Development of microfluidic and low-energy emulsification methods for the production of monodisperse morphologically-complex nanocarriers : application to drug and contrast agent encapsulation

Shukai Ding

UNIVERSITÉ DE STRASBOURG

ÉCOLE DOCTORALE DE PHYSIQUE ET CHIMIE-PHYSIQUE

Institut Charles Sadron, CNRS UPR 22

THÈSE présentée par :

Shukai DING

soutenue le : **30 Novembre 2016**

pour obtenir le grade de : **Docteur de l'université de Strasbourg**

Discipline/ Spécialité : Physique/Génie des procédés d'émulsification et de polymérisation

Development of microfluidic and low-energy emulsification methods for the production of monodisperse morphologically-complex nanocarriers. Application to drug and contrast agent encapsulation

THÈSE dirigée par :

M. Christophe Serra — Professeur, Université de Strasbourg

RAPPORTEURS :

M. Guo-Hua Hu — Professeur, Université de Lorraine

M. Eric Allémann — Professeur, Université de Genève, Suisse

AUTRES MEMBRES DU JURY :

M. Thierry Vandamme — Professeur, Université de Strasbourg

I would like to dedicate my thesis to beloved parents, family members & teacher for their love, guidance and prayers

RESUME DE THESE

Développement de méthodes d'émulsification microfluidique et basse énergie pour la production de nanovecteurs monodisperses de morphologies complexes. Application à l'encapsulation d'un principe actif ou d'un agent de contraste

1. Introduction

Au cours du dernier quart de siècle, les nanovecteurs ont suscité un intérêt grandissant dans le domaine pharmaceutique. Différents types de nanovecteurs ont ainsi été développés (nanoparticules polymères, liposome, polymèrosomes, hydrogels etc.) en vertu des avantages qu'ils procurent notamment pour la délivrance contrôlée/ciblée de principes actifs et le transport d'agents de contraste. Ils sont généralement obtenus par l'émulsification d'un fluide dans un autre qui lui est immiscible. Toutefois, les procédés conventionnels d'élaboration ne permettent qu'un contrôle limité de leurs caractéristiques (taille et morphologies) ce qui retarde leur développement. En effet, on observe avec les procédés discontinus classiques une variabilité de leurs caractéristiques d'un lot à un autre. Ceci résulte essentiellement de l'impossibilité de promouvoir un mélange parfaitement homogène dans tout le volume du réacteur.

Par ailleurs, des techniques avancées de mélange et d'émulsification ont été développées au cours des dix dernières années. Lors de cette thèse, deux techniques avancées ont été utilisées pour produire des nanovecteurs aux propriétés contrôlées encapsulant un principe actif ou un agent de contraste. Un premier lieu la microfluidique, c.-à-d. la science et technologie de la manipulation de volumes de fluide de l'ordre du nanolitre dans des microcanaux, qui permet en autre le control très précis du mélange de deux fluides immiscibles. En second lieu des méthodes d'émulsification basse énergie, basées sur la formation spontanée de nanoémulsions lorsque leur composition ou les conditions physiques (température notamment) sont changées, qui présentent un réel potentiel pour produire des nanoémulsions sans grande dépense d'énergie.

Les objectifs de cette thèse furent double : 1) mettre en œuvre ces techniques avancées pour produire des nanovecteurs monodisperses de morphologies complexes, 2) encapsuler un principe actif ou un agent de contraste.

Quatre différents types de nanovecteurs furent ainsi développés : des nanoparticules (NPs) de poly(méthyl méthacrylate) (PMMA) encapsulant soit un petite molécule bioactive hydrophobe (Kétoprofène) ou soit un agent de contraste (Fe_2O_3 NPs), des doubles émulsions

ou nanohydrogels contenant une sonde fluorescente (5(6)-carboxyfluorescéine) dans leur structure interne et enfin des nanolipogels (un réseau réticulé de polyacrylate gonflé par une huile de grade pharmaceutique) encapsulant des nanoparticules de Fe_2O_3 ou d'or.

2. Résultats choisis

2.1 Nanovecteurs polymères produits par des méthodes microfluidiques

2.1.1. Production de nanoparticules sèches de PMMA chargées de Kétoprofène- par couplage d'une nanoprécipitation assistée par micromélangeur et d'un séchage par pulvérisation

Ces nanovecteurs ont été produits par un procédé en deux étapes dont le schéma global est représenté en **Figure 1**. Les nanoparticules polymère pharmacologiquement chargées furent synthétisées au moyen de trois différents types de micromélangeurs : une simple jonction en T (bilamination, Swagelok, France), un micromélangeur interdigital haute pression à mutilamination (HPIMM, IMM, Allemagne) et un micromélangeur à jet d'impact (K-M 3, Fujifilm Corporation, Japon). Une solution de THF[1] à 1 wt.% de PMMA fut tout d'abord préparée et additivée avec un surfactant (Cremophor ELP, 0.5 wt.%) et la quantité souhaitée de Kétoprofène (0.5 wt.%). La solution résultante (solution de polymère) ainsi que la solution de non-solvant du polymère (eau ultrapure) furent pompées séparément au moyen de deux pompes CLHP[2] à des débits variant entre 3 et 7 mL/min dans chaque port d'entrée des micromélangeurs. La nanoprécipitation commença rapidement dans la chambre du micromélangeur lorsque que les deux solutions entrèrent en contact. Le THF diffusa alors rapidement dans la phase aqueuse laissant le MMA dans un état de sursaturation qui le conduisit à précipiter sous forme de nanoparticules.

Les suspensions colloïdales de nanoparticules de PMMA qui en résultèrent furent alors collectées à la sortie des micromélangeurs puis laissées toute une nuit dans une hotte à température ambiante pour éliminer le THF. Ensuite, les solution dénuées de solvant furent additivées avec du Mannitol (5 wt.%) et du SDS[3] (0.3 wt.%) pour prémunir l'agrégation des NPs durant le séchage par pulvérisation (**Figure 1**). Les nanosuspensions ainsi formulées furent enfin séchées au moyen d'un mini sécheur à pulvérisation (B-290, Büchi, France) sous les conditions suivantes : une température d'injection de 100°C, un débit d'aspiration de 100% et un débit d'entrée de 10 % (**Figure 1**). Une fois récupérées, les nanoparticules sèches furent stockées and un endroit sec pour éviter une reprise hygrométrique.

[1] Tétrahydrofurane

[2] Chromatographie en phase liquide à haute performance

[3] Sodium dodécyl sulfate

La taille et la distribution en taille de ces NPs furent déterminées par diffusion dynamique de la lumière (DDL) au moyen d'un granulomètre laser (Zetasizer Nano ZS, Malvern, France). Le laser hélium-néon (4 mW) était réglé sur 633 nm, l'angle de diffusion fixé à 173° et la température maintenue à 25°C. L'indice de polydispersité de la taille des particules (PDI) est une mesure de la largeur de la distribution en taille et il est communément admis qu'une valeur de PDI de 0.2 ou moins correspond à des particules monodisperses. La mesure de la distribution en taille des nanosuspensions fut faite en trois exemplaire en versant 0.02 mL de d'une nanosuspension and 1 mL d'eau ultrapure. Pour les nanoparticules sèches, ces dernières ont été préalablement redispersées à la même concentration que précédemment dans de l'eau ultrapure et plongées dans un bain à ultrasons pendant 5 min (89202, Bioblock Scientific, France). Ensuite leur taille a été déterminée en suivant le même protocole que celui utilisé pour les nanoparticules non séchées.

La quantification du Kétoprofène s'est effectuée par spectrophotométrie UV à 259 nm (UV-2401 PC, Schimadzu, Japan). Le rapport et l'efficacité d'encapsulation furent déterminés comme suit : pour les nanosuspensions avant séchage, le THF fut tout d'abord éliminée, puis 10 mL de la solution résultante furent centrifugés (Optima L-90 K Ultracentrifuge, Rotor Type 90 Ti, Beckman Coulter, France) à 45,000 Tr/min et 23°C pour éliminer le Kétoprofène non encapsulé. The surnageant fut ensuite utilisé pour mesurer le rapport (ER) et l'efficacité (EE) d'encapsulation conformément aux deux équations suivantes :

$$\mathbf{EE} = \frac{m_{KP}^{tot} - m_{KP}^{super}}{m_{KP}^{tot}} \qquad \textbf{Eq. 1}$$

$$\mathbf{ER} = \frac{m_{KP}^{tot} - m_{KP}^{super}}{m_{KP}^{tot} - m_{KP}^{super} + m_{Polym}^{NPs}} \qquad \textbf{Eq. 2}$$

où m_{KP}^{tot} et m_{KP}^{super} représentent respectivement les fractions massiques de Kétoprofène dans la solution initiale et dans le surnageant. Le numérateur du membre de droite de l'équation 1 représente ainsi la masse de Kétoprofène encapsulée dans les nanoparticules de PMMA par volume d'échantillon (10 mL). m_{Polym}^{NPs} est la concentration massique théorique de polymère dans l'échantillon calculée sur la base de la quantité de polymère utilisée dans la formulation initiale. Ainsi EE et ER représentent la fraction massique de la quantité initiale de Kétoprofène encapsulée et celle de Kétoprofène par nanoparticule respectivement. Pour les nanoparticules sèches, la même procédure a été employée après qu'elles eurent été redispersées dans l'eau ultrapure comme ce fut le cas pour la détermination de leur taille par DDL.

Les tests de libération du Kétoprofène furent effectués en chargeant un boudin de dialyse (diamètre 16 mm, MWCO 12-14 kDa, Medicell International, UK) avec 10 mL d'une nanosupension non séchée ou reconstituée à partir des nanoparticules sèches. Puis ce boudin fut immergé dans 250 mL d'une solution tamponnée de phosphate salin (pH=7.4, C=0.1M) agitée mécaniquement à 37°C. Régulièrement, la solution fut échantillonnée (aliquots of 3 mL) et le volume prélevé remplacé par la même quantité d'une solution

tamponnée fraîchement préparée afin d'assurer des conditions affamées (*sink conditions*). Puis la concentration massique de Kétoprofène dans les aliquots fut déterminée comme précédemment décrit par spectrophotométrie UV.

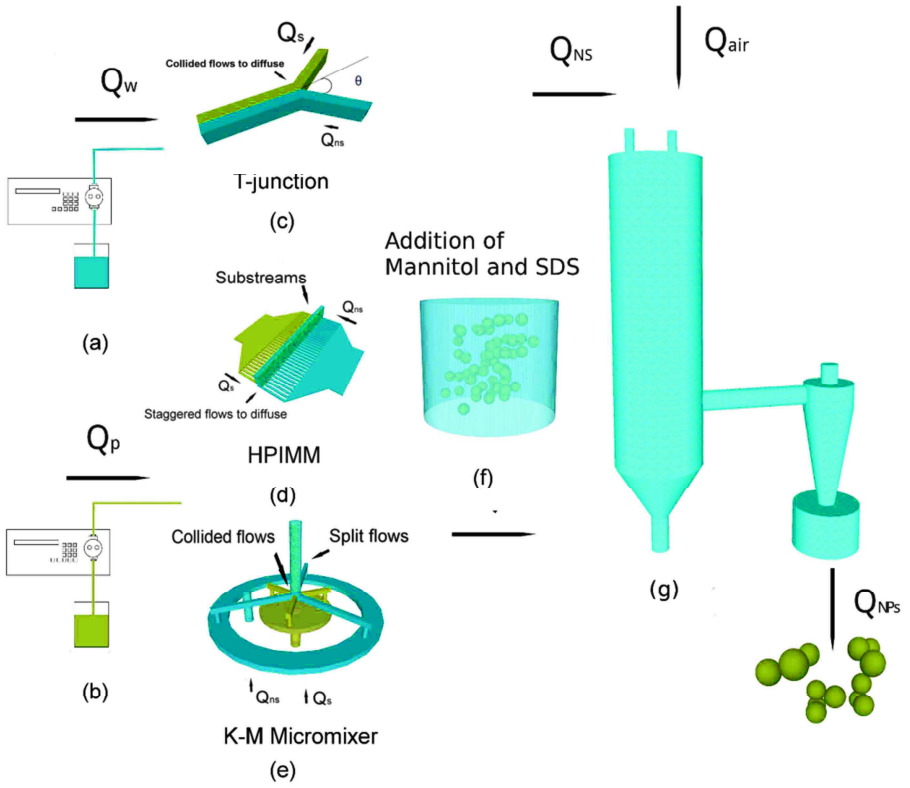

Figure 1. Schéma du procédé en deux étapes pour la production de nanoparticules sèches de PMMA chargées de Kétoprofène. Pompe pour les solutions de non-solvant (a) et polymère (b); jonction en T (c), HPIMM (d) and K-M (e) micromélangeurs; nanosuspension après nanoprécipitation (f); sécheur à pulvérisation (g).

L'influence des caractéristiques du micromélangeur et du débit de la phase aqueuse sur la taille des nanoparticules de PMMA chargées non séchées fut étudiée (**Figure 2**). On observe que lorsque le débit augmente, les particules sont plus petites ce qui est en accord avec le fait que le mélange est bien meilleur lorsque le débit des fluides à mélanger est plus grand[4]. Parmi les trois micromélangeurs testés, la jonction T produit toujours les plus grosses NPs alors que le K-M donne les plus petites. Pour ce dernier, le mélange résulte de la combinaison d'une haute énergie et de la diffusion moléculaire qui est beaucoup plus efficace que la simple diffusion moléculaire, qu'elle s'opère sur une distance courte (HPIMM) ou plus longue (jonction en T). On peut penser que le micromélangeur K-M fournit assez d'énergie pour une nucléation rapide tandis que la diffusion moléculaire va induire la croissance des nanoparticules de PMMA. Ainsi, le micromélangeur K-M apparaît comme le

[4] Hessel V., H. Löwe and F. Schönfeld, Micromixers—a review on passive and active mixing principles, Chem. Eng. Sci., 60 (8-9) (2005)2479-2501.

meilleur système et permet d'obtenir des nanoparticules monodisperses de PMMA chargées d'une taille de 110 µm et d'un PDI inférieur à 0,2.

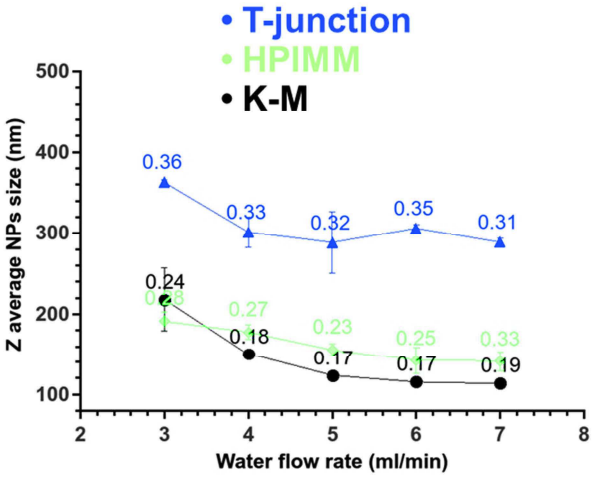

Figure 2. Effet du débit de la solution aqueuse sur la taille des nanoparticules de PMMA chargées en Kétoprofène pour les trois micromélangeurs testées. Le débit de la solution de polymère a été fixé à 1 ml/min. Les étiquettes des points indiquent la valeur du PDI.

La **Figure 3**a présente la taille des particules de PMMA chargées en médicament obtenus avec le micromélangeur K-M avant et après séchage pour deux débits d'eau différents. On observe que l'étape de séchage par pulvérisation n'altère que peu la qualité des nanoparticules de PMMA obtenues après nanoprécipitation puisque la taille et le PDI ne varient pas de façon significative. L'efficacité d'encapsulation (EE) et le rapport d'encapsulation (ER) pour les nanoparticules sèches ont été déterminés pour les deux tailles de nanoparticules de la **Figure 3**a et sont présentés dans la **Figure 3**b. A la fois le EE et le ER augmentent lorsque la taille des NPs augmente (par exemple lorsque le débit d'eau diminue, voir **Figure 2**). Ceci résulte du plus grand rapport surface sur volume des particules les plus petites qui favorisent ainsi une diffusion plus efficace du Kétoprofène à la surface des microparticules.

Enfin les propriétés de libération des nanoparticules ont été déterminées et les résultats obtenus pour les particules non séchées et redispersées après séchage produites avec deux débits d'eau différents sont affichés dans la **Figure 4**. Il est d'abord observé que plus les particules sont petites, plus grande est la quantité de Kétoprofène libérée. Ceci est dû à nouveau au rapport surface sur volume qui est plus élevé pour les petites nanoparticules. On peut également voir que les profils de libération pour des nanoparticules non séchées et celles redispersées sont les mêmes. Cependant la quantité cumulée libérée par les nanoparticules séchées par pulvérisation est toujours inférieure de 10 à 15% par rapport à celles qui ne furent pas séchées. Cela est probablement dû à la perte de médicament pendant le processus de séchage qui implique de l'air chaud à 37°C. Enfin, quelle que soit la taille des nanoparticules de PMMA, une libération prolongée est atteinte avec une quantité maximale de médicament libérée qui est atteinte après 6 heures.

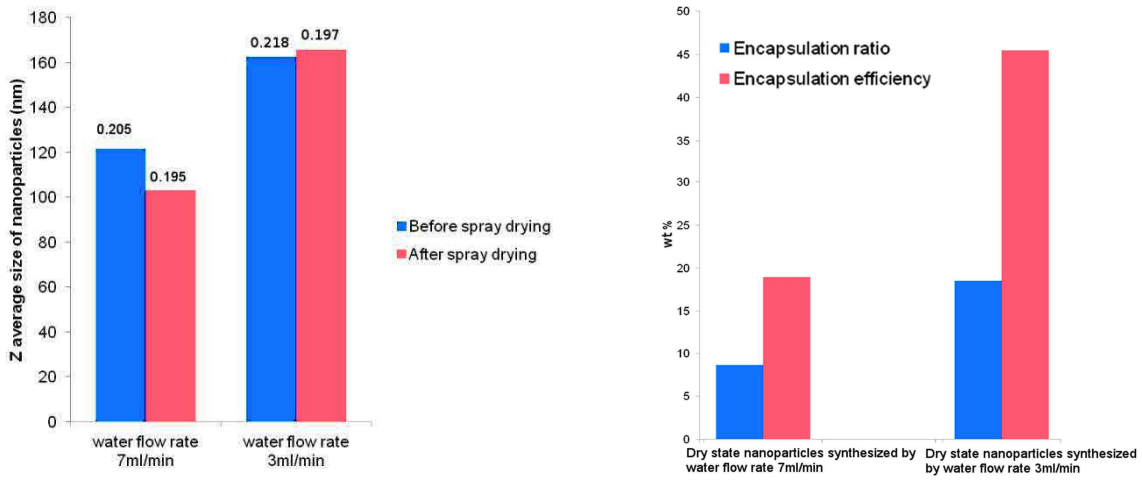

a) b)

Figure 3. a): influence du séchage par pulvérisation sur la taille des nanoparticules obtenues avec le micromélangeur K-M pour deux débits d'eau différents. b) efficacité d'encapsulation (EE) et rapport d'encapsulation (ER) des nanoparticules de PMMA chargées en Kétoprofène obtenues avec les deux débits d'eau différents.

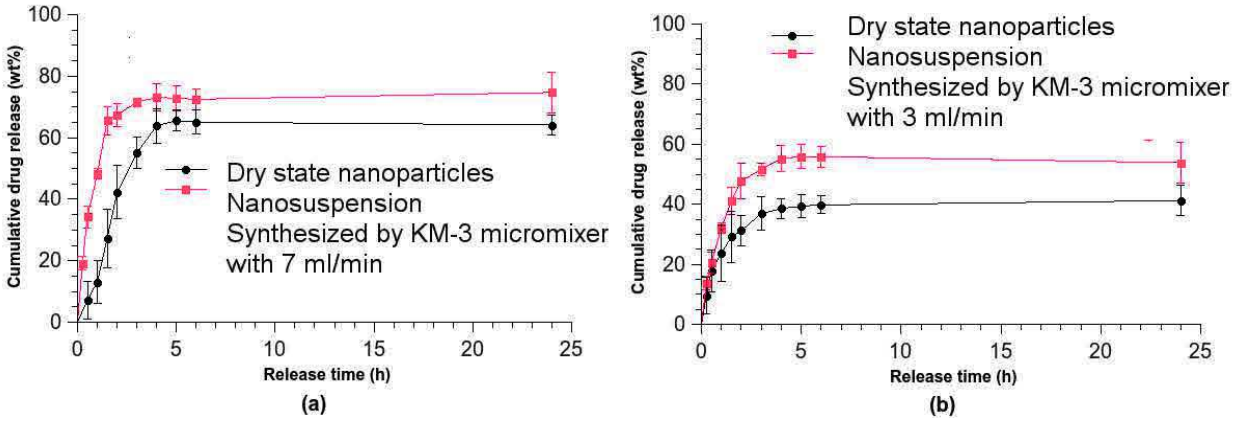

Figure 4. Profil de libération du principe actif modèle pour des nanoparticules séchées par pulvérisation puis redispersées et des nanoparticules non séchées et toutes deux produites avec deux débits d'eau différents: 7 ml/min (a) et 3 ml/min (b).

Ainsi, ce procédé en deux étapes est une stratégie efficace pour obtenir des nanovecteurs pulvérulents à base de polymères, chargés de principe actif, présentant une libération prolongée et pouvant être stockés et facilement redispersables pour une utilisation ultérieure; sans parler de la possibilité de dimensionner à une échelle plus grande la procédure.

2.1.2. Production microfluidique de nanoparticules de PMMA chargée en SPIONs

De manière similaire, la technique de nanoprécipitation assistée par micromélangeur (**Figure 5**a) fut appliquée pour encapsuler des nanoparticules d'oxyde de fer superparamagnétiques (SPIONs). Ainsi des nanoparticules de PMMA d'une taille de 200 nm ont été chargées avec des SPIONs de 6 nm à hauteur de 60% en poids. Cependant les nanoparticules de PMMA ne présentaient pas une morphologie sphérique, en raison du mécanisme intrinsèque de précipitation nucléation/croissance. En outre, la teneur en matière solide totale des nanosuspensions obtenues était très faible (0,05% en poids de PMMA). Aussi, pour résoudre ces deux inconvénients, une méthode d'émulsification basée sur un fort écoulement élongationnel fut considérée (**Figure 5**b). Un mélange hexane/dichlorométhane (50% en vol.) composée d'une solution de PMMA (5 mg/L) et de SPIONs (6,67 mg/L) a été émulsifié dans une solution aqueuse contenant 2% en poids d'un agent tensio-actif (Cremophor) au moyen d'un écoulement alternée (100 cycles à 50 mL/min) à travers la restriction brutale d'un microcanal (micromélangeur). Après l'évaporation des solvants organiques laissés pendant une nuit à température ambiante, des nanoparticules de PMMA chargées en agent de contraste magnétiques, monodisperses, sphériques et d'une taille de 100 nm ont été obtenues dans une solution aqueuse à une concentration de 0,1.% en poids de PMMA.

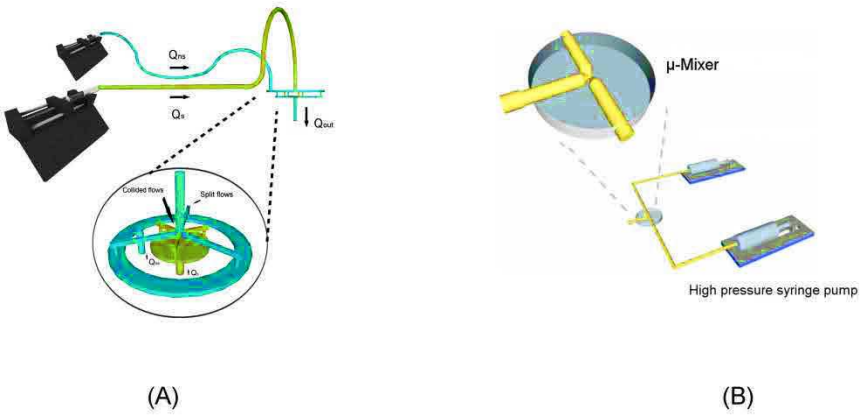

Figure 5. Description schématique des systèmes microfluidiques utilisés pour la nanoprécipitation assistée par micromélange (a) et l'émulsification microfluidique sous flux élongationnel (b).

2.2. Nanovecteurs produits par des méthodes basses énergie

2.2.1. Production d'émulsions et de nanohydrogels doubles fluorescents par couplage d'un microfluidiseur et d'une émulsification spontanée

Ces nanovecteurs ont été produits au moyen d'une procédure en deux étapes dont le schéma d'ensemble est présenté dans la **Figure 6**. Le procédé 1 est conçu pour produire une double nanoémulsion, quant au procédé 2 il permet d'obtenir des nanohydrogels entourés par une enveloppe huileuse (appelés plus tard nanohydrogels doubles pour raison de simplicité).

Dans le procédé 1, la première étape consiste en la préparation d'une solution diphasique obtenue par addition d'une quantité donnée d'une phase aqueuse (AP), composée d'une solution tamponnée de phosphate salin (PBS) mélangé avec différentes quantités en poids de Maltodextrine 01915 (épaississant) et de 5 (6) - carboxyfluorescéine (5 (6) -CF), dans une phase huileuse (OP), composée de Labrafac 1349 (un mélange de triglycérides d'acides caprique et caprylique de grade pharmaceutique) et un agent tensio-actif non ionique à faible HLB[5] (PGPR 476). Les teneurs en poids des différents composés par rapport à l'une ou l'autre des deux phases (aqueuse ou huileuse) sont données dans la Table 1. Dans le procédé 2, un monomère (acrylamide, AM), un photoarmorceur (GENOCURE DMHA) et un agent de réticulation (N, N'-méthylène-bisacrylamide, MBA) ont été ajoutés à la phase aqueuse précédente (Table 2). Une fois préparé, chacune des deux solutions ci-dessus a été prémélangée par vortex pendant 1 min (Heidolph Top-mix 94323, Bioblock Scientific, Allemagne) puis chauffé à 50°C avec vortex (Thermomixer C, Eppendorf, France) à 1000 Tr/min pendant 3 min, et enfin émulsifiée dans un Ultraturrax (IKA T25M, Allemagne) à 24.000 Tr/min pendant 3 minutes pour finalement produire une émulsion prémixée. Ensuite, la nanoémulsion primaire w_1/O a été obtenue en passant l'émulsion précédente dans un microfluidiseur commercial (LV1, Microfluidics Corp., USA). Les tailles et les PDI des nanoémulsions primaires obtenus par des mesures DDL sont rapportés dans la Table 1.

[5] Equilibre hydrophile-lipophile

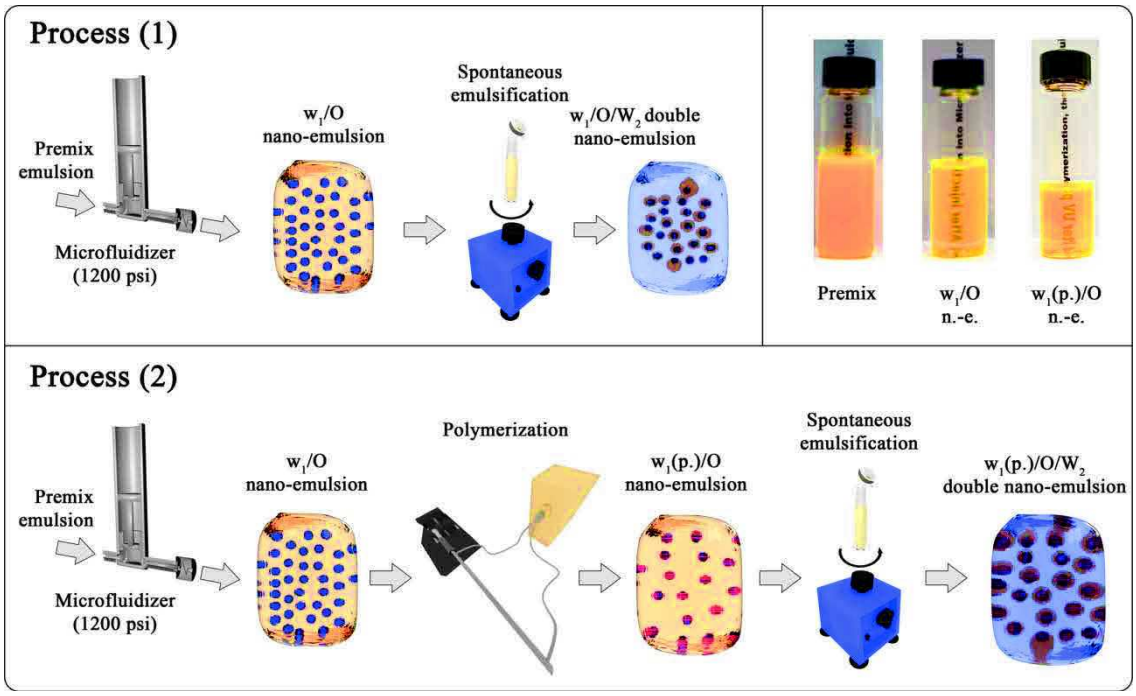

Figure 6. Dessins schématiques des procédés en deux étapes pour produire soit des nanomémulsions fluorescentes doubles (procédé 1) ou des doubles nanohydrogels fluorescentes (procédé 2). Dans le premier procédé, l'émulsion prémixée est injectée dans le microfluidiseur à haute pression pour obtenir une émulsion primaire de nanogouttelettes d'eau dans la phase huileuse (w_1/O) qui est ensuite utilisée dans l'émulsification spontanée pour obtenir la double nanoémulsion ($w_1/O/W_2$). Dans le procédé 2, l'émulsion prémixée contenant de l'acrylamide, un agent de réticulation et un photoamorceur est injectée dans le microfluidiseur à haute pression afin d'obtenir une émulsion primaire polymérisable de nanogouttelettes eau/acrylamide dans la phase huileuse (w_1/O). Ensuite, l'émulsion primaire est polymérisée par irradiation UV pour obtenir les nanohydrogels en phase huileuse ($w_1(p.)/O$) qui a été ensuite utilisé dans l'émulsification spontanée pour obtenir les nanohydrogels doubles ($w_1(p.)/O/W_2$). L'encart montre l'aspect de l'émulsion primaire avant et après le passage dans le microfluidiseur, et après polymérisation

Dans l'ensemble, le processus de nanoémulsification apparaît efficace, donnant des diamètres hydrodynamiques inférieurs à 200 nm qui peuvent descendre jusqu'à 50 nm, et des valeurs de PDI variant de 0,15 à 0,05, témoignant ainsi de la bonne monodispersité de la suspension. Le paramètre le plus important qui influe sur la taille des nanogouttelettes est la concentration en agent tensio-actif. L'augmentation de la teneur en poids de PGPR induit une diminution de la taille des nanogouttes de la phase aqueuse produites par le microfluidiseur, quelle que soit la viscosité de la phase aqueuse (c.-à-d. la teneur en poids de Maltodextrine) et quelle que soit la teneur en poids de la phase aqueuse. Ainsi les teneurs en poids de Maltodextrine et de la phase aqueuse ne semblent pas avoir un impact réel. Ce résultat est probablement lié au phénomène qui crée et stabilise les gouttelettes pendant l'émulsification. En effet, un rapport entre la viscosité des phases continue et dispersée allant de 1:10 à 1: 100 est nécessaire pour permettre et optimiser le fractionnement des gouttelettes. Avec une teneur minimale en poids de Maltodextrine de 30% en phase aqueuse, c'est précisément ce que nous avons obtenu. Ensuite, les autres paramètres clés

sont les teneurs en poids de la phase aqueuse et du PGPR dans l'huile. Les deux paramètres vont influencer, respectivement, le nombre de gouttelettes créées et leur stabilisation potentielle avant coalescence pendant le processus l'émulsification. On peut ainsi comprendre l'effet de la concentration de PGPR sur la taille résultante des gouttelettes, qui en raison d'une meilleure stabilisation des nanogouttes après génération permet d'en obtenir de plus petites.

Table 1. Composition et taille des émulsions primaire obtenues dans le procédé 1

Entrée	Phase aqueuse (AP)			Phase huileuse (OP)			Taille (nm)	PDI
	AP (wt.%)	Maltodextrine (wt.%/AP)	PBS Sol.* (wt.%/AP)	OP (wt.%)	Labrafac (wt.%/OP)	PGPR (wt.%/OP)		
1	19	72	28	81	98.75	1.25	195	0.12
2	19	72	28	81	99.25	0.75	193	0.06
3	25	72	28	75	92.86	7.14	150	0.12
4	15	72	28	85	93.75	6.25	123	0.03
5	10	30	70	90	94.12	5.88	111	0.15
6	15	30	70	85	93.75	6.25	111	0.10
7	25	30	70	75	92.86	7.14	110	0.08
8	25	50	50	75	92.86	7.14	104	0.12
9	15	50	50	85	93.75	6.25	101	0.15
10	10	40	60	90	87.50	12.5	55	0.16
11	13	50	50	87	90.62	9.375	55	0.28
12	10	50	50	90	87.50	12.5	50	0.11
13	10	60	40	90	87.50	12.5	77	0.08

* no 5(6)-CF dans la solution de PBS

Pour le procédé 2 (**Figure 6**), l'émulsion primaire polymérisable obtenue suite au microfluidiseur a été ensuite pompée à travers un tube en PTFE[6] de 1,6 mm de diamètre interne placée à l'intérieur d'une longueur de 20 cm de tube en acier inoxydable dont les deux extrémités sont reliées au moyen de deux jonctions en T (Swagelok, France) à deux guides d'ondes lumineuses d'une source d'UV (Lightningcure LC8, Hamamatsu, Japon) fonctionnant à une longueur d'onde de 365 nm et une intensité appropriée (environ 140 mW / cm2). Le temps de séjour de l'émulsion primaire sous la lumière UV fut d'environ 120s

[6] Polytétrafluoroéthylène

ce qui était suffisant pour polymériser l'acrylamide à l'intérieur des nanogouttelettes conduisant à la formation de nanohydrogels dans l'huile en raison de la présence de l'agent de réticulation MBA. Les tailles et les PDI des nanoémulsions primaires polymérisées obtenus par des mesures DDL sont rapportés dans la Table 2.

A partir de cette table, on peut noter que la présence de l'agent de contraste fluorescent (5 (6) -CF) et des composés de polymérisation (AM, MBA & DHMA) n'affectent en rien la taille des nanogouttelettes de la phase aqueuse (voir les entrées 1 et 3 de la Table 2 et l'entrée 12 de la Table 1 ainsi que les entrées 1-4 de la Table 2, respectivement).

Dans la deuxième étape, l'émulsification spontanée a été promue en ajoutant rapidement une quantité donnée d'un émulsifiant non ionique de grade pharmaceutique (Cremophor ELP) à l'émulsion primaire (polymérisée ou non) à la température ambiante suivi par 1 min de vortex (Heidolph Top-mix. 94323, Bioblock scientifique, Allemagne). Enfin, une quantité donnée de solution de PBS a été ajoutée rapidement à température ambiante à l'émulsion précédente puis agitée au vortex pendant 10 min avec le même appareil. Ainsi des nanogouttelettes d'eau (procédé 1) ou des nanohydrogels (procédé 2) contenant à la fois le 5(6)-CF et tous deux entourés par une couche de Labrafac ont été obtenus. Les caractéristiques de ces doubles nanovecteurs sont présentées dans la Table 3 et la Table 4.

Table 2. Composition et taille des émulsions primaire obtenues dans le procédé 2

Entrée	Phase aqueuse (AP)							Phase huileuse (OP)			Taille (nm)	PDI
	AP (wt %)	Maltodextrine (wt.%/AP)	PBS sol. (wt.%/AP)	5(6)-CF (mM in PBS sol.)	AM (wt.%/PBS)	MBA (wt.%/AM)	DHMA (wt.%/AM)	OP (wt.%)	Labrafac (wt.%/OP)	PGPR (wt.%/OP)		
1	10	50	50	50	-	-	-	90	87.50	12.5	58	0.17
2	10	50	50	50	40	10	5	90	87.50	12.5	50	0.13
3	10	50	50	200	40	10	5	90	87.50	12.5	53	0.23
4	10	50	50	50	40	2	5	90	87.50	12.5	47	0.17

Les deux paramètres suivants ont été utilisés pour décrire l'influence des teneurs en poids de Cremophor et de la solution de PBS ajoutés au cours de la deuxième étape sur les caractéristiques des nanovecteurs doubles obtenus.

$$\mathbf{SOR}(\%) = \frac{m^{CRE}}{m^{CRE}+m^{PE}} \quad \textbf{Eq. 3}$$

$$\mathbf{SOWR}(\%) = \frac{m^{CRE}+m^{PE}}{m^{ELP}+m^{CRE}+m^{PBS}} \quad \textbf{Eq. 4}$$

où m^{CRE} , m^{PE} et m^{PBS}représentent respectivement la masse de Cremophor, de l'émulsion primaire et de la solution de PBS employés pour l'émulsification spontanée.

Table 3. Rapport entre les teneurs en tensio-actif et en huile (SOR) employées dans l'émulsification spontanée du procédé 1 et caractéristiques des nanoparticules obtenues

Teneur en poids de Maltodextrine dans la phase aqueuse de l'émulsion primaire (w_1)								
40 wt.%*			50 wt.%$			60 wt.%£		
SOR (%)	Taille (nm)	PDI	SOR (%)	Taille (nm)	PDI	SOR (%)	Taille (nm)	PDI
20	178	0.51	20	161	0.31	20	168	0.37
25	156	0.34	25	137	0.13	25	153	0.29
30	127	0.17	30	113	0.15	30	119	0.13
35	103	0.12	35	113	0.22	35	98	0.11
40	83	0.14	40	81	0.12	40	87	0.15

* Basée sur l'entrée 10 de la Table 1 contenant en plus 50 mM de 5(6)-CF
$ Basée sur l'entrée 12 de la Table 1 contenant en plus 50 mM de 5(6)-CF
£ Basée sur l'entrée 13 de la Table 1 contenant en plus 50 mM de 5(6)-CF

Table 4. Rapport entre les teneurs en tensio-actif et en huile (SOR) employées dans l'émulsification spontanée du procédé 2 et caractéristiques des nanoparticules obtenues pour trois compositions différentes de la phase aqueuse primaire (w_1)

Composition A **Entrée 2 de la** Table 2			Composition B **Entrée 3 de la** Table 2			Composition C **Entrée 4 de la** Table 2		
SOR (%)	Taille (nm)	PDI	SOR (%)	Taille (nm)	PDI	SOR (%)	Taille (nm)	PDI
30	130	0.21	30	145	0.37	30	162	0.39
35	120	0.21	35	133	0.23	35	128	0.20
40	106	0.22	40	116	0.22	40	111	0.25

Après avoir obtenu les émulsions primaires, les nanoémulsions doubles $w_1/O/W_2$ ont été préparées par un procédé d'émulsion spontanée, qui est une méthode à basse énergie. Étant donné que le SOWR (Eq. 4) a été reconnu avoir aucune influence sur les propriétés de la nanoémulsion[7], il a été fixé à 40%. D'autre part, un paramètre clé influençant la taille des nanovecteurs doubles est la quantité de Cremophor rajoutée à l'émulsion primaire (SOR, Eq. 3), qui varie de 20 à 40%. Comme on s'y attendait, l'augmentation de la valeur du SOR induit de manière significative la réduction de la taille et du PDI des nanovecteurs doubles pour les deux procédés. La teneur en poids de Maltodextrine a été trouvée affecter grandement la taille de l'émulsion primaire (Table 1 and Table 2), mais a un impact modéré sur la taille des nanovecteurs doubles. Cela signifie que l'émulsification spontanée n'est pas pas affectée par la composition de la phase aqueuse dans l'émulsion primaire. En effet, une fois que l'agent

[7] Nicolas Anton and Thierry F. Vandamme, The universality of low-energy nano-emulsification, Int. J. Pharm., 37 (1-2) (2009) 142-147.

tensio-actif non ionique Cremophor est mélangé avec l'émulsion primaire, il semble conserver les gouttelettes internes. Ensuite, le mélange de cette phase huileuse avec du PBS provoque la solubilisation immédiate du Cremophor par le tampon, et se traduit par l'émulsification spontanée. Lorsque l'on compare la taille des nanovecteurs doubles obtenues avec le procédé 1 et 2, pour les mêmes paramètres de fonctionnement (Table 3 pour une teneur en poids de Maltodextrine de 50% et la composition A de la Table 4), il semble que la présence de poly(acrylamide) dans les nanogouttelettes primaire induit une augmentation modérée de la taille. En outre, comme on le voit dans la Table 4, la composition de phase aqueuse affecte très sensiblement la taille finale des nanovecteurs doubles. Lorsque la concentration en 5(6)-CF augmente ou lorsque la teneur en poids de MBA est diminuée, les nanogouttelettes doubles résultantes ont une taille qui augmente. Cela peut résulter d'un changement de la tension interfaciale entre la phase aqueuse et la phase huileuse.

Pour évaluer l'efficacité d'encapsulation de l'agent de contraste fluorescent 5(6)-CF dans les nanovecteurs doubles (Eq. 5), 0,8 mL de l'émulsion double recueillie à l'issue du procédé 1 ou 2 a été injecté dans une colonne de dessalage (PD-10 , GE Healthcare, États-Unis) pour séparer la 5(6)-carboxyfluorescéine libre située dans la phase continue principale (W_2) de l'émulsion double $w_1/O/W_2$ de celle encapsulée dans les nanovecteurs doubles. Ensuite, la solution libre de tout nanovecteur a été recueillie et analysée par spectrophotométrie UV pour déterminer la concentration massique de l'agent de contraste fluorescent non encapsulé.

$$\mathbf{EE_f}(\%) = \frac{m_{5(6)-CF}^{primary} - m_{5(6)-CF}^{uncap}}{m_{5(6)-CF}^{primary}} \qquad \textbf{Eq. 5}$$

où $m_{5(6)-CF}^{primary}$ et $m_{5(6)-CF}^{uncap}$ représentent respectivement la concentration massique de la 5(6)-carboxyfluorescéine dans l'émulsion primaire et celle qui n'a pas été encapsulée. Les résultats sont regroupés dans la Table 5. Il est à noter la quantité $m_{5(6)-CF}^{primary}$ fut déterminée par une méthode d'extraction sélective et spectrophotométrie UV.

Pour le procédé 1, l'efficacité d'encapsulation obtenue pour un SOR de 20% et une teneur en poids de Maltodextrine de 50% est environ de 19%. Cependant, on peut observer que, lorsque le SOR diminue, la taille et le PDI des nanovecteurs doubles augmentent (voir la Table 3), mais l'efficacité d'encapsulation augmente également (Table 5). Cela est probablement dû à la polydispersité plus élevée qui permet aux plus grandes nanogouttelettes d'être moins affectées par le processus d'émulsification. Un résultat similaire a été obtenu pour une teneur en poids de Maltodextrine de 40%, probablement pour les mêmes raisons. Lorsque la teneur en poids de Maltodextrine est augmentée à 60%, une légère augmentation de la valeur d'encapsulation est obtenue entre 7 et 12% avec l'augmentation du SOR. Du fait que la Maltodextrine n'affecte principalement que la viscosité de la phase aqueuse w_1, on peut imaginer que cette augmentation de la quantité de 5(6)-CF encapsulée peut être liée à une

rétention légèrement plus élevée de la sonde fluorescente pendant l'émulsification.

Table 5. Efficacité d'encapsulation de la 5(6)-CF pour différents rapports entre les teneurs en tensio-actif et en huile (SOR), différentes compositions de la phase aqueuses et des compositions en phase huileuse identiques à celles reportées dans la **Table 2**.

	Phase aqueuse (procédé 1)			**Phase aqueuse (procédé 2)**		
EE_f (%) / **SOR (wt.%)**	**Maltodextrine (40 wt.%/AP) 5(6)-CF (60 wt.%/AP)**	**Maltodextrine (50 wt.%/AP) 5(6)-CF (50 wt.%/AP)**	**Maltodextrine (60 wt.%/AP) 5(6)-CF (40 wt.%/AP)**	**Composition A** **Entrée 2 de la** Table 2	**Composition B** **Entrée 3 de la** Table 2	**Composition C** **Entrée 4 de la** Table 2
20	n/a	19.1	n/a	n/a	n/a	n/a
25	n/a	n/d	n/a	n/a	n/a	n/a
30	2.9	n/d	7.2	57.9	17.6	56.8
35	3.0	n/d	8.1	55.6	14.3	55.4
40	2	n/d	12.2	55.4	23.4	56.6

n/d: 5(6)-CF non détectée

D'autre part, lorsque la phase interne w_1 est polymérisée et transformée en un hydrogel (procédé 2), des efficacités d'encapsulation supérieures à 55% ont été obtenues, ce qui est probablement lié au fait que le polymère crée une cage d'eau qui ralentit les fuites de 5(6)-CF pendant et après l'émulsification spontanée. Il est intéressant de noter que pour les deux valeurs testées, la teneur en poids de l'agent de réticulation (MBA) n'a pas d'influence sur les résultats, ce qui signifie que les chaînes de poly(acrylamide) dans les nanogouttelettes de w_1 sont suffisamment réticulées pour conserver la sonde fluorescente. Une autre expérience a été réalisée en augmentant la concentration de la sonde jusqu'à 200 mM. Dans ce cas, l'efficacité d'encapsulation est diminuée pour atteindre des valeurs proches de 20%. Il en résulte que la capacité d'encapsulation maximale a dû être atteinte et que l'excès de 5(6)-CF est en grande partie expulsé vers la phase continue W_2.

2.2.2. Production de nanolipogels chargés en agent de contraste par émulsion spontanée

Pour produire des nanolipogels, l'émulsion w_1/O du procédé 1 (**Figure 6**) a été remplacée par un mélange contenant un monomère acrylate difonctionnel (diacrylate de tripropylèneglycol, TGPDA), un photoamorceur (1-hydroxycyclohexylphénylcétone, HCPK) et le Labrafac. Ce mélange a ensuite été utilisé comme la phase huileuse pour l'émulsification spontanée (addition/vortex successifs de Cremophor et solution de PBS). Après la formation des nanogouttelettes de TPGDA/Labrafac, le monomère a été polymérisé par irradiation UV avec le même dispositif que celui utilisé dans le procédé 2 (**Figure 7**). Ainsi des nanolipogels

dont la matrice fut composée de poly(TPGDA) gonflée par de l'huile Labrafac ont été obtenus. Il a été constaté que la présence de TPGDA dans la phase huileuse favorise l'émulsification spontanée. En effet, pour un SOR de 50% et en l'absence de TPGDA, les nanogouttelettes de Labrafac atteignirent une taille de 143 nm (PDI = 0,19) ; tandis qu'avec une teneur en poids de TPGDA de 40%, les nanolipogels présentèrent une taille beaucoup plus petites de 57 nm et furent plus monodisperses (PDI = 0,07).

Ainsi, la présence de TPGDA présente deux avantages par rapport à l'émulsification spontanée couramment utilisée. Premièrement, elle permet d'obtenir de plus petites tailles et des nanoparticules dont la distribution en taille est plus étroite. Deuxièmement, pour atteindre une taille de nanoparticules donnée, elle nécessite moins de quantité de Cremophor. Cela ouvre une nouvelle perspective pour obtenir des nanoparticules semi-solides par émulsification spontanée ce qui n'a jamais été obtenu auparavant. En outre, comme preuve de concept, des nanoparticules d'oxyde de fer (6 nm) ou des nanoparticules d'or (6 nm) ont été encapsulées dans la matrice de ces nanolipogels sans en affecter leur taille. Par conséquent, cela illustre la possibilité de préparer des nanolipogels chargés en agent de contraste par émulsification spontanée.

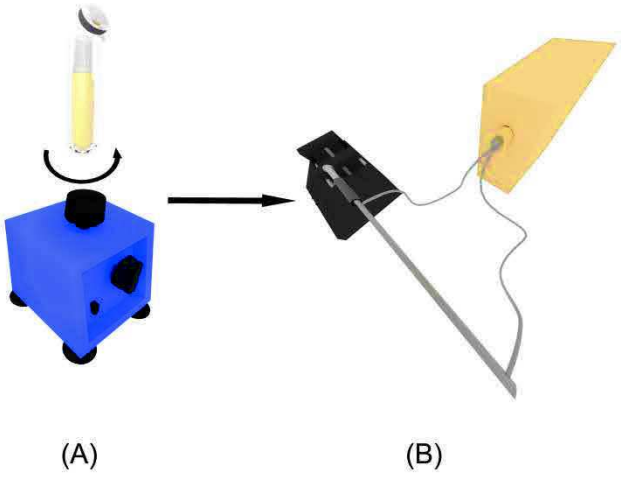

Figure 7. Dessins schématiques des étapes d'émulsification spontanée (a) et de la polymérisation sous flux continu par irradiation UV (b).

3. Conclusion

Au cours de ce travail de thèse trois méthodes différentes, à savoir la nanoprécipitation assistée par micromélangeur, l'émulsification microfluidique sous flux élongationnel et l'émulsification spontanée, ont été appliquées avec succès pour produire une grande variété de nanovecteurs dont la cargaison était soit un médicament modèle ou un agent de contraste.

La première méthode a permis de produire des nanoparticules monodisperses de PMMA

chargée en Kétoprofène dont la taille a pu être facilement variée de 200 nm jusqu'à 110 nm par augmentation du débit de non-solvant (eau). Une fois produits, les nanovecteurs ont été séchés au moyen d'un appareil commercial de séchage par pulvérisation. La taille de ces nanoparticules a été modérément affectée par le processus de séchage alors que le profil de libération prolongé du principe actif a été modifié de façon significative avec la taille des NPs (augmentation avec la réduction de taille) et avec l'étape de séchage par pulvérisation (systématiquement inférieur de 10 à 15% selon la taille des NPs). Toutefois, il a été observé que des nanoparticules chargées peuvent être simplement produites, séchées, stockées puis redispersées ultérieurement tout en présentant un taux de libération décent (au-dessus de 40% après plus de 6 heures). Cette méthode a également été utilisée pour produire des nanoparticules de PMMA de 200 nm chargées de nanoparticules d'oxyde de fer superparamagnétiques (SPIONs) avec une teneur en poids allant jusqu'à 60%.

La deuxième méthode a été utilisée pour doubler la fraction massique de ces nanoparticules chargées en agent de constate magnétique dans la suspension colloïdale finale et obtenir des nanoparticules plus sphériques de taille inférieure (100 nm).

La troisième méthode a été développée pour produire des nanoémulsions doubles ($w_1/O/W_2$) dont les nanogouttelettess intérieures furent chargées avec une sonde fluorescente (5(6)-carboxyfluorescéine). Cette méthode fut composée de deux étapes: i) la préparation, au moyen d'un microfluidiseur commercial, de l'émulsion primaire w_1/O dont la phase aqueuse (w_1) était composée d'une solution de PBS mélangé avec l'agent de contraste et l'épaississant (Maltodextrine) tandis que la phase huileuse (O) contenait une huile de grade pharmaceutique (Labrafac) et un tensio-actif non ionique à faible HLB (PGPR); ii) l'émulsification spontanée de la phase huileuse primaire par addition d'un émulsifiant non ionique (Cremophor), suivie d'une grande quantité de solution de PBS (W_2). La taille de l'émulsion primaire (50-200 nm) a été modérément affectée par la teneur en poids de l'épaississant (augmentant légèrement avec la quantité de Maltodextrine) mais fut largement affectée par la teneur en poids du tensio-actif dans la phase huileuse (diminuant fortement avec la quantité de PGPR). Si comme pour l'émulsion primaire, la teneur en poids de Maltodextrine a un effet modéré sur la taille des nanogouttelettes double, la teneur en poids du Cremophor dans l'émulsion primaire (SOR) est par contre le paramètre principal qui contrôle la taille finale de la double nanoémulsion. Une augmentation du SOR de 20 à 40% induit une forte diminution de la taille des nanovecteurs doubles de 160 jusqu'à 80 nm. Lorsque la phase aqueuse de l'émulsion primaire (w_1) contient une formulation polymérisable (monomère acrylamide, agent de réticulation et photoamorceur), ce procédé en deux étapes a permis la production de nanohydrogels de poly(acrylamide) entourés par une enveloppe huileuse (Labrafac). Ces doubles nanohydrogels ont permis d'augmenter de manière significative l'efficacité d'encapsulation de la sonde fluorescente (EE (f)) jusqu'à 50% par rapport celle de 2 à 12% obtenue sans ajout de monomère.
L'émulsification spontanée a également été utilisée pour produire des nanolipogels lorsque l'émulsion w_1/O précédente a été remplacée par un mélange lipophile composé d'un

monomère acrylate difonctionnel (tripropylèneglycol diacrylate, TPGDA), un photoamorceur et le Labrafac. Après addition d'une solution de Cremophor et du tampon PBS, des nanogouttelettes de ce mélange lipophile ont été obtenues et ensuite polymérisée par irradiation UV pour former des nanolipogels en suspension dans une phase aqueuse dont la matrice fut composée de poly(TPGDA) gonflé par le Labrafac. On a constaté que la taille de ces nanolipogels dépendait du paramètre SOR et de la teneur en poids du TPGDA dans le mélange lipophile et pouvait atteindre des valeurs aussi faibles que 57 nm. Enfin ces nanolipogels ont pu être chargés avec des nanoparticules magnétiques ou auriques pour servir potentiellement de nanovecteurs d'agent de contraste.

TABLE OF CONTENT

Chap 3. POLYMERIC NANOCARRIERS PRODUCED BY MICROFLUIDIC METHODS

CHAPTER 1
INTRODUCTION

Over the past 25 years, nanocarriers have attracted a considerable interest in pharmaceutics. Thus, different types of nanocarriers have been designed (e.g. polymeric nanoparticles, liposomes, polymerosomes, hydrogels etc.) as they offer unique benefits in terms of targeted/controlled drug release or as contrast agent cargos. They all share the feature of being produced from the emulsification of a given fluid into another immiscible one. But conventional preparation methods provide a poor control on nanocarrier's characteristics (e.g. size and morphology) which severely impede their further development. Indeed one observes variability in these characteristics when batch methods are employed for their production. This is mainly due to the poor ability to promote a homogenous mixing within the whole volume of the vessel.

On the other hand, advanced technologies for mixing and emulsification have been developed over the last decade. In this thesis, two types of advanced technologies have been applied to support stable and controllable properties of drug/contrast agent loaded nanocarriers. First of all, microfluidics, the science and technology of manipulating nanoliter volumes in microscale fluidic channels, has sufficiently ability to accurately control mixing rate of immiscible fluids. Second, low-energy emulsification methods, which rely on the spontaneous formation of nanoemulsions when either their composition or the surrounding conditions (mainly temperature) are changed, present a real potential to produce high quality nanoemulsions without much raw energy.

The aims of this PhD thesis were two-fold: 1) to apply such advanced technologies for the production of monodisperse morphologically-complex nanocarriers and 2) to encapsulate a drug or a contrast agent. To fulfill our goal, three different methods, namely micromixer-assisted nanoprecipitation, microfluidic-assisted elongational-flow emulsification and spontaneous emulsification, were successfully applied to produce a large variety of nanocarriers whose cargo was either a model drug or a contrast agent.

This manuscript is composed of 5 chapters. Beside the current one, the 2sd chapter is dedicated to the literature background and comprises two different sections. The first section reviews the different microfluidic nanoprecipitation systems employed for preparing pure drug or polymeric drug-loaded nanoparticles. The second section reviews the two-step methods allowing the production of micro- and nano double emulsions.

Chapter 3 presents a novel two-step method to get dry-state Ketoprofen-loaded PMMA[1] nanoparticles by combination of a microfluidic-assisted nanoprecipitation technique and conventional spray dryer. Effects of micromixing principle (multilamination or impact jet), ratio of non-solvent to polymer solutions flow rates and spray-drying step on nanoparticles size, size distribution, encapsulation efficiency and encapsulation ratio as well as drug release profile were thoroughly investigated.
This microfluidic-assisted nanoprecipitation technique was also adopted to produce PMMA nanoparticles loaded with iron oxide nanoparticles of smaller size. In parallel, these composite contrast agent nanocarriers were produced by a microfluidic-assisted elongational-flow nanoemulsification process for which effects of operating parameters were assessed.

Chapter 4 deals with the production of double nanocarriers, i.e. either water nanodroplets or PA[2] nanohydrogels loaded with a model drug (5(6)-carboxyfluorescein) and both surrounded by an oil shell (Labrafac[3]), using a new two-step method. The first step consisted in preparing a primary w_1/O[4] nanoemulsion by means of a commercial microfluidizer. In the second step the spontaneous emulsification of the oil phase was promoted to get the final $w_1/O/W_2$[5] double nanoemulsions. Effects of operating parameters, such as surfactant to oil ratio,

[1] Poly(methyl methacrylate)

[2] Poly(acrylamide)

[3] A mixture of capric and caprylic acid triglycerides as a model of parenteral-grade oil

[4] Water-in-Oil

[5] Water-in-Oil-in-Water

concentration of thickener or amount of drug etc., on primary emulsion and double nanoemulsion sizes as well as drug release properties were studied.

The spontaneous method was also used to produce contrast agent-loaded nanolipogels composed of either a mixture of TPGDA[6] and Labrafac or a crosslinked poly(TPGDA) matrix swollen by Labrafac which were loaded with iron oxide or gold nanoparticles of smaller sizes.

Finally Chapter 5 concludes about the work accomplished during this PhD and gives some perspective for future work.

[6] Tripropyleneglycol diacrylate

CHAPTER 2
BACKGROUND LITERATURE

2.1 Microfluidic nanoprecipitation systems for preparing pure drug or polymeric drug loaded nanoparticles: an overview

ABSTRACT

This review gives an overview of the different microfluidic setups used to produce either pure drug or drug-loaded polymeric nanoparticles. We propose a description of the different fluidic principles reported in the literature, explaining their respective design and configuration in parallel with the technical challenges related to the nanoprecipitation of the polymer, in relation with the results obtained, e.g., particle size, distribution and productivity.

2.1.1 Introduction

Over the past decade, a growing interest has been concentrated on polymeric nanoparticles (NPs) as drug delivery carriers to treat different types of disease[1-3]. Compared with conventional drug vehicles, such as liposomes, polymeric NPs were shown to increase the stability of drugs and to control their release properties[4, 5], owing to their tailored sizes, morphologies and the possibility to use biodegradable polymers. Moreover, NPs induce specific interactions with cells and tissues and notably can promote accumulation of drugs to target specific sites. On the other hand, using biodegradable polymers allows the sustained drug release at targeted sites, which can be controlled over days or weeks [6]. These particular properties constitute major advantages which have stirred the research effort in this field [7]. The main experimental ways for generating pure drug or polymer NPs can be namely listed as: solvent evaporation [8], salting-out [9], emulsification-solvent diffusion process [10], supercritical fluids that replace the solvent in the precipitation techniques [11], polymerization [12], and nanoprecipitation [13]. Among these techniques, we chose in the present review to focus on the nanoprecipitation since it is a simple, fast and reproducible method [14-16], and also widely used to produce NPs[17-20].

Polymeric and pure drug NPs were firstly prepared through nanoprecipitation by Fessi and co-workers [13]. The main principle driving the process is a fast mixing of a material solution (polymer and/or pure drug in a solvent) with a non-solvent of the material. Herein, ideally the solvent should be miscible with the non-solvent. The structure material (i.e. polymer and/or drug) should be free-soluble in the solvent and insoluble in the non-solvent. Controlling the size of the NPs passes through the optimization of process parameters as well as the formulation and physicochemical parameters, like the chemical nature of the solvent and non-solvent, the respective solubility of the material in both phases, their concentrations, the surfactant properties

of the polymer and/or drug, and potentially the presence of additional co-surfactant molecules (stabilizers).

In fact, the solvent transfer is one of the main parameters governing the nanoprecipitation [21], likely related to the miscibility between solvent and non-solvent which controls the speed of the mass transfer. On the other hand, the literature has shown that it is possible to precisely tune this transfer with microfluidic tools, which eventually improve the control on the NPs size. Microfluidics, the science and technology of manipulating nanoliter volumes in microscale fluidic channels, has impacted a wide range of fields including biological analysis, chemical synthesis, single cell analysis, and tissue engineering [22].

After George M. Whitesides's group [23] reported on the preparation of microfluidic systems by poly(dimethylsiloxane) replication of negative microstructures photolithographed on a silicon wafer in 1998, a very intense research was initiated and has now drastically widened the application of microfluidic systems. The influence of microfluidic technologies on chemical reactions has been widely described [24]. Particularly, a microfluidic system was designed to synthesize nanoscale materials by emulsification under high pressure homogenizer [25]. In the recent years, microfluidic systems were adapted to control the mixing rate between solvent and non-solvent phase, and clearly showed advantageous results in term of NPs size control, compared to classical batch processes for nanoprecipitation. The earliest example has reported the fine control of the mixing of two phases at nanoliters level within few microseconds with a flow-focusing silicon-based micromixer [26]. This method was later adapted for the nanoprecipitation of PLGA derivative NPs, providing the pioneer report on the controlled nanoprecipitation in microfluidic setup [27]. These works initiate a great research effort to explore the potentials of such novel microfluidic platforms for the elaboration of polymer and pure drug NPs by nanoprecipitation.

In this review, our objective was not to focus on micromixer particularly; however, the formulation of nanoparticles was mostly performed in micromixers. This is why the description of micromixer-based nanoprecipitation occupies the largest part of the review. Microfmixers provide a very efficient and controlled mixing between the polymer solvent and non-solvent, and the different geometries available allow adapting the NPs size and production rates to the needs of the formulator. For each flow pattern, practical examples reported in literature were presented in the Figure 1 of each section. It is noteworthy that other many other microfluidic systems instantiated based on the same principles exists, but since not applied for nanoprecipitation they were not described here.

Many tailored microfluidic systems operating under different fluidic principles were developed to prepare NPs. However, in many cases, researchers are mostly interested in the applications of NPs for drug delivery and diagnostics. Although mixing by microfluidic systems have been

reviewed in many papers [22, 28], it is somehow difficult for a non-microfluidic expert to select the right microfluidic platform for a given application without the help of dedicated expertise. To that extent, the present paper aims at presenting and comparing the most recent microfluidic research trends as well as the different basic fluidic principles. Thus this review proposes to give non-microfluidic experts a guide to choose the most adequate microfluidic platform to synthesize their own NPs.

2.1.2 Theoretical considerations of nanoprecipitation and advantages of microfluidic systems

The literature reviews two theories which may explain the formation of polymeric NPs by nanoprecipitation[6]: a dispersion mechanism such as the spinodal decomposition which is classified as a 'mechanical mechanism' and the classical nucleation and growth mechanism. In the 'mechanical' process, the solvent solution is broken into small chunks of fluids which are dispersed into the non-solvent solution. [29-32]. On the opposite, in the nucleation and growth process, nuclei are first produced when the polymer reaches a supersaturation state due to the solvent diffusion into the non-solvent solution. Then the nuclei grow by molecular deposition of polymer chains at their surface.[33-35]. However, both mechanisms require an efficient mixing between the polymer and non-solvent solutions. In case of nucleation and growth process, which is the process likely to be encountered with microfluidic systems, the faster the mixing, the smaller are the NPs.

Compared with conventional nanoprecipitation batch methods, advantages of microfluidic system lay in their excellent ability to manipulate nanoliter flows. Microfluidic systems such as micromixers can drastically reduce the mixing path of solvent and non-solvent down to few tens of micrometers, resulting in a very fast mixing achieved by diffusion within few milliseconds down to microseconds [26]. Thus, due to this fast and efficient mixing, different physicochemical properties of NPs can be obtained by controlling the ratio of flow rates of the non-solvent to the solvent solution or by changing the configuration of the micromixer. It usually results in the production of smaller particles compared to conventional methods [36, 37]. In addition, microfluidic systems are usually operated in continuous flow which supports the potential of NPs production at large scale. Another advantage of continuous production is the possibility to maintain over time the same quality of the product, a much important feature for the pharmaceutical industry. Finally, the laminar flow observed most of the time in microfluidic system ensures predictable and reproducible mixing conditions across fluidic interfaces [38].

Microfluidic systems exhibit thus many advantages but still face some challenges: their relatively low productivity due to their small internal volume and low flow rates, and finally the possibility of system blocking by solid particles accumulation.

2.1.3 The different working principles of micromixers

2.1.3.1 Molecular diffusion and kinetic energy

Molecular diffusion is to be found in channel-based micromixers. In such systems, the solvent and non-solvent are split into thin staggered lamellas owing to microchannels. Nanoprecipitation was simply driven by the molecular diffusion of solvent into the non-solvent lamellas. Depending on the lamellas width (i.e. microchannel width, typically around 30 µm), the diffusion and thus the nanoprecipitation can be achieved within few milliseconds. Ultimately, NPs are collected at the outlet channel (**Fig. 1 (c)**). Such micromixers are called interdigital multilamination micromixers and are commercially available from different suppliers. They allow the production of polymeric NPs with tunable sizes and narrow size distributions simply by adjusting the ratio of the flow rates of the non-solvent to the solvent solution and the microchannel width. The higher the former or the smaller the later, the smaller are the NPs.

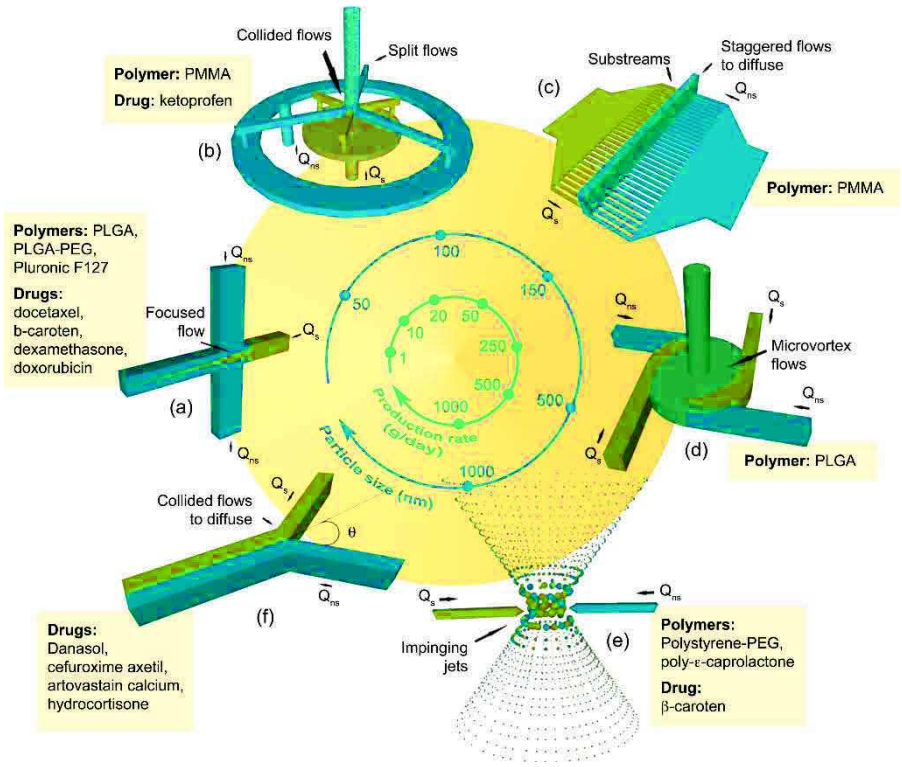

Figure 1. Overview illustration of NPs synthesized by mainly microfluidic systems (a) Schematic diagram of a hydrodynamic flow focusing micromixer. (b) Schematic diagram of combination kinetic energy and molecular diffusion. (c) Schematic diagram of achieving molecular diffusion by microchannels. (d) Schematic diagram of multi-inlet vortex mixer. (e) Schematic diagram of a confined impinging jets micromixer. (f) Schematic diagram of introducing kinetic energy by collided flows. Qns and Qs represent the non-solvent and solvent flows respectively.

By employing a high pressure interdigital multilamination micromixer (HPIMM, IMM) of 20 µm microchannels width (Fig. 2(a)), Bally et al. [39] succeeded to prepare poly(methyl methacrylate) (PMMA) NPs down to 100 ± 16 µm in size at a flow rate ratio equal to 10 and for a 1 wt.% polymer solution flowing at 0.8 mL/min. It is observed that the batch process consisting in slowly pouring dropwise the polymer solution in a stirred volume of non-solvent does not allow making variation of the NPs size and always produces bigger particles (245 ± 38 nm) than the interdigital multilamination micromixer. Moreover the batch process produces large aggregates when the polymer concentration is higher than 1 wt.% while the microfluidic process allows handling polymer solutions with a concentration up to 5 wt.% [40].

Other micromixers rely on high energy to promote an efficient mixing. Such microfluidic systems have been designed to promote and intensive shear rate as the effective driving force for mixing [41] when the non-solvent and solvent flows at high velocities in large microchannels. Squared-shape Y-type micromixers, with inlet and outlet dimensions of 300-500 µm and 300-800 µm respectively, are ones of the simplest kind of such micromixers (Fig. 1 (f)). The mixing efficiency can be controlled by the ratio of non-solvent and solvent flow rates as well as by varying the inlet angle θ.

Chen's group [42-44] used a Y-type micromixer to synthesize pure drug NPs, i.e. without polymer. The operating parameters were studied to obtain optimum results, including the ratio of flow rates and composition of the drug solution (Fig. 2(b)). Thus danazol NPs were synthesized in order to improve their dissolving rate for better bioavailability [42]. No surfactant was used to avoid hampering the crystal growing. By varying the ratio of drug and non-solvent solutions flow rates and temperatures, authors found that the supersaturation influences greatly the physicochemical properties of dazazol NPs. As such, they observed a rapid decrease in NPs size resulting in 100 % drug dissolution within 5 min, whereas only 35 % of raw danazol was obtained in same conditions. In a second paper, authors prepared amorphous cefuroxime axetil (CFA) NPs and found that the Y-shape micromixer allows to get NPs that hve also a higher dissolution rate [43]. These results proved that the microfluidic system has the ability to produce not only crystalline NPs but also amorphous ones. They compared the commercial CFA obtained by spray-drying (30~50 µm in size with large size distribution) and the microfluidic NPs they produced (300 nm in size and monodisperse) and highlighted the advantage of relying on a microfluidic system.

On the other hand, Ali et al. [45, 46] reported the formulation of hydrocortisone (HC) NPs, a practically water insoluble glucocorticoid drug, synthesized with a similar Y-shape micromixer coupled with a tangential flow filtration system, in order to concentrate the NPs suspension (Fig. 2 (c)). The different process parameters and microfluidic system configuration were studied. They found that almost similar results (around 300 nm) were obtained between the wet milling and microfluidic methods [46]. However with the later, NPs were prepared with less energy than with the former. In addition, the NPs synthesized with the microfluidic system presented amorphous state as seen by X-ray powder diffraction patterns (XRPD) and differential scanning calorimetric (DSC) compared to the crystalline NPs produced by the

wet milling method. NPs prepared by both methods presented a longer sustain release time (8~9 h) compared with the 4~5h of commercially available HC powder.

Ultimately it turned out that Y-shape micromixers do not have the ability to control the NPs size as easily as the HPIMM micromixer. They are indeed lacking the benefit of molecular diffusion over a short path like in interdigital multilamination micromixers. Therefore combination of molecular diffusion and high energy seems the best approach for high productivity and low NPs sizes. Such combination was brought by the K-M impact jet micromixer introduced by Mae and coworkers [47, 48]. The structure consists of three steel plates, namely the inlet, mixing and outlet plates. The two inlet fluids are first split into multiple flows (3 or 5) thanks to microchannels having a typical width of 150 µm. The resulting flows then converge to a single pin hole of typical 300 µm diameter where they are mixed as a result of their frontal collision. Finally the resulting mixture flows in the outlet microchannel of the last plate (**Fig. 1 (b)**).

In such micromixer, mixing by molecular diffusion plays an equivalent role as compared to the kinetic energy mixing [48]. This type of micromixer was first used to produce fine pigment NPs [49] but was also employed for the preparation of ketoprofen loaded PMMA NPs. [37] The NPs sizes were controlled between 100 and 150 nm and NPs size distribution was quite narrow (with a polydispersity index (PDI) less than 0.2 as seen by DLS, Zetasizer ZS 90, Malvern). The PDI is a mathematical definition accounting for the relative error between curve fit and experimental values. The PDI discloses the quality of the dispersion, from values lower than 0.2 for suitable measurements and good-quality of the colloidal suspensions, to values close to 1 for poor-quality samples, which in other words either do not present droplets sizes in the colloidal range, or exhibit a very high polydispersity. Drug loaded NPs showed controllable sustain release properties simply by varying the ratio of the non-solvent flow rate to the solvent solution flow rate. Encapsulation efficiency was controlled from 20 % to 50 % (**Fig. 2 (d)**).

2.1.3.1Hydrodynamic Flow Focusing

If the reduction of microchannel width is an efficient strategy to speed up the mixing, it has also some limitation imposed by microfabrication techniques. The hydrodynamic flow focusing (HFF) or sheath flow is another method to reduce the diffusion path but has virtually no limitation. Micromixers based on HFF are widely used to prepare NPs or hybrid NPs by nanoprecipitation [27, 38]. A typical HFF micromixer comprises four microchannels, with possibly different dimensions (**Table 1**), and always operates in laminar flow regime. The solvent solution is flowing through the main inlet channel and squeezed by two side flows of the non-solvent solution (**Fig. 1 (a)**). As a result, the solvent undergoes a strong hydrodynamic flow focusing effect that reduces its width virtually down to 0.1 µm as observed by Knight et al. [26]: a value much smaller than the typical 100 µm or 30 µm promoted in Y-type or interdigital multilamination micromixers respectively [45]. This results in a better control of the NPs characteristics like smaller size and

narrow size distribution. Note that the flow focusing extent can be controlled by the ratio of the flow rates of main inlet flow to the side flows.

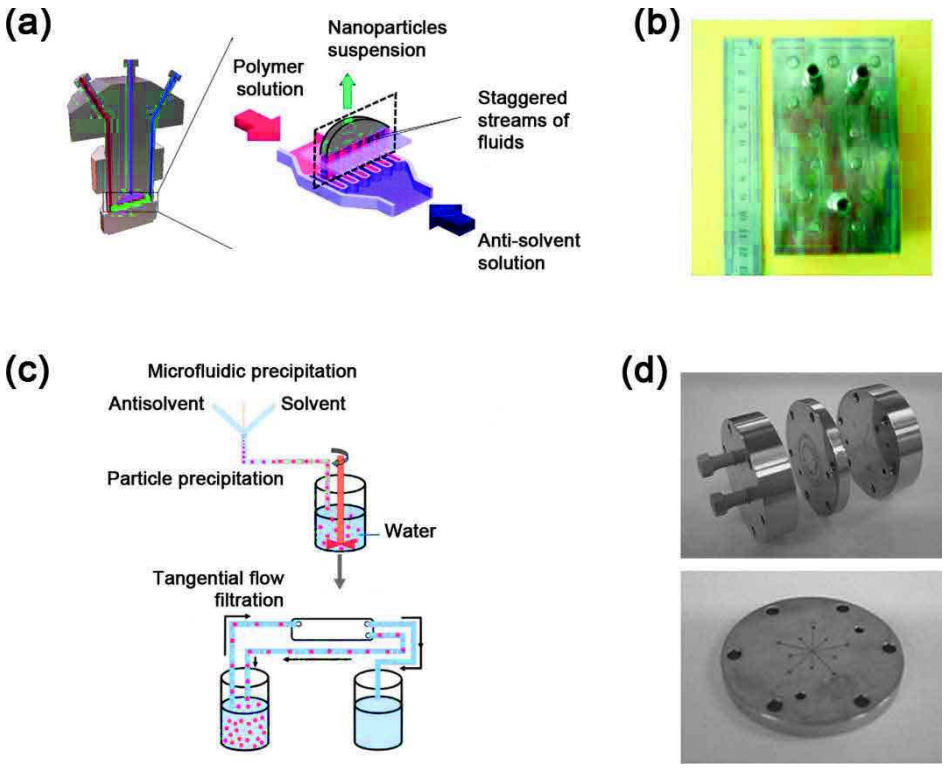

Figure 2. Microfluidic setups based on molecular diffusion and kinetic energy (a) HPIMM micromixer used by Bally et al. [39], (b) Y-type micromixer used by Chen's group. [43], (c) Y-type micromixer coupled with tangential flow filtration system designed by Ali et al. [45], (d) K-M micromixer used by Nicolas et al. [37].

The HFF mixing principle was first introduced by Knight et al. in 1998 [26] and then adapted in 2008 [27] for the production of amphiphilic poly(lactic-co-glycolic acid)-b-poly(ethylene glycol) (PLGA-PEG) NPs, for which acetonitrile served as the polymer solvent (**Fig. 3 (a)**). When PLGA was added to the final PLGA-PEG polymer, the microfluidic system showed a better control on the NPs size compared to the batch process. Indeed, for the HFF technology, the size increased from 24 nm to only 34 nm when the PLGA weight content was increased from 0 to 20 wt%, whereas for the batch method, the NPs size increased from 30 to 105 nm.

Interestingly, when Karnik et al. [27] admixed the polymer solution with a model drug (docetaxel, Dtxl) to get drug-loaded PLGA-PEG NPs, drug encapsulation efficiency was increased from 20 wt% to 50 wt% compared with the batch method. They also found that the final NPs size increased when Dxtl was added to the polymer solution. Thus authors investigated the water/acetonitrile ratio (so-called cloud point) at which polymer precipitated by gradually adding water to a solution of polymer with or without Dtxl in acetonitrile. Polymer alone was observed to precipitate for a water/acetonitrile ratio of 25% v/v, the presence of Dtxl shifted this

value up to 45 % v/v. It indicates that Dtxl starts precipitating after the polymer. Hence a rapid mixing may actually yield to slightly lower drug encapsulation efficiencies as some drug may be "locked out" of the NPs that have already been formed before the drug starts to precipitate. Capretto et al. [38] proposed an Y-type HFF setup that was used to prepare β-carotene loaded Pluronic F127 copolymer NPs by nanoprecipitation using THF solution and water as solvent and non-solvent respectively (**Fig. 3 (b)**). When only Pluronic F127 was used, a mean NPs diameter of 130 nm was obtained. When β-carotene was used alone, it was found that β-carotene precipitated immediately due to its higher hydrophobicity. As a result, aggregation of big particles completely blocked microchannel. When both β-carotene and copolymer composed the solvent solution, obtained NPs showed a much smaller size, of around 70 nm. Thus the two previous papers [27, 38] have clearly demonstrated that the composition of polymer solution has a significant influence on final NPs size as well as the superiority of the microfluidic approach compared to its batch counterpart, in terms of potential to control the NPs size. Palocci's group. [50] to propose a novel HFF microfluidic device by assembling commercial stainless steel micro-capillary tubes with cross junctions (**Fig. 3 (c)**). Dexamethasone was used to get drug-loaded PLGA NPs (35 to 350 nm). Encapsulation efficiency was found to reach values up to 93 %, whereas by batch method encapsulation efficiency reached a ceiling value of only 60 %.

To increase the throughput production of HFF micromixers, Kang et al. [51] conceived a three-layer poly(dimethyl siloxane) (PDMS) micromixer comprising 100 parallel flow focusing microchannels (**Fig. 3 (d)**). The parallel flow focusing micromixer was then adopted to prepare NPs, similarly using PLGA-PEG amphiphilic polymer. The results indicated the device was quite robust in producing reproducibly highly monodisperse NPs regardless the molecular weight of both copolymers and their weight content compared to the batch method. Lim et al. [52] reported the same structure to synthesis NPs. According to the results of Kang et al. [51], monodisperse NPs obtained from high molecular weight polymers were difficult to prepared by batch method due to uncontrollable mixing process resulting in NPs aggregation. Thus in order to use higher molecular weight polymers and to increase the polymer weight content in solvent solution as well as to avoid unexpected clogging, a 3D flow focusing geometry was developed by Rhee et al. [53, 54] (**Fig. 3 (e)**). This 3D HFF micromixer was successfully used for the production of NPs from $PLGA_{95K}$-PEG_{5K} having a high molecular weight and introduced at a weight content up to 5% (w/v) in acetonitrile. Sun et al. [55] proposed another 3D HFF micromixer based on the original concept of "origami chip" and applied this new device to the production of doxorubicin loaded PLGA NPs. The resulting NPs sizes obtained with the flat system (i.e. 2D device) were compared to those produced with the double spiral and arc systems (**Fig. 3 (f)**). While the minimum size obtained with the former was 100 nm, in same condition of flow rates, the last two systems produced much more monodisperse NPs sizes around 70 nm which was attributed to the significant reduction in mixing time (from 29 s down to 15 s) as simulated by CFD. Encapsulation efficiency of Doxorubicin reached 50 wt%.

2.1.3.2 Turbulence

Turbulence-based micromixers were conceived to solve for the low throughput of the aforementioned micromixers. Thus Johnson and Prud'homme [56, 57] developed the first kind of turbulence-based micromixers. This confined impinging jets micromixer (CIJM) was such designed that the solvent and non-solvent solutions were injected into the inlets (diameter 1 mm or 2 mm) at high velocities (2.8 m/s, 2.6 m/s) to form jets, the two jets collided inside a chamber of small dimensions (diameter 5 mm), the product was collected at outlet (diameter 2 mm) (**Fig. 1 (e)**). As such an intensive mixing is achieved within few milliseconds which was demonstrated by CFD simulations and microscopic particle-image velocimetry (μPIV)[58]. This innovative CIJM system was used by several authors for the fabrication of block copolymer NPs containing organic actives[59, 60] and to investigate the influence of its dimensions [61] and operating parameters [35, 62] on the NPs size (**Fig. 4 (a)**). In brief, β-carotene loaded Polystryene (10 monomers)-block-poly(ethylene oxide)(68 monomers) NPs, Poly-ε-caprolactone NPs and doxorubicin loaded poly(methoxypolethyleneglycolcyanoacrylate-co-hexadecylcyanoacrylate) NPs were successfully prepared by such CIJM system. Two inlet channel dimensions (1 mm and 2 mm) were tested; smaller NPs sizes were obtained with the narrower inlet channel. Authors also found that any increase in both fluids flow rates (from 3 ml/min to 120 ml/min) induced a decrease in NPs size from 600 to 200 nm.

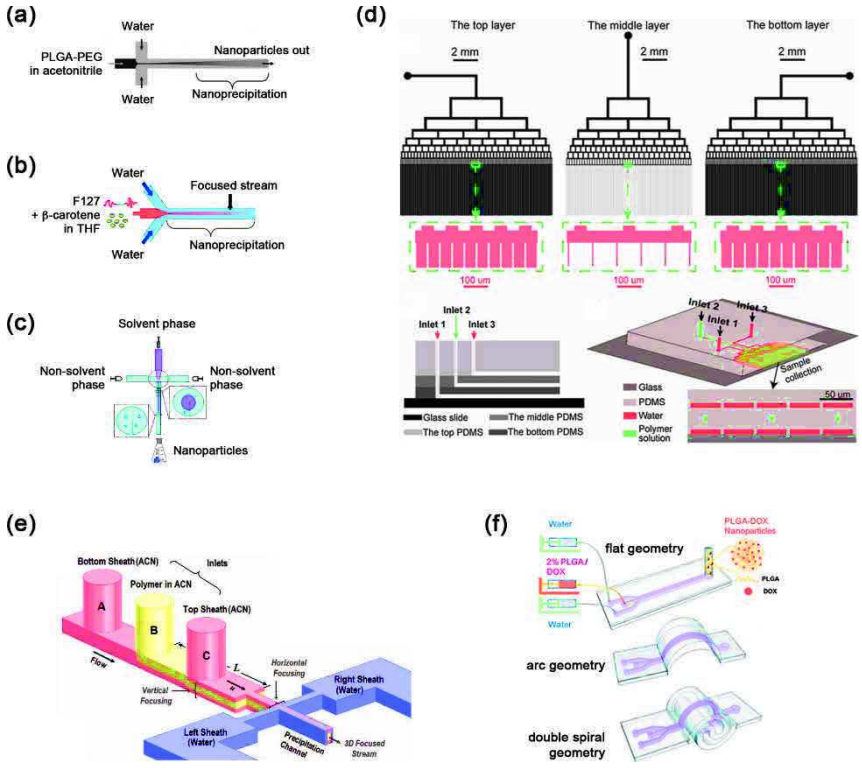

Figure 3. Different kinds of hydrodynamic flow focusing micromixer: (a) T-type flow focusing micromixer used by Karnik et al. [27], (b) Y-type flow focusing micromixer used by Capretto et al. [38], (c) flow focusing micromixer by assembling

commercial stainless steel micro-ca pillary tubes and cross junctions used by Palocci et al. [50], (d) Parallel flow focusing micro-mixer used by Kang et al. [51], (e) 3D flow focusing micromixer used by Rhee et al. [53], (f) 3D origami micromixer used by Sun et al. [55].

Fox's group [63] provided another example of turbulence-based micromixers by introducing the concept of on multi-inlet vortex mixer (MIVM) for flash nanoprecipitation (Fig. 1 (d)). This micromixer was designed to alleviate the limitation of the CIJM that requests equal flows of solvent and non-solvent streams to provide constant NPs properties. Authors investigated the flows inside the micromixer by microscopic particle image velocimetry (μPIV) and confocal microscopy. The results revealed that MIVM has the ability to perform a fast mixing promoted by turbulence obtained at high Reynolds numbers[64-68]. The potential of MIVM on encapsulating drug was successfully verified by the synthesis of lipid-polymer hybrid (LPH) NPs by Zhang and coworker [69] (Fig. 4 (b)). LPH NPs take advantage of the unique strengths of polymeric NPs and liposomes. Authors thus succeeded to synthesize 80 nm PLGA NPs surrounded by a functionalized lipid poly(ethylene glycol) 2000 (lipid-PEG) shell thanks to the MIVM platform. Recently a mesoscale version of the MIVM was developed, 16 times bigger than the microscale version aforementioned [70].

Eventually, turbulence was combined with other working principles to increase the productivity and reach much higher production rates than single working principle microfluidic devices such as HFF micromixers for instance. Thus Langer and coworkers [71] designed a microfluidic chip based on the HFF micromixer but incorporating microvortices in the precipitation region (Fig. 4 (c)). As a consequence, same LPH NPs as investigated by Zhang and coworker [69] were produced at a rate up to 0.3g/h with sizes ranging from 30 to 170 nm while preventing any clogging owing to the focusing flow. Interestingly, at the polymer/lipid weight ratio of 10 %, NPs size decreased from 93 to 55 nm with increased Reynolds number. Another example of combined working principles micromixer was reported by Karnik and coworkers [72] to increase the productivity by introducing turbulence and HFF technology (Fig. 4 (d)). Different types of NPs were synthesized such as: PLGA-PEG, polystyrene and iron oxide NPs. Different drugs were similarly encapsulated in these NPs such as: docetaxel and insulin. The results not only showed that the NPs size (around 50 nm) synthesized with such micromixer was significantly smaller than that prepared by conventional method (120.9 ± 6.9 nm) [73], but that the encapsulation loading (~ 2 wt.%) was higher than one obtained by batch method (~ 1 wt.%). Furthermore, the production rate achieved was 2.19 g/min, which is equivalent to 3.15 kg/d and 1.15 ton/yr.

2.1.3.1Other principles

Due to the limitations of microchannel-based devices that are easily clogged or plugged during processing, specialized materials and fabrication procedures are required [74]. Accordingly, many researchers attempted to simplify the fabrication of microfluidic devices. To this end, Xie et al. proposed a shear microfluidic setup for generating PLGA NPs (140 to 500 nm in size) that only

comprised general laboratory equipment like a 30-gauge needle (inlet channel) and a plastic tubing (dispersing channel). This example shows that conventional lab instruments can be simply adapted for the synthesis of polymeric NPs, however the polymer solution flow rate was quite low and fixed at 3.2 µL/min (Fig. 5 (a)).

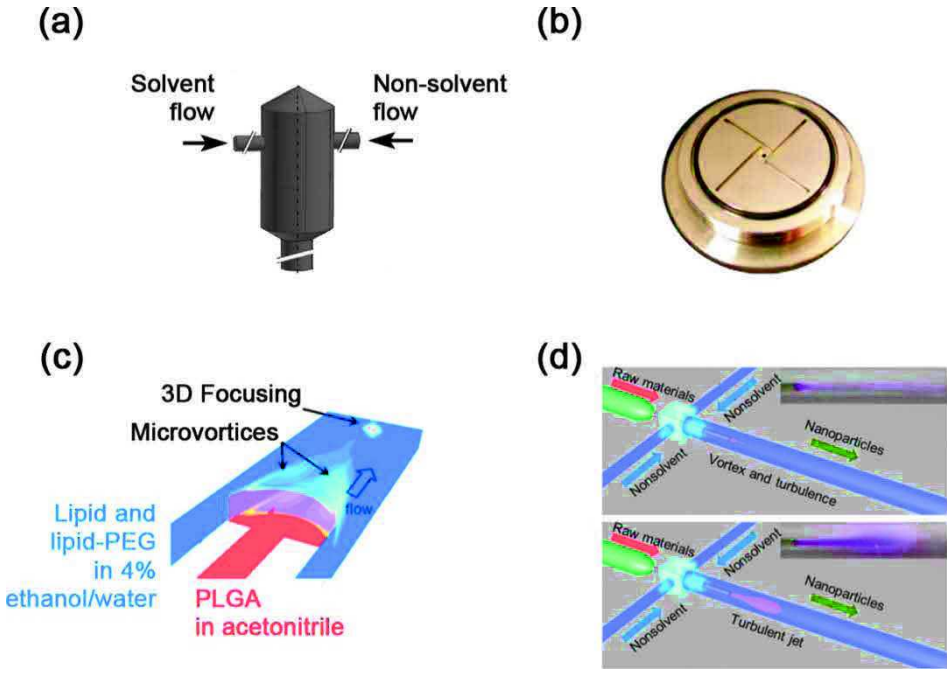

Figure 4. Different kinds of turbulence-based micromixers: (a) Confined impinging-jets reactor used by Lince et al. [62], (b) Multi-inlet vortex micro-mixer used by Fox and coll. [67], (c) The micromixer combined micro-vortices and 3D focusing used by Robert Langer et al. [71], (d) The micromixer combined jet flows and flow focusing used by Karnik et al. [72].

NPs were also synthesized by a microfluidic device whose working principle is based on the so-called chaotic advection which enables enhancement of mixing in laminar regime [24]. An example is the so-called Tesla mixer [75] which operates by continuously stretching and refolding volumes of the two fluids to be mixed. This micromixer can be integrated with a flow focusing section to improve even more the mixing performance [76] (Fig. 5 (b)). LPH hybrid NPs composed of a PLGA core surrounded by lecithin/DSPE-PEG shell were synthesized with such microfluidic system. The influence of mixing on self-assembly of hybrid NPs was studied by two methods, the slow mixing achieved by pipetting the solvent solution into a solution of water or PBS without sonication or heating and the rapid mixing achieved by the microfluidic system. For the case of slow mixing, a small fraction of the lipid-PEG was deposited on the surface NPs while the rest just formed a lipid phase in the resulting mixture. In contrast, uniform lipid-PEG coverage around PLGA core resulted in the formation of homogeneous LPH NPs under rapid mixing. To demonstrate the versatility of the microfluidic platform, authors successfully produced hybrid quantum dot NPs with an average size of 60 nm. On the other hand, instead of

using this chaotic micromixer for mixing the polymer and non-solvent solutions, it can also be used to mix the precursors of the solvent solution prior to the final mixing with the non-solvent (Fig. 5 (c)) [77]. Such a system allows a fast screening of the respective role of the different components in the formulation. Another example includes a rotating tubing [36], that allows to reach a high surface to volume ratio (Fig. 5 (d)) but at the expend of high raw energy. Consequently non-solvent and solvent undergo very intense and rapid mixing along the tube. As a result, the nanoprecipitation was implemented at a high throughput. Authors succeeded to produce pure meloxicam crystalline NPs with sizes decreasing down to 20 nm when increasing the tube rotational speed up to 1500 rpm. When coated with a polymer (poloxamer 188), 30 nm drug-loaded NPs exhibited different encapsulation efficiencies depending on the polymer concentration: from 57.6% to 97.6% for poloxamer concentrations of 0.15% and 2% respectively. Furthermore the drug dissolution rate after 10 min varied from 60% to 90% for uncoated and coated drug NPs obtained with a 2% poloxamer concentration compared to 10% and 20% for the batch respectively. In an attempt to reach throughput close to industrial levels, Douroumis and Fahr [78] and later on Dong et al. [79] developed two processes relying on a static mixer (Fig. 5 (e)) in order to produce NPs of poorly water-soluble drugs (Table 1).

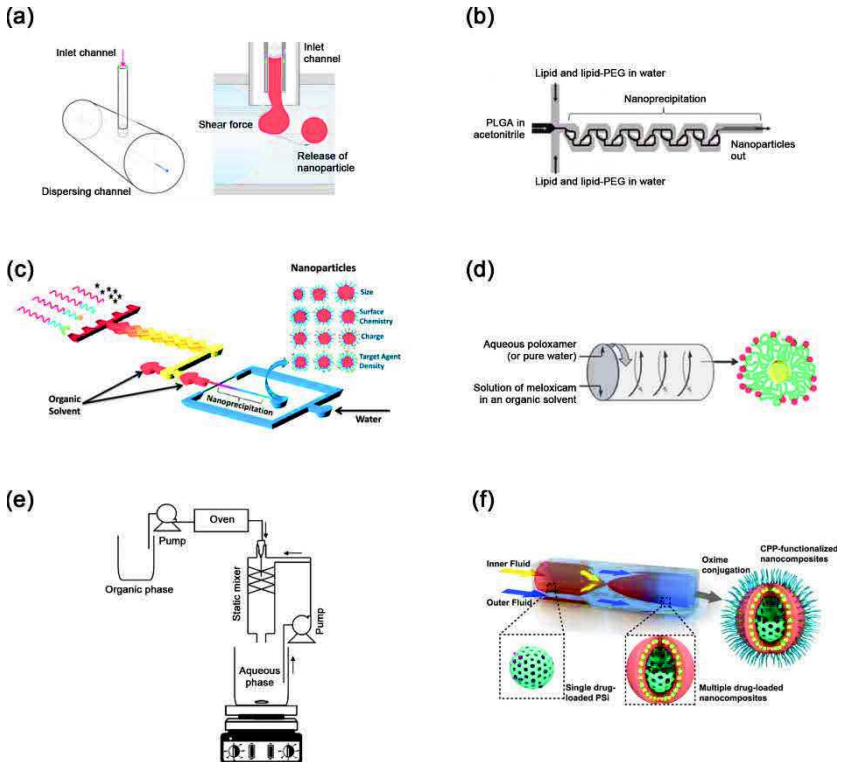

Figure 5. Microfluidic devices based on other principles: (a) Hydrodynamic force micromixer used by Xie et al. [81], (b) micromixer combining flow focusing and tesla structures used by Karnik et al. [76], (c) micromixer system combining flow focusing and multi-inlet structure used by by Karnik et al. [77], (d) Microfluidic system based on the intensification process used by Colin et al. [36] (e) Microfluidic system based on static mixer used by Douroumis et al. [78] (f) microfluidic system based on co-flow focusing used by Dongfei et al. [80]

They succeeded to operate their setup at an overall flow rate between 1.0 and 3.0 L/min. However the produced NPs had sizes not lower than 500 nm. Finally Dongfei et al. [80] reported a microfluidic co-flow focusing platform allowing the synthesis of complex nanostructures such as core-shell NPs (Fig. 5 (f)).

2.1.4 Quality or productivity, is it a trade-off problem?

The overview we disclosed showed that the choice of a microfluidic device to produce pure drug or drug-loaded polymeric NPs seems to be a matter of trade-off between size/quality and productivity. Table 1 presents a global summary comparing, by working principle, all fluidic setups, ranges of NPs size and production rates.

It appears that systems only based on kinetic energy give bigger particles than all other types of devices of same group, likely due to the longer diffusion path. On the other hand, their advantage clearly lies in flow rates (*i.e.* productivity) much higher than the others, up to 80 mL/min for solvent solution. As for microchannel-based micromixers like for the HPIMM [39], they allow to produce the smallest particles sizes. However one cannot decrease the microchannels width to get even smaller NPs without increasing the pressure drop. Reducing the later can be achieved by lowering the flow rates of non-solvent and solvent solutions but in turn the productivity will be reduced. The best compromise for this group seems to be the K-M micromixers which combine molecular diffusion and high energy mixing. Indeed it has the potential for high throughput production of small polymeric NPs. Another benefit of the K-M micromixers is their robustness and easy handling [37].

When adopting HFF micromixers, the size of the particles is dramatically reduced (ranging from 10 to 300 nm) but the productivity is sensitively much lower (from 0.3 µL/min to 0.5 mL/min for the solvent solution). However HFF micromixers can be largely suitable for a fast screening as they can be readily, prototyped like high energy T-type micromixers [23, 81].

The real potential for increasing the productivity comes with the introduction of turbulences. Solvent solution flow rate can thus be increased up to 40 mL/min while the NPs size remains quite small and well controlled (50 – 300 nm).

As for the micromixers working on other principles, they do not decrease the size of the NPs nor increase the productivity significantly but rather solve technical issues such as microchannel clogging or specific microfabrication problems.

Finally, to date, quality and productivity is still a problem of trade-off, currently intensively studied by many research groups.

2.1.5 Summary

Historically, nanoparticle carriers for therapy and diagnosis were developed after the first liposomal drug carrier was presented in 1973 [82]. Since then, there has been a constant and very intensive research activity in this field. One of the latest developments in the production of drug-loaded polymer nanoparticles begun with the advent of microfluidics when new microfabrication procedures allowed the production of microfluidic devices.

Indeed drug-loaded polymer nanoparticles can be effortless produced with the help of micromixers coupled to the so-called solvent displacement method, i.e. the nanoprecipitation of a polymer in solution which was possibly admixed with the desired drug. Nowdays there is a large variety of microfluidic devices, from the simplest ones using off-the-selves components to the most complex ones requiring multistep photolithographic procedures, that can address quite efficiently the inherent problem of size reproducibly and constant quality encountered with the conventional batch-type reactors [83]. Not to mention that microfluidic-engineered nanocarriers usually exhibit a higher drug encapsulation rate and promote a reproducible and better controlled drug release profile. Yet, microfluidic-assisted nanoprecipitation processes have major bottlenecks that still impede their further use. Though actual micromixer-assisted nanoprecipitaion processes satisfy the requirements for the production of pure drug or drug loaded polymeric NPs, they lack for some of them high throughput and high-quality NPs as well as the ability to produce at the same time libraries of NPs having different compositions.

For instance HFF micromixers meet the requirement for the rapid design of NPs of different compositions but at the cost of a rather low productivity. In contrast Y-type micromixers allow high productivity but are often associated to low-quality NPs. To that extent, jet and vortex micromixers seem to be the best compromise, but they can face microchannels clogging which will adversely affect the productivity on a long run. Finally, in the selection of the best microfluidic device for a given application, one has to keep in mind about the simplicity of the microfabrication and handling of the device (i.e. time of fabrication, cleaning issues etc.). Thus, at the moment, it seems that there is no ideal design that can meet the requirements of NPs size reproducibly and constant quality, high production rate and clogging free.

However computational fluid dynamics (CFD) has been routinely used to design micromixers in order to maximize the mixing efficiency [84-87] and on the other hand theoretical models of polymer nanoprecipitation have been developed successfully to account for the formation mechanism of polymer rnanoparticles [88, 89]. Therefore, it is foreseen that coupling both aforementioned approaches (CFD and theoretical models) would be the best strategy to numerically design this ideal micromixer. Such strategy has been scarcely reported in the literature [38, 90, 91] and is largely underused but has surely a great potential for significant advances in this field.

In conclusion, it is expected that micromixer-assisted nanoprecipitation processes will be in the future the focus of intensive academic an industrial researches because they are bearing the promise to rapidly produce libraries of drug-loaded nanocarriers for gene and drug delivery screening. Furthermore Dongfei et al. [80] opened a new route to the synthesis of multi-domain multi-drug loaded NPs whose peculiar morphology will most likely allow to investigate new release strategies, like synergetic or sequential releases of incompatible drugs as it has been demonstrated with polymeric microcarriers [92-94]

Table 1. Results from the microfluidic-assisted nanoprecipitation in literature for preparation of pure drug or polymeric drug loaded nanoparticles

Ref.	Size range of NPs	PDI	Solvent flow rate	Solvent	Polymer	Drug	Non-solvent	Stabilizer	NPs production rate (g/day)	Configuration of microfluidic system	Microfluidic system
Molecular diffusion and kinetic energy											
39	100 to 174 nm	< 0.3	0.2 to 1.5 mL/min	THF	Linear and branched PMMA (Mw for linear polymer molecular 7900 to 23000 g/mol, Mw for branched polymer 7900 and 7500 g/mol) Concentration in solvent: from 1 wt% to 5 wt%.	-	Water	Cremophor ELP. Concentration in solvent: 0.5 wt% / polymer.	7.88 to 106	Inlet: Squared -shaped 20 µm*20 µm. Outlet: Squared-shaped 60 µm*20 µm	HPMM commercial steels micromixer
42	360 nm to 55 µm (filtered by 0.45 µm)	n/a	4 to 80 mL/min	Ethanol	-	Saturated Danazol. Concentration in solvent: 2 % w/w.	Water	-	115.2 to 2304	Inlet: Squared-shaped 300 µm*300 µm. Outlet: Squared-shaped 600 µm*300 µm	Y-type steels micromixer
43	250 to 1100 nm (filtered by 0.22 µm)	n/a	2 to 16 mL/min	Acetone	-	Cefuroxime axetil. Concentration in solvent: 3 wt% to 7 wt%.	Isopropyl ether	-	86.4 to 1612.8	Inlet: Squared -shaped 400 µm*500 µm Outlet: Squared -shapedl 800 µm*500 µm	Y-type steels micromixer
44	210 to 2500 nm	n/a	2 to 16 mL/min	Methenol	-	Atorvastain calcium. Concentration in solvent: 3 wt% to 6 wt%.	Isopropanol	-	86.4 to 1382.4	Inlet: Squared -shaped 400 µm*500 µm Outlet: Squared -shapedl 800 µm*500 µm	Y-type steels micromixer
46	300 nm	0,18	1 mL/min	Ethanol	-	Hydrocortisone. Concentration in solvent: 1,25 wt%.	Water	Kollidon 30 PVP 0.2 % w/v, Hydroxypropylmethylcellulose HPMC (6 cP) 0.5 % w/v, Tween 80 0.1 % w/v in non-solvent.	18	Cylinder, Diameter 500 µm, inlet angle 10 °	Y type commercial chip
45	80 to 500 nm	0,21	0.25 to 1.5 mL/min	Ethanol	-	Hydrocortisone. Concentration in solvent: 1,25 wt%.	Water	Kollidon 30 PVP 0.2 % w/v, Hydroxypropylmethylcellulose HPMC (3.5- 6.5 cP) 0.5 % w/v, Sodium lauryl sulphate SLS 0.05 % w/v in non-solvent	3.6 to 21.6	Cylinder, Diameter 100, 500, 1000 µm, inlet angle 10, 75, 50 °	Y type commercial chip
37	100 to 150 nm	< 0.2	1 mL/min	THF	PMMA 15200 g/mol. Concentration in solvent: 1 wt%.	Ketoprofen (0.5 wt %/polymer)	Water	Cremophor ELP. Concentration in solvent: 0.5 wt% / polymer.	21.6	Inlet: Squared -shaped 150 µm*150 µm Outlet: Cylinder, Diameter 300 µm	K-M steels micromixer
Hydrodynamic Flow Focusing (HFF)											
82	70 to 80 nm	n/a	0.3 to 10 µL/min	Acetonitrile	PLGA15k-PEG3.4k. Concentration in solvent: 5 wt%.	Docetaxel. Concentration in solvent: 0.5 % w/v.	Water	-	0.00276 to 0.092	Squared -shaped 20 µm wide, 60 µm high	T-type HFF chip fabricated by standard micromolding process
38	100 to 200 nm	n/a	0.04 mL/min	THF	Pluronic F127 (Mw 12600 g/mol).Concentration in solvent: from 1.26 % w/v to 15.75 % w/v.	E-carotene. Concentration in solvent: from 0.063 % w/v to 1.57 % w/v.	Water	-	0.72 to 9.072	Squared -shaped 50 µm wide, 150 µm high	Y-type HFF chip by a photolithography/wet etching process
50	35 to 350 nm	low polydispersity	1 to 500 µL/min	Acetonitrile	PLGA 50 Kda. Concentration in solvent: 0.2 % w/v.	Dexamethasone. Concentration in solvent: 0.025 % w/v.	Water	-	0.00288 to 1.44	Cylinder, Diameter from 150 to 600 µm	T-type HFF assembled by a steels micro-capillary tubes
53	20 to 200 nm	n/a	5 µL/min	Acetonitrile	PLGA-PEG (PLGA27K-PEG5K, PLGA45K-PEG5K and PLGA95K-PEG5K). Concentration in solvent: 1 % , 3 % and 5 % w/v.	-	Water	-	0.072 to 0.36	Cylinder, Diameter from 100 and 200 µm	3D HFF realized by 2D conventional HFF chip process
51	50 to 200 nm	n/a	0.5 to 2 mL/h	Acetonitrile	PLGA-PEG (PLGA27K-PEG5K, PLGA55K-PEG5K and PLGA95K-PEG5K). Concentration in solvent: 1 % , 3 % and 5 % w/v.	-	Water	-	0.12 to 2.4	One inlet flow was divided into 100 substreams (the middle layer)/240 (top and bottom layers) tributary channels. 5 µm width 6 µm height of channels for polymer solution 45 µm width 7 µm height of channels for water solution	Multichannels HFF chip fabricated by soft lithographic technique
55	70 to 230 nm	< 0.13	0.3 to 2.5 mL/min	Mixture of dimethylformamide and trifluoroethanol	PLGA. Concentration in solvent: around 2 wt %.	Doxorubicin (0.6 wt%/polymer)	Water	Tween 20. Concentration in non-solvent: 0.1 % w/v.	8.64 to 72	Serrated -shaped 300 µm wide, 300 µm high	3D origami chip by bonding two polydimethylsiloxane layers after oxygen plasma
Turbulence											
59	60 to 1000 nm	n/a	n/a	THF	Polystyrene (10 monomers)-block-poly(ethylene oxide(68 monomers). Concentration in solvent: 0.32 wt% or 2.6 wt% (included drug).	E-carotene (from 0.063 % w/v to 1.57 % w/v)	Water		n/a	n/a	CIJM micromixer fabricated by microdrilling
62	200 to 600 nm	n/a	3 to 120 mL/min	Acetone	Poly-e-caprolactone. Concentration in solvent: 0.5 wt% (Mw 14000 g/mol) and 0.15 wt% (Mw 80000).	-	Water	-	6.48 to 864	Inlet channels diameter: 1 and 2 mm (Two inlet jets per fluid). Cylindrical chamber of 5mm of internal diameter. Outlet channel diameter: 2 mm	CIJM micromixer fabricated by microdrilling
69	100 to 200 nm	n/a	1 to 25 mL/min	Acetonitrile	PLGA (inherent viscosity ~ 0.82 dL/g). Concentration in solvent: 0.1, 0.25, 0.5 and 1 % w/v.	-	Aqueous solution containing 4 wt% ethanol	1,2-Distearoyl-sn-glycero-3-phosphoethanolamine-N-carboxy poly(ethylene glycol) 2000 (DSPE-PEG) 0.01 % w/v and L-a-phosphatidylcholine 0.025 % w/v in non-solvent.	1.44 to 360	Inlet channels: 1.1 mm width. Reaction chamber: 6mm diameter. Outlet channel: 1.3 mm diameter	MIVM steels micromixer
71	30 to 170 nm	n/a	0.2 to 1 mL/min	Acetonitrile	PLGA: Concentration in solvent: 0.1% or 0.5 % w/v.	-	Aqueous solution containing 4 wt% ethanol	Lecithin and DSPE-PEG (The molar ratio of lecithin to DPSE-PEG 7:3) PLGA-lipid : 5, 10, 25, 50, 100 wt%. in non-solvent	0.28 to 7.2	n/a	Micromixer based on the micro-vortices
72	50 to 100 nm	n/a	20 to 40 mL/min	Acetonitrile	PLGA-PEGa (concentration in solvent:1 % w/v), Polystyrene, siRNA-polyelectrolyte (polyethylenimine PEI25k, Branched) and Polyplex	Docetaxel, insulin (concentration none available)	Water	-	288 to 576	Needle 23G for jet, outer diameter:0.6414 mm, inner diameter:0.337 mm	Coaxial turbulent jet mixer fabricated by off-the-shelf components
Other principles											
75	140 to 500nm	n/a	5.2 µl/min	Acetonitrile	PLGA (Resomar RG502). Concentration in solvent: 1 % , 4 % w/v.	-	Water	PVA. Concentration in non-solvent: 1 % w/v (87 % - 89 % Hydrolyzed)	0.0921 to 0.23	Needle 30G: inner diameter: 0.11 mm. Tygon tubing for dispersing phase. The needle was inserted in the interior at 50 % of tubing diameter.	Fluidic Nanoprecipitation System assembled by general lab equipment
77	35 to 180 nm	n/a	5 to 10 µL/min	Acetonitrile THF	PLGA (inherent viscosity 0.82 dL/g). Concentration in solvent: 0.1% w/v. Quantum dot. Concentration in solvent: 0.05 % w/v.	-	Aqueous solution containing 4 wt% ethanol	Lecithin and DSPE-PEG (0.01 % to 0.001 % w/v, lecithin/DSPE-PEG, 6.4:1.6 by mol) in non-solvent.	0.0072 to 0.0144	Mixing channel: 50 µm wide, 60 µm high	The micromixer combined HFF with Tesla structure
36	30 to 180 nm	>0.2	18 mL/min	Benzyl alcoho.	Pulvaraner 188. Concentration in solvent: 0.15, 1 and 2 % w/v.	Meloxicam. Concentration in solvent: 0.2 % w/v.	Water	-	38.88 to 518.4	Rotating tube: hollow thin walled cylinder 6cm diameter and 30 cm length	Intensified micromixer based on a rotating surface
79	1 to 4 µm	n/a	50 mL/min	Two different solvents tested: ethyl alcohol, acetone	-	Many different drugs tested: Progesterone (PRG), E-Methasone valerate 17 (BMZ), Carbamazepine (CBZ), Oxcarbazepine (OXC)	Aqueous solution of hydroxypropylmethycellulose (Menilose 90SH-100, HPMC 60 SH-50) (concentration non available)	Lutrol F127. BPS-5. Lipoid S75 in non-solvent (concentration on available)	n/a	Static mixer: 10-30 mixing elements. Each elements: 3.2 mm diameter, 3.2 mm length. Offset 90 ° each other	The systems developed from a commercial static mixer

2.1.6 References

1. Gelperina S, Kisich K, Iseman MD et al. The potential advantages of nanoparticle drug delivery systems in chemotherapy of tuberculosis. American journal of respiratory and critical care medicine. 2005;172:1487-90.
2. Labhasetwar V, Song C, Levy RJ. Nanoparticle drug delivery system for restenosis. Advanced Drug Delivery Reviews. 1997;24:63-85.
3. Mohanraj VJ, Chen Y. Nanoparticles – A Review. Tropical Journal of Pharmaceutical Research. 2006;5:561-73.
4. Vila A, Sanchez A, Tobio M et al. Design of biodegradable particles for protein delivery. Journal of Controlled Release. 2002;78 15-24.
5. Mu L, Feng SS. A novel controlled release formulation for the anticancer drug paclitaxel (Taxol): PLGA nanoparticles containing vitamin E TPGS. Journal of Controlled Release. 2003;86:33-48.
6. Mora-Huertas CE,Fessi H, Elaissari A. Polymer-based nanocapsules for drug delivery. International journal of pharmaceutics. 2010;385:113-42.
7. Singh R, Lillard Jr JW. Nanoparticle-based targeted drug delivery. Experimental and molecular pathology. 2009;86:215-23.
8. Scholes PD, Coombesa AGA, Illurn L et al. The preparation of sub-200 nm poly (lactide-co-glycolide) microspheres for site-specific drug delivery. Journal of Controlled Release. 1993;25:145-53.
9. Allémann E, Gurny R, Doelker E. Preparation of aqueous polymeric nanodispersions by a reversible salting-out process: influence of process parameters on particle size. International journal of pharmaceutics. 1992;87:247-53.
10. Quintanar-Guerrero D, Ganem-Quintanar A, Allémann E et al. Influence of the stabilizer coating layer on the purification and freeze-drying of poly(D, L-lactic acid) nanoparticles prepared by an emulsion-diffusion technique. Journal of Microencapsulation. 1998;15:107-19.
11. Tom JW, Debenedetti PG. Particle formation with supercritical fluids- a review. Journal of Aerosol Science. 1991;22:555-84.
12. Couvreur P, Kante B, Roland M et al. Polycyanoacrylate nanocapsules as potential lysosomotropic carriers: preparation, morphological and sorptive properties. Journal of Pharmacy and Pharmacology. 1979;31:331-2.
13. Fessi H, Puisieux F, Devissaguet JP et al. Nanocapsule formation by interfacial polymer deposition following solvent displacement. International journal of pharmaceutics. 1989;55:R1-4. (• Polymeric NPs was firstly synthesized by nanoprecipitation)
14. Govender T, Stolnik S, Garnett MC et al. PLGA nanoparticles prepared by nanoprecipitation: drug loading and release studies of a water soluble drug. Journal of Controlled Release. 1999;57:171-85.
15. Rao JP, Geckeler KE. Polymer nanoparticles: Preparation techniques and size-control parameters. Progress in Polymer Science. 2011;36:887-913.
16. Schubert S, Delaney JT Jr et al.. Nanoprecipitation and nanoformulation of polymers: from history to powerful possibilities beyond poly(lactic acid). Soft Matter. 2011;7:1581-8.
17. Barichello JM, Morishita M, Takayama K et al. Encapsulation of hydrophilic and lipophilic drugs in PLGA nanoparticles by the nanoprecipitation method. Drug development and industrial pharmacy. 1999;25:471-6.
18. Chorny M, Fishbein L, Danenberg HD et al. Lipophilic drug loaded nanospheres prepared by nanoprecipitation : effect of formulation variables on size , drug recovery and release kinetics. Journal of Controlled Release. 2002;83:389-400.
19. Legrand P, Lesieur S, Bochot A et al. Influence of polymer behaviour in organic solution on the production of polylactide nanoparticles by nanoprecipitation. International journal of pharmaceutics. 2007;344:33-43.
20. BilatiU, Allémann E, Doelker E. Development of a nanoprecipitation method intended for the

entrapment of hydrophilic drugs into nanoparticles. European journal of pharmaceutical sciences : official journal of the european federation for pharmaceutical sciences. 2005;24:67-75.

21. Chen JF, Zheng C, Chen GT. Interaction of macro and micromixing on particle size distribution in reactive precipitation Chemical Engineering Science. 1996;51:1957-66. (• It is effective control NPs size and distribution method by increasing mixing efficiency of nanoprecipitation has explained)
22. Mae K. Advanced chemical processing using microspace. Chemical engineering science. 2007;62:4842-51.
23. Duffy DC, McDonald JC, Schueller OJA et al. Rapid Prototyping of Microfluidic Systems in Poly(dimethylsiloxane). Analytical chemistry. 1998;70:4974-84.
24. deMello AJ. Control and detection of chemical reactions in microfluidic systems. Nature. 2006;442:394-402.
25. El-Shabouri MH. Positively charged nanoparticles for improving the oral bioavailability of cyclosporin-A. International journal of pharmaceutics. 2002;249:101-8.
26. Knight JB, Vishwanath A, Brody JP et al. Hydrodynamic Focusing on a Silicon Chip: Mixing Nanoliters in Microseconds. Physical Review Letters. 1998;80:3863-6.
27. Karnik R, Gu F, Basto P et al. Microfluidic platform for controlled synthesis of polymeric nanoparticles. Nano letters. 2008;8:2906-12. (• Polymeric NPs was synthesized by hydrodynamic flow focusing microfluidic system)
28. Hessel V, Löwe H, Schönfeld F. Micromixers –a review on passive and active mixing principles. Chemical engineering science. 2005;60:2479-501.
29. Galindo-rodriguez S, Allémann E, Fessi H et al. Associated with Nanoparticle Formation in the Salting-out , Nanoprecipitation Methods. Pharmaceutical research. 2004;21:1428-39.
30. Molpeceres J, Guzman M, Aberturas MR et al. Application of central composite designs to the preparation of polycaprolactone nanoparticles by solvent displacement. Journal of pharmaceutical sciences. 1996; 85:206-13.
31. Quintanar-Guerrero D, Allémann E, Doelker E et al. A mechanistic study of the formation of polymer nanoparUcles by the emulsification-diffusion technique. Colloid and polymer science. 1997;275:640-7.
32. Thioune O, Fessi H, Devissaguet JP et al. Preparation of pseudolatex by nanoprecipitation: influence of the solvent nature on intrinsic viscosity and interaction constant. International journal of pharmaceutics. 1997;146:233-8.
33. Aubry J,Ganachaud F, Cohen Addad JP et al. Nanoprecipitation of Polymethylmethacrylate by Solvent Shifting: 1. Boundaries. Langmuir. 2009;25:1970-9.
34. Beck-Broichsitter M, Rytting E, Lebhardt T et al. Preparation of nanoparticles by solvent displacement for drug delivery: A shift in the “ouzo region” upon drug loading. European journal of pharmaceutical sciences. 2010;41:244-53.
35. Lince F, Marchisio DL, Barresi AA. Strategies to control the particle size distribution of poly-epsilon-caprolactone nanoparticles for pharmaceutical applications. Journal of colloid and interface science. 2008;322:505-15.
36. Dev S, Swaminathan IK, Raston CL. Nanosized drug formulations under microfluidic continuous flow. Lab on a chip. 2011;11:3214-7.
37. Anton N, Bally F, Serra CA et al. A new microfluidic setup for precise control of the polymer nanoprecipitation process and lipophilic drug encapsulation. Soft Matter. 2012;8:10628. (• The ketoprofen encapsulated PMMA NPs was synthesized by KM microfluidic system)
38. Capretto L, Cheng W, Carugo D et al. Mechanism of co-nanoprecipitation of organic actives and block copolymers in a microfluidic environment. Nanotechnology. 2012;23:375602.
39. Bally F, Garg DK, Serra CA et al. Improved size-tunable preparation of polymeric nanoparticles by microfluidic nanoprecipitation. Polymer. 2012;53:5045-51. (• Poly(methyl methacrylate) (PMMA) NPs was successfully synthesized by HPIMM microfluidic system)
40. Bally F. Continuous-flow synthesis of branched macromolecular architectures in microsystems : towards

biomedical applications. 2011.
41. Mohr WD, Saxton RL, Jepson CH. Mixing in Laminar-Flow Systems. Industrial & engineering chemistry. 1957;49:1855-6.
42. Zhao H, Wang JX, Wang QA et al. Controlled Liquid Antisolvent Precipitation of Hydrophobic Pharmaceutical Nanoparticles in a Microchannel Reactor. Industrial & engineering chemistry research. 2007;46:8229-35. (• Pure drug NPs was synthsized by Y-type microfluidic system)
43. Wang JX, Zhang QX, Zhou Y et al. Microfluidic synthesis of amorphous cefuroxime axetil nanoparticles with size-dependent and enhanced dissolution rate. Chemical engineering journal. 2010;162:844-51.
44. Zhang HX, Wang JX, Shao L et al.. Microfluidic Fabrication of Monodispersed Pharmaceutical Colloidal Spheres of Atorvastatin Calcium with Tunable Sizes. Industrial & engineering chemistry research. 2010;49:4156-61.
45. Ali HSM, York P, Blagden N. Preparation of hydrocortisone nanosuspension through a bottom-up nanoprecipitation technique using microfluidic reactors. International journal of pharmaceutics. 2009;375:107-13.
46. Ali HSM, York P, Ali HMA et al. Hydrocortisone nanosuspensions for ophthalmic delivery: A comparative study between microfluidic nanoprecipitation and wet milling. Journal of controlled release. 2011;149:175-81.
47. Aoki N, Mae K. Effects of channel geometry on mixing performance of micromixers using collision of fluid segments. Chemical engineering journal. 2006;118:189-97.
48. Nagasawa H, Aoki N, Mae K. Design of a New Micromixer for Instant Mixing Based on the Collision of Micro Segments. Chemical engineering & technology. 2005;28:324-30.
49. Nagasawa H, Nakao M. Organic pigment fine particles and method of producing same. United state patent. 2009:US 7,503,972 B2.
50. Chronopoulou L, Sparago C, Palocci C. A modular microfluidic platform for the synthesis of biopolymeric nanoparticles entrapping organic actives. Journal of Nanoparticle Research. 2014;16:2703.
51. Kang X, Luo C, Wei Q et al. Mass production of highly monodisperse polymeric nanoparticles by parallel flow focusing system. Microfluidics and nanofluidics. 2013;15:337-45.
52. Lim JM, Bertrand N, Valencia PMet al. Parallel microfluidic synthesis of size-tunable polymeric nanoparticles using 3D flow focusing towards in vivo study. Nanomedicine: nanotechnology, biology and medicine. 2014;10:401-9.
53. Rhee M, Valencia PM, Rodriguez MI et al. 3D Hydrodynamic Focusing for Confined Precipitation of Nanoparticles within Microfluidic Channels. 14th International Conference on Miniaturized Systems for Chemistry and Life Sciences. 2010:992-4.
54. Rhee M, Valencia PM, Rodriguez MI et al. Synthesis of Size-Tunable Polymeric Nanoparticles Enabled by 3D Hydrodynamic Flow Focusing in Single-Layer Microchannels. Advanced materials. 2011;23:H79-H83.
55. Sun J, Xianyu Y, Li M et al. A microfluidic origami chip for synthesis of functionalized polymeric nanoparticles. Nanoscale. 2013;5:5262-5.
56. Johnson BK, Prud'homme RK. Chemical processing and micromixing in confined impinging jets. AIChE journal. 2003;49:2264-82.
57. Johnson BK, Prud'homme RK. Mechanism for Rapid Self-Assembly of Block Copolymer Nanoparticles. Physical review letters. 2003;91:118302. (• Polystyene-poly(ethylene oxide) NPs was synthesized by CIJM microfluidic system)
58. Liu Y, Olsen MG, Fox RO. Turbulence in a microscale planar confined impinging-jets reactor. Lab on a chip. 2009;9:1110-8.
59. Johnson BK, Prud'homme RK. Flash NanoPrecipitation of Organic Actives and Block Copolymers using a Confined Impinging Jets Mixer. Australian journal of chemistry. 2003;56:1021.
60. Valente I, Celasco E, Marchisio DL et al. Nanoprecipitation in confined impinging jets mixers: Production, characterization and scale-up of pegylated nanospheres and nanocapsules for pharmaceutical use. Chemical engineering science. 2012; 77:217-27.

61. Lince F, Marchisio DL, Barresi AA. Smart mixers and reactors for the production of pharmaceutical nanoparticles: Proof of concept. Chemical engineering research and design. 2009;87:543-9.
62. Lince F, Bolognesi S, Stella B et al. Preparation of polymer nanoparticles loaded with doxorubicin for controlled drug delivery. Chemical engineering research and design. 2011;89:2410-9.
63. Liu Y, Cheng C, Liu Y et al. Mixing in a multi-inlet vortex mixer (MIVM) for flash nano-precipitation. Chemical Engineering Science. 2008;63:2829-42.
64. Cheng JC, Olsen MG, Fox RO. A microscale multi-inlet vortex nanoprecipitation reactor: Turbulence measurement and simulation. Applied physics letters. 2009;94:204104.
65. Cheng JC, Fox RO. Kinetic Modeling of Nanoprecipitation using CFD Coupled with a Population Balance. Industrial & engineering chemistry research. 2010;49:10651-62.
66. Shi Y, Fox RO, Olsen MG. Confocal imaging of laminar and turbulent mixing in a microscale multi-inlet vortex nanoprecipitation reactor. Applied physics letters. 2011;99:204103.
67. Shi Y, Cheng JC, Fox RO et al. Measurements of turbulence in a microscale multi-inlet vortex nanoprecipitation reactor. Journal of micromechanics and microengineering. 2013;23:075005.
68. Shi Y, Fox RO, Olsen MG. Micromixing visualization and quantification in a microscale multi-inlet vortex nanoprecipitation reactor using confocal-based reactive micro laser-induced fluorescence. Biomicrofluidics. 2014;8:044102.
69. Fang RH, Chen KNH, Aryal S et al. Large-scale synthesis of lipid-polymer hybrid nanoparticles using a multi-inlet vortex reactor. Langmuir. 2012;28:13824-9. (• PLGA NPs was synthesized by MIVM microfluidic system)
70. Liu Z, Ramezani M, Fox RO et al. Flow Characteristics in a Scaled-up Multi-inlet Vortex Nanoprecipitation Reactor. Industrial & engineering chemistry research. 2015:4512-25. (•• The MIVM microfluidic system have been scaled-up to 16 times, it will be applied to produce NPs by microfluidc system in industtrial-scale.)
71. Kim Y, Chung BL, Ma M et al. Mass production and size control of lipid-polymer hybrid nanoparticles through controlled microvortices. Nano letters. 2012;12:3587-91.
72. Lim JM, Swami A, Gilson LM et al. Ultra-high throughput synthesis of nanoparticles with homogeneous size distribution using a coaxial turbulent jet mixer. ACS Nano. 2014;8:6056-65. (•• PLGA-PEG NPs was systhesized by off-the-shelf compnents microfluidc system. Only the size did not keep the range of 50~100 nm, but the production rate also reached 288~576 g/day.)
73. Cheng J, Teply BA, Sherifi I et al. Formulation of functionalized PLGA–PEG nanoparticles for in vivo targeted drug delivery. Biomaterials. 2007;28:869-76.
74. Quevedo E, Steinbacher J, McQuade DT. Interfacial polymerization within a simplified microfluidic device: capturing capsules. Journal of the american chemical society. 2005;127:10498-9.
75. Hong CC, Choi JW, Ahn CH. A novel in-plane passive microfluidic mixer with modified Tesla structures. Lab chip. 2004:109-13.
76. Valencia PM, Basto PA, Zhang LF et al. Single-Step Assembly of Homogenous Lipid− Polymeric and Lipid−Quantum Dot Nanoparticles Enabled by Microfluidic Rapid Mixing. ACS Nano. 2010;4:1671-9.
77. Valencia, Pridgen EM, Rhee M et al. Microfluidic Platform for Combinatorial Synthesis and Optimization of Targeted Nanoparticles for Cancer Therapy. ACS Nano. 2013;7:10671-80.
78. Douroumis D, Fahr A. Nano- and micro-particulate formulations of poorly water-soluble drugs by using a novel optimized technique. European journal of pharmaceutics and biopharmaceutics. 2006;63:173-5.
79. Dong Y, Ng WK, Hu J et al. A continuous and highly effective static mixing process for antisolvent precipitation of nanoparticles of poorly water-soluble drugs. International journal of pharmaceutics. 2010;386:256-61.
80. Liu D, Zhang H, Mäkilä E et al. Microfluidic assisted one-step fabrication of porous silicon acetalated dextran nanocomposites for precisely controlled combination chemotherapy. Biomaterials. 2015;39:249-59.
81. Qin D, Xia Y, Whitesides GM. Soft lithography for micro- and nanoscale patterning. Nature protocols.

2010;5:491-502.
82. Gregoriadis G. Drug entrapment in liposomes. FEBS LETTERS. 1973;36:292-6.
83. Lim JM, Karnik R. Optimizing the discovery and clinical translation of nanoparticles: could microfluidics hold the key? Nanomedicine. 2014;9:1113-6.
84. Aubin J, Fletcher DF, Xuereb C. Design of micromixer using CFD modelling. Chemical Engineering Science. 2005;60:2503–16.
85. Yang AS, Chuang FC, Chen CK et al. A high-performance micromixer using three-dimensional Tesla structures for bio-applications. Chemical Engineering Journal. 2015;263:444-51.
86. Khosravi PM, Faramarz H, Davoud J. Mixing enhancement in a passive micromixer with convergent-divergent sinusoidal microchannels and different ratio of amplitude to wave length. Computers & Fluids. 2014;105:82-90.
87. Hung CI, Wang KC, Chyou CK. Design and flow simulation of a new micromixer. JSME International Journal Series B-Fluids and Thermal Engineering. 2005;48:17-24.
88. di Pasquale N, Marchisio DL, Barresi AA. Model validation for precipitation in solvent-displacement processes. Chemical Engineering Science. 2012;84:671-83.
89. Cheng JC, Vigil RD, Fox RO, A competitive aggregation model for Flash NanoPrecipitation. Journal of Colloid and Interface Science. 2010;351:330-42.
90. Wang LG, Fox RO, Comparison of micromixing models for CFD simulation of nanoparticle formation. AICHE Journal. 2004;50:2217-32.
91. di Pasquale N., Marchisio DL, Carbone P et al. Identification of nucleation rate parameters with MD and validation of the CFD model for polymer particle precipitation. Chemical Engineering Research & Design. 2013;91:2275-90. [92] Khan IU, Serra CA, Anton N et al. Microfluidic conceived Trojan microcarriers for oral delivery of nanoparticles. International journal of pharmaceutics. 2015;493:7-15.
93. Khan IU, Serra CA, Anton N et al. Microfluidic conceived drug loaded Janus particles in side-by-side capillaries device. International journal of pharmaceutics. 2014;473:239-49.
94. Khan IU, Stolch L, Serra CA et al. Microfluidic conceived pH sensitive core–shell particles for dual drug delivery. International journal of pharmaceutics. 2015;478:78-87.

2.2 Development of two-step emulsification to prepare water-in-barrier-in-water systems

ABSTRACT

Water-in-barrier-in-water systems have been regarded as a general type of multifunctional carriers for the encapsulation of different types of molecules. Such systems are depicted as water droplets encapsulated in a bigger oil droplet or in a polymer matrix. In this review, we propose to discuss the different preparation processes, the effect of formulation and operating parameters on the properties of double emulsions or water-in-barrier-in-water systems. One principal preparation method for these systems is a two-step emulsification process which will be the focus of an important part of the current review.

2.2.1. Introduction

Water-in-barrier-in-water systems, in which the barrier can be a vegetable oil, a mineral oil or a polymer matrix, consist of hydrophobic globules suspended in an aqueous phase which, in turn, contain smaller dispersed aqueous droplets. The main benefit of this special structure is the possibility to encapsulate different and potentially incompatible molecules (e.g. hydrophobic and hydrophilic) in a single carrier. It may thus results in the smart combination of drugs in one cargo. This way has been considered as a better option to maximize therapeutic effect and reduce drug resistance by cocktail therapy especially those involving various bioactive molecules in many diseases (in particular, cancer, cardiovascular diseases) [1, 2]. Thus, it has stimulated substantial interest in pharmaceutics [3] including delivery in intracellular cell [4, 5], substitute blood [6], vaccines, vitamins, enzymes, and hormones [7, 8]. To satisfy this structure, different type of vehicles have been synthesized by different strategies including double emulsion [9], polymeric microparticles [10], nanoparticles [11], nanocapsules [12], micelles and liposomes [13, 14]. These special structures have been studied during the last quarter of century. Generally, the two-step emulsification has become the main process to obtain these vehicles. But, to some extent, vagaries of the two-step emulsification have prevented its clinic application until now. However, the lately progress of the two-step emulsification method has provided impetus to the development of such advanced carriers.

Many reviews have presented specific aspects of the preparation of water-in-barrier-in-water systems with the two-step emulsification method such as stability [15], transport

phenomena [16], the two-step emulsification-evaporation methods for polymeric particles [17], microfluidic systems [18] and so on. To the best of our knowledge, it has never been reported about a general description of the two-step emulsification methods for water-in-barrier-in-water systems and the relation between the process parameters, formulation and properties of such systems such as size, size distribution and stability. In addition, due to significant differences in the preparation methods of water-in-barrier-in-water systems and emulsions such as O/O/W emulsions, or W/W/O emulsions, which were generally considered as of same structure as W/O/W emulsions, these multiple emulsions will not be part of the scope of this review. This paper focuses only on the development of two-step methods for the preparation of water-in-barrier-in-water systems, which are considered as the most potential and efficient methods. The discussion is organized based on the principle of two-step emulsification process, rather than by types, sizes and nature of the emulsions neither by the type of encapsulated molecules. General understanding of the two-step emulsification will be discussed in the first section. The second section is divided into two parts. On the one side, the selection of appropriate surfactants to achieve a double emulsification is highlighted. On the other side, the most general methods to stabilize water-in-barrier-in-water systems will be presented. The third section focuses on polymeric particles prepared by the two-step emulsification-evaporation method. These polymeric systems deserve their own section as they have been considered as the most effective carrier to prolong the release of encapsulated molecules. The fourth section will be focused on a new class of devices that can prepare water-in-barrier-in-water systems. Indeed, microfluidic devices were recognized to offer a better control in mass and heat transport that makes chemical microprocesses more efficient than their lab or industrial counterparts. Thus, the use of microfluidic devices to obtain water-in-barrier-in-water systems has been a new and potent method. The limitations of batch methods such as low reproducible results and low control on droplet size and size distribution render the use of the microfluidic devices very attractive. However, the later suffer from a relative low throughput.

Table 2. Influence of oil phase's specific gravity on the type of emulsion [20]

Density	Type of emulsion	Texture	Stability
0.664[1]	O/W[6]	Fine[8]	Stable[9]
0.726[2]	O/W	Fine	Stable
0.803	O/W	Fine	Stable
0.818	O/W	Fine	Stable
0.82[3]	O/W	Medium	Moderately stable
0.828	O/W	Coarse	Unstable
0.839	--	--	Separates immediately
0.849	--	--	Separates immediately
0.856	--	--	Separates immediately
	O/W	Coarse	Unstable
0.857	W/O[7]	Fine	Stable
	W/O	Medium	Moderately stable
0.869[4]	W/O	Medium	Stable
0.874	W/O	Fine	Stable
0.884	W/O	Fine	Stable
0.895[5]	W/O	Fine	Stable

1. Isohexane (boiling point = 77 ºC)
2. Iso-octane (boiling point = 118 ºC)
3. Boiling range = 130~150 ºC at 67 mm Hg. Of vacuum.
4. Boiling range = 210~230 ºC at 67 mm Hg. Of vacuum.
5. Boiling range = over 270 ºC at 67 mm Hg. Of vacuum.
6. O/W = oil-in-water, W/O= water-in-oil
7. Both types coexist in the same emulsion.
8. A fine texture is one in which the oil or water droplets average 0.02 mm or less, in an emulsion of medium texture the globules vary from 0.02 to 0.5 mm and a coarse emulsion is one in which the dispersed oil or water drops are over 0.5 mm in diameter.
9. Stability is purely a relative term here. Since most emulsions were treated with electrolytes, they were not allowed to stand, except in a few instances, for more than 15 minutes. An emulsion which showed little or no sign of separating during that time was recorded as “stable.” A “moderately stable” emulsions was stable for several minutes only. An “unstable” emulsion separated in less than a minute.

2.2.2. General consideration of the two-step emulsification

2.2.2.1. Intrinsic instability of double structure

The double emulsion as the first example of water-in-barrier-in-water systems was firstly presented in 1925 by William Seifriz [20] when he was researching how the specific gravity of the oil phase influences on the type of emulsion. Thus he investigated the formation of W/O or O/W emulsions with an aqueous dispersion of casein (a phosphoprotein, as a stabilizing agent, 0.2 % w/v) with different oil phases having various specific gravities. For given operating conditions, the results indicated that heavy oils (specific gravity above 0.857) tend to form W/O emulsions while stable O/W emulsions were formed for oils which specific gravity was lower than 0.820 (Table 2). When the specific gravity of the oil phase was comprised between 0.820 and 0.857 a phase separation or an unstable emulsion were observed.

Whereas William Seifriz investigated the effect of electrolyte concentration on the type of emulsions produced with petroleum oil, it found that electrolytes have the ability to reverse the W/O emulsion to O/W emulsion or to stabilize the O/W emulsion. Interestingly, an emulsion of straw-oil, which had a specific gravity of 0.882, presented an uncommon behavior. Sometimes it can't be emulsified at all. But sometimes, it can form a complex system consisting of a coarse oil-in-water emulsion, which includes oil globules (1 mm) encapsulating a fine water-in-oil emulsion. This was the original model for double emulsion which was formed near the reversal point (the point for which the W/O emulsion can be easily reversed to the O/W emulsion under the effect of electrolytes). So, the double emulsion was found as a very instable and sensitive system and was considered later as a transition state from W/O emulsions to O/W emulsions [21]. The reasons of this intrinsic instability include the free energy, osmotic pressure, and Laplace pressure [22]. The oil phase as the barrier of water-in-barrier-in-water systems induces a difference in the osmotic pressure between the innermost phase and external phase. Higher osmotic pressure in external phase induces the swelling of the inner water droplets. In contrast, lower osmotic pressure results in the shrinkage of the inner water droplets. The rupture of the oil droplets is thus induced by the rapid passage of water from the innermost phase to the external phase promoting by this osmotic pressure difference. As for the Laplace pressure inside droplets, it depends on the droplets size and surface tension. Laplace pressure is inversely related to the droplet size. Thus the pressure of inner droplets is much higher than the pressure of the oil droplets. This may ultimately lead to the inner droplets collapse and rupture.

Despite their inherent instability, double emulsions have the great advantage to possibly encapsulate multi components and thus have attracted a lot of interest. This

special structure was firstly considered to encapsulate insulin in the late 1960s [23]. Afterward, most of the researches were directed toward the W/O/W emulsions stability. As a result, the advent of two-step emulsification has offered the impetus to obtain double emulsions, due to control of osmotic pressure and Laplace pressure during each emulsification process.

2.2.2.2. General method to achieve the two-step emulsification

As aforementioned, the first double emulsion was discovered as an unexpected reward. Until 1976, a reliable method for preparing double structures was not yet established. Matsumoto et al. [24] presented the first two-step emulsification procedure for preparing double emulsions in 1976. Firstly, a W/O emulsion was prepared and then the W/O/W emulsion was obtained by using the primary W/O emulsion as the oil phase for the second emulsification step. Since then, the two-step emulsification method has been the main approach to get double emulsions [25]. Nevertheless, the one-step emulsification method to get double structures has been the focus of numerous researches driven by the simplicity of the process. The progress in one-step emulsification has been recently reviewed by Clegg et al. [26]. Thus the one-step emulsifications method can be classified in three categories: 1) double emulsions were formed by the use of microfluidic systems, 2) different type of block copolymers were introduced as surfactant to get double emulsions and 3) particles were used as stabilizing agent to get double emulsion by so-called Pickering phenomenon.

2.2.3. Preparation of double emulsions

2.2.2.3. Choosing surfactant for preparation double emulsions

For the two-step process, choosing a surfactant for each emulsification steps is important to get a stable final product. Basically, a hydrophobic surfactant characterized by a HLB lower than 7 (most commonly around 3-4) should be chosen for the preparation of the primary W/O emulsion. In contrast, a hydrophilic surfactant (HLB higher than 10) should be chosen for the second W/O/W emulsification.

In early stage of researching, Garti et al. [28] reported different methods to get stable W/O emulsions by suitable selection of surfactant. Initially, stable W/O and W/O/W emulsions were obtained by use of combination of different emulsifiers such as the mixture of span 80 and tween 80, in which the overall apparent HLB value was tuned by different ratios of the two surfactants for different types of emulsions. The inner aqueous phase separation from the continuous aqueous phase for a given time was used as the standard to evaluate the stability of W/O emulsions. Finally, an optimum

stability of W/O emulsions was obtained by use of brij 93 (HLB of 4.9, 8 wt.%) or span 80 + span 85 (HLB 4, 10 wt.%) as surfactant, in which any separation of water droplets from the oil phase was not observed and water droplets size can be modified from 0.5 to 3 µm.

For formation of W/O/W emulsions, when the concentration of the hydrophilic surfactant (Tween 80) in the external phase was increased from 2 to 7 wt.%, the encapsulation efficiency decreased from 66% down to 18%. It was explained by the fact that increasing the surfactant concentration induced the formation of smaller oil droplets which in turn promoted the rupture of inner water droplets. Authors showed that a balance exists between the encapsulation efficiency and the size of the double emulsion, related to the concentration of hydrophilic surfactant. The phenomenon was also observed at different size level of double emulsions [27]. Two explanations were summarized from literature: 1) higher concentration of hydrophilic surfactant results in smaller size and lower efficiency due to the rupture of water droplets[28]; 2) increasing affinity within mixed micelles of hydrophilic surfactant in external phase, the hydrophobic surfactant will be pumped outside of oil droplet. It resulted in the lower efficiency [27]. Besides, the author proposed a way to increase the encapsulation efficiency and stability at same time by the combination of ionic-surfactant and nonionic surfactant in external phase [28, 29]. However, in practice, the use of ionic surfactant induced some incompatibilities with the encapsulation of ionic drugs. Furthermore, Garti et al. [27] suggested that optimum values of HLB and concentration of hydrophilic emulsifier in external phase exist to get the highest encapsulation efficiency. The mixture of span 20 and tween 80 were adopted to investigate the effect of the HLB value (9 to 15) in the external phase on the encapsulated efficiency for W/O emulsions. The different optimum HLB values of hydrophilic surfactant were obtained for different concentrations of surfactant in external phase. They showed that a lower concentration of hydrophilic emulsifier in external phase resulted in the requirement of a higher HLB to obtain higher efficiency. When varying concentration of hydrophobic surfactant in middle phase, a higher concentration will result in a higher optimum HLB value of hydrophilic emulsifier to get higher encapsulation efficiency at same concentration of hydrophilic surfactant in external phase. It was explained that the migration of hydrophobic surfactant from the interface between middle phase (oil) and inner phase to interface between middle phase and external phase, which results in the decrease of apparent HLB value in the external interface [30].

Though low HLB values (less than 4) were used as a standard for selection of hydrophobic surfactant for preparation of W/O emulsions, there are still many types of surfactant with different structures but same HLB value. Thus, additional standards were introduced for the selection of hydrophobic surfactant: 1) more rigid hydrophobic

surfactants will confer more stability of W/O emulsion; 2) the selection of hydrophobic surfactant should be based on the nature of the oil. Similarly, a surfactant with a high degree of unsaturation (structural stiffness) is preferable to get more stable W/O emulsions. Based on above two principles, emulsifier should be selected rigid with a high degree of unsaturation to obtain the best stability of water droplets in vegetable oils [31].

The different types of double emulsions can be classified based on the number of water droplets in global droplets (Figure 6). Authors demonstrated that the different types of double emulsions can be obtained by a proper selection of the hydrophilic surfactant. Thus, double emulsions were synthesized with three types of hydrophilic surfactant at 2 wt.% (Briji 30, Triton X-165 and combined surfactant by Span 80 and Tween 80) in the external phase in which span 80 (5 wt %) was used as hydrophobic surfactant in middle phase. The three types of double emulsions shown in Fig. 1 are: 1) microcapsules, one oil droplet including one inner aqueous droplet, 2) multivesicular droplets for which one oil droplet encapsulate numerous inner aqueous droplets and microcapsules, 3) microspheres with a complex inner structure inside oil droplet [32]. Whereas in the other paper, different concentrations of span 80 in middle phase was investigated to obtain different types of double emulsions, teen 80 (1 wt.%) was used in external phase. However, additional stabilizing agent (bovine serum albumin, BSA) was added into inner phase to get more stable double emulsions. It was demonstrated that different types of double emulsions can also be prepared from microcapsules to microspheres with a concentration of Span 80 ranging from 1 to 10 wt.% in middle phase [33].

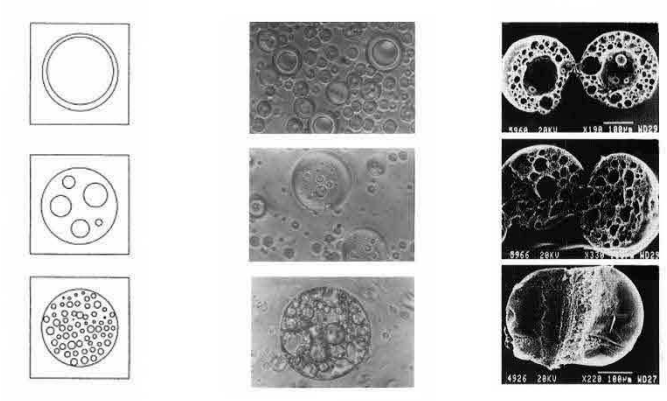

Figure 6. Three typical types of water-in-barrier-in-water structures with different materials. Left: sketch of double emulsions, middle: double emulsions as seen by an optical microscope which correspond to the electronic micrographs on the right handside [32,34]**.**

Also polymeric microparticles synthesized by the two-step emulsification-evaporation presented the same three types observed in the double emulsions in which BSA was

admixed in the inner phase (Figure 6). In summary, three main emulsions have been observed and controlled by the selection of an appropriate hydrophilic surfactant or by the concentration of the hydrophobic stabilizing agent. This methodology can be generally used to get different types of water-in-barrier-in-water systems by two-step emulsification without limitation of the barrier materials.

To summarize, we discussed above the general idea about the selection of surfactant: 1) for W/O emulsions, low HLB, good rigidity of surfactant and similarity between the nature of oil and surfactant are needed to be compatible with the W/O emulsions. Increasing concentration of hydrophobic surfactant in middle phase similarly results in more stable double emulsion, higher encapsulation efficiency, and more complex structure of double emulsion (microsphere); 2) for W/O/W emulsions, high HLB of the hydrophilic surfactant is needed to get stable emulsions., the stability of the double emulsions decreased with concentration of hydrophilic surfactant in external phase, which induces smaller size of the double emulsion, lower encapsulation efficiency, types of hydrophilic surfactant will decide the type of double emulsions; 3) there exist an optimum HLB value of hydrophilic surfactant to obtain highest encapsulation efficiency of double emulsion, the optimum HLB depends on the concentration of hydrophilic and hydrophobic surfactants.

2.2.2.1. Methods for stabilizing double emulsions

The low stability of double emulsions is a limitation to the application of double emulsions in pharmaceutics. However, the two-step emulsification supports many possibilities to improve the stability of double emulsions. To make double emulsions be valuable in practice, increasing stability of double emulsions have been investigating in many literature reports. First, stability can be increased by the use of hydrophobic surfactant in high concentration (span 80, 30 wt.%)[24]. Unfortunately, the migration of hydrophobic surfactant from interface between inner phase and middle phase to interface between middle phase and external phase will result in the low effective concentration of hydrophobic surfactant in interface between inner phase and middle phase and higher HLB value of hydrophilic surfactant is necessary to obtain the optimum encapsulation efficiency. Thus, it is imperative to get more stable systems by other methods. Garti et al. [35] reported the possibility to use polymeric surfactant to increase the stability of W/O emulsions. A such, soybean oil was firstly radically polymerized and then reacted with polyglycerol to provide some hydrophilic property. The different molecular weights of the as such synthesized polymeric surfactant were obtained ranged from 881 to 3758 g/mol. The stability of W/O emulsions increased with molecular weight of polymeric surfactant. It was found that excellent stability of W/O emulsions (50 wt.% inner phase kept in W/O emulsion) could be obtained by at low concentration of polymeric surfactant (3 - 5 wt.%)

compared with the same level of double emulsions synthesized at high concentration of non polymeric surfactant (20 -25 wt.%) [35].

Surfactants with three different chain lengths were employed to stabilize W/O emulsions [36]: 1) low molecular weight classical emulsifiers such as Span 80; 2) medium molecular weight macromolecules such as polyglycerol polyricinoleate (ETD or PGPR) and 3) high molecular weight grafted silicone lipophilic surfactant (Abil EM-90). The encapsulation efficiency was represented by migration of NaCl from inner phase into external phase after formation of double emulsions, which was tested by the conductivity of external phase. The results of encapsulation efficiency apparently decreased following the order: Abil EM-90 >ETD >Span 80. It was explained that the hydrophobic surfactant with higher molecular weight will produce higher effective concentration in middle phase at same concentration of hydrophobic surfactant compared with the one with smaller molecular weight due to less hydrophobic surfactant migration from W/O interface to O/W interface. In parallel, Florence et al. [37] postulated to improve the stability of double emulsions by formation of polymeric gel in an aqueous phase, which can be inner phase or external phase. A polyoxyethylene-polyoxypropylene ABA block copolymer (poloxamer) and acrylamide were added into inner phase or external phase, respectively. After emulsification, the gel is formed by crosslinked ABA block copolymer or polymerized acrylamide by UV irradiation [38]. The formation of the gel gave a more stable double emulsion. However, it has the disadvantage of possible drug degradation due to irradiation. Thus, these authors proposed enhancing the stability of double emulsion by the interfacial complexion of macromolecules and nonionic surfactants [39]. A type of crosslinked polyacrylic acid or BSA was added in the inner phase to complex with a low HLB surfactant (poloxamer) at the interface between inner phase and middle phase. The result presented a white film formed at the interface between inner phase and middle phase. In contrast, no visible film was formed when poloxamer and BSA or polyacrylic acid weren not added into the formulation to prepare double emulsions. It proved that the complex between polyacrylic acid or BSA and poloxamer surfactant can form the film at the interface between two phases. This formation of the film was explained by the interaction of hydrophobic and hydrogen binding. Besides, BSA presented the same ability to form the film. After using the system (the complex of BSA and poloxamer surfactant), the release of sulphane blue in double emulsions was decreased under 10 wt.% after 6 hr, whereas the release was over 40 wt.% without the complex formed [39]. At same time, the effect of BSA concentration in inner phase on encapsulation efficiency was investigated, the encapsulation efficiency was increased around 20 wt.%, when BSA (2 wt.%) was added to the inner phase, compared with inner phase without BSA, and finally encapsulation efficiency reached up to 80 wt.% [33]. After 30 days, it still kept over 60 wt.%. Garti et al. [40] investigated the

complex between BSA and Span 80 for improving the stability of the double emulsion by adding BSA in the inner phase or external phase respectively. In consequence, BSA was shown to improve the stability of double emulsions. NaCl was used as maker to research the encapsulation efficiency and release. The release of NaCl in double emulsion was assayed when BSA (0.2 wt.%) was added in the inner phase. The release rate was from 8 to 20 wt.% for 5 and 20 h respectively, much smaller than the release rate from 35 to 52 wt.% when the double emulsions were prepared without BSA in the inner phase. In addition, when BSA was added in the external phase, the smaller size of double emulsion was obtained. And the synthesized double emulsions size distribution has not changed after 6 weeks. It was explained that the formed film at the interface can impact elasticity and resistance to prevent the rupture of inner water droplet, but it has not ability to prevent coalescence of oil droplet.

Emulsions can also be stabilized by the complex of hydrophilic molecular and hydrophobic molecular at interface of water-oil. For example, the use of colloidal microcrystal line cellulose as "mechanical stabilizers" of double emulsions [41], and different biopolymers have been used in the inner phase based on the principle, such as gelation, caseins, whey protein, chitosan and cyclodextrins [35, 42-54]. In contrast, stable emulsions have been synthesized over the past decades by Pickering mechanism, in which inorganic nanoparticles were used instead surfactants to stabilize the oil/water interface. Thus, W/O emulsion's stability problem was hoped to be solved by the use of Pickering mechanism. The review about preparation of double emulsions by this way have been well organized by Clegg et al. [26].

It is noteworthy that Kawashima et al. [67] succeeded to produce double emulsions more stable by use of a solute concentration gradient between the inner phase and external phase. The method of stabilization was based on the formation of hypertonic inner aqueous phase. The sodium chloride or glucose was incorporated in the inner phase as the solute. Encapsulation efficiency and stability of double emulsions were investigated. It was found that a higher concentration of solute in the inner phase than in the external phase was helpful to get more stable double emulsions and higher encapsulation efficiencies while the other way around decreased the encapsulation efficiency. The explanation of this phenomenon was addressed when the primary emulsion were used to form double emulsions by adding of external phase with lower solute concentration, different osmotic pressure between inner phase and external phase increased the size of the inner droplets due to swelling and collapse of inner droplets and thickness of oil droplets at same time due to same oil volume with less interface of inner droplets and oil phase. Such loss of encapsulation efficiency evidenced the rupture of global droplets and salt migration from the inner phase into the external phase.

2.2.4. Polymeric particles synthesized by the two-step emulsification-evaporation methods

Due to the fast growing field of pharmaceutics and the advent of biopolymers such as Poly(lactide-co-glycolide) (PLGA), Poly(lactic acid) (PLA) and Polycaprolactone (PCL), the appetence of hydrophilic drugs encapsulation such as protein by polymeric particles has been dramatically increased. To encapsulate hydrophilic molecules and prolong the drug release, biopolymer microparticles, as the second example of water-in-barrier-in-water systems, were initially synthesized by modifying the two-step emulsification method.

The commonly method adopted was the encapsulation of a hydrophilic compound based on its direct dispersion into a polymeric organic solution by help of mechanic mixing. The encapsulated hydrophilic compound by modifying the two-step emulsification method offered better reproducibility and easy control during process[56]. Ogawa et al. [57, 58] firstly introduced the modifying two-step emulsification method to prepare polymeric microparticles. The standard of the process was proposed as follows: 1) polymer is dissolved in the solvent, which is immiscible with water, the polymer solution is emulsified with water to form W/O emulsion; 2) the W/O emulsion is poured into the external aqueous phase to get W/O/W emulsion; 3) the solvent is evaporated, the polymer precipitates and forms solid particles. Similarly, a hydrophilic analogue of luteinizing hormone was encapsulated into the matrix of polymeric microparticles by Ogawa et al. [57, 58]. Synthesized PLA or PLGA were dissolved in dichloromethane as the oil phase. However, since no hydrophobic surfactant was added into the oil phase, a broad size distribution of microparticles (37~125 μm) was obtained. After the preparation of double emulsions, the microparticles in the wet state were sized using sieves of different apertures to get different size of microparticles. On the other hand, effect of inner phase gelation on the encapsulation efficiency has been investigated. Incorporation of gelatin in inner phase increased the encapsulation efficiency to 70.7 wt.% compared with the microparticles prepared without gelatin (6.7 wt%).

Langer et al. reported encapsulated proteins (BSA and tetanus toxoid) in PLGA microparticles by the two-step emulsification-evaporation method [56, 59]. Figure 7(ㅣ) present a typical picture of PLGA microparticles synthesized by this method.

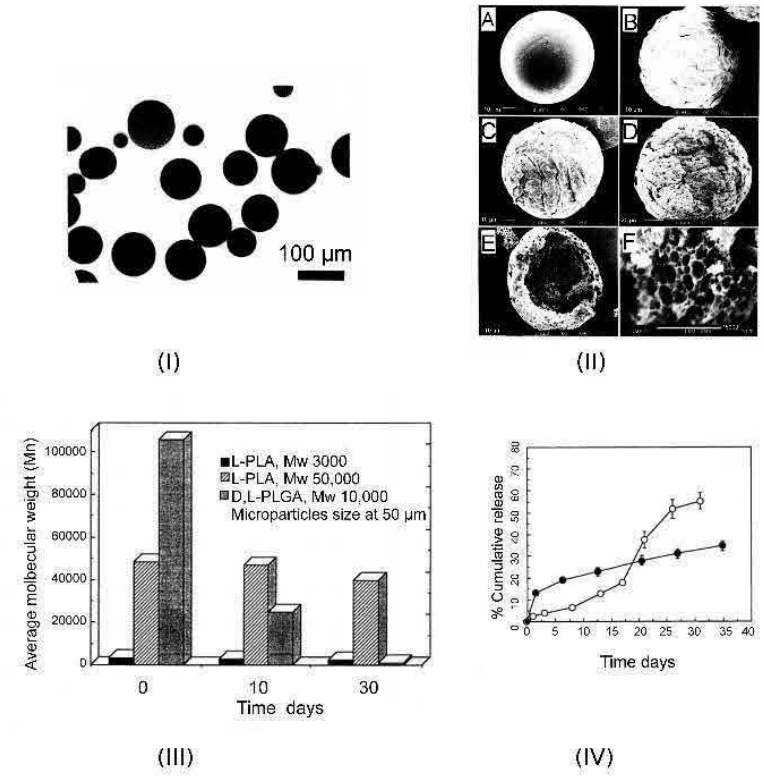

Figure 7. (I) Picture of typical PLGA microparticles synthesized with the two-step emulsification-evaporation method by phase contrast light microscopy [58]. (II) Typical degradation processes of PLGA microparticles synthesized with the two-step emulsification-evaporation methods without hydrophobic surfactant by SEM, (A) immediately after preparation, (B) after 1 day, (C) after 4 days, (D) after 7 days, (E), after 14 days (F) and after 76 days [59]. (III) Typical molecular degradation rate of microparticles synthesized with the two-step emulsification-evaporation methods between PLA and PLGA [59]. (IV) Cumulative release of tetanus toxoid from microspheres prepared with different polymers, filled symbols, PLA (Mw 3000); open symbols, PLGA (Mw 100,000)

W/O emulsions were also prepared without lipophilic surfactant. The typical degradation progress of PLGA microparticles was also expressed by a series of photos displayed in Figure 7(II). Initially, the PLGA microparticles had a smooth surface. Small micropores (diameter less that 0.1 µm) scattered all over the surface of microparticles were observed after one day, microparticles were slightly cremated, shrank due to dehydration. After 4 days in releasing medium, small pores scattered all over the microsphere size increased with time. After 14 days the microspheres were highly porous, however, it kept their spherical shape. Until 76 days, microparticles just kept porous remnants.

The influence of lipophilic surfactant, type and molecular weight of polymer has been investigated on the size and morphology of microparticles as well as on the degradation of the polymer chains. The results were presented when L-α-phosphatidylcholine, a lipophilic surfactant, was added into the oil phase, the microparticles became smaller and porous. Moreover, for higher molecular weights of polymer, bigger microparticle were obtained [56].

Degradation of polymer chain was assayed by dissolving microparticles in the organic solvent to obtain the change of molecular weight at given incubation time. However the fast degradation of PLGA chains during incubation were observed compared to the PLA chains in Figure 7(III), the proteins release curves presented opposite trends. PLGA microparticles presented slower release rate, in which only 8 wt.% of proteins in PLGA microparticles was released after 3 days compared to the 30 wt.% proteins release for PLA microparticles at the same time. It indicated that the release of protein mainly depended on the diffusion through channels in initial stage, in which the reduction in molecular weight has less influenced on the structure of microparticles. After initial stage, a critical increase of porosity induced a higher release rate (Figure 7(Iv)).Nihant et al. [34] studied the influence of different parameters on the properties of PLA microparticles. BSA was chosen as stabilizer for the inner phase. Similarly to the results obtained by Florence et al. (Figure 6), the typical three type of double emulsions were reflected in microparticles by the stabilizer concentration in the inner phase.

Yang et al. [60, 61] reported on the influence of solvent evaporation temperature on the property of PLGA microspheres during the solidification process. The process was recorded by microscope. The size and size distribution of microparticles increased with temperature. When the range of temperature was fixed from 5°C to 42°C, the size of the microparticles changed from 88 to 130 μm respectively (Figure 8(I)). It was explained that the global droplets kept the viscosity solution low during evaporation at low temperature until the critical concentration of polymer in organic solvent is reached, at which the low viscous solution transformed into solid state. Thus, low viscosity solution of droplets has ability to keep homogeneous size under shearing force. In contrast, as the microparticles rapidly transformed from a low viscosity solution to a solid state at higher temperature resulting from the to rapidly evaporation of solvent, the size and size distribution of microparticles have been significantly influenced by shearing forces induced by stirring. In addition, the morphology of microparticles was similarly investigated with different temperature. It was observed (Figure 8(II)) that the synthesized microparticles had a porous steucture. It results from the low concentration of PLGA (3% w/v) and PVA (0.05% w/v) in inner phase. More porous and thicker polymeric barriers were obtained at lower temperature, whereas the microparticles prepared at higher temperature presented a more homogeneous polymeric barrier (Figure 8(II)).

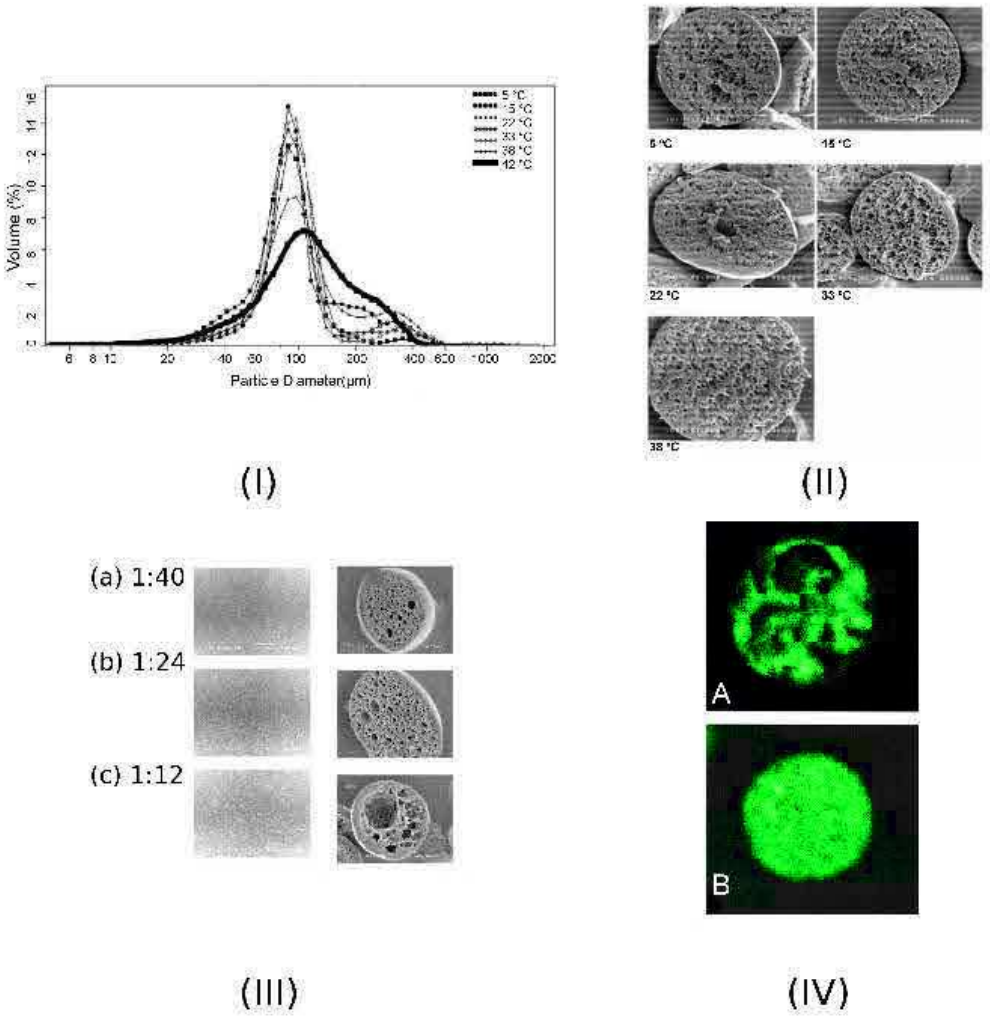

Figure 8. (I) Size distribution of PLGA microspheres with respect to the temperature during solvent evaporation [61]. (II) Surface morphology and inner structure of PLGA microparticles with different ratio of inner phase and solvent phase. 5000× The size of the bar in surface morphology is 5 μm and in inner structure is 10 μm [60]; cross-sectional of PLGA microparticles by SEM with different temperatures [61]. (IV) Effect of different concentrations of hydrophilic surfactant (PVA) in inner phase on the distribution of drug (BSA) inside PCL (Mn 10000) microparticles (A) 0.025 wt % (B) 0.1 wt % [10].

Moreover, different volume ratios of inner and middle phase were investigated, related to the structure of surface and inner structure of microparticles (Figure 8(III)). The higher ratio of inner phase and middle phase, the higher the porosity of the surface and inner network. Besides, the microparticles size increased from 61.4 to 81.9 μm with the ratio of inner phase and solvent phase. However, encapsulation efficiency has been slightly affected by the ratio, the burst release has been initially increased from 9.75 to 76.6 % at release curve, in which burst release was relate to the rapid release phenomenon in initially stage release. It was the result of releasing molecules loosely attached to the interface between particles and external phase.

When the hydrophilic surfactant PVA was added into the inner phase or outer phase, PCL was chosen as barrier materials for microparticles because more hydrophobic

property of PCL resulted in less interaction with hydrophilic surfactant compared to PLGA. The effect of PVA concentration in inner phase was investigated on the inner structure of microparticles. It was shown that low PVA concentration in inner phase (0.025%) induced more coalescence of inner water droplets with each other and formed interconnecting water channel in the inner structure of microparticles. As a consequence the encapsulation efficiency was lower (42.8 wt.%). Whereas the microspheres fabricated at a higher PVA concentration (0.5%) in the inner phase presented a more uniform encapsulated cargo distribution and higher encapsulation efficiency (70 wt.%) as shown in Figure 8(Iv) [10] (obtained by fluorescent labeling).

The size of microparticles decreased with the concentration of PVA in the external phase. Different volume ratios of inner phases and middle phase and concentrations of polymer in middle phase were studied. When a low volume of inner phase and a higher concentrated polymer solution was applied, it appeared more difficult to break bigger global droplets into small ones during the second emulsification step, resulting in an increase of the size of the microparticles.

When BSA was used as a marker to investigate the encapsulation efficiency and loading rate of microparticles, higher concentrations of BSA were found to increase the loading rate while the encapsulation efficiency was decreased, which resulted in a higher loss of BSA during the emulsification. Finally, the size of microparticles was controlled between 60-120 μm, the encapsulation efficiency was modified from 40 to70 wt.% respectively [10]. Rosca et al. [62] proposed the relation among the inner water droplets size and global droplets size and inner structure of PLGA microparticles. The different types of microparticles structures were obtained by different evolutions of the transformation from double emulsions to microparticles upon solvent evaporation.

It was found that the morphology of the microparticles depended mainly on the relation between the diameter of the inner droplets (Di) and global droplets (Dg). When Di ≈ Dg, the polymer barrier was so thin that it could not resist to the inward forces originating from the Laplace pressure and osmotic pressure between the inner and external phases. Thus this polymeric layer broke down during the solvent evaporation, the global particle cannot be created as seen in Figure 9(I) (III). When Di << Dg, the global particle was generated due to the formation of thicker polymeric barriers (Figure 9(II)). However, the diameter of the global particle resulted from all the formulation parameters: emulsification energy input, polymer concentration, surface active agent concentration, phase volumes, phase viscosities and so forth [62].

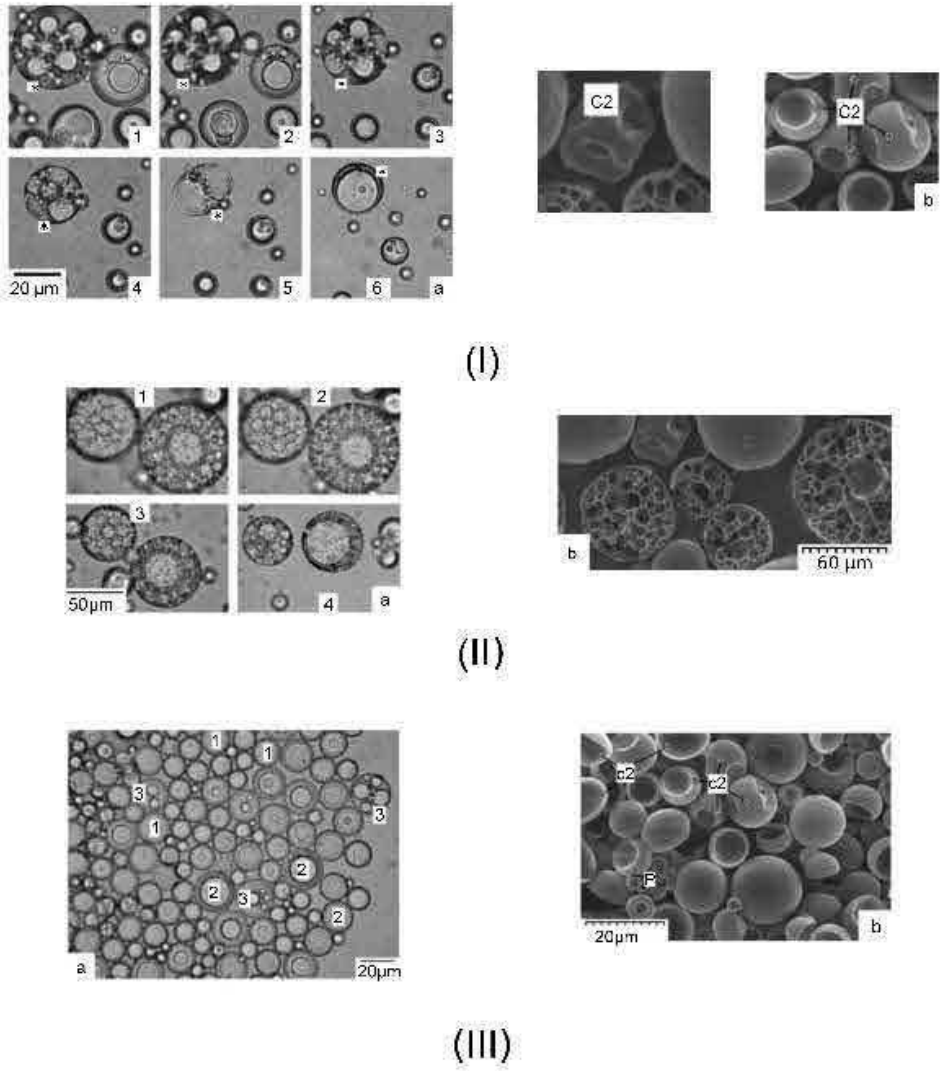

Figure 9. Evolution from double emulsions to solid PLGA microparticles and relation between the diameters of two phases and type of microparticles (I) a. Double emulsions synthesized for PLGA at 5% w/v, 1400 rpm by homogenizer for second step (II) a. Double emulsions synthesized for PLGA at 10% w/v, 1 % w/v, 500 rpm by homogenizer for second step (III) a. Double emulsions synthesized for PLGA at 5% **w/v, 1% w/v, 8000 rpm by** homogenizer for second step. All SEM micrographs b. correspond to a in left after solvent evaporation [62].

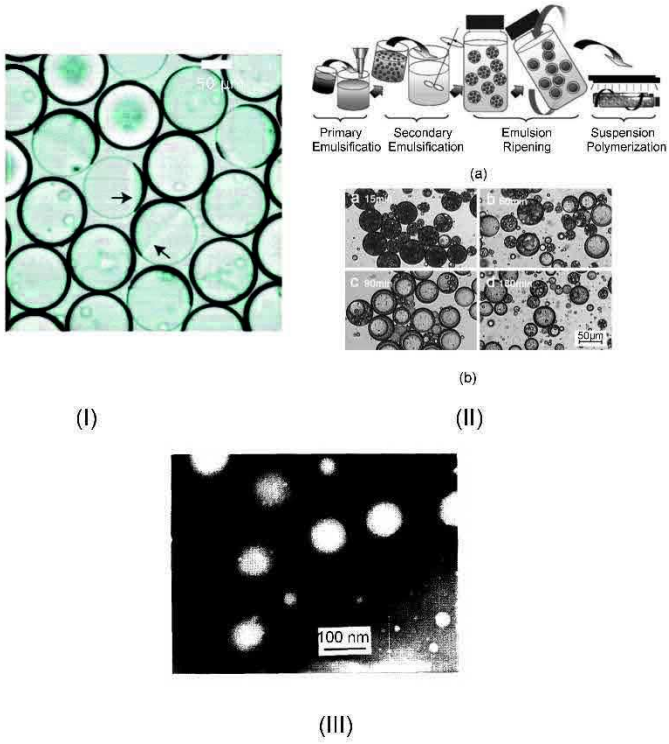

Figure 10. (I) Microcapsules synthesized by microfluidic coaxial flow method. Arrows represent the dewetting phenomenon [63]. (II) (a) Flowchart of the preparation of double emulsion templated mcirocapsules, (b) evolution of transformation of double emulsion with different ripening times [65]. (III) TEM microphotograph of typical BSA-loaded PLGA nanoparticles [66]

Though the polymeric microparticles have been synthesized by two-step emulsification method, the inner structure of the obtained polymeric microparticles remained quite complicated. It means the obtained microparticles kept a microsphere or a multivesicular structure, which have been described as the latter two classic types of double emulsions. Weitz et al. [63] firstly presented a new method to prepare homogeneous polymeric microcapsules using a microfluidic coaxial flow method by simply assembling three tubes (Figure 10(I)) . Polymeric microcapsules have been synthesized with two types of diblock polymer: polystyrene-block-poly (ethylene oxide)(PS-PEO) and PBA-PAA poly(normal-butyl acrylate)-poly(acrylic acid) [64]. The transformation from double emulsion to polymeric microparticles during evaporation of organic solvent has been followed by microscope. A dewetting phenomenon was observed during the evaporation of the organic phase. It was thought the initial formation of the polymeric barrier separated instantly from organic solvent at high concentration of polymer, from which the shape of microcapsules is based on the dewetting phenomenon. The dewetting phenomenon was clearly presented during the evaporation (Figure 10(I)) . The concentration of polymer in organic has been classified into three categories: low concentration (0.01 wt.%), middle concentration (0.1 wt/%) and high concentration (1~1.5 wt.%).Firstly it was not possible to form stable polymeric microcapsules at low concentrations. When the concentration of

polymer was increased up to the middle concentration, stable microcapsules were obtained due to the dewetting phenomenon with resolubilization of polymeric barrier. At high concentrations of polymer, the microcapsules will be formed with thicker patches due to the dewetting instability.Gao et al. [65] firstly adopted the coalescence of inner droplets after preparation of double emulsions to obtain the polymeric microcapsules by batch method, in which the method was denoted as "emulsion ripening" (Figure 10(II)). However, to prevent the droplets breaking during emulsions ripening process, the double droplets were polymerized and crosslinked with methyl methacrylate as monomer, trimethylolpropane trimethacrylate as crosslinker and Azobis(2,4-dimethylvaleronitrile) as radical photoinitiator .

Finally, the different types and physicochemical properties of polymeric microcarriers prepared by the two-step emulsification method have been shown. The effect of process parameters has been elucidated. The polymeric microcarriers as an example of water-in-barrier-in-water systems have presented the merit of the stability, biocompability and easy releasing control with the help of a biopolymer.

As the development of drug delivery and interest in nanocarriers for drug delivery and targeting were increasing, the encapsulation of hydrophilic molecules in nanocarriers has stimulated an extensive research activity. Blanco et al. firstly modified the two-step emulsification-evaporation method to get nanocarriers [66]. The typical picture of PLA nanoparticles synthesized is presented in Figure 10(III). A sonicator was used instead of the homogenization or mechanical stirring for preparation of nanoparticles during the two-step emulsification. BSA-loaded PLGA nanoparticles have thus been successfully prepared from 320 nm to 530 nm depending on the molecular weight of PLGA. It showed us the two-step emulsification has ability to produce water-in-barriers-in-water systems at the nanoscale. Tobío et al. [67] used PLA-PEG block polymer to encapsulate a model protein antigen, tetanus toxoid (TT) by two-step emulsification method. PLA-PEG polymer nanoparticle size was controlled at 142.8 nm compared with PLA nanoparticle of 153 nm.

Bonneaux et al. [68] used a two-steps sonication method to prepare double emulsions by using different molecular weights of PLA (from 1938 to 90000 Da) and by varying different process parameters. It was emphasized that using rotating evaporator did not influence the size of the nanoparticle at room temperature. Finally, the size of PLA nanoparticles reached around 200 nm. HSA (human serum albumin) was used as a marker to calculate encapsulation efficiency, which was varied from 20 to 30% by increasing volume ratio of inner phase.

As a result, different phenomena are observed for PLGA and PLA nanoparticles with respect to different molecular weights. The nanoparticles size increased with a

decrease in the molecular weight of PLA and an increase in in the molecular weight of PLGA. It was explained that the nanoparticles size depend on the property and molecular weight of polymer. PLA has more hydrophobic property than PLGA. The lower the molecular weight of PLA, the lower is the viscosity of polymer solution, and the faster is the exchange of polymer in between global droplets through the external phase. In contrast, the hydrophilic moiety of PLGA increased with the molecular weight. More hydrophilic property facilitated the exchange of the polymer in between the global droplets. Doelker et al. [69] studied the influence of sonication parameters on the preparation of nanoparticles. The exposure time and energy of sonication were systematically investigated. Simultaneously, the nanoparticles were prepared by vortex mixing instead of sonication at each emulsification step. The results were compared with the nanoparticles prepared only with sonication. It was observed that the duration of exposure time at second emulsification step has a greater influence on the nanoparticle size than at the first step emulsification. The energy of sonication has two thresholds for preparation of the nanoparticles, in which energy less than low energy threshold cannot produce nanoparticles, whereas energy higher than the second threshold will result in a high polydispersity index of nanoparticles due to the non-uniform energy dissipation. In this paper, the threshold was found between 20-65 W. Concerning the use of a vortex mixing during the first step, similar nanoparticle sizes to those produced with the sonicator were obtained. It suggested it is not necessary to use sonication for both emulsification steps. However, replacing sonication by vortex mixing at second step cannot produce individual nanoparticles as polymer aggregates were obtained. All this results support one idea, the selection of emulsification process will be more important than the variation of the other parameters [59, 70]. Fessi et al. [11] adopted polycaprolactone (PCL) to synthesize nanoparticles by two-steps of sonication with sonication (500 W, 20 kHz). They studied the influence exposure time of sonication during the first step emulsification and second step emulsification on the size of obtained polymeric nanoparticle. It presented the exposure time of sonication at first step did have not significantly influence on the size of finally nanoparticles. Whereas, the PCL nanoparticles size decreased with the exposure time of sonication during the second step emulsification. Sonication frequency, PVA concentration in the external phase, PCL concentration in the middle phase and the volume of external phase have been investigated. All these parameters in the two-step emulsification have a maximum limitation of influence on the size of particles. Over the threshold, the nanoparticles size cannot be further decreased. Finally, the smallest PCL nanoparticles were synthesize at 219 nm. Ma et al. [71] synthesized conjugated bis(□-cyclodextrin) (β-7-membered sugar ring molecular, commonly used as solubilizing agents to increase water-solubility of lipophilic compounds and enhance bioavailability of drug) into PLGA to encapsulate BSA by two-steps emulsification with sonication. It was found that the encapsulation efficiencies were ranging from 80 to 90 wt.%, which have

apparently increased compared to the encapsulated HSA PLA nanoparticles (encapsulation efficiency 20 to 30 wt.%) and encapsulated HSA PLGA nanoparticle (encapsulation efficiency at around 60 wt.%). However, the smallest size of nanoparticles was around 300 nm. It is to be noted that the nanoparticles were synthesized with sonication (30 W), bigger size might be resulting from the applied lower energy during the process.

2.2.5. Microfluidic systems

Microfluidic technologies have been widely developed over the past decades. They have been the cornerstone of intensive researches for the production of particles owing to the possibility to control finely segments of fluids. For water-in-barrier-in-water systems, due to a vigorous mixing in batch processes, the turbulent shear force resulted in a broad size distribution of the inner water droplets and double droplets. In addition, it is difficult to precisely control the number of inner droplets in the oil droplets by conventional methods [72].However, the control of the number of inner droplets is very important to control the release rate of encapsulated substance. Thus, there is an increasing interest to produce water-in-barrier-in-water systems by microfluidic methods. However, there are also some drawbacks in many aspects. A main problem of microfluidic systems comes from the need of different surface properties in microchannels. For the two-steps process, a hydrophobic surface of microchannels satisfies the requirement for the formation of W/O emulsion. Indeed it will prevent a phase inversion (water phase flowing along the wall of the device) during the first step, whereas a hydrophilic surface of microchannels is required to form the W/O/W emulsion for protecting the hydrophobic global droplets during the second process. Nisisako et al. [73] reported the formation of monodisperse double emulsions prepared by microfluidic systems with two T-shaped microchannels and Pyrex glass as chip materials, in which W/O emulsions and W/O/W emulsions were formed at a first T-shaped microchannels and second T-shaped microchannels, respectively (Figure 11(ı)).

Based on different fabrication methods and surface modification of microchannel surface, two types of chips were designed to synthesize double emulsions. The first one was a two T-shaped microchannels with different surface properties, and the second was fabricated on two separated chips joined with PTFE tubes. The surface of the first T-junction was treated to be hydrophobic by a saline-coupling agent .

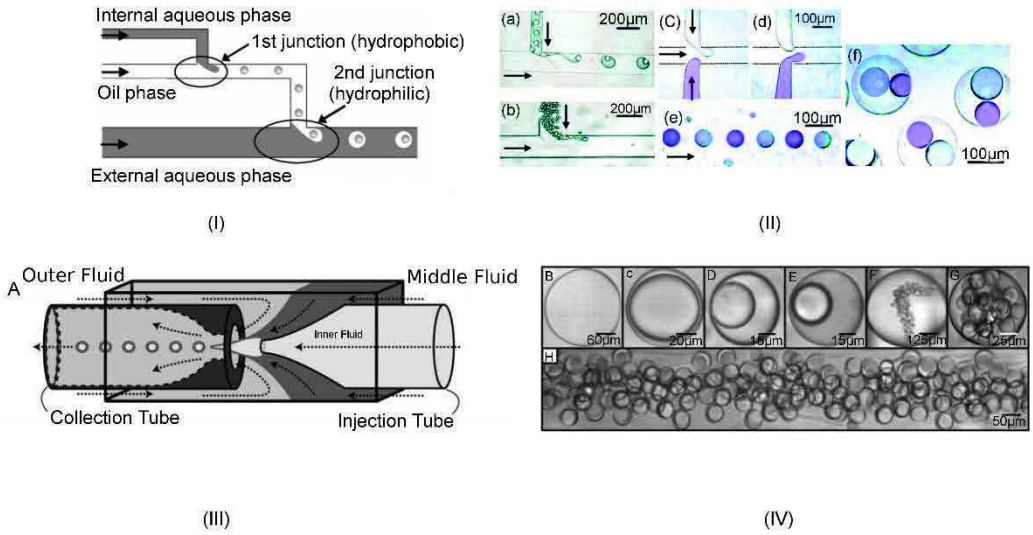

Figure 11. (I) Basic concept for preparing double emulsions (W/O/W) using T-shaped microchannels. (II) different types of double emulsion synthesized by T-junction microfluidic system [73]. (III) Schematic diagram of the coaxial microcapillary fluidic device. (IV) different types of double emulsions synthesized by coaxial microcapillary fluidic device [9]

These two types of chip have distinct advantages and drawbacks. Two T-shaped microchannels were fabricated in one chip, which resulted in the smoother connection to render a more controllable process. At the same time, one of complex partial modification of surface in microchannels was needed to satisfy the process. However, there were many efforts to achieve the purpose [74]. When two T-shaped microchannels were fabricated in separate chips, the configuration of connection introduced some disorder in the primary W/O emulsions, which brought a poor controllable process. In contrast, the modification of surface in microchannels became easier to operate. Alternately, one can prevent to modify the surface properties of a chip by employing an appropriate combination of materials. For example, poly(dimethylsiloxane) (PDMS) chips and glass chips satisfied the requirement of different surface properties. It offered the opportunity for scaling up the productivity of emulsions by removing the partial surface modification during fabrication.

As results, it was found that the number of water droplets can be controlled in one oil globule by modifying the flow rate of middle phase from 12 to 1 m/h (Figure 11(II)). The size of water droplets also were modified between 10~45 μm, and the oil globule size can be controlled between 95~220 μm.

Weitz et al. [75]designed a microfluidic systems, which adopted flow focusing and selective withdrawal technique, to synthesize double emulsions by assembling cylindrical glass capillary nested within a square glass tube (Figure 11(III)) [9]. The inner and middle phases were pumped through the capillary tube and around the

capillary respectively while the external phase was pumped through the square glass tube with opposite direction. The double emulsions were delicately formed at the entrance of the collection tube.

Through the assembly of capillaries and collection tubes of different sizes, different morphologies of double droplets can be synthesized (Figure 11(Iv)). The thickness of middle phase in the double emulsion can be also modified. In addition, the design actually prevented the device from partial surface modification. However, the low throughput is the other main drawback of microfluidic systems. To increase production rate, the parallelization of several single double droplets generators is commonly observed. Microfluidic systems have more remarkable advantages than the conventional method in the precise control of double emulsions structure [76], which is important for the preparation of multiple properties cargo and control of each phase volume fraction [77]. Different types of microfluidic systems based on the aforementioned two microfluidic systems have been developed to address different drawback in microfluidic systems. Those for the production of double emulsions have been reviewed Chong et al.[18]. Moreover, due to the easy control of the fluid elements, the preparation of double emulsions showed exceptional flexibility in obtaining other types of particles [78], such as lipid vesicles [79], mesoporous hydroxyapatite [80], polymersomes [81], microgel [82], gas-filled microparticles, nonspherical colloidosomes [83], hollow particles [84] and high-order multiple emulsions [72].

To date, for microfluidic systems, partial surface modification, and production rate were generally considered as the main problems. However, many effort have been devoted on surface modification [74, 85] and increasing production rate by different technologies such as parallel microfluidic systems [86-88].

2.2.6. General consideration of the preparation of water-in-barrier-in-water particles by two-step emulsification method

Water-in-barrier-in-water systems was prepared by two-step emulsification method, at first step, the W/O emulsion was firstly prepared by homogenization process or sonication, then W/O/W emulsions were prepared by emulsification of primary emulsion in the external phase. Different materials have been used for the barrier such as strew oil, vegetable oil or polymer. Different parameters in process and materials presented huge influence on the physicochemical and encapsulation properties of product. Discerning of the two-step emulsification method will help us to fast obtain the optimum properties of product. Regarding water-in-barrier-in-water systems as a general system, it was directly related to the two-step emulsification method and not

limited to the barrier materials. The idea will help us to find a general rule for two-step emulsification method and distinct of the water-in-barrier-in-water systems with different materials. As well-known, different applications in pharmaceutics associated different requirement of properties of these systems. For example, nanocarriers were required for targeting. Among considerable properties of water-in-barrier-in-water systems, the suitable size and size distribution are prerequisite for potential applications in pharmaceutics. These properties can influence many functions including degradation, flow properties, clearance and uptake mechanisms of carriers [89].

Considerable researches have been conducted to obtain different sizes. However, the development of now processes did not attract much attention from researchers, although it will definitely impact on final product.

The double emulsions firstly have been observed by William Seifriz [20]. Hand-shaking was used to prepare double emulsions in (Figure 12(Ⅰ)). The results presented a coarse emulsions. Thereafter, in the early stage of the development of the two-step emulsification method, double emulsions were prepared by the simple mechanical stirring or checker (Figure 12(Ⅲ), in which the detail information of equipment are presented in table 3. As such the size of the double emulsions ranged from 5 to 30 μm. The double emulsions size strongly depended on the stirring rate. When stirring rate was extremely low, for example Kawashima et al. used 390 rpm and 630 rpm to prepare W/O emulsion and W/O/W emulsions, respectively [90], the size of double emulsions was large and polydispersed (8 to90 μm, Figure 12(Ⅱ)). Exception of results from Matsumoto et al. [24], it was declared the size of synthesized double emulsion can be achieved at 2 μm by a special pin-mixer and high speed homogenization (Figure 12(Ⅵ)). However, it was thought that the result originated from the incorporation of high concentration of Span 80 (30 wt.%). Further, Kawashima et al. [90] introduced a method to decrease the polydispersiyty and large size of double emulsions, in which the double emulsions firstly synthesized by conventional method then extruding the double emulsion by porous membrane, finally the obtained double emulsion was redispersed in additional external phase (Figure 12(Ⅴ)). The size of double emulsion was decreased down to 3.64 μm. Kim et al. [91]reported double emulsions synthesized by two-step emulsification with sonication. The double emulsion size varied from 1.3~1.6 μm. Ohwaki et al. [92] claimed that the size of W/O emulsions were obtained at 100~200 nm when formulated by high pressure homogenizer. However, the prepared double emulsion after second emulsification was still in the micron range (Figure 12(Ⅳ)). Okochi et al. [93]proposed the concept of the mixed emulsification for the formation of single emulsion. The size of W/O emulsion was around 256 nm by use of a combination of sonication and homogenizer. It was concluded that producing fine and homogeneous emulsions can be reached by

combination of multi emulsification process, in which size and size distribution of emulsions can be reduced step by step. Besides, a double emulsions were synthesized by membrane emulsification method, the results presented size distribution profile of membrane method was sharper than the stirring method.

Leal-Calderon et al. [27] used a new technology to get monodisperse 400 nm W/O emulsions after coarse emulsification by mechanical mixing, which was called fractionated crystallization technique (Figure 12(v)). However, the method involved multi-purification [94]. Following the pioneering work of Talyor [95], an efficient method for producing quasi-monodisperse double emulsion by couette mixer was proposed (Figure 12(vIII)) [96].

When polyols and PGPR were incorporated in the middle phase, extremely small W/O emulsion sizes were produced by the combination of rotor-stator emulsifier and high-pressure homogenizer. The size of W/O emulsions (0.2 μm) obtained with this method was much lower compared to the W/O emulsions size of 1.8 μm produced without any polyols and that of 0.8 μm with high-pressure homogenizer without any polyols [97].

A new type of emulsification called a dual-feed process by high-pressure microfluidizer was applied to second step emulsification to obtain double emulsions. The size of the double emulsion was decreased down to 3-4 μm with an incorporation of polysaccharides and protein in external phase [43]. Yafei et al. [98] reported extremely complicated process to obtain submicron size double emulsion (0.7 to2 μm), though the production rate seemed to be excessively low since a multi-fractionation centrifugation stage was applied after each step of sequential emulsifications.

In contrast, for polymeric particles, Ogawa et al. [58] firstly introduced the two-step emulsification to encapsulate a hydrophilic drug in a polymeric microparticle matrix. Rotor-stator emulsifier and a turbine-shaped mixer were employed for the two steps. The prepared microparticles had extremely broad size distribution so that the sieves had to be used to separate the different microparticles sizes. As for the development of emulsification methods, more advanced technologies were considered for the preparation of polymeric double particles which allowed to reduce and narrow the size and size distribution of microparticles microparticles respectively [56]. Encapsulated hydrophilic molecules in nanocarriers have been also considered. Alonso et al. synthesized nanoscale polymeric particles by two-step emulsification with sonication [66]. It was found that the emulsification methods employed had a great influence on the property of double emulsions.

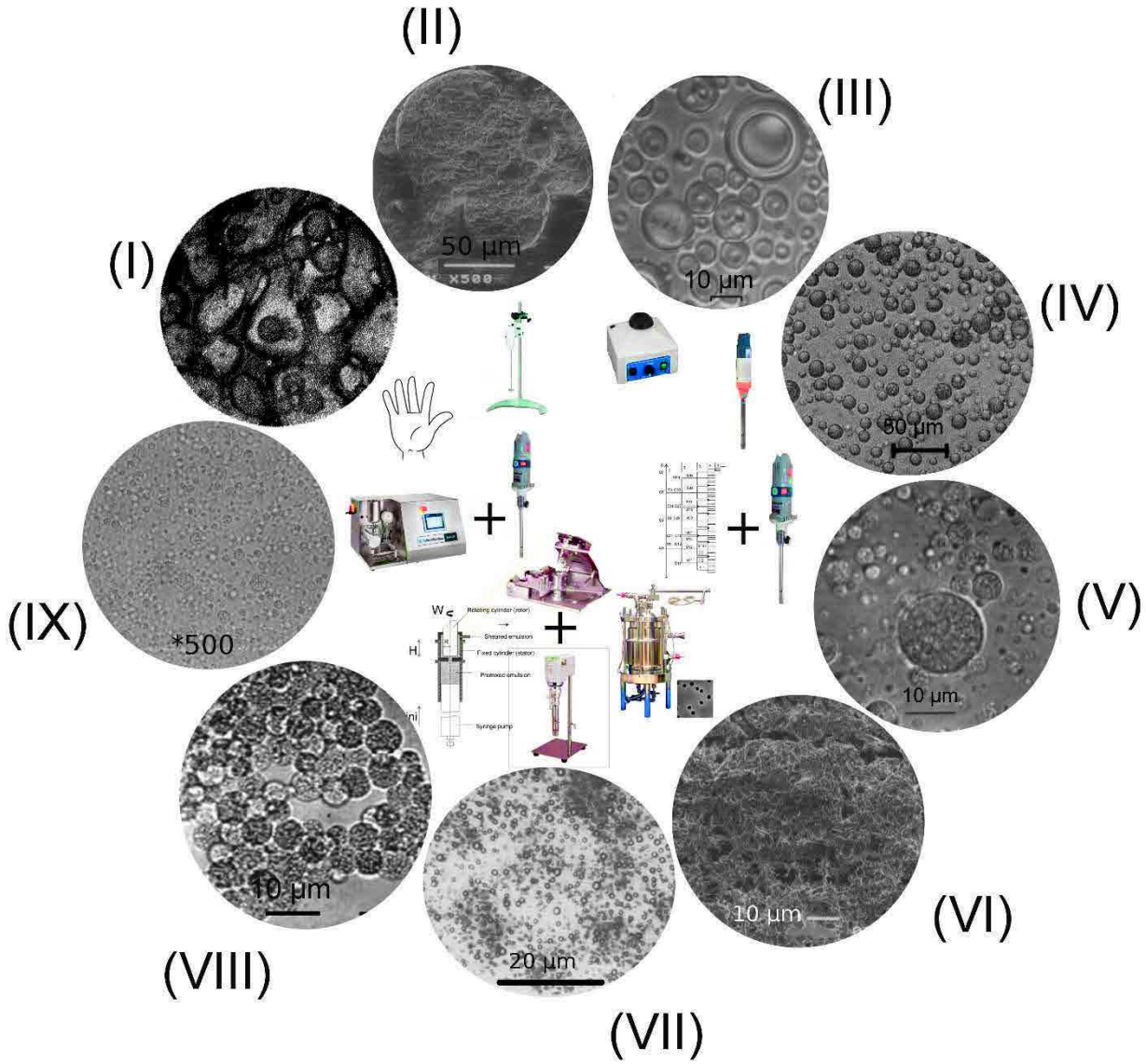

Figure 12. Evolution of relationship between water-in-barrier-in-water size and process. (I) Double emulsions synthesized by one-step emulsification with hand-shaking [20]. (II) Double emulsions synthesized by two-step emulsifications with mechanical stirring [90]. (III) Double emulsions synthesized by two-step emulsifications with small vibrating mixer [32]. (IV) Double emulsions synthesized by Ultraturrax (X1020, Ystral) [92]. (V) Double emulsions synthesized by a fractionated crystallization technique [94] and Ultraturrax [27]. (VI) Double emulsions synthesized by extrusion of a primary emulsions prepared by method (II) through a porous membrane [90]. (VII) Double emulsions synthesized with pin-mixer and Ultraturrax (Tokushu Kikakogyo Co., Japan) for W/O and W/O/W emulsions, respectively [24]. (VIII) Double emulsions synthesized by couette mixer [96]. (IX) Double emulsions synthesized by Ultraturrax and Microfludizer [36].

Recently, the advantages of microfluidic systems have completely solved the poor control drawback of the two-step emulsification method for the preparation of water-in-barrier-in-water systems of micron sizes [73]. The microfluidic systems stimulated the new prospective for a precise control of double emulsions, in which the number of water droplets included in one global droplet can be accurately controlled by the flow rate of middle phase and inner phase.

However the biggest challenge still lies in the development of efficient methods that can produce nanosized water-in-barrier-in-water systems.

2.2.7. Summary

Preparation of stable water-in-barrier-in-water systems with highly controllable sizes has become the development direction of two-step emulsification methods. However, microfluidic systems have well solved the size control problem at microscale. Furthermore, the combination of protein, polysaccharides and polymeric surfactant or pickering stabilizing agents allowed obtaining stable micronsized double emulsions. In contrast, polymeric materials tend to be the privileged strategy to obtained nanozised systems although some researchers still tried to find methods to get double nanoemulsions without polymer as barrier material [99, 100]. To avoid the destabilization of the O/W emulsion during the second step emulsification, low energy methods could be considered in conjunction with an efficient emulsification method for the first step (like the high pressure microfluidizer). Among low energy methods, the spontaneous emulsification presents some advantages. The emulsification is promoted by the addition of an external compound dissolved in the external phase (water) that will trigger the nanoemulsification and thus can be carried out under gentle stirring.

Thus it is believed that the next breakthrough in the production of double polymeric nanoemulsions may come from the combination of spontaneous emulsification and standard nanoemulsification methods.

Table 3. Information in literature for different type of water-in-barrier-in-water systems based on the two-step emulsification method

Information in literature for preparation double emulsions

Author	Published year	Oil	Emulsification Process	Encapsulated molecule	Inner phase	Oil phase	Outer phase	W/O emulsion size	Inner phase: middle phase (v/v)	W/O/W emulsion size	Primary emulsion:external phase (v/v)	Encapsulation efficieny(wt.%)
R.H. Engel	1968	Trioctanoin	Sonifier	Insulin	ZnCl2 (0.003 M) Insulin (100 u/ml) solution	Palmitic acid (0.03 M) in trioctanion	Sodium lauryl sulphate (1 w/v %) solution	/	7.2 ml : 10.8 ml	/	4.5 ml : 13.5 ml	/
Sachlo Matsumoto	1976	liquid paraffine (same as light mineral in wiki)	Pin-mixer (Aluminum-vessel 4.2 cm depth and 7.5 cm inner diameter; Stirrer, four-pins (3.9 cm length 0.26 cm diameter) rotor; 88 rpm) for W/O emulsions; Ultraturrax 100~ 12000 rpm for W/O/W emulsions	Glucose	Glucose 0.5 wt% aqueous phase	Span-80 (30 wt %) in liquid paraffin	Tween-20 0.5% aqueous solution	2 µm	72:28	about 2 µm	51:49	90.00%
A. T. Florence	1981	Isopropyl myristate	Small vibrating mixer	/	Water	Oil containing Span 80 (5 wt%)	Water containing 2% wt/wt surfactant as follows: Brij 30, Triton X-165, or a 3:1 Span 80:Tween 80 mixture.	2~3 µm	1:1	8~25 µm	1:1	/
Nissim Garti	1983	Paraffinic oil	Magnetic strring	Chloropromazin hydrochloride	Aqueous drug solution (55 mg/ml of the drug)	Paraffinic oil (containing 8-10 wt %, of oil soluble emulsifiers) The different emulsifiers were researched, 8 wt % of Brij 93 having an HLB of 4.9, or 10 wt % Span 80 + Span 85 having an HLB of 4 .	Water(3-5 wt%, emulsifier) Span 20 + Tween 80, Triethanolamine + Oleic acid (1:1 wt)	0.5~3 µm	3:7	5~15 µm	3:7	100.00%
Nissim Garti	1984	Light mineral oil	Homogenization (Silverson homogenizer) for W/O emulsions, Magnetic strring for W/O/W emulsions	NaCl	NaCl solution (1 wt %)	Brij 92 in light mineral oil	Span 20 + Tween 80 (HLB=11) glucose solution (5.5 wt%)(equalize the osmotic pressure caused by the NaCl.)	/	30 :70-x (Here, x represent the concentration of surfactant)	/	20:80-X(wt%) Here, x represent the concentration of surfactant	30.00%
A.T. Florence	1986	Isopropylmyristate	Whirlimixer	NaCl	BSA (0.05~2.0 wt %) NaCl 1.25 wt % solution	Span 80 (1~10 wt%) in isopropylmyristate	Water containing 1% w/v Tween 80 adding sorbitol to the external aqueous phase, appropriate concen-trations being calculated from its NaCl equivalent osmolarity (5.48% sorbitol = 0.9% NaCl).	2~3 µm	1:1	8~25 µm	1:1	50 ~80%
A. T. Florence	1986	Isopropylmyristate	Mechanical strring (1200 rpm) for W/O emulsions, Non-disruptive method (Whirlimixer) for W/O/W emulsions	Sulphane Blue	Crosslinked polyacrylic acid (crosslinked by allyl sucrose, of 56-68 % carboxylic acid group content was used in the complexation reaction. molecular weight approximately 3 X 10 6)were adjusted to pH 7.2-7.3 by adding 1 N NaOH) or 0.2 wt % BSA of 0.1 wt % sulphane blue solution	5% Poloxamer 331 in isopropyl myristate	aqueous hydrophilic surfactant solution	/	1;1	/	1:1	/
Kamlesh P. Oza	1989	Heavy mineral oil	Polytron Homogenization	NaCl	Avicel RC591 colloidal microcrystalline cellulose (CMCC 2 wt % or 1 wt %) solution	Span 80 (2 wt %) or Span 85 in heavy oil phase	CMCC (2 wt % or 1 wt %) dispersion	/	1:9 or 4:6	24~30 µm	1:4 or 1:1	
Yoshiaki Kawashima	1991	liquid paraffin	Mechanical strring (390 rpm) for W/O emulsions, 630 rpm for W/O/W emulsions. Prepared W/O emulsions or W/O/W emulsions is extruded by porous membranes	NaCl	NaCl 0.02 M aqueous solutions	70% (w/w) liquid paraffin and 30% (w/w) Span 80	Tween 20 (0.5 % w/v) aqueous solution	3.52 µm (Before struded membrane), 2.25 or 2.5 (After struded membrane)	5:3	8~90 µm (Before extruded by membrane) 3.64 or 4.41 (After struded membrane)	1:1	67~98 %
Takayuki Ohwaki	1993	liquid paraffin	Ultraturrax with U-shaped blade (7.3 mm diameter, 12 mm height) at bottom of a cylinder (7.8 mm internal diameter, 10.2 mm external diameter , 25000 rpm)	Secretin	Sodium alkylsulfonate in buffer(PH 6.33), sodium chloride(0~1.8 % w/v) coccine (0.2 % w/v) or Secretin (0.064 % w/v) solution	Span 80 (10% w/v) in liquid paraffin	PSML 20 (1.5% w/v) buffer solution	100~200 nm	8:5 (v/v)	14~20µm	1:1 (v/v)	/
Nissim Garti	1994	Paraffinic oil	Ultraturrax homogenizer (8000~24500) rpm, 15 min for W/O emulsions, Microfludizer for W/O/W emulsions	NaCl	NaCl solution	Span 80, STD, PG80, Or Grafted silicone lipophilic surfactant (Silicone-based poly(ethylene-glycol) copolymer in paraffinic oil, concentration of surfactant set at 10 wt %	Hydrophilic poly (siloxane)-graft-poly(oxyethylene) (Number of EO grups ranging from 7,12,16, 45, grafting dentsity or percentage of substitution, 16, 32,52 %, molecular weight 2250~13300) solution, concentration of surfactant set 2 wt %	Below 0.5 µm with narrow size distribution	3:7	4.5 µm	1:4	/
Chong-Kook Kim	1995	Liquid paraffin	Ultrasonicator	Cytarabine	Cytarabine solution	Span (30 wt %, Span 20, 80) in liquid paraffin	Tween (0.5 wt % Tween 20, 80) solution	/	2:5	1.3~1.6 µm	1:4	60~80 wt %
F. Leal-Calderon	1998	Dodecane	Machanical strring then Fractionated crystallization technique for W/O emulsions, Ultraturrax for W/O/W emulsions	NaCl	NaCl (0.1 M) in water	Span 80 in the dodecane (1:1 Weight mixture).	SDS , TTAB (0.0008 mol/l) and Tween 80 in water	400 nm	1:1 After dilluted in dodecane to 10 % by volume	10 µm polydisperse	1:9	/
Hideaki Okochi	2000	The mixture of several vegetable oils and iodo-poppy oil (Lipiodol, which is added to adjust specific gravity (1.27 g/ml).) In particular, soybean oil or isopropyl myristate was used when the drug was added .	Complex of homogenzation and Ultrasonicator for W/O emulsions, Homogenization for W/O/W emulsions (External phase was poured into the W/O emulsions)	Vancomycin (VCM)	VCM (5 % w/v) saline solution	HCO-40 (5 %) in the mixture of soybean oil (70 wt %) and Lipiodol (30 wt %)	Pluronic F-88 (0.5 wt % ~5 wt %) solution	250~500 nm	1:4	20 ~100 µm for soybean oil; aorund 15 µm for isopropyl myristate (lower viscosity compared with soybean oil)	1:1	55~90 wt %
F. Leal-Calderon	2001	Dodecane or Commercial sunflower oil (Stora)	Mechanical strring for premxing W/O emulsions and W/O/W emulsions. Then Couette-type mixer consisting of two concentric cylinders (Inner culinder of radius 20mm. Outer cylinder immoblle, Gap bwtween the stator and the rotor 100 µm) for W/O emulsions and W/O/W emulsions	NaCl	NaCl (0.2M) in water	Admul Wol 1403 (10 wt %, Polyrycinoleate of polyglycerol) , Arlacel p135 (polyethylene-30 dipolyhydroxystearate) ; Arlacel 186 (glyceryl monooleate) in oil phase	NaCl solution or glucose (0.4M) /surfactant Synperonic PE/F 68 provided (5%, Triblock copolymer of ethylene oxide (EO) and propylene oxide (PO), The average formula 75 EO/30 PO/75 EO). To increase the viscosity of the external water phase,we added a polysaccharide, alginate HF120L (2 wt%)	0.3µm	2:3~3:1	2 ~7 µm	7:3 or 3:2	95%
F. Leal-Calderon	2001	Alkane oils such as dodecane and hexadecane	Couette-type mixer consisting of two concentric cylinders (Inner culinder of radius 20mm. Outer cylinder immoblle, Gap bwtween the stator and the rotor 100 µm) for coarse W/O emulsions and high pressure jet homogenizer JH-1 for W/O/W emulsions	NaCl	NaCl (0.2M) in water	Span 80 (2 wt %) in oil phase	SDS (CMC/100, or CMC/10 CMC= 8 * 10 -3 mol/L) glucose (11.5 wt %) solution	0.36 µm	< 1:4	4 µm	< 1:4	/
Nissim Garti	2002	Mixture of mono glyceride oleate (GMO) and medium chain fatty acid trglycerides (MCT, C8~C10)	Complex of homogenzation and High pressure homogenizer (3000 atm) for W/O emulsions, High pressure Homogenizer (600 atm) for W/O/W emulsions	Vitamin B1	Glucose (16.7 wt %) aqueous phase	PGPR (11.4 wt %) in Mixture of mono glyceride oleate (GMO 2.8 wt %) and medium chain fatty acid trglycerides (MCT, C8~C10)	Whey protein isolate (WPI 2~6 wt %) and Xanthan gum (0.1 or 0.5 wt %) water solution	/	3:47 w/w	3~4 µm	1:5 w/w	60~90 wt %
Hu Gang	2006	Dodecane	Homogenizer or sonication for crude W/O emulsions prepared by machainic mixing and fractionation through centrifugation, Machanical mixing then polycarbonate membrane (0.01 to 20 µm) back and forth five times then fractionation through centrifugation	/	NaCl (0.1 M) Dextran (9 * 10 -5 M) water solution	Arlacel P 135 dodecane solution	NaCl (0.1 M) solution	0.1 µm	1:1 or 1:5	0.7 ~ 2 µm	1:10	/

Information in literature for preparation polymeric particles

Author	Published year	Solvent	Polymer	Process	Encapsulated molecule	Inner phase	Middle phase	Outer phase	Diluted phase	Inner phase: middle phase (v/v)	Primary emulsions:external phase (v/v)	double emulsion/ Dilluted emulsion (v/v)	W/O/W emulsion size	Encapsulation effeciency
Yasuaki Ogawa	1988	Dichloromethane	PLA (Mw 22500), PLGA (Mw 14000)	Homogenizer for W/O emulsions, turbine-shaped mixer for W/O/W emulsions	leuprolide acetate	Leuprolide acetate(8 % w/v) water or geltin solution	PLA or PLGA dichloromethane solution	Polyvinyl alcohol (0.5 %) solution	/	1:4	1:8	/	125,88, 74, 44, and 37 µm (The hardened microcapsules in the wet state were sized using sieves having apertures)	2~70 wt %
Robert Langer	1991	Methylene chloride	PLGA (75:25 Mw 5000, 10000, 14000)	Vortex mixer or probe sonicated for W/O emulsions. Magnetic strring for W/O/W emulsions	Fluorescein isothiocyanate-labled bovine serum albumin) (FITC-BSA) and FITC-labeled horseradish peroxidase (FITC-HRP)	Protein (20 % w/v) solution	PLGA (100 % w/v) methylene chloride solution	PVA (1 %) solution	PVA (0.1 %) solution	1:20	1:2	1:100	55-99 µm (sized using sieves with apertures of 100 µm)	60 ~90 wt%
Robert Langer	1993	Methylene chloride	PLA (Mw 3000, 50000) and PLGA (50:50 Mw 100000 Resomer RG 506)	Sonication (50 W 10 sec) for W/O emulsion, Homogenization at 15000 rpm for 10 sec	Tetanus toxoid	Tetanus toxoid solution	Polymer (PLA 20~50 % w/v PLGA 10~20 % w/v) ethylene chloride solution or Polymer lipophilic surfactant L-α-phosphatidylcholine (0.3 % w/v) in chloroform	PVA(1%) solution	PVA (0.1 %) solution	1:20	1:1	1:100	10~50µm	/
Nicole Nihant	1994	Methylene chloride	PLA (Mn 51000)	Ultraturrax for W/O emulsions, A four-pitched blade impeller (800 rpm) for W/O/W emulsions	BSA	BSA solution	PLA (9 wt %) methylene chloride with or without Pluronic F68	PVA (2.5 wt %) solution	PVA (0.1 %) PBS solution	1:5(v/g)	1:25 (v/g/v)	/	>100µm	/
M.J. Alonso	1997	Ethyl acetate	PLGA (50:50 Mw 15000 Resomer RG 502, Mw 43000 RG 503 and Mw 50000 503 H)	Sonication (15 W 15 s)	FITC-BSA	FITC-BSA (4 % w/v) solution	PLGA (20 % w/v) ethyl acetate solution	PVA (1 % w/v)	PVA (0.3 % w/v)	1:20	1:2	1:50	320 ~ 530 nm	20 wt %~70 wt % (with PVA obtained 20 wt %)
M.J. Alonso	1998	Ethyl acetate	PLA (Mn 50000) PLA-PEG (PLA Mn 45000 PEG Mn 5000)	Sonication (15 W 15 s)	Tetanus toxoid	Tetanus toxoid (10 % w/v) solution or gelatine (2 %) added as stabilizer	PLA or PLA-PEG (5 % w/v) ethyl acetate solution	Sodium cholate (1 % w/v) solution	Sodium cholate (0.3 % w/v)	1:20	1:2	1:50	130~150nm	30 ~35 wt %
F. Bonneaux	1998	Methylene chloride	Mw 90 000 , 50000 , 17400, 1	Sonication	HSA	Water or Human serum albumin (HSA 2 %) solution used as a 20% injectable solution)	PLA (2.5 wt %) methylene chloride solution	PVA (5 % w/v) solution	PVA (0.1 % w/v) solution	1:20	1:2	1:20	200±5 nm	20~30 wt %
Yi-Yan Yang	2000	Dichloromethane	LGA(65:35 Mw 40 000–75 00	Sonication for W/O emulsions, Machenic strring for W/O/W emulsions	BSA	BSA (4 % w/v) phosphate-buffered saline (PBS) (pH 7.4) solution containing PVA (0.05% w/v)	PLGA (3 % w/v) methylene chloride solution	PVA (0.05 wt %) PBS solution	640 ml PBS with 0.05% PVA	1:24	1:20	25:64	88~130 µm	58%
Eric Doelker	2003	Ethyl acetate	PLGA (50:50 Mw 34,000 Da , Resomer RG 503)	Sonicator (20~65 W 2~20 s) for W/O emulsions, Sonicator/Vortex for W/O/W emulsions	Methylene blue	Water	20 % w/v) ethyl acetate	PVA (2 %) solution	PVA (0.3 %) solution	1:20	1:2	1:5	250-350 nm	16~20%
sif Daniel Ros	2004	Dichloromethane	PLGA(50:50 Mw 45000–75000)	Homogenizer for W/O emulsion, or Homogenizer or Machenic strring W/O/W	/	PVA (1% w/v) water solution	PLGA dichloromethane solution	PVA water solution	500 ml of 0.1% w/v PVA solution	1:10	1:6	1:16	10 m	/

Information in literature for microfluidic systems

Author	Published year	Oil	Configuration of microfludic systems	Encapsulated molecule	Inner phase	Middle phase	outer phase	W/O emulsion size	W/O/W emulsion size
Takasi Nisisako	2004	Corn oil	Micro-chips which based on T-junction: One-chip and two chip One-chip module (Number represent width*depth) Type1:first junction:60*25 µm Second juntion:130*65µm;type2: 40*10 180*75,type3: 85*35 225*100 Two-chip module:80*40 (130 - 220)*90	/	Water	Lecithin (0.5 wt %) or tetraglycerin-condensed ricinoleic acid ester (1.0 wt %, CR-310) in corn oil	Sodium dodecyl sulfate or decaglycerol monostearate (0.5 wt %) water solution	52 µm (including 4.7~11.9 droplets in one oil globule)	83 µm
D. A. Weitz	2005	/	Microcapillary device. Based on coaxial flow and flow focusing, (Typical inner diameters of the tapered end of the injection tube range from 10 to 50 µm, and the orifice in the collection tube of the injection tube range from 50 to 500 µm)	/	water	Polymer (70 % can be photopolymerized Norland Optical Ahesiive) 30 % acetone or Poly(butyl acrylate)-b-poly(acrylic acid) (PBA-PAA) (2 wt%) toluene and tetrahydrofuran (7:3 v/v)	water	10 ~50 µm	50~500 µm

2.2.8. References

1. S. Sengupta, D. Eavarone, I. Capila, G. Zhao, N. Watson, T. Kiziltepe, R. Sasisekharan, Temporal targeting of tumour cells and neovasculature with a nanoscale delivery system, Nature, 436 (2005) 568-572.
2. D. Lane, Designer combination therapy, Nature Biotechnology, 24 (2006) 163-164.
3. S.S. Davis, I.M. Walker, Multiple Emulsions as Targetable Delivery System, in: Methods in Enzymology, 1987, pp. 51-64.
4. H. Hillaireau, P. Couvreur, Nanocarriers' entry into the cell: Relevance to drug delivery, Cellular and Molecular Life Sciences, 66 (2009) 2873-2896.
5. M. Petro, H. Jaffer, J. Yang, S. Kabu, V.B. Morris, V. Labhasetwar, Tissue plasminogen activator followed by antioxidant-loaded nanoparticle delivery promotes activation/mobilization of progenitor cells in infarcted rat brain, Biomaterials, 81 (2016) 169-180.
6. M. Lu, C. Zhao, Q. Wang, G. You, Y. Wang, H. Deng, G. Chen, S. Xia, B. Wang, X. Li, L. Shao, Y. Wu, L. Zhao, H. Zhou, Preparation , characterization and in vivo investigation of blood-compatible hemoglobin-loaded nanoparticles as oxygen carriers, Colloids and Surfaces B: Biointerfaces, 139 (2016) 171-179.
7. K. Pays, J. Giermanska-Kahn, B. Pouligny, J. Bibette, F. Leal-Calderon, Coalescence in surfactant-stabilized double emulsions, Langmuir, 17 (2001) 7758-7769.
8. U. Bilati, E. Allémann, E. Doelker, Nanoprecipitation versus emulsion-based techniques for the encapsulation of proteins into biodegradable nanoparticles and process-related stability issues, AAPS PharmSciTech, 6 (2005) E594-E604.
9. A.S. Utada, E. Lorenceau, D.R. Link, P.D. Kaplan, H.a. Stone, D.a. Weitz, Monodisperse double emulsions generated from a microcapillary device, Science 308 (2005) 537-541.
10. Y. Yang, Morphology, drug distribution, and in vitro release profiles of biodegradable polymeric microspheres containing protein fabricated by double-emulsion solvent extraction/evaporation method, Biomaterials, 22 (2001) 231-241.
11. M. Iqbal, J.P. Valour, H. Fessi, A. Elaissari, Preparation of biodegradable PCL particles via double emulsion evaporation method using ultrasound technique, Colloid and Polymer Science, 293 (2015) 861-873.
12. S.H. Hu, S.Y. Chen, X. Gao, Multifunctional nanocapsules for simultaneous encapsulation of hydrophilic and hydrophobic compounds and on-demand release, ACS Nano, 6 (2012) 2558-2565.
13 S. Matsumoto, M. Kohda, S.I. Murata, Preparation of lipid vesicles on the basis of a technique for providing W/O/W emulsions, Journal of Colloid And Interface Science, 62 (1977) 149-157.
14. T.M. Allen, P.R. Cullis, Liposomal drug delivery systems: From concept to clinical applications, Advanced Drug Delivery Reviews, 65 (2013) 36-48.
15. N. Garti, A. Aserin, Double emulsions stabilized by macromolecular surfactants, Advances in Colloid and Interface Science, 65 (1996) 37-69.
16. N. Garti, Progress in Stabilization and Transport Phenomena of Double Emulsions in Food Applications, Food Science & Technology, 30 (1997) 222-235.
17. M. Iqbal, N. Zafar, H. Fessi, A. Elaissari, Double emulsion solvent evaporation techniques used for drug encapsulation, International Journal of Pharmaceutics, 496 (2015) 173-190.
18. D.T. Chong, X.S. Liu, H.J. Ma, G.Y. Huang, Y.L. Han, X.Y. Cui, J.J. Yan, F. Xu, Advances in fabricating double-emulsion droplets and their biomedical applications, Microfluidics and Nanofluidics, 19 (2015) 1071-1090.
19. D.a. LaVan, T. McGuire, R. Langer, Small-scale systems for in vivo drug delivery, Nature biotechnology, 21 (2003) 1184-1191.
20. W. Seifriz, Studies in emulsions, J. Phys. Chem., (1925) 587-600.
21. A.T. Florence, D. Whitehill, Stability and Stabilization of Water-in-Oil-in-Water Multiple Emulsions, a, (1985).
22. A. Aserin, Multiple Emulsions, Wiley Subscription Services, Inc., A Wiley Company, 2007.
23. R.H. Engel, S.J. Riggi, M.J. Fahrenbach, Insulin: Intestinal absorption as Water-in-Oil-in-Water Emulsions, Nature, 219 (1968) 857-857.
24. S. Matsumoto, Y. Kita, D. Yonezawa, An attempt at preparing water-in-oil-in-water multiple-phase emulsions, Journal of Colloid And Interface Science, 57 (1976) 353-361.
25. M. Frenkel, R. Shwartz, N. Garti, Multiple emulsions. I. Stability: Inversion, apparent and weighted HLB, Journal of Colloid And Interface Science, 94 (1983) 174-178.
26. P.S. Clegg, J.W. Tavacoli, P.J. Wilde, One-step production of multiple emulsions: microfluidic, polymer-stabilized and particle-stabilized approaches, Soft Matter, 12 (2016) 998-1008.

27. M. Ficheux, L. Bonakdar, F. Leal-Calderon, J. Bibette, Some Stability Criteria for Double Emulsions, Langmuir, 14 (1998) 2702-2706.
28. N. Garti, M. Frenkel, R. Shwartz, Multiple Emulsions. Part Ii: Proposed Technique To Overcome Unpleasant Taste of Drugs, Journal of Dispersion Science and Technology, 4 (1983) 237-252.
29. S. Magdassi, M. Frenkel, N. Garti, On the Factors Affecting the Yield of Preparation and Stability of Multiple Emulsions, Journal of Dispersion Science and Technology, 5 (1984) 49-59.
30. S. Magdassi, M. Frenkel, N. Garti, R. Kasan, Multiple emulsions II: HLB shift caused by emulsifier migration to external interface, Journal of Colloid And Interface Science, 97 (1984) 374-379.
31. N. Garti, G.F. Remon, Relationship between nature of vegetable oil, emulsifier and the stability of w/o emulsion, International Journal of Food Science & Technology, 19 (1984) 711-717.
32. A.T. Florence, D. Whitehill, Some features of breakdown in water-in-oil-in-water multiple emulsions, Journal of Colloid And Interface Science, 79 (1981) 243-256.
33. J.A. Omotosho, T.K. Law, T.L. Whateley, A.T. Florence, The stabilization of w/o/w emulsions by interfacial interaction between albumin and non-ionic surfactants, Colloids and Surfaces, 20 (1986) 133-144.
34. N. Nihant, C. Schugens, C. Grandfils, R. Jerome, P. Teyssie, Polylactide microparticles prepared by double emulsion/evaporation technique. I. Effect of primary emulsion stability, in, 1994, pp. 1479-1484.
35. R. Goubran, N. Garti, Stability of water in oil emulsions using high molecular weight emulsifiers, Journal of Dispersion Science and Technology, (1988) 131-148.
36. Y. Sela, S. Magdassi, N. Garti, Polymeric surfactants based on polysiloxanes-graft-poly (oxyethylene) for stabilization of multiple emulsions, Colloids and Surfaces A: Physicochemical and Engineering Aspects, 83 (1994) 143-150.
37. A.T. Florence, D. Whitehill, Multiple W/O/W emulsions stabilized with poloxamer and acrylamide gels, Journal of Pharmacy and Pharmacology, 32 (1980) 64P-64P.
38. A.T. Florence, D. Whitehill, Stabilization of water / oil / water multiple emulsions polymerization of the aqueous phases, J. Pharm. Pharmacol, (1982) 687-691.
39. T.K. Law, T.L. Whateley, a.T. Florence, Stabilisation of w/o/w multiple emulsions by interfacial complexation of macromolecules and nonionic surfactants, Journal of Controlled Release, 3 (1986) 279-290.
40. N. Gaiti, a. Aserin, Y. Cohen, Mechanistic considerations on the release of electrolytes from multiple emulsions stabilized by BSA and nonionic surfactants, Journal of Controlled Release, 29 (1994) 41-51.
41. K. Oza, S. Frank, Multiple Emulsions Stabilized By Colloidal Microgrystalline Cellulose, Journal of Dispersion Science and Technology, 10 (1989) 163-185.
42. S.C. Yu, A. Bochot, G. Le Bas, M. Chéron, J. Mahuteau, J.L. Grossiord, M. Seiller, D. Duchêne, Effect of camphor/cyclodextrin complexation on the stability of O/W/O multiple emulsions, International Journal of Pharmaceutics, 261 (2003) 1-8.
43. A. Benichou, A. Aserin, N. Garti, Double emulsions stabilized by new molecular recognition hybrids of natural polymers, Polymers for Advanced Technologies, 13 (2002) 1019-1031.
44. a. Benichou, a. Aserin, N. Garti, Double emulsions stabilized with hybrids of natural polymers for entrapment and slow release of active matters, Advances in Colloid and Interface Science, 108-109 (2004) 29-41.
45. T.K. Law, T.L. Whateley, a.T. Florence, Multiple Emulsions Stabilized by Protein: Nonionic Surfactant Interfacial Complexation, Woodhead Publishing Limited, 2005.
46. S.M. Hodge, D. Rousseau, Continuous-phase fat crystals strongly influence water-in-oil emulsion stability, Journal of the American Oil Chemists' Society, 82 (2005) 159-164.
47. P. Sipos, I. Csoka, S. Srcic, K. Pintye-Hodi, I. Eros, Influence of preparation conditions on the properties of Eudragit microspheres produced by a double emulsion method, Drug Development Research, 64 (2005) 41-54.
48. D. Chognot, M. Leonard, J.-L. Six, E. Dellacherie, Surfactive water-soluble copolymers for the preparation of controlled surface nanoparticles by double emulsion/solvent evaporation, Colloids and Surfaces B: Biointerfaces, 51 (2006) 86-92.
49. J. Jiao, D.J. Burgess, Multiple Emulsion Stability: Pressure Balance and Interfacial Film Strength, Multiple Emulsions: Technology and Applications, (2007) 1-27.
50. A. Benichou, A. Aserin, N. Garti, W/O/W double emulsions stabilized with WPI-polysaccharide complexes, Colloids and Surfaces A: Physicochemical and Engineering Aspects, 294 (2007) 20-32.
51. R. Lutz, A. Aserin, L. Wicker, N. Garti, Double emulsions stabilized by a charged complex of modified pectin and whey protein isolate, Colloids and Surfaces B: Biointerfaces, 72 (2009) 121-127.

52. R. Lutz, A. Aserin, L. Wicker, N. Garti, Release of electrolytes from W/O/W double emulsions stabilized by a soluble complex of modified pectin and whey protein isolate, Colloids and Surfaces B: Biointerfaces, 74 (2009) 178-185.
53. H.J. Yang, I.S. Park, K. Na, Biocompatible microspheres based on acetylated polysaccharide prepared from water-in-oil-in-water (W1/O/W2) double-emulsion method for delivery of type II diabetic drug (exenatide), Colloids and Surfaces A: Physicochemical and Engineering Aspects, 340 (2009) 115-120.
54. E. Bouyer, G. Mekhloufi, V. Rosilio, J.L. Grossiord, F. Agnely, Proteins, polysaccharides, and their complexes used as stabilizers for emulsions: Alternatives to synthetic surfactants in the pharmaceutical field?, International Journal of Pharmaceutics, 436 (2012) 359-378.
55. W.L. Shanyang Lin, Zero-order or first-order release kinetics of water-in-oil-water multiple emulsion of lipiodol dependent on the types of surfactans, Biol Pharm Bull., (1992).
56. M.J. Alonso, S. Cohen, T.G. Park, R.K. Gupta, G.R. Siber, R. Langer, Determinants of Release Rate of Tetanus Vaccine from Polyester Microspheres, Pharmaceutical Research, 10 (1993) 945-953.
57. Y. Ogawa, M. Yamamoto, H. Okada, T. Yashiki, S. Tsugio, A New Technique to effciently Entrap Leuprolide Acetate into Microcapsules of Polylactic Acid or Copoly(Lactic/Glycolic) Acid, Chemical & pharmaceutical bulletin, 36 (1987) 1095-1104.
58. Y. Ogawa, M. Yamamoto, S. Takada, H. Okada, T. Shimamoto, Controlled-release of leuprolide acetate from polylactic acid or copoly(lactic/glycolic) acid microcapsules: Influence of molecular weight and copolymer ratio of polymer, Chemical & Pharmaceutical Bulletin, 36 (1988) 1502-1507.
59. S. Cohen, T. Yoshioka, M. Lucarelli, L.H. Hwang, R. Langer, Controlled delivery systems for proteins based on poly(lactic/glycolic acid) microspheres, Pharmaceutical Research, 8 (1991) 713-720.
60. Y.Y. Yang, T.S. Chung, X.L. Bai, W.K. Chan, Effect of preparation conditions on morphology and release profiles of biodegradable polymeric microspheres containing protein fabricated by double-emulsion method, Chemical Engineering Science, 55 (2000) 2223-2236.
61. Y.Y. Yang, H.H. Chia, T.S. Chung, Effect of preparation temperature on the characteristics and release profiles of PLGA microspheres containing protein fabricated by double-emulsion solvent extraction/evaporation method, Journal of Controlled Release, 69 (2000) 81-96.
62. I.D. Rosca, F. Watari, M. Uo, Microparticle formation and its mechanism in single and double emulsion solvent evaporation, Journal of Controlled Release, 99 (2004) 271-280.
63. R.C. Hayward, A.S. Utada, N. Dan, D.a. Weitz, Dewetting instability during the formation of polymersomes from block-copolymer-stabilized double emulsions, Langmuir, 22 (2006) 4457-4461.
64. E. Lorenceau, A.S. Utada, D.R. Link, G. Cristobal, M. Joanicot, D.a. Weitz, Generation of polymerosomes from double-emulsions, Langmuir, 21 (2005) 9183-9186.
65. F . Gao, Z.G. Su, P. Wang, G.H. Ma, Double emulsion templated microcapsules with single hollow cavities and thickness-controllable shells, Langmuir, 25 (2009) 3832-3838.
66. M.D. Blanco, M.J. Alonso, Development and characterization of protein-loaded poly(lactide-co-glycolide) nanospheres, European journal of Pharmaceutical and biopharmaceutics, 43 (1997) 287-294.
67. M. Tobío, R. Gref, a. Sánchez, R. Langer, M.J. Alonso, Stealth PLA-PEG nanoparticles as protein carriers for nasal administration, Pharmaceutical Research, 15 (1998) 270-275.
68. M.F. Zambaux, F. Bonneaux, R. Gref, P. Maincent, E. Dellacherie, M.J. Alonso, Influence of experimental parameters on the characteristics of poly (lactic acid) nanoparticles prepared by a double emulsion method, Journal of Controlled Release, 50 (1998) 31-40.
69. U. Bilati, E. Allémann, E. Doelker, Sonication parameters for the preparation of biodegradable nanocapsules of controlled size by the double emulsion method, Pharmaceutical development and technology, 8 (2003) 1-9.
70. M.C. Julienne, M.J. Alonso, J.P. Benoit, Preparation of poly (D,L-lactide/glycolide) nanoparticles of controlled particle size distribution: application of experimental designs, Drug development and industrial pharmacy, 8 (1992) 1063-1077.
71. H. Gao, Y. Wang, Y. Fan, J. Ma, Ethylenediamino bridged bis(β-cyclodextrin)/poly(DL-lactic-co-glycolic acid) nanoparticles prepared by modified double emulsion method: Effect of polyvinyl alcohol on nanoparticle properties, Journal of Applied Polymer Science, 107 (2008) 571-576.
72. L.Y. Chu, A.S. Utada, R.K. Shah, J.W. Kim, D.a. Weitz, Controllable monodisperse multiple emulsions, Angewandte Chemie - International Edition, 46 (2007) 8970-8974.
73. S. Okushima, T. Nisisako, T. Torii, T. Higuchi, Controlled production of monodisperse double emulsions by two-step droplet breakup in microfluidic devices, Langmuir, 20 (2004) 9905-9908.
74. Z. Bai, B. Wang, H. Chen, M. Wang, Spatial wettability patterning of glass microchips for water-in-oil-in-

water (W/O/W) double emulsion preparation, Sensors and Actuators, B: Chemical, 215 (2015) 330-336.
75. I. Cohen, H. Li, J.L. Hougland, M. Mrksich, S.R. Nagel, Using selective withdrawal to coat microparticles, Science 292 (2001) 265-267.
76. H. Hirama, T. Torii, One-to-one encapsulation based on alternating droplet generation, Scientific Reports, 5 (2015) 15196-15196.
77. C.X. Zhao, D. Chen, Y. Hui, D.a. Weitz, A.P.J. Middelberg, Stable Ultrathin-Shell Double Emulsions for Controlled Release, ChemPhysChem, 02138 (2016) 1553-1556.
78. H.C. Shum, D. Lee, I. Yoon, T. Kodger, D.A. Weitz, Double Emulsion Templated Monodisperse Phospholipid Vesicles, Langmuir, 24 (2008) 7651-7653.
79. L.R. Arriaga, S.S. Datta, S.-h. Kim, E. Amstad, T.E. Kodger, F. Monroy, D.A. Weitz, Ultrathin Shell Double Emulsion Templated Giant Unilamellar Lipid Vesicles with Controlled Microdomain Formation, Small, (2014) 950-956.
80. H.C. Shum, A. Bandyopadhyay, S. Bose, D.a. Weitz, Double emulsion droplets as microreactors for synthesis of mesoporous hydroxyapatite, Chemistry of Materials, 21 (2009) 5548-5555.
81. C.S. Ho, J.W. Kim, D.a. Weitz, Microfluidic fabrication of monodisperse biocompatible and biodegradable polymersomes with controlled permeability, Journal of the American Chemical Society, 130 (2008) 9543-9549.
82. C.-H. Choi, H. Wang, H. Lee, J.H. Kim, L. Zhang, A. Mao, D.J. Mooney, D.a. Weitz, One-step generation of cell-laden microgels using double emulsion drops with a sacrificial ultra-thin oil shell, Lab on a Chip, 16 (2016) 1549-1555.
83. D. Lee, D.a. Weitz, Nonspherical colloidosomes with multiple compartments from double emulsions, Small, 5 (2009) 1932-1935.
84. W. Wang, M.J. Zhang, R. Xie, X.J. Ju, C. Yang, C.L. Mou, D.a. Weitz, L.Y. Chu, Hole-shell microparticles from controllably evolved double emulsions, Angewandte Chemie - International Edition, 52 (2013) 8084-8087.
85. B. Thompson, C.T. Riche, N. Movsesian, K.C. Bhargava, M. Gupta, N. Malmstadt, Engineered hydrophobicity of discrete microfluidic elements for double emulsion generation, Microfluidics and Nanofluidics, 20 (2016) 1-5.
86. T. Nisisako, T. Ando, T. Hatsuzawa, High-volume production of single and compound emulsions in a microfluidic parallelization arrangement coupled with coaxial annular world-to-chip interfaces, Lab on a Chip, 12 (2012) 3426-3426.
87. L.R. Arriaga, E. Amstad, D.a. Weitz, Scalable single-step microfluidic production of single-core double emulsions with ultra-thin shells, Lab on a Chip, 15 (2015) 3335-3340.
88. M.B. Romanowsky, A.R. Abate, A. Rotem, C. Holtze, D.a. Weitz, High throughput production of single core double emulsions in a parallelized microfluidic device, Lab on a Chip, 12 (2012) 802-802.
89. J.a. Champion, Y.K. Katare, S. Mitragotri, Particle shape: A new design parameter for micro- and nanoscale drug delivery carriers, Journal of Controlled Release, 121 (2007) 3-9.
90. Y. Kawashima, I.T. Hino, H. Takeuchi, T. Niwa, K. Horibe, Shear-Induced Phase Inversion and Size Control of Water / O / Water Emulsion Droplets with Porous Membrane, Journal of Colloid and Interface Science, 145 (1991).
91. C.-k. Kim, S.-c. Kim, H.-j. Shin, K. Mi, K.-h. Oh, Y.-b. Lee, I.-j. Oh, Preparation and characterization of cytarabine-loaded W/O/W multiple emulsions, International Journal of Pharmaceutics, 124 (1995) 61-67.
92. T. Ohwaki, M. Nakamura, H. Ozawa, Y. Kawashima, T. Hino, H. Takeuchi, T. Niwa, Drug Release from the water-oil-in-water multiple emulsion in vitro. II. Effects of the addition of hydrophilic surfactants to the internal aueous compartment on the release rate of secretin, Biol Pharm Bull., 41 (1993) 741-746.
93. H. Okochi, M. Nakano, Preparation and evaluation of w/o/w type emulsions containing vancomycin, Advanced Drug Delivery Reviews, 45 (2000) 5-26.
94. J. Bibette, Depletion interactions and fractionated crystallization for polydisperse emulsion purification, Journal of Colloid And Interface Science, 147 (1991) 474-479.
95. G.I. Taylor, The formation of emulsions in definable fields of flow, Proceedings of the royal society of london. Series A, 29 (1934) 501-523.
96. J. Bibette, V. Schmitt, F. Leal-Calderon, C. Goubault, K. Pays, D. Olea, P. Gorria, J. Bibette, V. Schmitt, F. Leal-Calderon, Shear rupturing of complex fluids: Application to the preparation of quasi-monodisperse water-in-oil-in-water double emulsions, Langmuir, 17 (2001) 5184-5188.
97. A. Benichou, A. Aserin, N. Garti, Polyols, High Pressure, and Refractive Indices Equalization for Improved

Stability of W/O Emulsions for Food Applications, Journal of Dispersion Science and Technology, 22 (2001) 269-280.
98. Y. Wang, T. Zhang, G. Hu, Structural evolution of polymer-stabilized double emulsions, Langmuir, 22 (2006) 67-73.
99. J.a. Hanson, C.B. Chang, S.M. Graves, Z. Li, T.G. Mason, T.J. Deming, Nanoscale double emulsions stabilized by single-component block copolypeptides, Nature, 455 (2008) 85-88.
100. Y. Zhao, J. Zhang, Q. Wang, J. Li, B. Han, Water-in-oil-in-water double nanoemulsion induced by CO(2), Physical chemistry chemical physics, 13 (2011) 684-689.

CHAPTER 3

POLYMERIC NANOCARRIERS PRODUCED BY MICROFLUIDIC METHODS

Preface

In the literature background chapter, it was reported the great potential of polymeric nanoparticles as drug delivery and contrast agent carriers. It was also mention that nanoprecipitation is an effective method to produce pure drug or polymeric nanoparticles. Coupled with the use of a micromixer, this method has the capability to solve the inherent problem of size reproducibility and constant quality encountered with conventional batch-type reactors. For practical reasons which include long-term storage and handling easiness, the colloidal suspension of polymeric nanoparticles produced by micromixer-assisted nanoprecipitation processes should be converted into dry-state nanoparticles.

Thus, in the next section, a new two-step procedure was developed to produce drug-loaded dry-state nanoparticles by combining micromixer-assisted nanoprecipitation and spray drying. Different micromixing principles will be investigated for the first time and their effect on nanoparticles size will be assessed. The possible alteration of nanoparticles properties (e.g. size and drug release profile) upon drying process will be also studied.

This chapter is partially adapted from the two following articles:

(1) Shukai Ding, Christophe A. Serra, Wei Yu, Nicolas Anton and Thierry F. Vandamme, Production of dry-state ketoprofen-encapsulated PMMA NPs by coupling micromixer-assisted nanoprecipitation and spray drying, ***in preparation****.*

(2) Shukai Ding, Mohamed F. Attia, Justine Wallyn, Christophe A. Serra, Nicolas Anton, Wei Yu and Thierry F. Vandamme, Microfluidic-assisted production of SPIONs-encapsulated PMMA nanoparticles, ***in preparation****.*

3.1 Production of dry-state ketoprofen-encapsulated PMMA NPs by coupling micromixer-assisted nanoprecipitation and spray drying

ABSTRACT

We present a two-step process to produce dry-state Ketoprofen-loaded poly(methyl methacrylate) nanoparticles (NPs) with controllable size and tunable drug release profile. A colloidal suspension of drug-loaded nanoparticles was first obtained from a micromixer-assisted nanoprecipitation process and then transferred into a commercial spray dryer. After the first step, highly monomodal NPs in the size range 100 to 210 nm were obtained as seen by the low polydispersity index value (ca. PDI ~ 0.2) returned by a dynamic light scattering detector. Physicochemical properties, encapsulation efficiency/ratio and drug release kinetics of NPs before and after drying were determined. Results showed that the NPs size was not significantly affected by the spray drying while encapsulation parameters and drug release rate were slightly decreased compared to the non spray-dried NPs. A sustained drug release was observed over 6 hours and the drug release rate (up to 70%) was found to vary with the size of the NPs which in turn is a function of the flow rate ratio between the polymer solution and the non-solvent-solution.

3.1.1 Introduction

During the last two decades, nanoparticles (NPs) have received an enormous attention due to their unique properties and are now used for many applications in pharmaceutics [1-4]. Thus, pure drug NPs are found to significantly increase dissolution rate [5] while drug-loaded polymeric NPs improve the stability and release properties of drug, owing to their tailored compositions and functionalities as well as the possibility to use of biodegradable materials [6,7]. However, discrepancies in NPs

quality from batch to batch operations still hamper further industrial development of drug-loaded NPs. Continuous-flow processes are usually associated to constant quality and thus represent an attractive alternative to batch operations.

Significant efforts have been imparted to prepare drug-loaded polymeric NPs by different methods such as emulsification-solvent evaporation [8], salting-out [9] or nanoprecipitation [10]. The latter is probably the simplest, fastest and more reproducible method and allows the production of stable colloidal suspensions of NPs (also called nanosuspensions) [11]. The first NPs prepared through this method were obtained by Fessi and coll. in 1989 [10]. The precipitation of a structure material, like polymer or drug, by mixing two streams of a solvent and non-solvent solution is the main principle driving the nanoprecipitation process. As such, the solvent should be miscible with the non-solvent while the structure material should be free-soluble in the solvent and insoluble in the non-solvent. Quality of the obtained NPs, mainly size and size distribution, is highly affected by the diffusion rate of the solvent into the non-solvent solution as well as by their relative flow rates and concentration of the structure material in solvent solution [12].

Recently microfluidics, the science and technology which allows manipulating nanoliter volumes in microscale fluidic channels, has become an enabling method to improve and accelerate the mixing performance in chemical processes [13-15]. It has thus driven many research groups to use microfluidic systems to prepare NPs [16,17,18]. Results have demonstrated that the quality of the obtained NPs was significantly better than those originating from non-microfluidic systems, e.g. smaller NPs sizes with much narrower size distributions. Thus microfluidic devices present a tremendous potential for the continuous-flow production of high quality NPs [19]. However when it comes to prepare pure drug or drug loaded polymer NPs, end-usage may request to store/transport the NPS before application.

To prevent a cost-intensive transportation and to ensure stability of the NPs on a long time, dry-state NPs may represent the best option. Therefore, once prepared, NPs

should be efficiently recovered and dried. There are two methods for drying a nanosuspension. The first one is the freezing drying technique [12,13]. This method is: i) time consuming due to a three-step procedure (freezing, primary and secondary drying), ii) highly energy demanding, iii) well adapted to water-based nanosuspensions and iv) scarcely operated in continuous-flow conditions. On this other hand, one can rely on the spray drying method to obtain dry-state NPs [20-25]. This is an extremely fast process since the nanosuspension's continuous phase (liquid) will be instantaneously evaporated. Furthermore, this method is much less time consuming that the previous one and can be operated continuously.

Lee *et al.* [20] and Li *et al.* [23] have prepared NPs of different sizes using a commercial nano spray dryer B-90 (Büchi) which comprises a piezoelectric-actuated steel membrane and an electrostatic collector. However, prior to spray drying, the NPs suspension needs to be filtered with a 0.45 μm filter to prevent the membrane fouling. Lee *et al.* used an aqueous solution of bovine serum albumin (BSA, hydrophilic property) as a model drug and Tween 80 as a crystal inhibitor. After drying, they obtained NPs whose size varied from 540 to 2609 nm. Li *et al.* also used the B-90 spray dryer to prepare different NPs such as sodium chloride (table salt, 517 to 993 nm), Furosemide (drug, 1.24 μm), pure wall materials (e.g. Arabic gum, whey protein, polyvinyl alcohol, Maltodextrin, 141 to 729 nm) but found that the particle size distributions were quite large as seen by SEM micrographs. In addition, authors prepared dried NPs from a 85 nm nanoemulsion (PDI=0.017) obtained by the spontaneous emulsification method using Vitamin E Acetate (VEA) as the oil phase and distilled water as the continuous phase. The nanoemulsion was first mixed with different pure wall materials and then dried using the B-90 spray dryer which ultimately led to NPs with a solid shell (pure wall material) and a liquid core composed of VEA. Unfortunately after drying, authors found that the re-dispersed nanoparticles had a higher size and a larger particle size distribution compared to the original VEA nanodroplets. The least increase was obtained with Maltodextrin for which 141 nm NPs were collected (PDI=0.167). This emphasizes that the nature of the

pure wall materials has a significant effect on the dried-state NPs features. Few years before, Freitas *et al.* [22] made the same observation when using a commercial mini spray-dryer 190 (Büchi) to prepare different types of dried solid lipid NPs. They found that the nature and concentration of the lipid (Cetylpalmitate, Compritol, Synchrowax) as well as the nature of pure wall materials (Mannitol, Lactose, Trehalose) played an important role on the property of re-dispersed NPs. Chaubal *et al.* [24] similarly concluded that Mannitol allowed the production of a dry-state Itraconazole powder that was flowable and easily re-dispersed.

A microfluidic spray dryer was developed by Weitz and coll. [21]. The setup was fabricated by poly(dimethylsiloxane) (PDMS) replication from a negative pattern engraved in a silicon wafer. Due to the intrinsic PDMS hydrophobicity, the microchannel had to be treated by oxygen plasma to prevent fouling, although the effect decreased over time. In addition, the setup was only designed for obtaining small amounts of product (solvent flow rate at 1-5 mL/hr). They injected a solution of poly(vinyl pyrrolidone) and Danazol (1.5 wt.%) into their device and obtained 4 µm droplets of drug/solvent. Upon evaporation at room temperature of the solvent, they finally got pure drug NPs (20 to 60 nm). Recently, they designed a new microfluidic device aiming at producing dried NPs by supersonic air speed reaching up to 600 m/s [25]. This PDMS-made nebulator was composed of six gas inlets positioned on either side of a main microchannel connected to two liquid inlets. Different compounds have been tested including CaCO3 NPs (20 nm), NaCl NPs (less than 15 nm) and Danazol NPs (20 to 40 nm). Nanoparticles can also be obtained with a microfluidic device promoting surface acoustic waves (SAW). This device was composed of a pair of aluminum-chromium interdigital transducers (IDTs) fabricated onto a 128° y-cut x-propagating lithium niobate (LiNbO3) piezoelectric substrate surface. Thus, mechanical oscillations can be produced by inverse piezoelectric effect resulting from a high frequency electrical signal delivered to the IDTs. As a result, a surface wave is generated and impacts a micron size droplet deposited on the substrate leading to its atomization into multiple nanodroplets. Higuchi *et al.* firstly applied SAW to fabricate

a pocket-size atomizer in 1995 [26]. Then, Friend *et al.* used it to synthesize poly(caprolactone) NPs (150-200 nm) [27]. Although the device can be operated continuously, the throughput is quite low (0.24 g/hr).

Although more efficient than conventional spray dryers in controlling the size of the dry-state NPs (lower sizes and narrower size distributions), these microfluidic devices suffer from a rather complicated microfabrication procedure and/or extremely low yields. Thus conventional spray-dryer seems still the best option for producing large amount of dried NPs. To solve for the large size distribution of NPs they suffer from, one may think to spray-dry a polymer nanosuspension instead of a structure material dissolved in a solvent. To that extent, this paper proposes to combine the advantages of micromixer-assisted nanoprecipitation in controlling the size of drug-loaded polymeric NPs and the possibility to obtained dry-state nanocarriers by conventional spray drying for storage and further re-dispersion before use. In particular several micromixers operating upon different mixing principles will be investigated in light of the NPs size and size distribution. Also, the effects of spray-drying on re-dispersed nanocarriers properties (encapsulation ratio and efficiency, drug release profile) will be assessed and compared with those of non spray-dried NPs.

3.1.2 Materials and procedure

3.1.2.1 Materials

Ketoprofen (as a hyhrophobic model drug, KP), Mannitol (a versatile stable excipient) and Cremophor ELP (a nonionic surfactant) were kindly gifted by Amoli Organics Ltd. (Mumbai, India), Roquette (Strasbourg, France) and Laserson (Etampes, France) respectively and used as received. Cremophor ELP is a polyoxiethylated castor oil with a number of ethylene oxide groups around 35, and has a molecular about 1,500 g/mol. This surfactant is a mixture of different oligomers of molecular weights following a poisson-like distribution centered on the one announced by the

manufacturer. This amphiphilic compound exhibits a hydrophilic–lipophilic balance (HLB) of about 12-14, and creates a stabilizing PEG-layer surrounding the polymeric NPs from their hydrophilic PEG moities. Methanol, tetrahydrofuran (THF), sodium dodecyl sulfate (SDS) were purchased from Sigma-Aldrich (Saint-Louis, USA) and Mannitol 90 from Roquette (Beinheim, France) All other chemicals (methyl methacrylate, copper (I) bromide, 1,1,4,7,10,10-hexamethyltriethylenetetramine, 2-ethyl bromoisobutyrate) used for the synthesis of the polymer were purchased from Sigma-Aldrich (Saint-Louis, USA) and used as received except 2-ethyl bromoisobutyrate initiator, which was distilled under vacuum prior to use and methyl methacrylate, which was passed through an alumina column, from Merck (Darmstadt, Germany) to remove inhibitors. Ultrapure water was obtained using the MilliQ filtration system (Millipore, Saint-Quentin-en-Yvelines, France).

3.1.2.2 Synthesis and characterization of poly(methyl methacrylate)

Poly(methyl methacrylate) (PMMA) was synthesized following the procedure reported in a previous paper [11]. In brief, PMMA was obtained by atom transfer radical polymerization (ATRP). Reagents include methyl methacrylate as monomer, copper (I) bromide as catalysis, 1,1,4,7,10,10-hexamethyltriethylenetetramine ligand. The reaction was carried out for 1.5 hrs in THF at 60°C in a magnetically stirred round bottom flask under a nitrogen atmosphere. Then the obtained polymer solution was filtrated through an alumina column to remove catalyst and poured in a large volume of methanol to precipitate PMMA. Dry state polymer was finally obtained after overnight vacuum at 30°C. PMMA was analyzed by gel permeation chromatography (PL-GPC 120 platform, Polymer Laboratories, Church Stretton, UK) in THF (at a flow rate of 1 mL/min at 35°C). The number-average molecular weight of the synthesized polymer was 15,500 g/mol (Đ = 1.37).

3.1.2.3 Preparation of nanosuspensions by micromixer-assisted nanoprecipitation

Purified PMMA (1 wt.%) was firstly dissolved in THF admixed with Cremophor ELP (0.5 wt.%) and required amount of Ketoprofen (0.5 wt.%). The resulting mixture (polymer solution) and non-solvent solution (Ultrapure water) were pumped separately by two 307 HPLC pumps (Gilson, Paris, France) at flow rates varying from 3 to 7 mL/min (Figure 1a,b), and mixed within different micromixers (Figure 1c,d,e). Nanoprecipitation started right away within the mixing chamber of the micromixers when both fluids were brought into contact. The resulting colloidal suspension of PMMA NPs was then directly collected at the outlet of the micromixers.

Three different micromixers operating under different mixing principles were employed (Table 1) and properties of the produced NPs were compared for the same operating parameters (concentrations and flow rates). First a 90° angle Y-type micromixer, i.e. a T-junction micromixer (SS-100-3, Paris Fluides Systèmes Technologies, Courtaboeuf, France) was used to mix polymer and non-solvent solutions (Figure 1c). This micromixer puts into contact a single stream of both fluids and relies on molecular diffusion to promote an efficient mixing in the outlet channel when its size is large and/or flow rates are rather low (i.e. in laminar regime, our case). A high pressure interdigital multilamination micromixer (HPIMM, IMM, Mainz, Germany) was also employed, in which molecular diffusion also contributes mainly to the mixing performance of polymer and non-solvent solutions. In such system, each inlet stream is split into 15 sub-streams of small width in staggered arrangement. Diffusion operates downstream in the flow focusing section (not represented in Figure 1d). Combination of molecular diffusion and high energy seems the best approach for high productivity and low nanoparticles sizes 19. Such combination was brought by the K-M impact jet micromixer (Fujifilm Corporation, Kyoto, Japan) introduced by Mae and coworkers [28,29]. The structure consists of three steel plates, namely the inlet, mixing and outlet plates. The two inlet streams are first split into 3 sub-streams thanks to microchannels. The resulting flows then converge to a single pin hole where

they are mixed as a result of their frontal collision. Finally the resulting mixture flows in the outlet microchannel of the last plate.

Table 1. Micromixers' characteristics

Type of micromixer	Y-type	HPIMM	K-M
Working principle	Molecular diffusion	Molecular diffusion	Impact mixing
Number of channels per inlet stream	1	15	3
Outlet channel width (w, µm)	-	45	-
Outlet channel height (h, µm)	-	60	-
Outlet channel diameter (µm)	1680	-	300

3.1.2.4 Reynolds numbers

Micromixers mixing efficiency will be discussed as a function of the Reynolds numbers achieved in the outlet of the devices for the different non-solvent (water) flow rates investigated (Table 2). Since the outlet channel of the HPIMM micromixer is not cylindrical, the Reynolds number has to be expressed as a function of the hydraulic diameter. The expression of the density and viscosity of the exiting fluid should also take into account the excess molar viscosity and volume of the THF-water mixture as well as the increase in density of the THF solution due to the addition of the polymer, surfactant and drug. For the detailed calculations, the reader may refer to the supporting information.

Table 2. Reynolds numbers in the outlet microchannel of the three micromixers for different water flow rates.

Type of micromixers	Water flow rate (mL/min)				
	3	4	5	6	7
T-Junction micromixer	39	52	67	81	96
HPIMM micromixer	33	44	56	68	81
K-M micromixer	218	291	373	456	540

Flow rate of the polymer solution was kept constant to1 mL/min

3.1.2.5 Production of dry-state NPs by spray drying

Once recovered, the nanosuspensions were left overnight in a fume hood at room temperature to remove THF. Then, the solvent-free solutions were admixed with Mannitol (5 wt.%) and SDS (0.3 wt.%) to prevent NPs from aggregation during spray drying (Figure 1f). The formulated nanosuspensions were finally dried with a mini spray dryer (B-290, Büchi, Rungis, France) under the following conditions: inlet temperature at 100°C, outlet temperature at 50°C, aspirator flow rate at 100%, inlet flow rate at 10% (Figure 1g). After spray drying, the dry state NPs were collected (Figure 1h) and stored in a dry atmosphere to prevent hygroscopic recovery.

3.1.2.6 Physicochemical and encapsulation properties of drug-loaded PMMA NPs

The size and size distribution of the NPs were assessed by dynamic light scattering (DLS) using a Malvern Nano ZS instrument (Malvern, Orsay, France). The helium-neon laser (4 mW) was operated at 633 nm, the scatter angle was fixed at 173° and the sample temperature was maintained at 25°C. The polydispersity index of the particle size distribution (PDI) is a measure of the broadness of the size distribution and it is commonly admitted that PDI values below 0.2 corresponds to monomodal distributions. Measurements of nanosuspensions size were performed in triplicates by pouring 0.02 mL of the nanosuspension into 1 mL of Ultrapure water. A given amount of dry-state NPs was completely re-dispersed in ultrapure water so as to get the same NPs concentration before spray drying. Then the resulting suspension was sonicated for 5 min at 35 kHz (89202, Biolock Scientific). Finally the size of NPs was determined following the same protocol as for non spray-dried NPs.

Ketoprofen quantification was performed by UV spectrophotometry with a Schimadzu UV-2401 PC spectrophotometer (Kyoto, Japan). A calibration curve was first obtained by plotting different known concentrations of Ketoprofen as a function of the peak intensity at 259 nm. Encapsulation ratio and efficiency were determined as follows: for nanosuspensions, once THF was removed from the suspension, 10 mL was taken to

remove the non-encapsulated Ketoprofen by ultracentrifugation (Optima L-90 K Ultracentrifuge, Rotor Type 90 Ti, Beckman Coulter, Paris, France) at 45,000 rpm and 23°C. The supernatant was used to measure encapsulation efficiency (EE) and encapsulation ratio (ER) accordingly to the two following equations:

$$\mathbf{EE} = \frac{m_{KP}^{tot} - m_{KP}^{super}}{m_{KP}^{tot}} \quad \text{Eq. 1}$$

$$\mathbf{ER} = \frac{m_{KP}^{tot} - m_{KP}^{super}}{m_{KP}^{tot} - m_{KP}^{super} + m_{Polym}^{NPs}} \quad \text{Eq. 2}$$

where m_{KP}^{tot} and m_{KP}^{super} represent the mass concentration of KP in the initial formulation and in the supernatant respectively. The numerator of the right hand part of Eq. 1 is the mass of KP encapsulated in PMMA NPs per volume of sample (10 mL). m_{Polym}^{NPs} is the theoretical mass concentration of polymer in the sample based on the initial amount of polymer used in the formulation. Thus EE and ER represent the total mass fraction of initial KP encapsulated and the mass fraction of KP per nanoparticle respectively. For dry-state NPs, the same procedure was applied once the NPs were completely re-dispersed in ultrapure water as for size determination by DLS measurements.

Release experiments of KP were performed by charging a dialysis tubing (diameter 16 mm, MWCO 12-14 kDa, Medicell Internatioannal, London, UK) with 10 mL of an original or re-dispersed NPs suspension. Then the dialysis tubing was immersed in a 250 mL phosphate buffered saline solution (pH=7.4, C=0.1M) gently stirred magnetically at 37°C. At predetermined time points, the solution was sampled (aliquots of 3 mL) and replaced by the same volume of fresh PBS to ensure sink conditions. Mass of KP in the aliquots was determined as previously described by UV spectrophotometry.

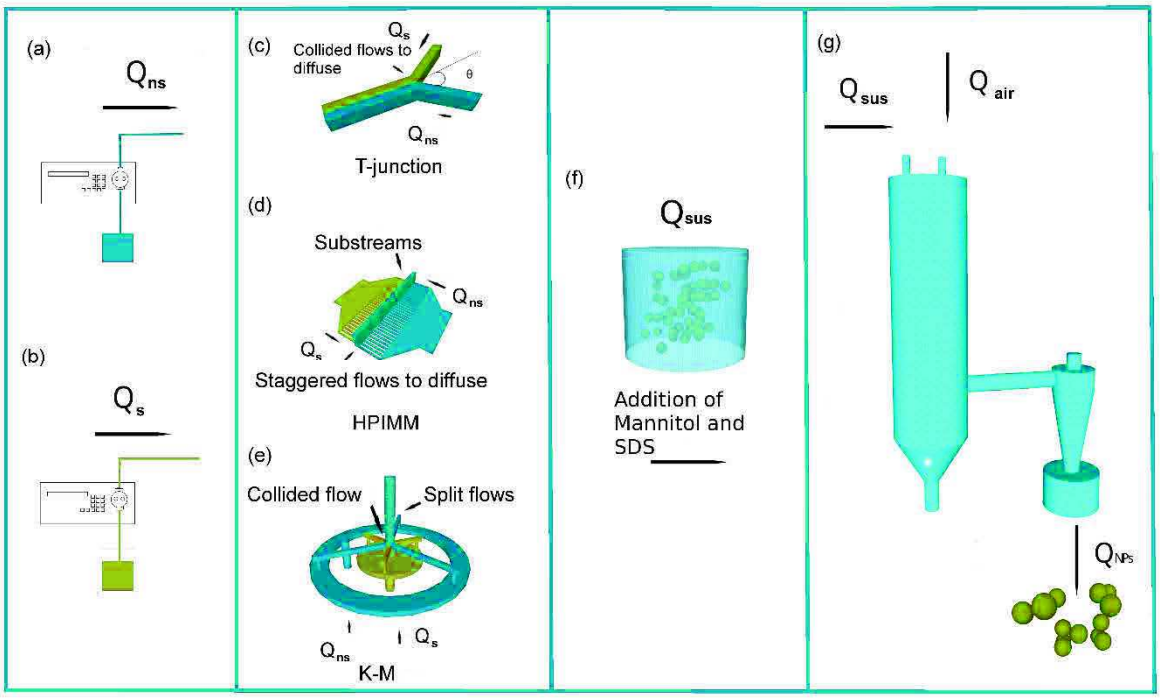

Figure 1. Schematic drawing of the whole two-step process to produce dry-state Ketoprofen-loaded PMMA NPs. Pumps for non-solvent (a) and polymer (b) solutions; T-junction (c), HPIMM (d) and K-M (e) micromixers; nanosuspension after nanoprecipitation (f); spray dryer (g). Q_s, Q_{ns}, Q_{sus}, Q_{air} and Q_{NPs} being the flow rate of the solvent (i.e. polymer solution), the polymer non-solvent, the nanosuspension, the spray drier air and the dried nanoparticles respectively.

3.1.3 Results and discussion

3.1.3.1 PMMA NPs

Unloaded PMMA nanoparticles have been synthesized with the aforementioned three micromixers for different water flows rate at a constant polymer feeding rate of 1 mL/min (Figure 2). It observed that whatever the micromixer used, the NPs size decreased when the water flow rate was increased. The T-junction micromixer always gave the biggest NPs with the highest PDI values. Although HPIMM and KM micromixers gave similar sizes at low water flow rates, the later achieved the production of the smallest and globally more monodispersed NPs at high water flow rates.

The key point for controlling NPs size in the microfluidic-assisted nanoprecipitation process is how fast operates the mixing between the polymer solution and the non-solvent solution. According to the nucleation and growth mechanism, the faster the mixing, the faster the polymer reaches a supersaturation state which induces its precipitation into a higher number of nuclei which then start to grow by adsorbing new macromolecules. As a result, lower size NPs are obtained providing that nuclei and nanoparticles aggregation are prevented [18,30,31,32,33,34,35]. Aggregation can be prevented by the surface adsorption of surfactant molecules [36]. In the present work, we used Cremophor ELP (a type of hydrophilic surfactant) to achieve stability of NPs. The decrease in NPs size with respect to the non-solvent flow rate is thus attributed to an enhanced and faster mixing due to a higher kinetic energy embarked by the water phase when its flow rate is increased.

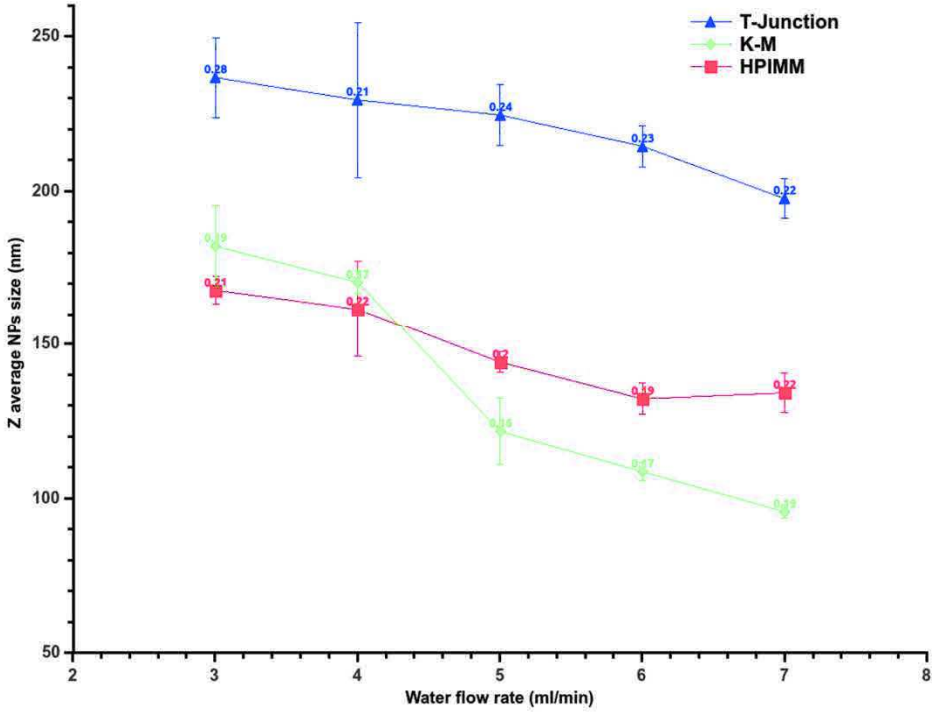

Figure 2. Effect of the water flow rate on the size of unloaded PMMA NPs for the three different micromixers. The polymer solution flow rate was fixed at 1 mL/min. Numbers represent the PDI value of each data point.

However, at fixed flow rates, the NPs size is also function of the flow condition promoted by the micromixer. In the mixing chamber of the micromixer, the size will

thus depend on how homogeneous is the mixing (i.e. how homogeneous is the nucleation) whereas at the micromixer outlet it will depend mainly whether the flow condition favors the growth of nuclei and/or NPs aggregation. One can consider that a rapid intermeshing of the streamlines of polymer and non-solvent solutions in the whole volume of the mixing chamber (i.e. at the place where the two fluids are put into contact) will favor a homogeneous nucleation as well as the rapid adsorption of surfactant molecules on the nuclei to further prevent aggregation. On the opposite, if the streamlines are not or weakly interpenetrated, the nucleation rate will be low. In the micromixer outlet, the former situation will favor nanoparticles aggregation while in the later situation the nanoparticles growth will be favored. To that extent, the best situation to get the smallest nanoparticles would be to have a strong intermeshing of the streamlines in the mixing chamber and a weakly intermeshing in the micromixer outlet.

For a T-Junction micromixer, Engler *et al.* [37] have numerically simulated the flow condition as a function of the Reynolds number (Re). They found (Figure S1) a stratified flow at low Re (around 7) for which the streamlines do not interpenetrate. When Re is increased up to 60, they observed a so-called vortex flow for which the streamlines bend with weak intermeshing. However when the Re is further increased (above 200), the streamlines start to strongly interpenetrate and give rise to the so-called engulfment flow. Considering the Re numbers for the T-junction micromixer reported in Table 2, at the best, the engulfment flow is obtained which explains the high NPs sizes that are produced with this micromixer.

For the HPIMM micromixer, the Reynolds number which are calculated for the different water flow rates are lower than those obtained for the T-junction micromixer (Table 2). However, this micromixer allowed producing lower NPs sizes (Figure 2). This apparent contradiction may be explained by considering the thickness of the two solutions lamellae. In the T-junction there is only one lamella per fluid whose maximum thickness corresponds to the radius of the outlet channel in case of equal

flow rates and same viscosity, i.e. 840 µm (Table 1). For the HPIMM, the two fluids are delaminated into 15 lamellae whose thicknesses are 45 µm (Table 1). Therefore, even if the Reynolds number is too low to promote an engulfment flow, the diffusion of the polymer solvent into the non-solvent is much faster in case of the HPIMM micromixer due to a shorter diffusion path.

For the impact jet micromixer, Mae and coll. [28,29] have assessed the mixing performance of different K-M micromixers (different numbers of inlet channels per fluid and outlet channel diameters) by carrying out the Villermaux-Dushman reaction [38] and compared their mixing efficiency with a multilamination micromixer very similar to the HPIMM micromixer used in this study. Authors also concluded that the Reynolds number is an important parameter which affects the mixing efficiency; the higher the Re, the better are the mixing performances. For the K-M micromixer (5 inlet channels per fluid and an outlet channel diameter of 360 µm) the most closely related to the one used in this study, they found that the mixing performance was higher than that of the multilamination micromixer whatever the Reynolds number. They also observed that for Re above 200, the K-M micromixer achieved almost ideal mixing as seen by the quasi total disappearance of the triiodide ion (measured by UV spectrophotometry) in the iodide–iodate reaction system. Although in the work of Mae and coll. none of the K-M micromixers investigated was the one we used in this study, we still can conclude that for Reynolds numbers higher than 300 (i.e. for water flow rates above 4 mL/min, Table 2), the K-M micromixer is the most efficient of the three micromixers investigated and allows the production of the smallest nanoparticles.

3.1.3.2 Drug-loaded PMMA nanoparticles

Ketoprofen-loaded PMMA NPs have been synthesized with the aforementioned three micromixers for different water flow rates and different concentrations of drug. The results are displayed in Figure 3 and Figure 4 respectively.

It is observed in Figure 3 that, like in the case of unloaded PMMA NPs, the size of the nanoparticles decreases with the water flow rate. Furthermore, the effect of the type of the micromixer seems to be the same as the T-junction micromixer still gives the biggest nanoparticles while the K-M micromixer generates the smallest. However, the sizes of drug-loaded PMMA NPs obtained with the T-junction are significantly higher than those without drug by an average value of 110 µm. For the two other micromixers, the difference is less than 40 nm. Presumably, these results may be explained by either a change in the physicochemical properties of the polymer solution (e.g. the interfacial tension between polymer solution and non-solvent) and/or by a change in the surface properties of the NPs which favor aggregation, both due to the presence of the drug.

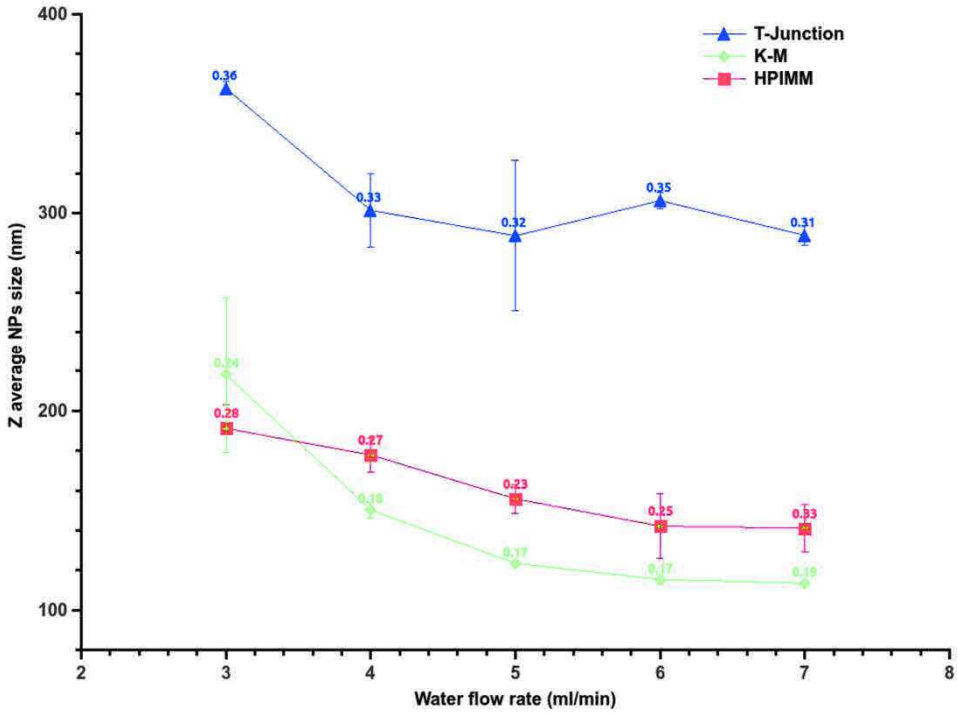

Figure 3. Variation of the size of Ketoprofen-loaded PMMA NPs as a function of the water flow rate for the three different micromixers. The polymer solution flow rate was fixed at 1 mL/min. Numbers represent the PDI value of each data point. The mass fraction of drug was fixed at 0.5 wt.%.

To discriminate between these two assumptions, the concentration of drug was increased up to 0.5 wt.%. Results for each micromixer are displayed in Figure 3. It is observed that the NPs sizes for the K-M micromixer are almost unaffected by the

concentration of Ketoprofen while for the two other micromixers they changed significantly; increasing globally for the T-junction micromixer as the concentration increases and following a non-monotonous variation for the HPIMM micromixer (increasing for a concentration of 0.25 wt.% then decreasing for 0.5 wt.%). Change in interfacial tension is probably not the primary cause of variation of NPs size because the K-M mixer would have exhibited a variation of the nanoparticles size with drug concentration. Therefore, it is believed that the presence of the drug in the polymer solution favors the NPs aggregation. However, the efficient intermeshing provided by the K-M micromixer allows a fast surfactant molecules adsorption onto the NPs surface preventing further aggregation. For the two other micromixers, the flow conditions are less favorable for such rapid adsorption leading to aggregation and consequently to an increase in NPs size.

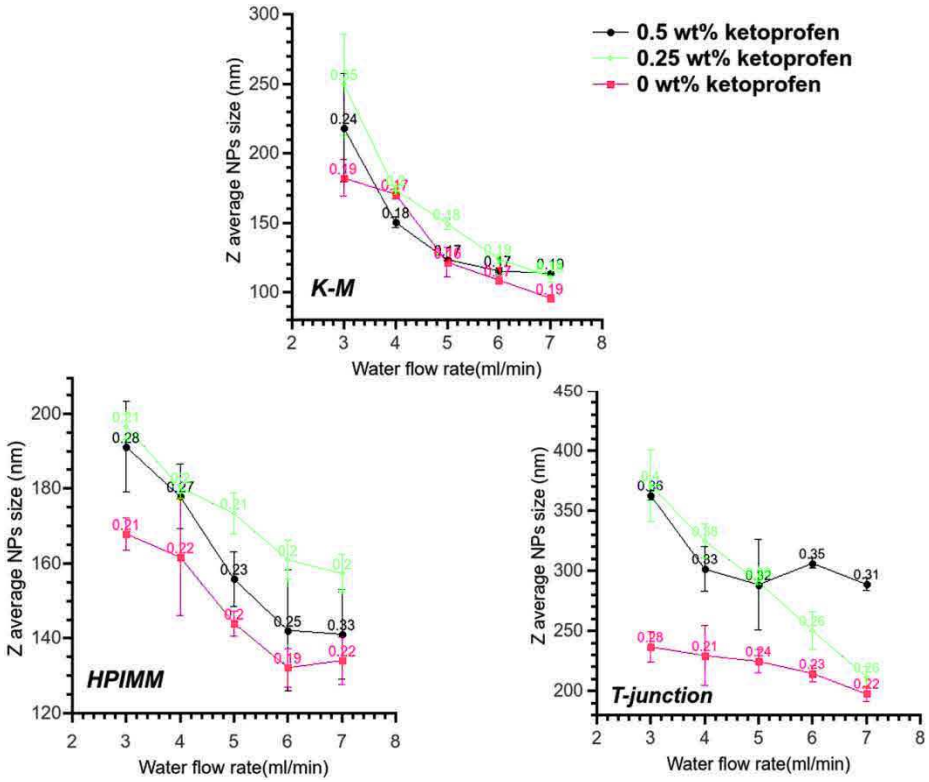

Figure 4. Effect of Ketoprofen concentration on the size of drug-loaded PMMA NPs for the three micromixers investigated. The polymer solution flow rate was fixed at 1 mL/min. Numbers represent the PDI value of each data point.

Another evidence of the difference in the flow condition promoted by the micromixers is the size distributions of the drug-loaded PMMA NPs (Figure 5). The narrower distribution is observed for the K-M micromixer while the T-junction micromixer induces the broadest one. Furthermore, for the latter a second peak in the micron range is visible witnessing the sever aggregation promoted by this type of micromixer.

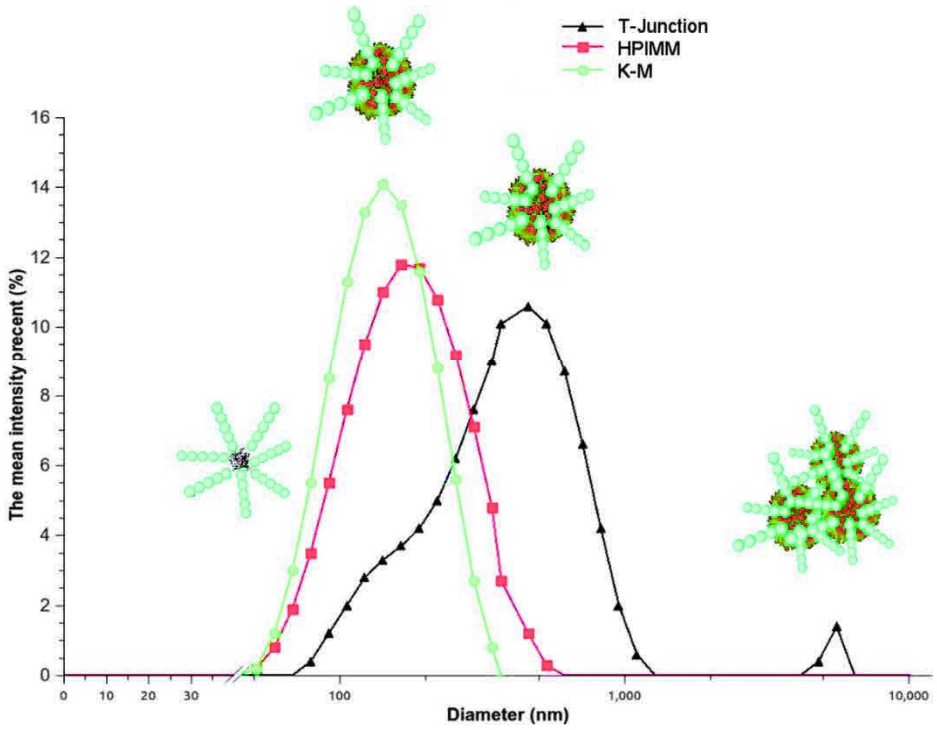

Figure 5. Size distribution of Ketoprofen-loaded PMMA NPs for the three micromixers. The polymer solution flow rate and water flow rate were fixed at 1 mL/min and 7 mL/min respectively. The mass fraction of drug was fixed at 0.5 wt.%.

3.1.3.3 Dry-state drug-loaded PMMA nanoparticles

It has been recognized that the spray drying may promote NPs aggregation. Indeed the inherent thermal history of the method can result in the recrystallization of hydrophilic surfactant, which compromises their ability to prevent aggregation of NPs. In addition, the thermal stress can destabilize the NPs themselves. Consequently, some researches have discussed the use of freeze drying to produce nanoparticles [39,40]. However thanks to the early work of Chaubal *et al.* [24], polymeric surfactants, ionic surfactants and sugars were found to efficiently protect NPs from aggregation during spray

drying. Specifically Mannitol, a polyalcohol sugar, was recognized to offer the most desirable NPs morphology and flowability and thus was used in this study to prevent NPs aggregation during the spray drying procedure.

Figure 6 presents the size of the re-dispersed spray-dried and non spray-dried drug-loaded PMMA NPs obtained with the K-M micromixer for two different water flow rates. The spray drying step was found not altering the quality of the PMMA NPs obtained after nanoprecipitation as the size and PDI do not vary significantly upon spray drying. This result demonstrates that high-quality dry-state drug-loaded NPs can be produced by combination of microfluidic-assisted nanoprecipitation and spray drying techniques.

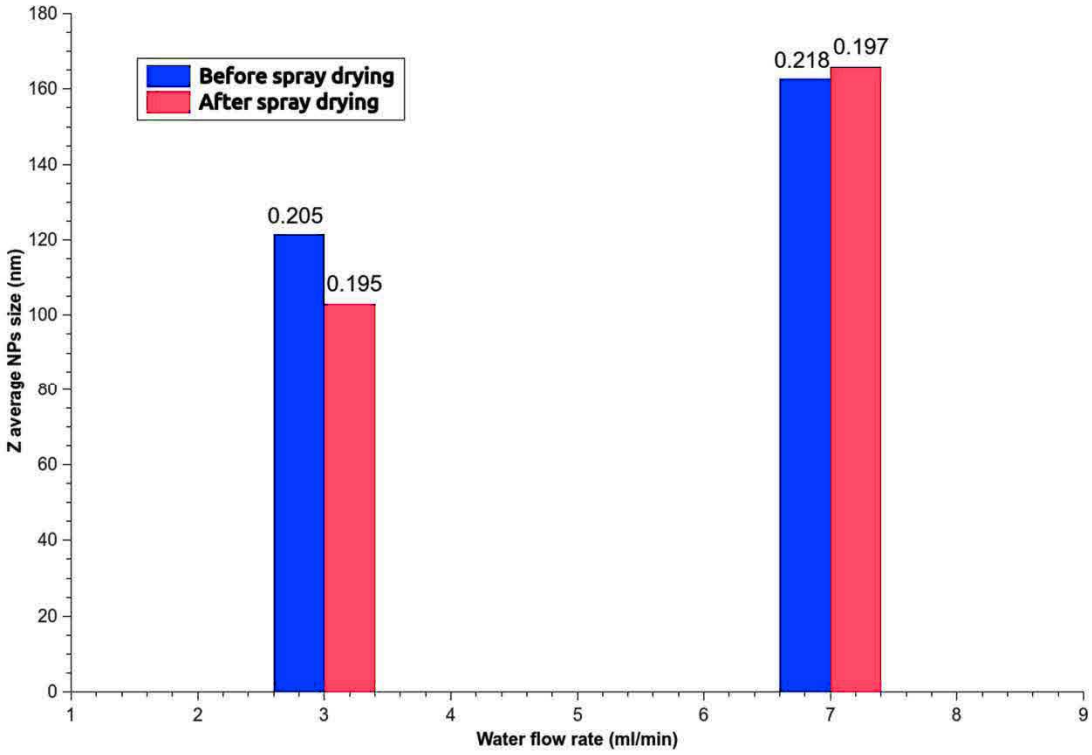

Figure 6. Drug-loaded NPs size obtained with the K-M micromixer before and after spray drying for two different water flow rates (3 and 7 mL/min). Numbers represent the PDI value of each data point.

3.1.3.4 Encapsulation efficiency/ratio and drug release profiles

Encapsulation efficiency (EE) and encapsulation ratio (ER) of non spray-dried and re-dispersed dry-state drug-loaded PMMA NPs were determined according to Eq. 1&2 for the two nanoparticles sizes of Figure 6 and are presented in Figure 7. Both EE and ER increase when the size of the NPs increases (i.e. when the water flow rate is decreased, see Figure 3). This may result from the higher surface to volume ratio of lower particle sizes (i.e. produced with high water flow rate) which promote a more effective diffusion of the Ketoprofen out of the NPs through the microparticles surface during the nanoprecipitation step. Globally re-dispersed dry-state drug-loaded PMMA NPs exhibit smaller EE and ER whatever the water flow rate used for their production. It means that these NPs have encapsulated a smaller mass of Ketoprofen in comparison with the non spray-dried nanoparticles. It is believed that during the spray drying process, some of the drug was lost probably due to the heat treatment they have undergone.

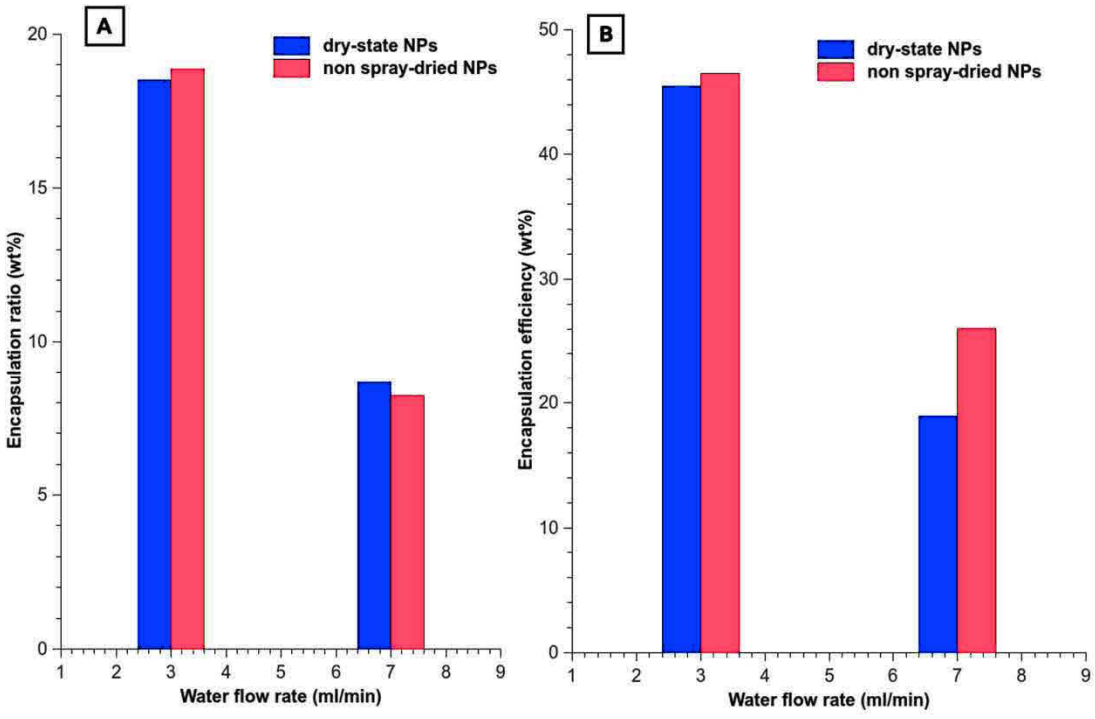

Figure 7. Encapsulation ratio (A) and encapsulation efficiency (B) of non spray-dried and re-dispersed dry-state drug-loaded PMMA NPs obtained with the K-M micromixer at two different water flow rates (3 and 7 mL/min). The polymer solution flow rate was fixed at 1 mL/min.

Finally, the cumulative release curves of Ketoprofen from non spray-dried and re-dispersed dry-state loaded PMMA NPs of two different sizes have been determined following the procedure described in the Materials and methods section. The results are presented in Figure 8. It is observed that non spray-dried NPs, whatever their size (i.e. whatever the water flow rate), exhibit the highest drug release rate. For all the samples the maximum release rates are obtained after 6 hours and are equal to 70% and 50% for non-spray-dried NPs and to 65% and 40% for the re-dispersed spray-dried NPs and for the smallest and biggest nanoparticles respectively. The higher release rate of the smallest NPs is a consequence of their higher surface to volume ratio like it was for the encapsulation efficiency/ratio. Concerning the lower drug release observed for the re-dispersed dry-state NPs (ca. 10% less), it is directly related to the lower encapsulation efficiency (Figure 7), i.e. to the lower amount of encapsulated drug. In case the drug release is driven by the difference of drug concentration between the nanoparticles and the release medium, smaller amounts of drug will slow down its diffusion towards the release medium. Therefore, at a given time, the drug release rate will be lower.

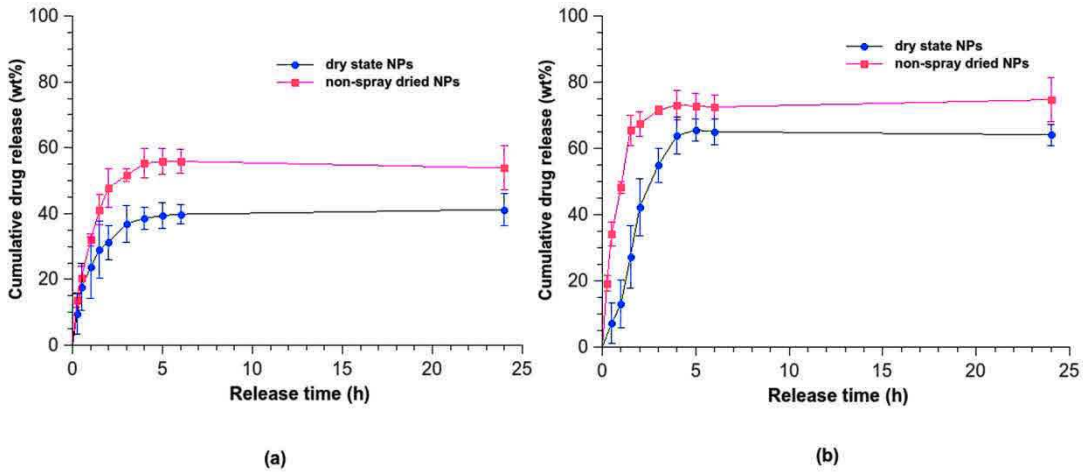

Figure 8. Cumulative drug release of non spray-dried and re-dispersed dry-state loaded PMMA NPs obtained with the K-M micromixer at two different water flow rate 3 mL/min (a) and 7 mL/min (b). The polymer solution flow rate was fixed at 1 mL/min.

3.1.4 Summary

A microfluidic method developed for the nanoprecipitation of polymers was combined with a commercial spray dryer to produce high quality feature-controlled dry-sate drug loaded polymer nanoparticles in the size range 100 to 200 nm. Aqueous suspensions of Ketoprofen-loaded PMMA nanoparticles were thus produced using different micromixers, operating according to two different mixing principles (multilamination and impact jet), by varying the flow rate ratio between the polymer solution (THF) and the non-solvent solution (water). Then the nanosuspensions were admixed with a polyalcohol sugar (Mannitol) to prevent nanoparticles aggregation during the spray drying. Among the three micromixers tested, it was found that he impact jet micromixer allowed producing the drug-loaded nanocarriers with the narrowest size distribution and a size decreasing when the water flow rate was increased. It was also observed that the spray drying did not affect significantly the size of the dry-state nanocarriers in comparison to the original size of the nanoparticles in suspension. However, the encapsulation efficiency of dry-state NPs was found to be slightly lower than that of non spray-dried nanoparticles but reached values of up to 45% for the biggest nanocarriers. Concerning the drug release profiles, both non spray-dried and dry-state drug-loaded nanoparticles exhibited a sustained release over 6 hours with drug release rate values as high as 70%. The latter was found to depend upon the size of the nanocarriers, increasing by decreasing their size, and was somehow 10% lower for the dry-state NPs.

In summary, this two-step process offers a new platform to rapidly formulate, potentially in a continuous manner, high-quality dry-state drug-loaded nanocarriers which size and drug release rate can be tuned simply by changing the operating conditions of the nanoprecipitation step.

In this section a two-step procedure aiming at producing dry-state drug-loaded polymeric nanoparticles was successfully developed. The key step was the production of a colloidal suspension of size-controlled nanoparticles by means of the so-called solvent displacement method (nanoprecipitation). This method was carried out in a

micromixer-assisted process to take advantage of the fast mixing promoting by such microfluidic devices. In the next section, this process will be used to produce polymeric contrast-agent nanocarriers. However the overall solid content of the obtained nanosuspensions will be quite low and nanoparticles will not have a spherical morphology. Therefore a microfluidic-assisted elongational-flow emulsification method will be introduced to solve for this problem.

3.1.5 Supporting information

Reynolds numbers

Micromixers mixing efficiency will be discussed as a function of the Reynolds numbers achieved in the outlet of the devices. Since for some micromixer the outlet channel is not cylindrical, the Reynolds number is defined with the hydraulic diameter (D_h) as follows:

$$Re = \frac{\rho \, v \, D_h}{\mu} \qquad \text{Eq. S3}$$

where v, ρ, and denote the velocity, the density and the dynamic viscosity of the fluid exiting the micromixer, i.e. the THF-water mixture, respectively.

The exit fluid velocity (Eq. 1) is defined considering the total flow rate of polymer and non-solvent solutions (q_{PS}, q_{NS} respectively) and the cross-section area (S) of the outlet channel of the micromixer:

$$v = \frac{q_{PS} + q_{NS}}{S} \qquad \text{Eq. S4}$$

When the micromixer outlet is a cylindrical channel (T-junction and K-M), the hydraulic diameter (Eq. 1) is simply equal to the diameter of the channel while for the HPIMM it is defined considering the cross-section area of flow (S) and wetted perimeter (P_w) according to the following equation:

$$D_h = \frac{4\,S}{P_w} \qquad \text{Eq. S5}$$

Considering that the HPIMM micromixer outlet is composed of 2x15 microchannels of width w and height h (Table 1), the wetted perimeter and cross section area are given by:

$$P_w = 60\ (w+h) \qquad \text{Eq. S6}$$

$$S = 30\ w\ h \qquad \text{Eq. S7}$$

The density of the exiting fluid (Eq. S1) may be calculated considering its mass flow rate and its volume flow rate:

$$\rho = \frac{\dot{m}}{\dot{V}} \qquad \text{Eq. S8}$$

The former ($\dot{m}$) depends on the density and flow rate of the polymer solution (PS) and non-solvent phase (NS) (Eq. S7). Given the amounts of polymer (1 wt.%), surfactant (0.5 wt.%) and drug (0.5 wt.%), the density of the polymer solution is given by Eq. S8 and mainly based on the density of the polymer solvent (THF).

$$\dot{m} = \rho_{PS}\, q_{PS} + \rho_{NS}\, q_{NS} \qquad \text{Eq. S9}$$

$$\rho_{PS} = 0.98\, \rho_{THF} \qquad \text{Eq. S10}$$

The exiting fluid volume flow rate ($\dot{V}$) depends on the total mole flow rate ($\dot{n}$), the molar fractions and molar volumes of the polymer solution (assumed to be equal to the molar fraction and molar volume of THF given the low mass fraction of PMMA, x_{THF} and $\underline{V}_{THF}$ respectively) and non-solvent (water, x_{THF} and $\underline{V}_{NS}$) as well as the excess molar volume of the water-THF mixture ($\underline{V}^{ex}$).

$$\dot{v} = \dot{n}\,(x_{THF}\,\underline{V}_{THF} + x_{NS}\,\underline{V}_{NS} + \underline{V}^{ex}) \qquad \text{Eq. S11}$$

The total molar flow rate ($\dot{n}$) is given by the following equation:

$$\dot{n} = \frac{\rho_{THF}\,q_{THF}}{M_{THF}} + \frac{\rho_{NS}\,q_{NS}}{M_{NS}} \qquad \text{Eq. S12}$$

Where M_{THF} and M_{NS} denote the molar mass of THF and non-solvent (water). Note that q_{THF} is considered to be equal to q_{PS}.

The molar fractions are calculated as follows:

$$x_{THF} = \frac{\frac{\rho_{THF}\,q_{THF}}{M_{THF}}}{\frac{\rho_{THF}\,q_{THF}}{M_{THF}} + \frac{\rho_{NS}\,q_{NS}}{M_{NS}}} \qquad \text{Eq. S13}$$

$$x_{NS} = \frac{\frac{\rho_{NS}\,q_{NS}}{M_{NS}}}{\frac{\rho_{THF}\,q_{THF}}{M_{THF}} + \frac{\rho_{NS}\,q_{NS}}{M_{NS}}} \qquad \text{Eq. S14}$$

Finally the exit fluid viscosity (Eq. 1) is defined considering the molar fractions (x_{THF}, x_{NS}) and the viscosity of the polymer solution (THF) and non-solvent (NS, water) as well as the excess viscosity (μ^{ex}) of the THF-water mixture:

$$\mu = x_{THF}\,\mu_{THF} + x_{NS}\,\mu_{NS} + \mu^{ex} \qquad \text{Eq. S15}$$

The two excess quantities ($\underline{V}^{ex}$, μ^{ex}) are obtained from the data compiled by Nayak *et al.* [42] on the THF-water mixture.

Figure

According to the numerical study conducted by Engler *et al.* [43], the flow regime inside a T-junction micromixer present three different hydrodynamic behaviors as seen by the streamlines which are significantly affected by Reynolds number.

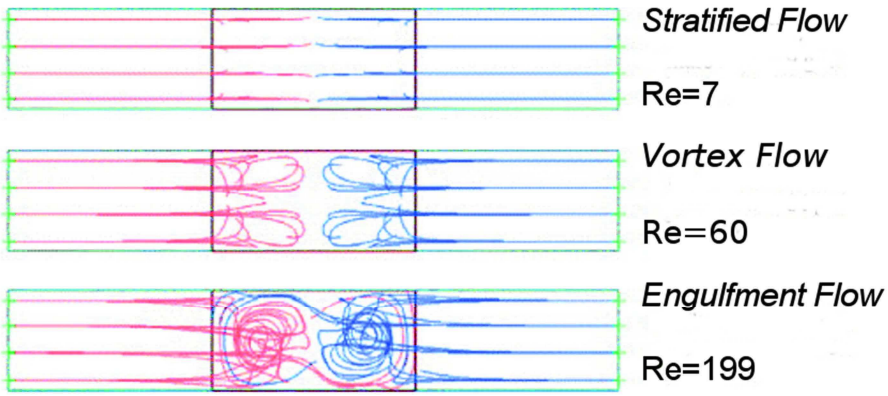

Figure S1. Streamlines inside a T-Junction micromixer for different Reynolds numbers. View of the mixing channel (left and right are the inlet channels).

3.1.6 References

1. Ferrari, M. Nature Reviews 2005, 5, 11.
2. LaVan, D. A.; McGuire, T.; Langer, R. nature biotechnology 2003, 21, 8.
3. Levy, L.; Sahoo, Y.; Kim, K.-S.; Bergey, E. J.; Prasad, P. N. Chemistry of Materials 2002, 14, 6.
4. Ferrari, M. nature nanotechnology 2008, 3, 2.
5. Wang Jie-Xin; Zhang Qian-Xia; Zhou Yue; Shao Lei; Jian-Feng, C. Chemical Engineering Journal 2010, 162, 844-851.
6. A. Vila; A. Sanchez; M. Tobıo; P. Calvo; Alonso, M. J. Journal of Controlled Release 2002, 78 15-24.
7. L. Mu; Feng, S. S. Journal of Controlled Release 2003, 86, 33-48.
8. Scholes P D; Coombesa A G A; Illurn L; Davisa S S; Vertb M; Daviesa M C. Journal of Controlled Release 1993, 25, 145-153.

9. Allémann E.; Gurny R.; E., D. International journal of pharmaceutics 1992, 87, 247-253.
10. Fessi H; F, P. International journal of pharmaceutics 1989, 55, R1-4.
11. Govender Thirumala; Stolnik Snjezana; MC, G. Journal of Controlled Release 1999, 57, 171-185.
12. Chen J. F.; Zheng C.; T., C. G. Chemical Engineering Science 1996, 51, (10), 1957-1966.
13. DeMello, A. J. Nature 2006, 442, 394-402.
14. Song, H.; Chen, D. L.; Ismagilov, R. F. Angewandte Chemie International Edition 2006, 45, (44), 7336-7356.
15. Parida, D.; Serra Christophe, A.; Bally, F.; Garg Dhiraj, K.; Hoarau, Y., Intensifying the ATRP synthesis of statistical copolymers by continuous micromixing flow techniques1. In Green Processing and Synthesis, 2012; Vol. 1, p 525.
16. Karnik, R.; Gu Frank; Basto Pamela; Cannizzaro Christopher; Dean Lindsey; Kyei-Manu William; Langer Robert; C, F. O. Nano letters 2008, 8, 2906-12.
17. Ali Hany S M; York Peter; Ali Ahmed M A; Nicholas, B. Journal of controlled release : official journal of the Controlled Release Society 2011, 149, 175-81.
18. Anton Nicolas; Bally Florence; Serra Christophe a.; Ali Ali; Arntz Youri; Mely Yves; Zhao Minjie; Marchioni Eric; Jakhmola Anshuman; Vandamme Thierry F. Soft Matter 2012, 8, 10628.
19. Ding, S.; Anton, N.; Vandamme, T. F.; Serra, C. A. Expert Opinion on Drug Delivery 2016, 1-14.
20. Lee, S. H.; Heng, D.; Ng, W. K.; Chan, H.-K.; Tan, R. B. H. International Journal of Pharmaceutics 2011, 403, (1–2), 192-200.
21. Thiele, J.; Windbergs, M.; Abate, A. R.; Trebbin, M.; Shum, H. C.; Forster, S.; Weitz, D. A. Lab on a Chip 2011, 11, (14), 2362-2368.
22. Freitas, C.; Müller, R. H. European Journal of Pharmaceutics and Biopharmaceutics 1998, 46, (2), 145-151.
23. Li, X.; Anton, N.; Arpagaus, C.; Belleteix, F.; Vandamme, T. F. Journal of Controlled Release 2010, 147, (2), 304-310.
24. Chaubal, M. V.; Popescu, C. Pharmaceutical Research 2008, 25, (10), 2302-2308.
25. Amstad, E.; Gopinadhan, M.; Holtze, C.; Osuji, C. O.; Brenner, M. P.; Spaepen, F.; Weitz, D. A. Science 2015, 349, (6251), 956-960.
26. Kurosawa, M.; Watanabe, T.; Futami, A.; Higuchi, T. Sensors and Actuators A: Physical 1995, 50, (1), 69-74.
27. James, R. F.; Leslie, Y. Y.; Dian, R. A.; Adam, M. Nanotechnology 2008, 19, (14), 145301.
28. Aoki Nobuaki; Mae Kazuhiro. Chemical Engineering Journal 2006, 118, 189-197.
29. Nagasawa, H.; Aoki, N.; Mae, K. Chemical Engineering & Technology 2005, 28, 324-330.
30. Nayak, J. N.; Aralaguppi, M. I.; Kumar Naidu, B. V.; Aminabhavi, T. M. Journal of Chemical & Engineering Data 2004, 49, (3), 468-474.
31. Chronopoulou Laura; Sparago Carolina; Cleofe, P. Journal of Nanoparticle Research 2014, 16, 2703.
32. Lim JM; Swami Archana; Gilson LM; Chopra Sunandini; Sungyoung, C. ACS Nano 2014, 8, 6056-6065.
33. Johnson Brian K.; Prud'homme, R. K. Australian Journal of Chemistry 2003, 56, 1021.

34. Dirksen, J. A.; Ring, T. A. Chemical Engineering Science 1991, 46, (10), 2389-2427.
35. Julien Aubry, F. G., Jean-Pierre Cohen Addad, Bernard Cabane. Langmuir 2009, 25, 1970-1979.
36. Lannibois, H.; Hasmy, A.; Botet, R.; Chariol, O. A.; Cabane, B. J. Phys. II France 1997, 7, (2), 319-342.
37. Engler, M.; Kockmann, N.; Kiefer, T.; Woias, P. Chemical Engineering Journal 2004, 101, (1–3), 315-322.
38. Guichardon, P.; Falk, L. Chemical Engineering Science 2000, 55, (19), 4233-4243.
39. Abdelwahed, W.; Degobert, G.; Fessi, H. European Journal of Pharmaceutics and Biopharmaceutics 2006, 63, (2), 87-94.
40. Abdelwahed, W.; Degobert, G.; Stainmesse, S.; Fessi, H. Advanced Drug Delivery Reviews 2006, 58, (15), 1688-1713.
41. Rabinow, B. E. Nat Rev Drug Discov 2004, 3, (9), 785-796.
42. Nayak, J.N.; Aralaguppi, M.I.; Naidu, B.V.K.; Aminabhavi, T.M. J. Chem. Eng. Data 2004, 49, 468-474
43. Engler, M.; Kockmann, N.; Kiefer, T.; Woias, P. Chem. Eng. J. 2004, 101, (1–3), 315-322.

3.2 Microfluidic-assisted production of SPIONs-encapsulated PMMA NPs

ABSTRACT

In this paper, super paramagnetic iron oxide nanoparticles (SPIONs, around 6 nm) encapsulated in poly(methyl methacrylate) nanoparticles (PMMA NPs) with controlled sizes ranging from 100 nm to 200 nm have been successfully produced. The hybrid polymeric nanoparticles were prepared following two different methods: (1) nanoprecipitation and (2) nanoemulsification-evaporation. These two methods were implemented in two different microprocesses based on the use of an impact jet micromixer and an elongational-flow microemulsifier respectively. SPIONs-loaded PMMA NPs synthesized by the two methods presented completely different physicochemical properties. The polymeric nanoparticles prepared with the micromixer-assisted nanoprecipitation method showed a heterogeneous dispersion of SPIONs inside the polymer matrix, an encapsulation efficiency close to 100 wt.% and an irregular shape. In contrast, the polymeric nanoparticles prepared with the microfluidic-assisted nanoemulsification-evaporation method showed a homogeneous dispersion, almost complete encapsulation and spherical shape. The properties of the polymeric nanoparticles have been characterized by DLS, TGA and TEM. In vitro cytotoxicity assays were also performed on the hybrid and pure PMMA nanoparticles.

3.2.1 Introduction

Magnetic nanoparticles (MNPs) have become one of the main scopes in nanomaterials dedicated to biomedical applications. Over the past decades, an ocean of research in pharmaceutical fields has been expanding showing how such magnetic nanomaterials are versatile and possess huge potentials for enhanced diagnosis of various diseases [1-4].

Among the different types of MNPs, superparamagnetic iron oxide nanoparticles (SPIONs) have attracted great attention due to the combined merits of atomic composition, crystal structure, and nanoscale effect. Indeed they offer good magnetic properties and thus present a huge potential as magnetic nanoprobes or nanoparticulate contrast agents for magnetic resonance imaging (MRI) in non-invasive diagnoses. As regards to in vivo aspects, SPIONs already exhibit two main advantages: i) their magnetic property within body can enlarge the signal during MRI and ii) their ultra small size leads to their fast distribution and good diffusion in intercellular space[5]. However, for in vivo applications, the design of SPIONs surface must be adapted in order to overcome a lack of stealth property which prevents SPIONs from achieving what they were introduced for. The hurdle that the unmodified SPIONs are facing is the fast opsonization (recognition and sequestration) by the reticuloendothelial system (RES) causing SPIONs metabolization and rapid excretion from body. Syntheses of SIPONs by general methods such as co-precipitation, microemulsion, and thermal decomposition, mostly provide lipophilic SPIONs due to the use of long carbon chain ligands as stabilizer agent during the synthesis process. It results in instability of SPIONs in biological environment, because they tend to aggregate to bigger particles. Efficient surface modification of SPIONs will not only prolong the circulation time in blood stream and impart bioactive function on the SPIONs surface, which will interact with the target site of cell as ligand-receptor pair, but also circumvent the aggregation of SPIONs in aqueous phase. The commonly used methods for surface modification of SPIONs have been implemented by directly inverting hydrophobic surfactant into hydrophilic ones [6, 7]. Although, the surface modification of SPIONs has been well developed, SPIONs still will face challenges in clinics. For example, SPIONs with ultras mall size may undergo fast biodegradation during in vivo assays [8].

Thus, to overcome a lack of stability and long-time retention, we have investigated in this study the encapsulation of SPIONs within a polymeric matrix as an inorganic-organic nanoassembly based on magnetic seeds embedded within polymeric

nanoparticles to prevent SPIONs from aggregation and impose stability in biological environment.

Actually, preliminary experiments have been endeavored in this respect [9]. Different monomer were applied to encapsulate the SPIONs by hydrolysis-condensation reaction or emulsification-polymerization with silica [10], polystyrene [11], poly(methyl methacrylate) (PMMA) [12, 13], or PMMA-DVB (DVB = divinylbenzene) [14]. Generally, the commonly used protocol was achieved by polymerization of monomer. However, the obtained nanohybrids showed some deficiencies regarding the coating materials and their impacts on the in vivo properties of nanohybrids, for example the molecular weight of the polymeric coat and the degradable rate or the toxicity of materials. Besides, the low entrapment efficiency of SPIONs and the poor control over the methods preclude them from being widespread use. To address these shortcomings, SPIONs-encapsulated polymeric nanoparticles have been synthesized by top-down methods, i.e. by starting from an already synthesized polymer and not from its monomer. We synthesized SPIONs-loaded PMMA NPs by nanoprecipitation and nanoemulsification-evaporation methods associated with microfluidic systems, which yielded nanohybrids with enhanced properties compared to those produced by conventional methods [15]. To the best of our knowledge, it has been reported no papers in the literature about the preparation of this type of nanoparticles by such methods and none of them relied on microfluidic systems. To that extent, it will be potent methods to encapsulate SPIONs in a polymeric matrix.

Basically, nanoprecipitation and nanoemulsification-evaporation methods have been prevalent strategies for production of polymeric nanoparticles. Fessi and coll. were the pioneers in the preparation of polymeric nanoparticles by nanoprecipitation [16]. They reported that nanoprecipitation, also known as solvent displacement process or interfacial deposition, was driven by the fast diffusion of a solvent, solubilizing the polymer, in a non-solvent of the polymer (most often an aqueous phase) in presence or

absence of surfactant to provoke polymer precipitation. Ideally, the solvent and the non-solvent used in the formulation should be miscible. In contrast, during the nanoemulsification-evaporation method, the solvent and non-solvent need to be immiscible. First, those two solvents are mixed to get an emulsion (micron-or nanosized) in which the organic solution of polymer is the dispersed phase while the non-solvent forms the continuous phase. Solvent from the emulsion droplets is then removed by evaporation to get solid polymeric nanoparticles.

Compared to other methods such as salting-out [17], supercritical fluids that replace the solvent in the precipitation techniques [18], polymerization [19], microfluidic-assisted methods to prepare nanoparticles offers some flexibility for the biological applications. One of the latest developments in the production of polymeric nanoparticles begun with the advent of microfluidics and its specific microfabrication procedures [20]. Extensive microfluidic systems have been explored to enhance the property of polymeric NPs [21-37] due to a better control over fluid flow at small scale, even at nanoliters [38]. In this current study, the microfluidic-assisted nanoprecipitation system and nanoemulsification-evaporation method have been adopted to synthesis unique physicochemical properties of SPIONs-loaded PMMA NPs aiming at allowing these nanohybrids particles to be used as potential MRI contrast agent with high concentration of encapsulated SPIONs encapsulated in a polymer shell surrounded by a PEGylated shell required to overcome the in vivo effect of their ultra small size.

3.2.2 Materials and procedure

3.2.2.1 Materials

Methyl methacrylate, copper (I) bromide, 1,1,4,7,10,10-hexamethyltriethylenetetramine and 2-ethyl bromoisobutyrate used for the synthesis of the PMMA and iron(III) acetylacetonate (Fe(aca)3) (97%), 1,2-dodecanediol (90%),

oleylamine (70%) and oleic acid (90%) used for the SPIONs synthesis were purchased from Sigma-Aldrich (Saint-Louis, USA) and used as received except 2-ethyl bromoisobutyrate initiator, which was distilled under vacuum prior to use and methyl methacrylate monomer, which was passed through an alumina column, from Merck (Darmstadt, Germany) to remove inhibitors. Ethanol, dichloromethane (DCM), diphenyl ether, hexane, methanol, tetrahydrofuran (THF) were purchased from Sigma-Aldrich (Saint-Louis, USA). Nonionic surfactant (Cremophor ELP) from BASF (Ludwigshafen, Germany) was kindly provided from Laserson (Etampes, France). Cremophor ELP is a parenteral grade nonionic surfactant made by reacting ethylene oxide to castor seed oil at an ethylene oxide to oil molar ratio of 35 [39]. MilliQ water was obtained using the MilliQ filtration system (Millipore, Saint-Quentin-en-Yvelines, France). Dimethyl sulfoxide (DMSO), and 3-(4,5-dimethylthiazol-2-yl)-2,5-diphenyltetrazolium bromide (MTT) solutions were purchased from Sigma-Aldrich (St. Louis, MO). Phosphate buffered saline (PBS), Dulbecco's modified Eagle medium (DMEM), and fetal bovine serum were purchased from PAN Biotech (Aidenbach, Germany).

3.2.2.2 Synthesis and characterization of PMMA

PMMA was synthesized by atom transfer radical polymerization technique (ATRP) using modified procedure from by Xu *et al.* [11]. Reagents include methyl methacrylate as monomer (19.91 mL), copper (I) bromide as catalysis (0.0876 g) and 1,1,4,7,10,10-hexamethyltriethylenetetramine as ligand (182.75 µL). The reaction was carried out for 1.5 hours in THF (19.8 mL) at 60°C in a magnetically stirred round bottom flask under a blanket of nitrogen. Then the as-prepared polymer solution was filtrated through an alumina column to remove catalyst and poured in a large volume of methanol to precipitate PMMA. Dry powder polymer was finally obtained after overnight vacuum at 30°C. Dry state polymer was finally obtained after overnight vacuum at 30°C. PMMA was analyzed by gel permeation chromatography (PL-GPC 120 platform, Polymer Laboratories, Church Stretton, UK) in THF (at a flow rate of 1

mL/min at 35°C). The number-average molecular weight of the synthesized polymer was 15,500 g.mol-1 (Đ = 1.37).

3.2.2.3 Synthesis of SPIONs

Fe(acac)3 (0.71 g, 2 mmol), 1,2-dodecandiol (2.02 g, 10 mmol), oleic acid (2 mL, 6 mmol), oleylamine (2 mL, 6 mmol) and diphenyl ether (20 mL) were mixed and magnetically stirred in a 100 ml round bottom flask. The mixture was heated to reflux (200°C) for 2 hours. The black-brown oily mixture was cooled to room temperature by removing the heating source and purified by dialysis against ethanol (~ 5 cycles). Ethanol was then removed from the product under vacuum. The resulting black product was finally suspended in THF or dichloromethane to reach a concentration of 15 mg of SPIONS per mL of organic solvent and form black ferrofluids referred as SPIONs-THF and SPIONs-DCM respectively. SPIONs composition was investigated by infrared spectroscopy on a Nicolet 380 FT-IR Spectrometer (Thermo Electron Corporation) which revealed absorption peaks of magnetite Fe3O4 iron oxide phase (588 cm-1) with a shoulder assigned to maghemite γ-Fe2O3, the oxidized form of magnetite, due to slight oxidation naturally occurring on SPIONs surface.

3.2.2.4 Physicochemical characterization of SPIONs-loaded PMMA NPs

3.2.2.4.1 Dynamic light scattering (DLS)

The size and size distribution of the hybrid NPs were assessed by dynamic light scattering (DLS) using a Malvern Nano ZS instrument (Malvern, Orsay, France). The helium-neon laser (4 mW) was operated at 633 nm, the scatter angle was fixed at 173° and the sample temperature was maintained at 25°C. The polydispersity index of the particle size (PDI) is a measure of the broadness of the size distribution and it is commonly admitted that PDI values below 0.2 corresponds to monomodal distributions. Measurements of nanosuspensions size were performed in triplicates by pouring dropwise the 0.02 mL nanosuspensions into 1 mL MilliQ water.

3.2.2.4.2 Transmission electron microscope (TEM)

To analyze the morphology and shape of the hybrid nanoparticles, TEM experiments were performed. A drop of the SPIONs-loaded PMMA NPs suspension was placed on a carbon grid (carbon type-A, 300 mesh, copper, Ted Pella Inc. Redding, PA) and dried at 40°C. Observations were carried out using a Philips Morgagni 268D electron microscope. In another experiment, a 5µl drop of the SPIONs-loaded PMMA NPs suspension was deposited onto a carbon film freshly glow discharged (Elmo, Cordouan Technologies) without negative staining. The contrast is, in that case, directly related to the atomic number of the diffusing atoms. So SPIONs are seen as black dots and the PMMA is invisible. The grids are observed in a Tecnai G2 operating at 200kV and the images are taken with an Eagle 2k2k ssCCD camera (FEI).

3.2.2.4.3 Thermal gravimetric analysis (TGA)

Thermogravimetric analysis (TGA) measurements were performed on a TGA 2 (Mettler Toledo). The mass losses of samples were assayed under nitrogen atmosphere from 35 to 700°C with a heating rate of 10°C/min.

3.2.2.5 *In vitro Cytotoxicity Assays (MTT Method)*

Cytotoxicity assays were performed using HeLa human cervix epithelial adenocarcinoma cells, and they were selected as a standard cancer cell line model. Cells were seeded in 96-well plates at a concentration of 104 cells per well in 100 µL of medium (DMEM) containing 10% FBS and 1 wt.% of commercial solution of penicillin and streptomycin. Cells were then incubated overnight at 37°C under a controlled atmosphere (5% CO2 and 80% H2O). Next, the culture medium was replaced by the same medium but containing variable concentrations of SPIONPs-loaded PMMA nanoparticles (see details below). After incubation for 24 h, the medium was removed and the cells were washed with PBS. Then, the wells were filled with cell culture medium containing MTT, incubated for 4 hours at 37 °C, and the formed formazan crystals were dissolved by adding 100 µL of DMSO. UV absorbance was measured at 570 nm with a microplate reader (Varioskan Flash, Thermo

Scientific, USA). Experiments were carried out in triplicate and expressed as a percentage of viable cells compared to the control group.

3.2.2.6 Preparation of SPIONs-loaded PMMA NPs by the micromixer-assisted nanoprecipitation method

Formulation of SPIONs-loaded PMMA NPs via microfluidic-assisted nanoprecipitation method was performed by using SPIONs-THF solution. Evaluation of the amount of SPIONs in THF was carried out by weighting the mass of SPIONs from an aliquot of SPIONs-THF after complete evaporation of solvent. The organic phase (THF) contained PMMA, non-ionic surfactant and SPIONs whereas the non-solvent phase was only MilliQ water. The organic phase was prepared by the successive addition of purified PMMA (50 mg) and Cremophor ELP (25 mg) to 5 mL of the dispersion of SPIONs in THF adjusted to 15 mg SPIONs/mL (total amount encapsulated = 75 mg of SPIONs). As illustrated in Figure 9, the microfluidic system consisted of two syringe pumps (PHD 2000, Harvard Apparatus) which were connected with a micromixer by two PTFE tubes (1.06 mm ID x 1.68 mm OD). The micromixer used was the K-M impact jet micromixer (Fujifilm Corporation, Kyoto, Japan) introduced by Mae and coworkers [24,40] and was composed of 3 microchannels (150 x 150 µm square) per inlet streams and an outlet channel of 300 µm in diameter. The organic phase and MilliQ water were pumped separately at different flow rates: the organic phase flow rate was fixed at 0.2 mL/min whereas the water flow rate was varied over a range of 2, 2.4, 2.8, 3, 3.2, 3.6 and 4 mL/min. Nanoprecipitation started right away within the mixing chamber of the micromixer when both fluids were brought into contact. The resulting colloidal suspension of SPIONs-loaded PMMA NPs was then directly collected at the outlet of the micromixer. The suspension was left at room temperature overnight to completely remove organic solvent to be ready for the measurements and characterizations.

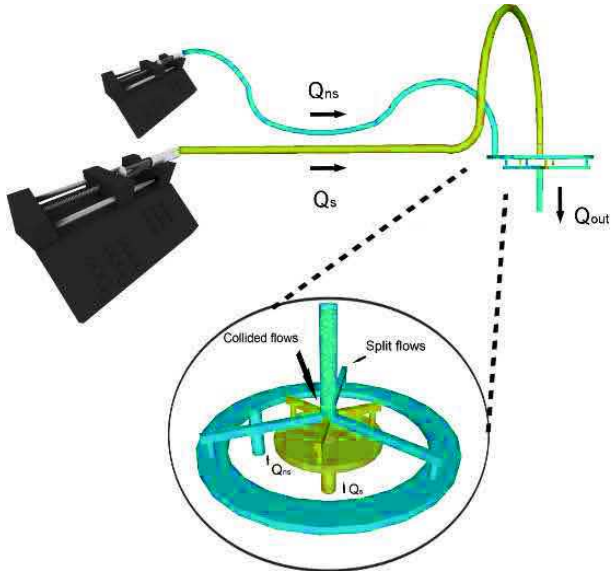

Figure 9. Schematic representation of the micromixer-assisted nanoprecipitation process (not at scale). Q_s, Q_{ns} and Q_{out} denote the flow rate of the polymer solution, non solvent and exit stream respectively

3.2.2.7 Preparation of SPIONs-loaded PMMA NPs by the microfluidic-assisted nanoemulsification-evaporation method

Formulation of SPIONs-loaded PMMA NPs via microfluidic-assisted nanoemulsification-evaporation method was performed by using SPIONs-DCM solution. Similarly, to compare with the micromixer-assisted nanoprecipitation, the concentration of SPIONs in DCM was adjusted to 15 mg SPIONs/mL. PMMA (10 mg/mL DCM) and hexane (1.5 mL) were added into SPIONs-DCM (1.5 mL). Mixture was then subjected to 10 min sonication to complete PMMA solubilization. The as-prepared suspension was used as organic phase during emulsification. The continuous phase was basically composed of Cremophor ELP (0.255 g) solubilized in MilliQ water (12.75 mL). The organic phase (2.25 mL) and aqueous phase (12.75 mL) were then vortexed for 1 min to form a premixed emulsion. The premix was then used as the raw material for the microfluidic-assisted nanoemulsification system. As illustrated in Figure 10, the emulsification system was mainly assembled with two mid-pressure syringe pumps (neMESYS Mid Pressure Module, Cetoni) which can work in opposite phase (withdraw/infuse), two 25 mL stainless steel syringes (Cetoni) and one PEEK tee (Valco Vici). The system was controlled by the supplier's software to accurately operate flow rate. The micromixer was fabricated to obtain three drilled cylindrical

microchannels having a diameter to either 250 or 150 µm. Two microchannels were connected to the stainless steel syringes with two PTFE tubes (1.06 mm ID x 1.68 mm OD). The third microchannel was used to collect the emulsion. During the process, both pumps were operated in opposite phases at the same reciprocating flow rate so that the premixed emulsions were transferred from one syringe to the other one through the microchannels acting as a restriction to the flow. A back and forth movement of the pump counts for one cycle. Different reciprocating flow rates and number of cycles were investigated on the physicochemical properties of NPs [41].

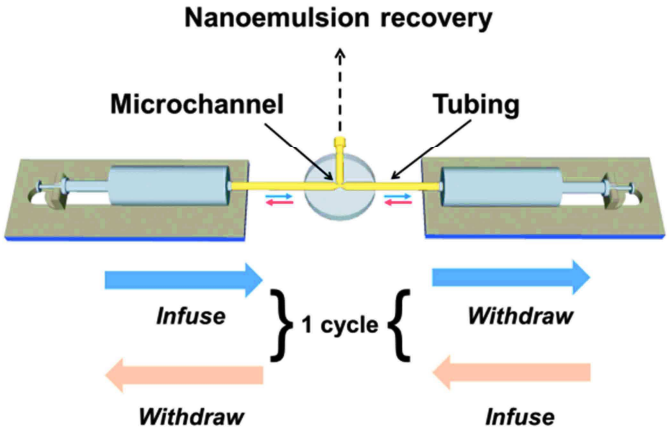

Figure 10. Schematic drawing of the microfluidic-assisted nanoemulsification process (not at scale)

3.2.3 Results and discussion

3.2.3.1 Physicochemical properties of SPIONs-loaded PMMA NPs

3.2.3.1.1 Micromixer-assisted nanoprecipitation method

This method has already been applied for the synthesis of drug-loaded PMMA NPs [22] in our previous work. The main component of the system is the micromixer, which can split each inlet phase into three sub-streams flowing in microchannels (150 x 150 µm square) and then collides the six flows to support the fast mixing of organic phase and aqueous phase by kinetic energy. The resulting suspension is collected in the outlet microchannel (300 µm diameter) which concentrated the collided six flows to improve molecular diffusion. The two key parameters, kinetic energy and molecular

diffusion, are thus required to achieve the nanoprecipitation of polymeric nanoparticles. So far, this micromixer has been reported as the most suitable device for the preparation of polymeric nanoparticles with enhanced properties [15]. As for the mixing process, it has also been proved that to ensure good physicochemical features to suspensions formulated via microfluidic-assisted nanoprecipitation, fast mixing remained one of the most important conditions to apply [42]. The mixing performance can be impacted by the difference of water and polymer solvent flow rates ratio. Indeed, a higher continuous phase flow rate compared to a low organic phase flow rate would support better performance of mixing due to the collided flows and the fast molecular diffusion in the outlet microchannels. We consequently selected in our study a constant flow rate (0.2 ml/min) for the polymer solution and a range of higher flow rates for the water phase to change the kinetic energy during the process.

The sizes of the nanoparticles that were obtained are displayed in Figure 11(a). Influence of kinetic energy on the size of PMMA NPs and SPIONs-loaded PMMA NPs has been assessed. For PMMA NPs, the size has apparently been greatly influenced by the water flow rate, decreasing sharply when the flow rate was increased. This phenomenon has been observed in different studies [21, 43-46] about the precipitation of a polymer or a pure drug and results from two reasons: 1) a higher water phase to polymer solution flow rate ratio induced a higher supersaturation of the polymer or drug, which initially resulted in smaller nuclei formation during the nanoprecipitation [47]; small nuclei formation is a key parameter to obtain nanoparticles whatever the mechanism they follow next to get bigger, i.e. growth or aggregation; 2) higher flow rates (organic phase or water phase) induce a higher kinetic energy resulting in higher Reynolds numbers, as such, the streamlines of the two phases intermesh rapidly decreasing the diffusion path of the polymer solvent into the non-solvent phase and thus speeding up the mixing [48]. For the SPIONs-loaded PMMA NPs, the size of the nanoparticles has been surprisingly slightly influenced by the ratio of water phase to polymer solution flow rate compared to pure PMMA NPs. This observation is unquestionably linked to the presence of SPIONs in the

formulation. One can hypothesize that the presence of inorganic nanoparticles in the polymer solution alters somehow the formation of nuclei or most probably their growth because the size of a nuclei is expected to be of the same order as SPIONs size. Therefore, due to the nuclei-growth mechanism, it is likely that SPIONs would be mostly present at the surface of the polymeric nanoparticles as TEM micrographs may suggest (Figure 16(a&b)). In such situation, the presence of SPIONs may favor the adsorption of further macromolecules and thus sustains the polymeric nanoparticles growth. When the water flow rate increases, the mixing is more intense and the SPIONs deposition on the surface of growing polymeric nanoparticles may be faster allowing them to grow even further. As a consequence the hybrid nanoparticles will have a bigger size than the pure PMMA NPs as stressed out by size distributions of unloaded and SPIONs-loaded PMMA NPs (Figure 11(b)).

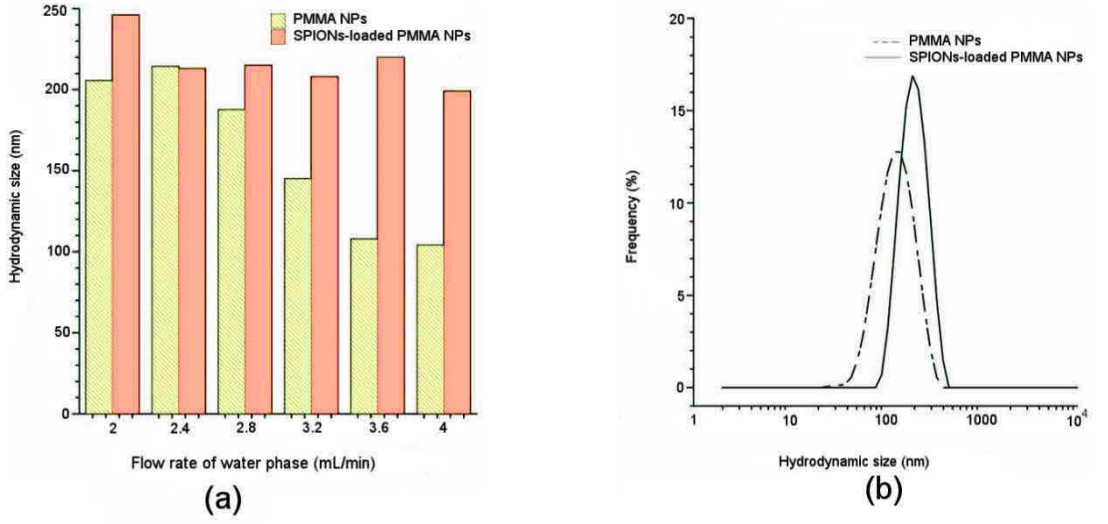

Figure 11. Size variations of SPIONPs-loaded PMMA NPs and PMMA NPs obtained by the micromixer-assisted nanoprecipitation method with respect to the water flow rate (a) and their distribution at a water and polymer solution flow rates of 4 mL/min and 0.2 mL/min respectively (b).

3.2.3.1.2 Microfluidic-assisted nanoemulsification-evaporation method

In contrast to the conventional shear flow emulsifiers (rotor-stator or high pressure homogenizer) or ultrasonicators, elongational-flow emulsifiers were recently proved to be more efficient in controlling the size and size distribution of a nanoemulsion in the

range 50-300 nm [49]. Furthermore, this kind of emulsifiers operates at low pressure (ca. 2.5 bars) and can accommodate high dispersed phase viscosities. However until now, we used a labscale or a microfluidic elongational-flow emulsifier to produce nanoemulsions composed of a monomer solution (MMA) as the dispersed phase and an aqueous continuous phase. Then the monomer nanodroplets were polymerized either by UV irritation or heating [33, 41]. In this study a microfluidic elongational-flow emulsifier was employed to emulsify a SPIONs/MMA solution or a SPIONS/MMA/solvent solution instead of a simple monomer solution (Table 3). Once the nanodroplets were formed, the solvent was removed by heating and let the polymer to form solid hybrid nanoparticles.

Table 3 Composition of the coarse emulsions used for the microfluidic-assisted nanoemulsification-evaporation method

Formulation	Organic Phase (0.75 mL)				Water Phase (4.25 mL)
	Hexane	MMA	SPIONs-DCM	PMMA	Cremophor ELP
1	×	0.75 mL	0.75 mL*	-	2 wt.%
2	×	×	0.75 mL	10 mg/mL DCM	2 wt.%
3	0.375 mL	×	0.375 mL	10 mg/mL DCM	2 wt.%

* after mixing with MMA, DCM was evaporated by heating the mixture at 70°C for 30 min

At first a solution of pure MMA was used to encapsulate SPIONs (Entry 1 of Table 3). However, the nanoemulsion produced with the microfluidic elongational-flow emulsifier was not stable. The emulsion fast separated into two layers after few minutes. Aggregation of SPIONs was observed in the upper water layer and also in the organic layer (Figure 12(1)). Afterwards, the SPIONs-DCM suspension was used as the organic phase in which PMMA was dissolved (Entry 2 of Table 3). The resulting coarse nanoemulsion was turbid and SPIONs aggregates were clearly visible (Figure 12(2)). It is assumed that the density of DCM (1.33 g/cm3) was probably too high to promote a fine emulsion. Therefore we prepared a third formulation (Entry 3 of Table 3) by mixing the SPIONs-DCM/PMMA solution with 50 vol.% hexane (density 0.65 g/cm^3) to lower down the density of the dispersed phase accordingly to Seifriz recommendations [50]. After the emulsification, a fine nanoemulsion was obtained

without evidence of SPIONs aggregation (Figure 12(3)). In the following, the results will be presented for nanoemulsions prepared with the formulation 3 of Table 3.

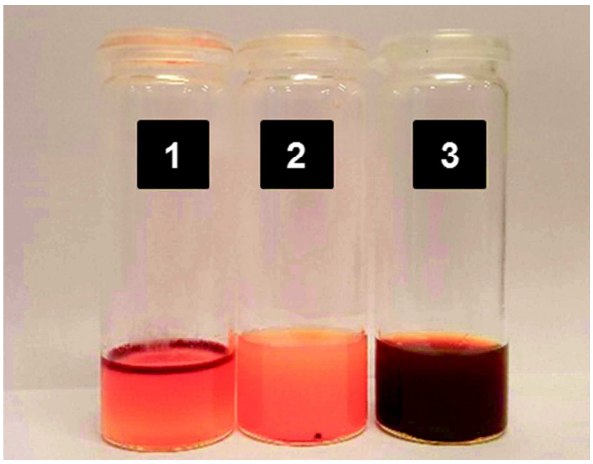

Figure 12. Optical micrographs of the samples 1, 2 and 3 of Table 3 (from left to right) after microfluidic-assisted nanoemulsification-evaporation. Nanoemulsification was performed with a bore size of 150 μm, a reciprocating flow rate of 50 mL/min and a number of cycles of 100.

The influence of the operating parameters, namely the number of cycles, the reciprocating flow rate (FR) and the bore size of the elongational-flow emulsifier, on the size of the SPIONs-loaded PMMA NPs produced is presented in Figure 13(a). A combination of a large bore size (250 μm) along with a low reciprocating flow rate (30 mL/min) induced the formation of the biggest nanoparticles whose size tended to decrease with an increase in the number of cycles. When the bore size was reduced down to 150 μm and the reciprocation flow rate increased up to 50 mL/min, the size also decreased. If one assumes that during the evaporation of hexane, there is no droplet fusion, this result complies with a previous study conducted on the nanoemulsification of a MMA solution [49]. In brief the smaller the bore size and the higher the reciprocating flow rate, the higher is the elongational strain rate ($\dot{\varepsilon}$) which is the driving force of the rupture of a big mother droplet into smaller daughter ones and thus the smaller are the nanodroplets. However, the value of the strain rate is not the same in the whole volume of the restriction being higher close to wall and smaller in the center. Therefore some time is required to decrease the size of the nanodroplets and ultimately reach a plateau value corresponding to the lowest size that can be ruptured for the highest value of $\dot{\varepsilon}$ imposed by the operating parameters used. In other

words, the size should decrease with the number of cycle and reach a constant value. This is pretty much what one observes in Figure 13(a). Figure 13(b) displays the two size distributions returned by the DLS measurements for unloaded and SPIONs-loaded PMMA NPS produced under same operating conditions. It observed that both distributions almost superimposed perfectly. It is known from our previous work, that a higher dispersed phase viscosity will generate bigger nanodroplets [49]. This result may thus be interpreted by the assumption that the addition of the SPIONs into the Hexane/PMMA dispersed phase did not alter too much its viscosity. However, given the concentration of SPIONs in the dispersed phase (5 mg/mL) and from the numerous SPIONs to be seen in the TEM micrographs (Figure 16(c)), this is unlikely. It is most probable that the high density of SPIONS would have significantly increased the density of the PMMA NPs to the point that DLS measurements had retuned much higher values than they should have been. This will be corroborated by the TEM micrographs that will exhibit plenty of loaded PMMA NPs smaller than 100 nm. In summary, the microfluidic-assisted nanoemulsification-evaporation method allowed producing SPIONs-loaded PMMA NPs which size was up to 100 nm.

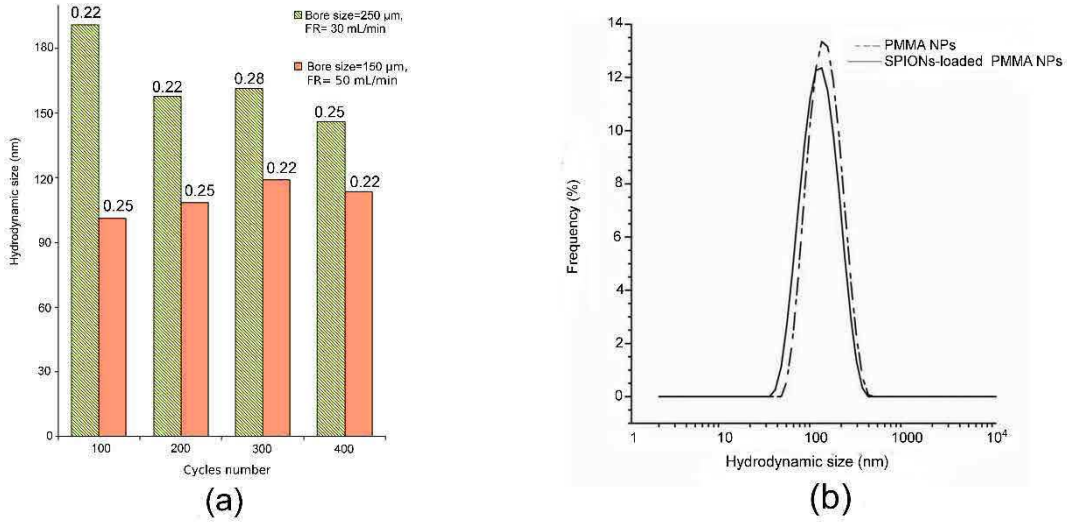

Figure 13. Effect of the number of cycles in the microfluidic-assisted nanoemulsification-evaporation method on the size of SPIONs-loaded PMMA NPs for two different micromixer bore sizes (250 and 150 µm) and two different reciprocating flow rates (30 and 50 mL/min) (a). Size distribution of two samples, SPIONs-loaded PMMA NPs and PMMA NPs, obtained for a number of cycles of 400, a micromixer bore size of 150 µm and a reciprocating flow rate of 50 mL/min (b).

3.2.3.2 Characterization of SPIONs-loaded PMMA NPs

To prove the presence of SPIONS inside PMMA NPs and to quantify the difference between the nanohybrid particles produced by the two methods used, thermal gravimetric analyses were performed on the dried SPIONs, SPIONs-loaded PMMA NPs either produced with the nanoprecipitation or nanoemulsification method and unloaded PMMA NPs. SPIONs thermogram (Figure 14a) exhibited a rapid loss of weight till 450°C then a plateau at 65% up to 650°C. The weight loss is attributed to the removal of all organic compounds (like the oleic acid) used in the synthesis of the inorganic nanoparticles and the plateau to bare SPIONs. PMMA thermogram (Figure 14d) indicates that past 450°C, all the polymer has been destroyed. Whatever methods used for their production, SPIONs-loaded PMMA NPs thermograms (Figure 14b,c) present a plateau between 450°C and 650°c which thus proves the presence of the inorganic NPs in the PMMA nanoparticles. However the plateau for those produced with the nanoemulsification methods is higher (20%) than that for the nanoprecipitation method (10%). This seems to indicate that the former method allows encapsulating twice as much SPIONS than the latter.

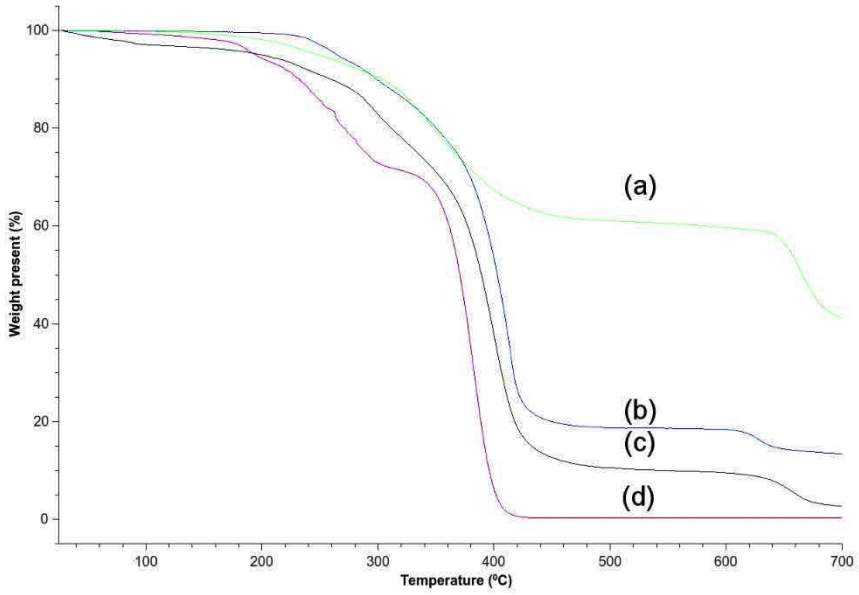

Figure 14. TGA curves of (a) SPIONs nanoparticles (b), SPIONs-loaded PMMA nanoparticles produced with the microfluidic-assisted nanoemulsification-evaporation method, (c) SPIONs-loaded PMMA nanoparticles synthesized by the micromixer-assisted nanoprecipitation method and (d) PMMA nanoparticles.

To check that SPIONS-loaded PMMA NPS had some magnetic properties, two nanosuspensions prepared accordingly to the two aforementioned methods were placed in two separated vials and observed in a magnetic field created by the proximity of a simple magnet. Before adding the magnetic field, the two samples were left side by side to rest for 30 min (Figure 15(a)). Then the magnet was placed in between the two samples overnight. In the morning of next day, a concentrated layer of SPIONs-loaded PMMA NPs was observed on one side of the vial close to the magnet (Figure 15(b)). This experiment sufficiently proved that the hybrid nanoparticles that were produced can be actuated by an external magnetic field. This ability is an important property which makes them suitable as MRI contrast agents.

Figure 15. Optical micrographs of the two SPIONs-loaded PMMA NPs suspensions obtained with the nanoprecipitation (right) and nanoemulsification (left) methods without magnetic field (a) and in presence of a simple magnet (b).

The morphology of the above two samples has been analyzed by TEM. SPIONs-loaded PMMA NPs prepared according to the micromixer-assisted nanoprecipitation method is shown in Figure 16(a&b). The micrographs indicate that the whole amount of SPIONs has been encapsulated in the matrix of PMMA NPs; there are indeed little isolated inorganic nanoparticles in the background. However, the SPIONs are unevenly distributed in or at the surface of the PMMA NPs (see insets of Figure 16(a)). Furthermore, the shape of these hybrid nanoparticles looks irregular and some hybrid nanoparticles seem to have been aggregated (Figure 16(b)). Morphology of SPIONs-loaded PMMA NPs prepared by the microfluidic-assisted nanoemulsification-evaporation method is displayed in Figure 16(c). One can clearly see round shape structures (spheres) containing a high amount of SPIONs. The size of the hybrid

nanoparticles varies from 20 nm up to 250 nm with a majority around 40 nm. The long arrows point to the PMMA nanoparticles containing the SPIONs and the short arrow points to the few free SPIONs. The difference in morphology and distribution of SPIONs for the two types of loaded PMMA NPs produced may be explained considering the inherent mechanism of organic nanoparticles formation of the two methods. For the nanoprecipitation method, the mixing is extremely fast and suggests that the formation of the loaded PMMA NPs is rapid. This means that the SPIONS and PMMA chains do not have enough time to rearrange. Indeed, once precipitated the PMMA is in its glassy state (Tg ~ 100 °C) which prevents any further rearrangement. In contrast, the nanoemulsification-evaporation method proceeds with a slow evaporation of the polymer solution which allows SPIONs and PMMA chains to rearrange resulting in the formation of spherical PMMA NPs with a homogeneous distribution of SPIONs.

3.2.3.1Cytotoxicity assay of SPIONs-loaded PMMA NPs

In vitro toxicity of SPIONs-loaded PMMA NPs suspensions was assessed by MTT test after incubation of the NPs for 24 hours with HeLa cells (cancer cell line model) at different SPIONS and PMMA concentrations (Figure 17). The toxicity was globally similar whatever method was used to produce the hybrid nanoparticles. The LD50 is around 5 mg/mL for SPIONPs-loaded PMMA NPs and 1 wt.% for pure PMMA NPs.

This means that the toxicity profiles are very low if compared with the SPIONs-based products reported in the literature. These experiments have been performed in direct contact with cells which thus were exposed to harsh conditions, but the cell viability remains high. This negligible toxicity could be attributed to the PMMA polymer and the PEGylated surfactant coating of the SPIONs, giving rise to biocompatible and stealth NPs which can be promising in in vivo experiments.

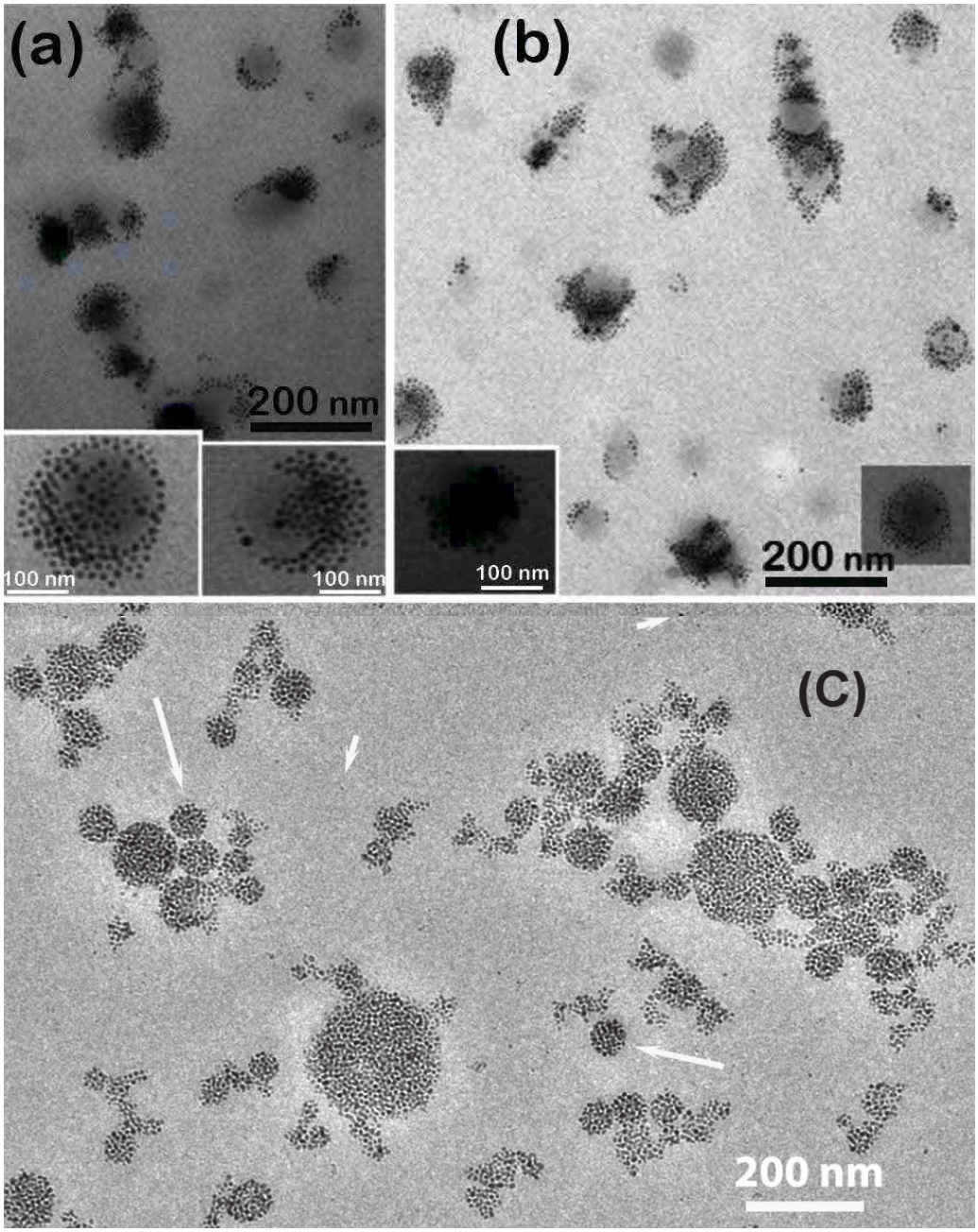

Figure 16. TEM micrographs of unstained SPIONs-loaded PMMA NPs obtained with the micromixer-assisted nanoprecipitation method (a and b). TEM of SPIONs-loaded PMMA NPs obtained with the microfluidic-assisted nanoemulsification-evaporation method (c).

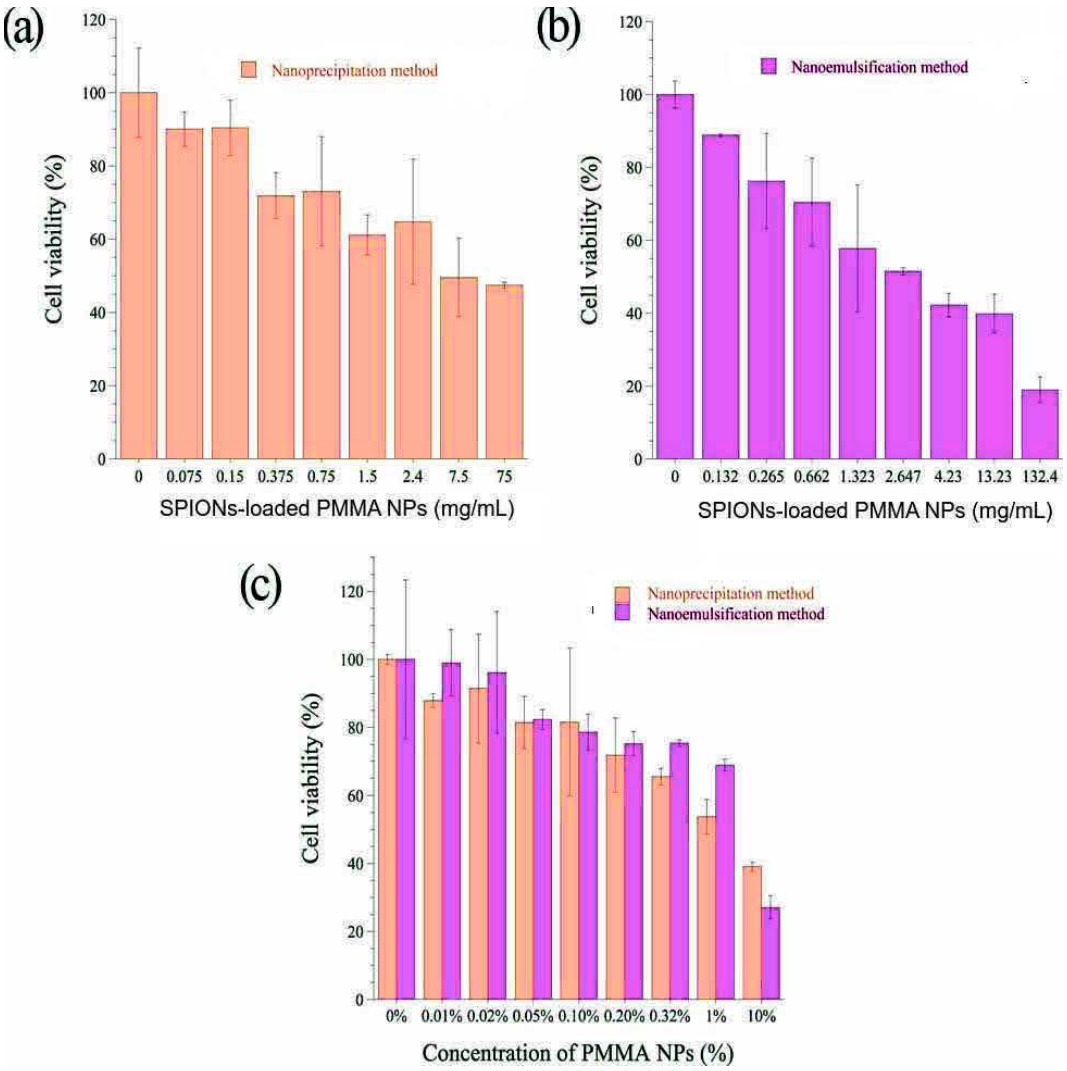

Figure 17. Cell viability measurements for different concentrations of SPIONS-loaded PMMA NPs obtained with the nanoprecipitation (a) and nanoemulsification (b) method. Cell viability measurements for different concentrations of pure PMMA NPs obtained by both methods (c). Experiments have been performed in triplicates.

3.2.4 Summary

Two different methods, namely nanoprecipitation and nanoemulsification-evaporation, were carried out in two different microfluidic devices (micromixer and elongational-flow microemulsifier respectively) to produce SPIONs-loaded PMMA NPs whose size could be tuned from 100 to 200 nm. However, the results shown that the morphologies of the hybrid nanoparticles and the distribution of SPIONs in the organic nanoparticles were different. The microfluidic-assisted nanoemulsification-evaporation method

allowed producing spherical nanoparticles with a homogeneous distribution of SPIONs while the second method produced irregular nanoparticles with an unevenly distribution of inorganic nanoparticles at the surface or in the PMMA NPs. These observations result from the inherent difference in the mechanism of particles formation induced by the two methods. In the first method, the rapid precipitation of PMMA chains induced by the fast diffusion of the polymer solvent into the non-solvent prevents their rearrangement; while for the second method the slow evaporation of the polymer solvent allows a not stop rearrangement of PMMA chains and SPIONs which ultimately leads to the formation of spherical nanoparticles and homogeneous distribution of SPIONs. Nevertheless, the two methods allowed producing SPIONs-loaded PMMA NPs that exhibit low cell toxicity and thus could serve as potential MRI contrast agents.

3.2.5 References

1. Stephen, Z.R., F.M. Kievit, and M. Zhang, Magnetite nanoparticles for medical MR imaging. Materials Today, 2011. 14(7-8): p. 330-338.
2. Pankhurst, Q.a., *et al.*, Applications of magnetic nanoparticles in biomedicine. Journal of Physics D: Applied Physics, 2003. 36(13): p. 167-181.
3. Pankhurst, Q.a., *et al.*, Progress in applications of magnetic nanoparticles in biomedicine. Journal of Physics D: Applied Physics, 2009. 42: p. 224001-224001.
4. Veiseh, O., J.W. Gunn, and M. Zhang, Design and fabrication of magnetic nanoparticles for targeted drug delivery and imaging. Advanced Drug Delivery Reviews, 2010. 62(3): p. 284-304.
5. Brightman, M.W., The distribution within the brain of ferritin injected into cerebrospinal fluid compartments. I. Ependymal distribution. Journal of Cell Biology, 1965. 26(1): p. 99-123.
6. Mahmoudi, M., *et al.*, Optimal design and characterization of superparamagnetic iron oxide nanoparticles coated with polyvinyl alcohol for targeted delivery and imaging. The journal of physical chemistry. B, 2008. 112(46): p. 14470-14481.
7. Chastellain, M., A. Petri, and H. Hofmann, Superparamagnetic Iron Oxide Nanoarticles for Biomedical Applications : a focus on PVA as a coating. Mat. Res. Soc. Symp. Proc., 2004. 789: p. 11-14.
8. Lu, Y., *et al.*, Modifying the Surface Properties of Superparamagnetic Iron Oxide Nanoparticles through A Sol – Gel Approach. Nano letters, 2002. 2(3): p. 183-186.
9. Landfester, K. and L.P. Ram rez, Encapsulated magnetite particles for biomedical application. Journal of

Physics: Condensed Matter, 2003. 15(15): p. S1345-S1361.

10. Santra, S., *et al.*, Synthesis and characterization of silica-coated iron oxide nanoparticles in microemulsion: The effect of nonionic surfactants. Langmuir, 2001. 17(10): p. 2900-2906.
11. Xu, X., *et al.*, Synthesis and utilization of monodisperse superparamagnetic colloidal particles for magnetically controllable photonic crystals. Chemistry of Materials, 2002. 14(3): p. 1249-1256.
12. Beyaz, S., T. Tanrisever, and H. Kockar, Emulsifier-free emulsion polymerization of methyl methacrylate containing hydrophilic magnetite nanoparticles. Macromolecular Research, 2010. 18(12): p. 1154-1159.
13. Guo, C., L. Zhou, and J. Lv, Effects of expandable graphite and modified ammonium polyphosphate on the flame-retardant and mechanical properties of wood flour-polypropylene composites. Polymers and Polymer Composites, 2013. 21(7): p. 449-456.
14. Liu, X., *et al.*, Surface modification and characterization of magnetic polymer nanospheres prepared by miniemulsion polymerization. Langmuir, 2004. 20(23): p. 10278-10282.
15. Ding, S., *et al.*, Microfluidic nanoprecipitation systems for preparing pure drug or polymeric drug loaded nanoparticles: an overview. Expert opinion on drug delivery, 2016. 5247(just-accepted).
16. Fessi, H. and F. Puisieux, Nanocapsule formation by interfacial polymer deposition following solvent displacement. International Journal of Pharmaceutics, 1989. 55: p. 1-4.
17. Allémann, E., R. Gurny, and E. Doelker, Preparation of aqueous polymeric nanodispersions by a reversible salting-out process: influence of process parameters on particle size. International Journal of Pharmaceutics, 1992. 87(1-3): p. 247-253.
18. Tom, J.W. and P.G. Debenedetti, Particle formation with supercritical fluids—a review. Journal of Aerosol Science, 1991. 22(5): p. 555-584.
19. Couvreur, P., *et al.*, Polycyanoacrylate nanocapsules as potential lysosomotropic carriers: preparation, morphological and sorptive properties. Journal of Pharmacy and Pharmacology, 1979. 31(1): p. 331-332.
20. Duffy, D.C., *et al.*, Rapid Prototyping of Microfluidic Systems in Poly(dimethylsiloxane). Analytical chemistry, 1998. 70(23): p. 4974-84.
21. Lim, J.M., *et al.*, Ultra-high throughput synthesis of nanoparticles with homogeneous size distribution using a coaxial turbulent jet mixer. ACS Nano, 2014. 8(6): p. 6056-6065.
22. Anton, N., *et al.*, A new microfluidic setup for precise control of the polymer nanoprecipitation process and lipophilic drug encapsulation. Soft Matter, 2012. 8(41): p. 10628-10628.
23. Liu, D., *et al.*, Microfluidic assisted one-step fabrication of porous silicon@acetalated dextran nanocomposites for precisely controlled combination chemotherapy. Biomaterials, 2015. 39: p. 249-59.
24. Nagasawa, H., N. Aoki, and K. Mae, Design of a new micromixer for instant mixing based on the collision of micro segments. Chemical Engineering and Technology, 2005. 28(3): p. 324-330.
25. Abou Hassan, A., *et al.*, Synthesis of iron oxide nanoparticles in a microfluidic device: preliminary results in a coaxial flow millichannel. Chemical Communications, 2008(15): p. 1783-1785.
26. Jahn, A., *et al.*, Preparation of nanoparticles by continuous-flow microfluidics. Journal of Nanoparticle Research, 2008. 10(6): p. 925-934.
27. Jahn, A., *et al.*, Microfluidic Mixing and the Formation of Nanoscale Lipid Vesicles. ACS Nano, 2010. 4(4):

p. 2077-2087.

28. Jahn, A., *et al.*, Controlled Vesicle Self-Assembly in Microfluidic Channels with Hydrodynamic Focusing. Journal of the American Chemical Society, 2004. 126(9): p. 2674-2675.
29. Johnson, B.K. and R.K. Prud'homme, Mechanism for Rapid Self-Assembly of Block Copolymer Nanoparticles. Physical Review Letters, 2003. 91(11): p. 118302.
30. Karnik, R., *et al.*, Microfluidic Platform for Controlled Synthesis of Polymeric Nanoparticles. Nano Letters, 2008. 8(9): p. 2906-2912.
31. Kim, Y., *et al.*, Mass Production and Size Control of Lipid–Polymer Hybrid Nanoparticles through Controlled Microvortices. Nano Letters, 2012. 12(7): p. 3587-3591.
32. Lim, J.-M., *et al.*, Parallel microfluidic synthesis of size-tunable polymeric nanoparticles using 3D flow focusing towards in vivo study. Nanomedicine: Nanotechnology, Biology and Medicine, 2014. 10(2): p. 401-409.
33. Rhee, M., *et al.*, Synthesis of Size-Tunable Polymeric Nanoparticles Enabled by 3D Hydrodynamic Flow Focusing in Single-Layer Microchannels. Advanced Materials, 2011. 23(12): p. H79-H83.
34. Shen, H., *et al.*, Self-assembling process of flash nanoprecipitation in a multi-inlet vortex mixer to produce drug-loaded polymeric nanoparticles. Journal of Nanoparticle Research, 2011. 13(9): p. 4109-4120.
35. Valencia, P.M., *et al.*, Single-Step Assembly of Homogenous Lipid–Polymeric and Lipid–Quantum Dot Nanoparticles Enabled by Microfluidic Rapid Mixing. ACS Nano, 2010. 4(3): p. 1671-1679.
36. Valencia, P.M., *et al.*, Microfluidic Platform for Combinatorial Synthesis and Optimization of Targeted Nanoparticles for Cancer Therapy. ACS Nano, 2013. 7(12): p. 10671-10680.
37. Zhang, C., *et al.*, Flash nanoprecipitation of polystyrene nanoparticles. Soft Matter, 2012. 8(1): p. 86-93.
38. Amstad, E., *et al.*, Production of amorphous nanoparticles by supersonic spray-drying with a microfluidic nebulator. Science, 2015. 349(6251): p. 956-960.
39. Janos Szebeni, F.M.M., Carl R. Alving, Complement Activation by Cremophor EL as a Possible Contributor to Hypersensitivity to Paclitaxel: an In Vitro Study. Journal of the National Cancer Institute, 1998. 90(4): p. 6.
40. Aoki, N. and K. Mae, Effects of channel geometry on mixing performance of micromixers using collision of fluid segments. Chemical Engineering Journal, 2006. 118(3): p. 189-197.
41. Yu, W., *et al.*, Development of an elongational-flow microprocess for the production of size-controlled nanoemulsions: application to the preparation of monodispersed polymer nanoparticles and composite polymeric microparticles. Macromol. React. Eng., 2016 (Accepted).
42. Chen, J., C. Zheng, and C. Gant Ang, Interaction of macro- and micromixing on particle size distribution in reactive precipitation. Chemical Engineering Science, 1996. 51(10): p. 1957-1966.
43. Wang, J.-X., *et al.*, Microfluidic synthesis of amorphous cefuroxime axetil nanoparticles with size-dependent and enhanced dissolution rate. Chemical Engineering Journal, 2010. 162(2): p. 844-851.
44. Karnik, R., *et al.*, Microfluidic platform for controlled synthesis of polymeric nanoparticles. Nano letters, 2008. 8(9): p. 2906-12.

45. Bally, F., *et al.*, Improved size-tunable preparation of polymeric nanoparticles by microfluidic nanoprecipitation. Polymer, 2012. 53(22): p. 5045-5051.
46. Kim, Y., *et al.*, Mass production and size control of lipid-polymer hybrid nanoparticles through controlled microvortices. Nano letters, 2012. 12(7): p. 3587-91.
47. Aubry, J., *et al.*, Nanoprecipitation of polymethylmethacrylate by solvent shifting: 1. Boundaries. Langmuir : the ACS journal of surfaces and colloids, 2009. 25(4): p. 1970-9.
48. Karnik, R., *et al.*, Microfluidic platform for controlled synthesis of polymeric nanoparticles. Nano letters, 2008. 8: p. 2906-12.
49. Yu, W., *et al.*, Development of an elongational-flow microprocess for the production of size-controlled nanoemulsions: batch operation. Macromol. React. Eng., 2016 (Accepted).
50. Seifriz, W., Studies in emulsions. J. Phys. Chem., 1925: p. 587-600.

CHAPTER 4

NANOCARRIERS PRODUCED BY LOW ENERGY METHODS

Preface

In previous chapter, two different microfluidic-assisted processes (nanoprecipitation and nanoemulsification) were developed to produce polymeric nanocarriers comprising a hydrophobic drug or a contrast agent embedded into a hydrophobic polymer matrix. However, to encapsulate a hydrophilic drug and to still benefit from an aqueous suspension of nanocarriers, the polymeric nanoparticles morphology should be modified.

Thus, in this chapter, double nanocarriers, comprising either water nanodroplets or hydrophilic polymer nanohydrogels loaded with a hydrophilic fluorescent probe and both surrounded by a shell of parental-grade oil, will be produced by means of a two-step process relying on the spontaneous emulsification method. This low energy method will be also applied to the production of contrast agent-loaded nanolipogels.

This chapter is partially adapted from the following article:

(1) Shukai Ding, Nicolas Anton, Wei Yu, Salman Akram, Marc Schmutz, Halina Anton, Andrey Kymchenko, Thierry F. Vandamme and Christophe A. Serra, A new method for the formulation of double nano-emulsion, in preparation.

(2) Shukai Ding, Nicolas Anton, Christophe A. Serra, Wei Yu and Thierry F. Vandamme, Production of contrast agent-loaded nanolipogels by spontaneous emulsification, in preparation.

4.1 A new method for the formulation of Double nano-emulsion

ABSTRACT

Double emulsions are very attractive systems for many reasons, mainly their ability to encapsulate hydrophilic and lipophilic molecules simultaneously in a single particle, as well as the possibility of protect hydrophilic fragile molecules from the continuous phase. Double emulsions is a technology widely present at scale decreasing up to the micrometer, however, reaching nanoscales with double nano-emulsions, with all new potential applications as nanomedicines or diagnosis agent, is a real challenge still in abeyance to date. In this study we propose an original two-step approach for the fabrication of double nano-emulsions with final size are below 200 nm. The process consists of the formulation of a primary water-in-oil (w_1/O) nano-emulsions by high-pressure homogenization, and re-emulsifying this primary emulsion by low-energy method to preserve the double nano-structure. Various characterization techniques were undertaken to prove the double structure and evaluating the encapsulation efficiency of a small hydrophilic probe in the inner aqueous droplets. Complementary fluorescence confocal and cryo-TEM experiments were conducted to achieve the characterization and prove the double structure of the nano-suspension.

4.1.1 Introduction

Aqueous core nano-vector have been prompted considerable researches over past the quarter of a century, which make barrier globules suspended in a aqueous phase, in turn, which contain smaller dispersed aqueous droplets [1-3]. Such a complex structure results in multi-functional nano-carrier able to encapsulate hydrophilic molecules, hence presenting a huge potential for pharmaceutical application. Double emulsions, that is to say water-in-oil-in-water, present the great advantage to allow co-encapsulating of hydrophilic molecules (in the inner aqueous compartments) and lipophilic one (in the lipophilic envelop) [4, 5]. The combination of several components of different natures in one single carrier is a serious solution to improve the efficiency of treatment, bringing a synergetic effect *in situ* [5, 6]. Thus, to satisfy this need, variety of vehicles have been designed, such as conjugated polymer nanoparticles [7-9], core-shell polymer nanoparticles [10, 11], liposome [12] and so forth. Besides, polymeric nanoparticles, who has ability of encapsulated hydrophilic

and hydrophobic drug at same time, can be synthesized by double emulsification-evaporation. Even if theoretically speaking these solutions seems fulfill the specifications of co-encapsulation, their main limitation remains their encapsulation efficiency. This point precisely made accelerate the research effort in order to provide efficient multifunctional nano-carrier.

One interesting and realistic candidate appears in the pattern of double emulsion structure; oil phase is used as hydrophobic barrier between two aqueous phases. This system not only meets requirement of cocktail therapy, but using directly hydrophilic and lipophilic phases guarantees the best possible encapsulation efficiency of both hydrophilic and lipophilic molecules. This is one of the main reason why double emulsions triggered substantial interest in pharmaceutical application such as drug delivery [13], cancer therapy [14], vaccine [15].

However up to know, the formulation constraints only restricted the fabrication of double emulsions at the micro-scale. The reason comes to the instability of the double structure when the scale reaches scales lower than 100 nm,[16],[17] probably due to the great increase of Laplace pressure in the inner aqueous droplets. Some strategies were used to reinforce the double structure and attempt stabilizing the particle, like, *e.g.*, replace oil phase for a lipophilic polymer / solvent phase (using PLA, poly(lactic acid)), giving rise to water/polymer/water vehicle, encapsulating hydrophilic proteins (HSA, human serum albumin) at around 20-30 %, without description of co-encapsulation of lipophilic component in the PLA phase [18]. An unique example describes the establishment of double nano-emulsions formulation through stabilization with very specific block co-polypeptides, with no development on the encapsulation efficiency and yields, and potential loading of hydrophilic molecules [19]. Actually, in spite of some reported examples, decreasing the scale range of nano-emulsions along with conserving the properties of double emulsions like high encapsulation, easy production and industrial scale-up, still remains a challenge in abeyance.

Microscopic water-in-oil-in-water double emulsion was firstly observed in 1925 [20], when W. Seifriz researched the type of emulsions with changing the specific gravity of oil phase and the type of electrolyte. Then, synthesis and application of double emulsion have extensively been investigated, and different methods of preparation have been developed. In general, the double emulsions are prepared according to two steps: The w_1/O emulsion is first prepared as primary, and then this primary emulsion

is used as oil phase with another aqueous phase, to formulate a direct second emulsion $w_1/O/W_2$.[21]·[22]

In the present papers, the formulation of double nano-emulsions is envisaged through transposing the classical method undertaken the fabrication of double emulsions, to the processes classically followed to generate nano-emulsions. It follows therefrom that the two dispersed phases are generated separately; the first emulsification provides the reverse emulsion w_1/O, followed by a second emulsification giving $w_1/O/W_2$. Similarly to micro-scale double emulsions, this methodology aims to insure the best encapsulation efficiency, but on the other hand, since the composition of the two aqueous phases is different, a special care needs to be devoted to the study of stability, drug leakage and equilibrium between osmotic pressure. This point can be followed by the encapsulation of a probes and determination encapsulation efficiency.

This transposition involves that the process integrates several constraints: the primary emulsion should be logically formed at nano-scale, this primary emulsion should present a size typically below 50 nm, small enough to allow the second nano-encapsulation. In addition, the primary emulsions should be stable enough to undergo the second emulsification process without breaking. Ideally, the second nano-emulsification should follow a soft emulsification to preserve the structure of inner droplets, that is to say a process involving low energy like spontaneous emulsification. Basically, the generating process used for nano-emulsions formulations are divided into high energy and low-energy methods [23]. High-energy methods involve the use of specific devices such as sonication or high-pressure apparatuses (like high pressure homogenizer or Microfluidizer®), whereas low-energy nano-emulsification used the physicochemical properties of the components to generate stable nano-emulsions.

In the present study, we propose to design a novel methodology to generate double emulsions at the nano-metric scale, through the first formation of a reverse w_1/O nano-emulsion by high-energy method, followed by re-emulsification of this primary emulsion by spontaneous emulsification.

Herein we focus to the development of a general emulsification method to get and understand the formulation of double nano-emulsion through a two-steps method. The primary w_1/O nano-emulsion was stabilized by low-HLB surfactants, and generated by high-pressure homogenizer. Then, double nano-emulsion was formulated, using a classical spontaneous emulsification process, simply replacing the oil for the primary

emulsion [24]. To stabilize primary emulsion, acrylamide sometimes was added into water droplet to acquire polyacrylamide hydrogel by UV-polymerization after first step. The results were researched with UV-polymerization or without UV-polymerization. From a broader perspective, the present work gives a clear example in which nano double emulsion was synthesized by general methods. Evaluation of the double structure was performed by cryo transmission electron microcroscopy (cryoTEM), fluorescent microcroscopy, and the encapsulation efficiency within the aqueous inner compartment was characterized through using a hydrophilic fluorescent probe placed in the first water phase.

4.1.2 Materials and procedure

4.1.2.1 Materials

Medium chain triglycerides used in the preparation of nano-emulsions was exclusively Labrafac® WL 1349 (Gattefossé S.A., Saint-Priest, France), a mixture of capric and caprylic acid triglycerides as a model of parenteral-grade oil. Nonionic surfactant (Polyglycerol polyricinoleate, PGPR, Pan Oil PGPR E476), used as low-HLB surfactant (HLB = 1.5 ± 0.5) for the preparation of primary nano-emulsion w/O, was kindly gift by Stéarinerie Dubois (Boulogne-Billancourt, France). PGPR is a lipophilic stabilizer largely used in many formulations, and *generally recognized as safe* for human consumption by the FDA. Nonionic surfactant Kolliphor ELP® (BASF, Ludwigshafen, Germany) is polyoxiethylated-35 castor oil, HLB = 12~14, used as hydrophilic surfactant in the secondary emulsification. Maltodextrin 01915 (MD) kindly obtained from Cargill (Saint-Germain-en-Laye , France). MD is a polysaccharide generally used as a food additive. Genocure* DMHA was provided from RAHN (U.S.A.), and 5(6)-Carboxyfluorescein (CF), N,N´-Methylene-bisacrylamide (MBA), acrylamide, potassium phosphate monobasic, sodium hydroxide were purchased from sigma (Saint-Louis, U.S.A.).

4.1.2.2 Preparation of carboxyfluorescein solution

Amount of CF was added to PBS (PH=7.4 UPS) which results in a drastic decrease of pH. 0.1 M Sodium hydroxide solution was used to increase pH until a completely transparent brown CF solution was obtained. Then, sodium hydroxide solution was continually added until reaching a pH value of 7.4.

4.1.2.3 Preparation of primary emulsions w1/O by high pressure microfluidizer

Let us focus on one of the most efficient high pressure device, the Microfluidizer® (Microfluidics Corp., Westwood, MA, USA) [25], and precisely the lab-scale model, LV1; It works on the principle of injecting coarse emulsion (premix aqueous phase and oil phase) into an interaction chamber by high pressure up to 1200 psi. Size decrease of emulsion droplets results to the great shear forces, which is supported by the special structure inside interaction chamber. Microfludizer have been used in the pharmaceutical industry [26, 27]. First step is the preparation of the inner aqueous w_1 and oily phases. Aqueous phase w_1 contains maltodetxin (C* Dry 01915), Milli-Q water or PBS, and fluorescent probe (CF solution). Other additives like polymerizing agents, crosslinkers and initiators can potentially be added. Oil phase was prepared by mixing the oil Labrafac WL® and PGPR. The proportions of the different components as well as the volume fraction of dispersed phase were the subjects of a part of the study. Both phases were roughly mixed in a 50 mL Falcon-type flack, with a volume around 10 mL. This coarse emulsion was mixed in a vortex for 1 min, and then setup in a Thermomixer (Eppendorf Thermomixer C, French) at 1000 rpm and 50°C for 3 min. The premix was finalized using an UltraTurrax® (IKA T25M Germany) operating at 24000 rpm, for 3 min. Next, the premix obtained was directly injected into the Microfludizer® operating at 1200 psi, to get the w_1/O nano-emulsion after one passage.

4.1.2.4 Nano-double emulsions produced by spontaneous nano-emulsification

Once the primary emulsion is generated, it is then used as oily phase for the spontaneous emulsification process, with or without a reinforcement of their structure by polymerization. Spontaneous emulsification takes benefit of the intrinsic physicochemical properties of the surfactants, co-surfactants and excipients in the formulation, to create the dispersion of oil phase at the nanometric scale, in the continuous one (aqueous). Low-energy nano-emulsification methods have been described through several methods, like, *e.g.*, spontaneous emulsification or phase inversion temperature methods, but were recently shown to be based on similar mechanisms [28]. In general, the formulation of nano-emulsion is performed by mixing one aqueous phase (that can be pure water) with the oily phase containing the high-HLB non-ionic surfactant (fully miscible in certain conditions of temperatures). When these phases are mixed, the water-miscible surfactants diffuse into the water phase, even so fast that turbulence thereby generated along with spinodal-like decomposition, causes oil nano-scaled droplets to form [29].

The idea here was to transpose the spontaneous nano-emulsification to serve the fabrication of double emulsions, using the primary emulsions as oil phase, assuming that spontaneous emulsification will be a smooth method that preserve the inner droplet structure. Thus, spontaneous nano-emulsification was performed by beforehand mixed primary emulsion with high-HLB nonionic surfactant at room temperature, and then by rapidly pouring PBS in it. This system was then homogenized (vortex), rapidly giving double nano-emulsions. The dispersion properties, size, polydispersity index (PDI) closely linked to the relative proportions between the different components, defined as *(i)* high-HLB surfactant / primary emulsion weight ratio: SOR = 100× $w_{surfactant}$ /($w_{surfactant}$ + w_{oil}), where *w* indicates the weight of the different compounds, and *(ii)* surfactant + oil/water weight ratio: SOWR = 100× $w_{surfactant+oil}$/($w_{surfactant+oil}$ + w_{water}). Influence of the SOR was studied, whereas the one of the SOWR was kept constant at 40% throughout this study (since its influence is negligible, only impacting on the droplet concentration).

4.1.2.5 Characterization of primary nano-emulsion

Nano-emulsion size distributions were assessed by dynamic light scattering (DLS, Malvern ZS 90). Primary emulsion was collected from outlet of microfluidizer, diluted by Labrafac WL®. The concentration of CF effectively present in the primary emulsion was performed by destroying a sample of the dispersion by heating at 70°C during 10 min along with addition of hydrophilic nonionic surfactant (at ratio 1:1). Then centifugation (14000 rpm 20 min, Eppendorf minispin Centifuge) allowed collecting the aqueous phase at the bottom of flack. The supernatant was removed and washed by dichloromethane three times. Then, dichloromethane was completely evaporated, CF dissolved in PBS, and quantified by UV-spectrometers. This quantification method was followed for every primary emulsion formulated and performed in triplicate.

4.1.2.6 Characterization of double nano-emulsion

Likewise, size distribution of double nano-emulsion was determined by DLS After a dilution with PBS. Evaluation of the fraction of CF encapsulated in the inner aqueous phase w_1 of double nano-emulsion was performed with a separation of the double nano-droplets from free dye potentially escaped in external water phase W_2. This separation is done by size exclusion chromatography using desalting column (PD-10 Sephadex® G-25 M, GE Healthcare). Before injection sample, columns were equilibrated with 25 mL of PBS (also used as eluent), and 0.8 mL of the sample was

deposed. We observed a clear boundary of pure PBS, between the first passage of double nano-emulsions (milky) and free dyes (colored), which ensures the efficiency of the separation. The concentration of free CF was finally assessed by UV spectrometers (experiment done in triplicate), giving the value of encapsulation efficiency *EE* as follow:

$$EE = \frac{w_{tot.} - w_{free}}{w_{tot.}}$$

where $w_{tot.}$ and w_{free} are the weight of the total amount of CF in the primary emulsion and the weight of the un-encapsulated CF, respectively. Values of *EE* were quantified by UV spectrophotometry on the free fraction, after separation with size exclusion chromatography. The double-structure of emulsion was imaged by cryogenic transmission electron microscopy (cryoTEM), after the sample dialysis to remove free surfactant in W_2 (1 mL sample into the dialysis membrane, Spectra/Por®, Spectrum Europe B.V., Breda, the Netherlands, cut-off 12 kDa, immersed 50 mL PBS for 12 h).

Double nano-emulsions structure was further characterized by confocal microscopy. By adding a lipophilic fluorescent probe in the oil phase in addition to CF in the aqueous inner compartments, this characterization technique aim to show the co-localization of the two dyes. Double nano-emulsions were loaded with extremely hydrophobic cyanine dye CY5LP. This dye was prepared as reported in previous studies.[30] In Brief, small hydrophilic counterion (*i.e.*, perchlorate) of a cationic cyanine dye 1,1′-dioctadecyl-3,3,3′,3′-Tetramethylindocarbocyanine (Dil) was replaced with a bulky hydrophobic tetraphenylborate (TPB) anion to form CY5LP. Double nano-emulsions were deposited in the 8 well imaging chamber (Ibidi-Biovalley) and imaged by the confocal microscope Leica SP2 using a 20× dry objective (Leica). CF was excited with a 488 nm laser and the emitted fluorescence was detected in the spectral range 500-550 nm, on the other hand, CY5LP was excited with a 632 nm laser and the emitted fluorescence was detected in the spectral range 650-710 nm.

Cryo-TEM experiments were done on double nano-emulsions. The primary emulsions corresponded to entry 2 of Table 2, and double emulsion was formulated adopting SOR = 30 wt.%. Then, the sample was dialyzed for 24h (Spectra/Por®, Spectrum Europe B.V., Breda, the Netherlands, cutoff 12 kDa) to remove free surfactants. The

vitrification of the samples was carried out in a homemade vitrification system. The chamber was held at 22°C and the relative humidity at 80%. A 5 µL drop of the sample was deposited onto a lacey carbon film covered grid (Ted Pella) rendered hydrophilic using an ELMO glow discharge unit (Cordouan Technologies). The grid is automatically blotted to form a thin film which is plunged in liquid ethane hold at -190°C by liquid nitrogen. In that way a vitrified film is obtained in which the native structure of the objects is preserved. The grid was mounted onto a cryo holder (Gatan 626) and observed under low dose conditions in a Tecnai G2 microscope (FEI) at 200 kV. Images were acquired using an Eagle slow scan CCD camera (FEI).

4.1.3 Results and discussion

As theoretically described above, the formulation of double nano-emulsion is a multistep process, schematically illustrated in Fig. 1. Two formulations conditions were investigated, without (process (1)) and with (process (2)) polymerization of aqueous inner phase w_1. In the first section below, we will focus on the study of the influence of the composition and formulation parameters on the properties of the primary emulsion w_1/O. In the process (2), acrylamide, MBA and DMHA are added to the carboxy fluorescence solution to convert the aqueous nano-droplets of the w_1/O nano-emulsion into hydrogel, after UV polymerization. The inset of Fig. 1 shows the aspect of the primary emulsion before and after the passage into the Microfluidizer®, and after polymerization. The premix appears totally turbid while the reverse nano-emulsion w_1/O or the polymerized reverse nano-emulsion w_1(p.)/O appears clear and translucent.

4.1.3.1 Impact of the composition on the properties of the primary nano-emulsion w_1/O

To summarize, the aqueous phase is composed of MilliQ water, maltodextrin (thickener), carboxyfluorescein (probe), and potentially acrylamide (monomer), crosslinker (MBA) and photoinitiator (DMHA). The oil phase is composed of Labrafac WL® (medium chain triglycerides) and PGPR (low-HBL stabilizer). We investigate the influence of the composition of these different components, on the size and size distribution of the w_1/O nano-emulsions, and report the results in Table 1. The different entries are sorted by size, to emphasize the potential impact on the formulation parameters on the nano-emulsion properties.

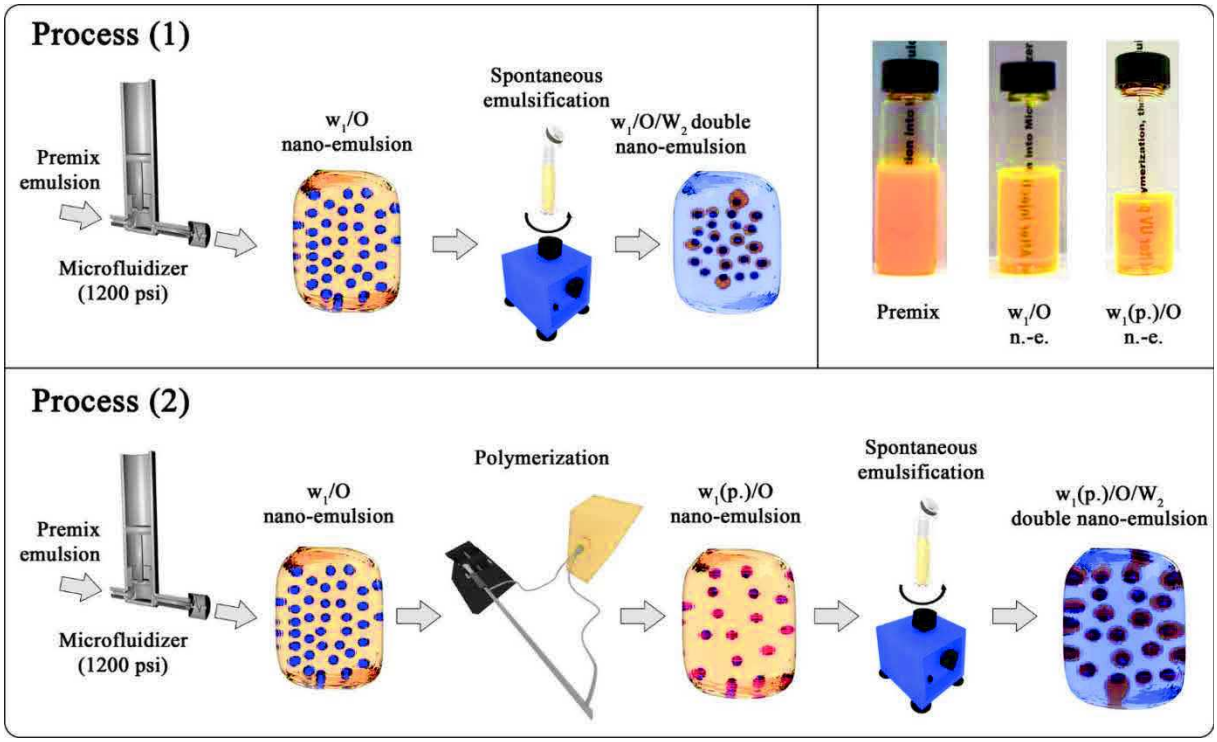

Figure 1. Schematic drawings of the two-step processes to produce either fluorescent double nanomemulsions (process 1) or fluorescent double nanohydrogels (process 2). In first process, the premix emulsion is injected into the high pressure microfluidizer® to obtain a primary emulsion of water nanodroplets in oil phase (w_1/O), which is then used in the spontaneous emulsification to get the double nanoemulsion ($w_1/O/W_2$). In process 2, the premix emulsion containing acrylamide, photoinitiator and crosslinker is injected into the high pressure microfluidizer® to obtain a polymerizable primary emulsion of water/acrylamide nanodroplets in the oil phase (w_1/O). Then the primary emulsion is polymerized by UV irradiation to get nanohydrogels in oil phase ($w_1(p.)/O$) which was then used in the spontaneous emulsification to get double nanohydrogels ($w_1(p.)/O/W_2$). Inset shows the aspect of the primary emulsion before and after the passage into the microfluidizer®, and after polymerization.

Overall, the nanoemulsification process appears efficient, giving hydrodynamic diameters below 200 nm that can reach ca. 50 nm, along with PDI values varying from 0.15 to 0.05 and hence witnessing the good monodispersity of the suspension. The most important parameter affecting nanodroplets size is the surfactant concentration. Increasing the weight content of PGPR induces a decrease in the size of the aqueous phase nanodroplets produced by the microfluidizer®, whatever the viscosity of the aqueous phase (i.e. whatever matodextrin weight content) and weight content of the aqueous phase. On the other hand, the weight contents of matodextrin in water $[MD]_{water}$ has a limited impact on the size, as we can observe it when $[PGPR]_{oil}$ is kept constant at 6.25 wt.%, . This result is likely correlated to the phenomenon that creates and stabilizes the droplets during processing. Indeed, a ratio between the viscosity of continuous and dispersed phases ranging from 1:10 and 1:100 is required to allow and optimize the fractionation of the droplets. With a minimum Maltodextrin weight

content of 30 wt.% of in aqueous phase, this is precisely what we obtained. Then, the other key parameters are the weight contents of the aqueous phase and PGPR in oil. Both parameters will influence, respectively the number of droplets created, and their potential stabilization before coalescence during emulsification. Now, one can understand the clear effect of the PGPR concentration on the resulting size of the droplets, definitively due to a better stabilization of the nanodroplets after generation.

For process 2 (Fig. 1), the resulting polymerizable primary emulsion was then pumped through a PTFE tubing (1.6 mm ID) placed inside a 20 cm long stainless tube which both ends were connected my means of two T-junctions (Swagelok, France) to the two light waveguides of an UV source (Lightningcure LC8, Hamamatsu, Japan) operating at a wavelength of 365 nm and suitable intensity (*ca.* 140 mW/cm^2). As such the residence time of the primary emulsion under the UV light was about 120s which was sufficient to polymerized acrylamide inside the nano-droplets resulting in the formation of nanohydrogels in oil due to the presence of the MBA crosslinker. Sizes and PDI of the obtained polymerized primary nanoemulsions as returned by DLS measurements are reported in Table 2. From this table it can be mentioned that the presence of the fluorescent contrast agent (CF) and polymerization compounds (AM, MBA & DHMA) do not affect too much the size of the aqueous phase nano-droplets (see entries 1 & 3 of Table 2 and entry 12 of Table 1 as well as entries 1-4 of Table 2 respectively).

4.1.3.2 Synthesis of double nano emulsions

After obtaining primary emulsion, the w1/O/W2 double emulsions are prepared by spontaneous emulsion method, which is a low energy method. Since the volume ration of water compared to the one of the primary emulsion (i.e. value of SOWR, see above) was recognized to not having substantial influence on the nano-emulsion properties,18 it was fixed to 40%. On the other hand, a key parameter basically influencing the droplet size is the high-HLB-to-oil ration (namely SOR, see above). SOR was varied from 20 to 40%, and the size of the resulting double nano-emulsion are reported in Tables 3 and 4. As expected, increasing the value of SOR induces the reduction of the double droplet size, even below 100 nm for SOR = 40%.21, 24 In addition, to ensure and confirm the limited impact of the viscosity of aqueous phase on the process, we have followed its impact on the size of the double droplets, selecting [MD]water = 40, 50 and 60 wt.%. Resulting size and PDI of the secondary double nano-emulsions formulated by process (1) and (2) are reported in Tables 3 and 4, and actually show that the suspension are very similar whatever the MD concentration.

Table 1. Composition and size of the primary emulsion in process 1

Entry	Aqueous phase (AP)			Oil phase (OP)			size(nm)	PDI
	AP (wt.%)	Maltodextrin (wt.%/AP)	PBS Sol.* (wt.%/AP)	OP (wt.%)	Labrafac (wt.%/OP)	PGPR (wt.%/OP)		
1	19	72	28	81	98.75	1.25	195	0.12
2	19	72	28	81	99.25	0.75	193	0.06
3	25	72	28	75	92.86	7.14	150	0.12
4	15	72	28	85	93.75	6.25	123	0.03
5	10	30	70	90	94.12	5.88	111	0.15
6	15	30	70	85	93.75	6.25	111	0.10
7	25	30	70	75	92.86	7.14	110	0.08
8	25	50	50	75	92.86	7.14	104	0.12
9	15	50	50	85	93.75	6.25	101	0.15
10	10	40	60	90	87.50	12.5	55	0.16
11	13	50	50	87	90.62	9.375	55	0.28
12	10	50	50	90	87.50	12.5	50	0.11
13	10	60	40	90	87.50	12.5	77	0.08

* no CF in PBS buffer solution

Table 2. Composition and size of the primary emulsion used in spontaneous emulsification in process (2).

Entry	Aqueous phase (AP)							Oil phase (OP)			Size (nm)	PDI
	AP (wt %)	Maltodextrin (wt.%/AP)	PBS sol. (wt.%/AP)	CF (mM in PBS sol.)	AM (wt.%/PBS)	MBA (wt.%/AM)	DHMA (wt.%/AM)	OP (wt.%)	Labrafac (wt.%/OP)	PGPR (wt.%/OP)		
1	10	50	50	50	-	-	-	90	87.50	12.5	58	0.17
2	10	50	50	50	40	10	5	90	87.50	12.5	50	0.13
3	10	50	50	200	40	10	5	90	87.50	12.5	53	0.23
4	10	50	50	50	40	2	5	90	87.50	12.5	47	0.17

This means that the spontaneous emulsification is not affected by the oil content, but still by the surfactant-to-oil ratio. Actually, once the high-HLB nonionic surfactant (Kolliphor ELP®) is mixed with the primary nano-emulsion, it seems to preserve the inner droplets. Then, mixing this oily phase with PBS induces the immediate solubilization of the Kolliphor ELP® by the buffer, and result in the spontaneous emulsification. Size distribution of primary and double emulsion of a representative sample is reported in Fig. 2 (entry 2 in Table 2 for primary emulsion and composition A in Table 4, with SOR = 40 wt.% for double emulsion). It is interesting to note that the primary emulsions w1(p.)/O is centered on 50 nm and the double emulsions w1(p.)/O/W2 reached 122 nm, with both a relatively good monodispersity. Even if the two distributions seem to overlap, they are still compatible with an engulfment of the former in the latter.

Table 3. Surfactant to oil ratio (SOR) used in spontaneous emulsion of process (1) and resulting double nanoparticles characteristics.

Weight content of Maltodextrin in aqueous phase of primary emulsion (w_1) for process 1								
40 wt.%*			**50 wt.%$**			**60 wt.%£**		
SOR (%)	Size (nm)	PDI	SOR (%)	Size (nm)	PDI	SOR (%)	Size (nm)	PDI
20	178	0.51	20	161	0.31	20	168	0.37
25	156	0.34	25	137	0.13	25	153	0.29
30	127	0.17	30	113	0.15	30	119	0.13
35	103	0.12	35	113	0.22	35	98	0.11
40	83	0.14	40	81	0.12	40	87	0.15

* Based on aqueous formulation of entry 10 of Table 1 containing 50 mM of 5(6)-CF
$ Based on aqueous formulation of entry 12 of Table 1 containing 50 mM of 5(6)-CF
£ Based on aqueous formulation of entry 13 of Table 1 containing 50 mM of 5(6)-CF

Table 4. Surfactant to oil ratio (SOR) used in spontaneous emulsion of process (2) and resulting double nanoparticles characteristics for three different compositions of primary aqueous phases (w_1).

Composition A **Entry 2 of Table 2**			**Composition B** **Entry 3 of Table 2**			**Composition C** **Entry 4 of Table 2**		
SOR (%)	Size (nm)	PDI	SOR (%)	Size (nm)	PDI	SOR (%)	Size (nm)	PDI
30	130	0.21	30	145	0.37	30	162	0.39
35	120	0.21	35	133	0.23	35	128	0.20
40	106	0.22	40	116	0.22	40	111	0.25

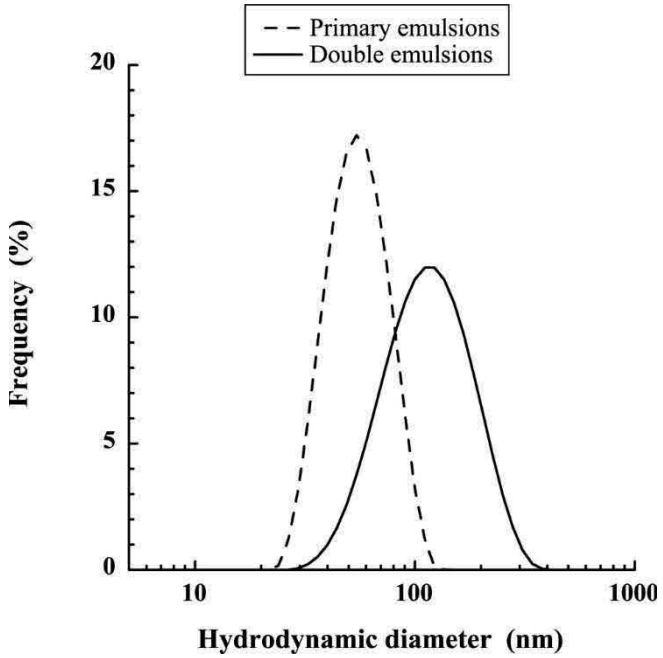

Figure 2. Size distribution of primary emulsion (w_1(p.)/O) corresponding to entry 2 in Table 2, and double emulsions (w_1(p.)/O/W_2) corresponding to composition A in Table 4, with SOR = 40 wt.%.

Considering the whole process of double nano-emulsion formulation, the critical question is to know if the secondary nano-emulsification preserves or not the inner aqueous nano-droplets. Indeed, spontaneous emulsification involves mixing oil with hydrophilic nonionic surfactant, which can potentially solubilize and destabilize hydrophilic materials, and the turbulences generated could, as well, induce their leakage towards the bulk phase W2. To this end, we worked out a method based on the encapsulation of a probe fluorescent probe, easily quantified by absorption. 5(6)-carboxyfluorescein was selected to plays this role, and was encapsulated in the inner aqueous phase w_1 at a concentration of 50 mM (200 mM was also tested for

comparison, see below). Once the double nano-emulsion was formulated, free CF is physically separated from the double nano-droplets by phase exclusion chromatography (PD10 Sephadex G25), and the free portion was quantified.

The first system is the double nano-emulsion (process (1)) with SOR = 20% and [MD] = 50 wt.%, quite polydisperse (PDI = 0.51) and sizing around 177 nm. Encapsulation efficiency obtained was up to ca. 19%. When the droplet size is reduced and monodispersity increased, along with increasing the SOR (concentration of high-HLB surfactant), the encapsulation drops to zero. This is likely due to the polydispersity that allows the bigger droplets to be less affected by the emulsification process. A similar result was obtained from [MD] = 40 wt.%, probably for the same reason. When [MD] is increased to 60 wt.%, a very slight rise of the encapsulation value was obtained, between 7 to 12% encapsulated. Owing to the fact that the MD mainly impact on the viscosity of the phase w1, one can imagine that this increase of CF encapsulation may be related to the slightly higher retention of CF during emulsification.

Table 5. 5(6)-CF encapsulation efficiency for different surfactant oil ratios (SOR), different aqueous phase compositions and same oil phase composition as in Table 2.

	Aqueous phase (process 1)			**Aqueous phase (process 2)**		
EE_f (%) / **SOR (wt.%)**	**Maltodextrin (40 wt.%/AP) 5(6)-CF (60 wt.%/AP)**	**Maltodextrin (50 wt.%/AP) 5(6)-CF (50 wt.%/AP)**	**Maltodextrin (60 wt.%/AP) 5(6)-CF (40 wt.%/AP)**	**Composition A** **Entry 2 of Table 2**	**Composition B** **Entry 3 of Table 2**	**Composition C** **Entry 4 of Table 2**
20	n/a	19.1	n/a	n/a	n/a	n/a
25	n/a	n/d	n/a	n/a	n/a	n/a
30	2.9	n/d	7.2	57.9	17.6	56.8
35	3.0	n/d	8.1	55.6	14.3	55.4
40	2	n/d	12.2	55.4	23.4	56.6

n/d: 5(6)-CF non detected

On the other hand, when the inner phase w_1 is polymerized and turned into hydrogels (process (2)), the double nano-emulsification allows a much greater encapsulation of CF, up to about 50%. Compared to the double nano-emulsion prepared with process (1), here the droplets integrate monomer, crosslinker and initiator and we saw above a limited impact on the size of both primary and double nano-emulsions. According to the same trend that the one observed for process (1), increasing the value of SOR

results in decreasing the double droplet size (see Table 4), *e.g.* from 130 nm, 120 nm and 106 nm, corresponding to SOR 30 wt.%, 35 wt.% and 40 wt.%. Compared with results in the process (1), the size and PDI are lightly increased, maybe related to the fact that more water droplets are encapsulated inside oil globules. However, in any event, converting internal aqueous droplets into hydrogels has a real impact on the encapsulation of the small hydrophilic probe. Values as high as 50-60 % encapsulated are significantly high, and likely related to the fact that crosslinked polyacrylamide creates a water cage that slows down the CF leakage during and after the spontaneous emulsification. It is interesting to note that the presence of crosslinker (MBA, 2 wt.%) has no influence on the results, meaning that the crosslinked polyacrylamide chains sufficiently packed and tangled in the w_1 nano-droplets to retain CF. Another experiment, similarly to the one was conducted with increasing the CF concentration to 200 mM. In that case, the encapsulation efficiency is decreased, roughly around 20%. It follows therefrom that the maximum encapsulation capability is reached and the excess of CF is largely expelled toward the W_2 bulk phase.

To summarize, the efficient encapsulation of small hydrophilic probe like CF is possible with a reinforcing the inner droplet of w_1 aqueous phase with the creation of a hydrogel. The crosslinked polymer chains synthetized are packed enough to prevent the leakage of at least half of the amount of CF, during the spontaneous emulsification, but reaches its limit when the probe concentration is increased. These results are quite important since they bring the evidence of the efficient encapsulation of hydrophilic molecules within nano-emulsion droplets. By the way these results go in the sense of proving that the nano-dispersion we obtained is compatible with a structure of double nano-emulsion with aqueous inner compartments, which is absolutely original with a two-step formulation method.

4.1.3.3 Microscopy

We have shown above that the supposed double nano-emulsions are able to encapsulate a small hydrophilic molecule (CF) with an efficiency that varies in function of the formulation conditions. The objective of this section is to perform further characterization that will confirm the double structure $w_1/O/W_2$ of these nanoparticles through fluorescence microscopy. To this end, aqueous phase contained CF as it was performed above, and oil phase was formulated encapsulated lipophilic dye, CY5LP, a lipophilic form of cyanine 5, stabilized by lipophilic counter ions.[30] Results are reported in Fig. 3.

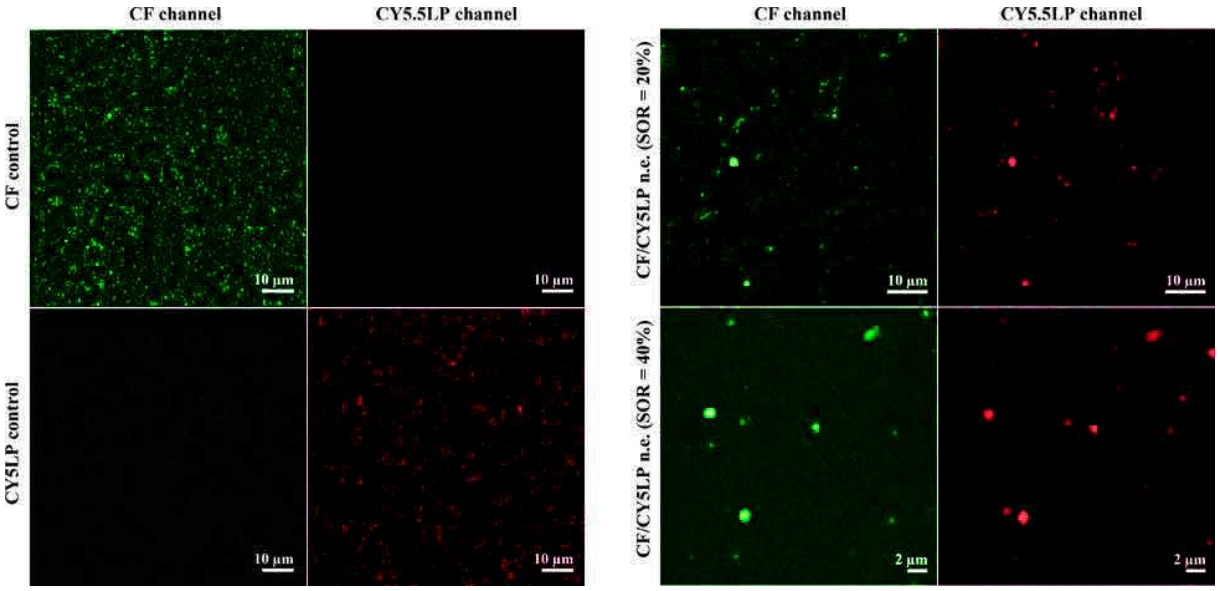

Figure 3. Fluorescence confocal microscopy of w_1(p.)/O/W_2 double nano-emulsions. Carboxyfluorescein (CF) and lipophilic cyanine 5 (CY5LP) are used as hydrophilic and lipophilic model dyes, respectively. CF control is double nano-emulsions containing only CF in aqueous core, and CY5LP is a nano-emulsion only containing CY5LP in oil phase.

On the one hand, control experiments were performed with formulations only containing one dye, either CF or CY5.5LP in order to show that the two signals do not overlap (Fig. 3, left). On the other hand, the same acquisition was performed on double nano-emulsions containing both dyes, with two different formulations differing in SOR values, 40% and 20%. Control experiments appeared very clear and the two emission spectra sufficiently separated to allow the differentiation between the two dyes. Regarding double nano-emulsions containing both drugs, the aim of this experiment was to show the co-localization of the green and red signals in order to corroborate the double structure. In Fig. 3, most of the visible nano-droplets effectively appear to nanoencapsulate both CF and CY5LP. However, to understand the picture, one have to remind *(i)* first that acquisitions were performed in liquid environment that can cause the potential mobility of the droplets between the two acquisitions, and *(ii)* that the droplet population present a log-normal distribution with very big droplets (high brightness) and very small ones (cloudy diffusing signal). Intermediate-sized droplets are still visible and likely subject to movement in liquid medium while bigger seem to stick on the support. These results confirm that hydrophilic molecules encapsulated in the inner aqueous core of the nanoparticules are overall co-localized with lipophilic molecules, this is an additional clue to prove the double structure of the nano-emulsions.

Cryo-TEM microscopy was finally conducted on w_1(p.)/O/W_2 dialyzed samples to observe the double structure of the nano-emulsions. Results are reported in Fig. 3, the core shell structures are seen with width ranging from a 10 nm up to 300 nm (long arrow). The inner part of the objects present a low contrast due to the presence of water. In the background a lot a small objects are seen (arrowhead), likely corresponding to the polymerized polymer without a core. Cryo-TEM results finished to dispel doubts regarding the core double structure of these new nano-carriers, however, they disclosed that the double structure is closer to a core / shell structure than a multi-core / shell structure as it is generally the case for double emulsions.

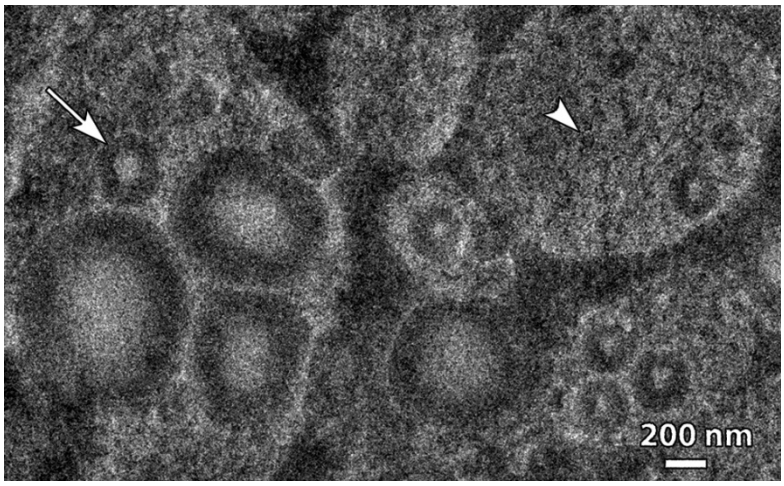

Figure 4. Cryo TEM micrographs of w_1(p.)/O/W_2 double nano-emulsions (The sample was synthesized by formulation of the primary emulsion at entry 2 table 2, and SOR fixed at 30 wt.%). The darkest areas are the supporting lacey film.

4.1.4 Summary

This work had the objective to create a double emulsion at a nanometric scale by a two-step process. The first primary nano-emulsions, so-called reverse nano-emulsion w_1/O was already a full formulation challenge, reached by high-pressure homogenizer (Microfluidizer®). The formulation of reverse nano-emulsions was shown mainly related to the composition of the system, namely to the concentration of low-HLB surfactant (PGPR) soluble in oil (medium chain triglyceride) and the quantity of maltodextrin in the aqueous phase that impacts on the viscosity of dispersed phase. We disclosed that a combination of $[PGPR]_{oil}$ > 7% and $[MD]_{water}$ > 50% is necessary to decrease the droplet size below 100 nm, and a combination $[PGPR]_{oil}$ > 12% and $[MD]_{water}$ > 50% drops the size below 50 nm. The second step of the process was the spontaneous emulsification of this primary nano-emulsion, giving rise of double nano-

emulsion $w_1/O/W_2$, and the characterization of the leakage of an encapsulated small hydrophilic molecule (CF). The results showed that encapsulation efficiency (EE) can strongly differ in function of the formulation parameters like the final size of the double droplets (reducing the EE) or the polymerization of the inner aqueous phase (increasing the EE up to *ca.* 58%). Further cryo-TEM and fluorescence microscopy have been conducted on the most efficient formulations, and corroborate the potential double structure $w_1/O/W_2$. We can conclude that developing a formulation of double nano-emulsion by a two-step approach is a real challenge, pioneered by this work, opening the door to numerous formulations and applications.

In this section drug-loaded double nanocarriers were successfully produced by means of a two-step process whose key step relied on the spontaneous emulsification method. This method was quite effective to generate at virtually no energy input size-controlled hydrophobic nanodroplets. In the next section this method will be applied for the production of nanolipogels composed of a mixture of either polymerized or non-polymerized bifunctional acrylate and parental-grade oil nanodroplets loaded with two different kinds of contrast agent nanoparticles of smaller size.

4.1.5 References

1. Seifriz, W., *Studies In Emulsions 3* The Journal of Physical Chemistry, 1924. **29**(6): p. 10.
2. Becher, P., *Emulsions: Theory and practice.* 1965.
3. Mahrhauser, D.-S., C. Fischer, and C. Valenta, *Double emulsions based on silicone-fluorocarbon-water and their skin penetration.* International Journal of Pharmaceutics, 2016. **498**: p. 130-133.
4. Garber, A.J., *Benefits of combination therapy of insulin and oral hypoglycemic agents.* Archives of Internal Medicine, 2003. **163**(15): p. 1781-1782.
5. Lane, D., *Designer combination therapy for cancer.* Nat Biotech, 2006. **24**(2): p. 163-164.
6. Kemp, J.a., et al., *"Combo" nanomedicine: Co-delivery of multi-modal therapeutics for efficient, targeted, and safe cancer therapy.* Advanced Drug Delivery Reviews, 2016. **98**: p. 3-18.
7. Rubinfeld, B., et al., *Identification and immunotherapeutic targeting of antigens induced by chemotherapy.* Nat Biotechnol, 2006. **24**(2): p. 205-9.
8. Gu, H., et al., *Facile One-Pot Synthesis of Bifunctional Heterodimers of Nanoparticles: A Conjugate of Quantum Dot and Magnetic Nanoparticles.* Journal of the American Chemical Society, 2004. **126**(18): p. 5664-5665.
9. Santra, S., et al., *Conjugation of Biomolecules with Luminophore-Doped Silica Nanoparticles for Photostable Biomarkers.* Analytical Chemistry, 2001. **73**(20): p. 4988-4993.
10. Burns, A., H. Ow, and U. Wiesner, *Fluorescent core-shell silica nanoparticles: towards "Lab on a Particle" architectures for nanobiotechnology.* Chemical Society Reviews, 2006. **35**(11): p. 1028-1042.
11. Wu, S.-H., Y. Hung, and C.-Y. Mou, *Compartmentalized Hollow Silica Nanospheres Templated from Nanoemulsions.* Chemistry of Materials, 2013. **25**(3): p. 352-364.

12. Allen, C., D. Maysinger, and A. Eisenberg, *Nano-engineering block copolymer aggregates for drug delivery.* Colloids and Surfaces B: Biointerfaces, 1999. **16**(1–4): p. 3-27.
13. Engel, R.H., S.J. Riggi, and M.J. Fahrenbach, *Insulin: Intestinal Absorption as Water-in-Oil-in-Water Emulsions.* Nature, 1968. **219**: p. 2.
14. Khopade, A.J., K.S. Nandakumar, and N.K. Jainb, *Lectin-Functionalized Multiple Emulsions for Improved Cancer Therapy.* Journal of Drug Targeting, 1998. **6**: p. 285-292.
15. Vermaj, R. and T.N. Jaiswal, *Protection, humoral and cell-mediated immune responses in calves immunized with multiple emulsion haemorrhagic septicaemia vaccine.* Vaccine, 1997. **15** p. 7.
16. Florence, A.T. and D. Whitehill, *Stability and Stabilization of Water-in-Oil-in-Water Multiple Emulsions*, in *Macro- and Microemulsions*. 1985, American Chemical Society. p. 359-380.
17. S. S. Davis, H.P.R., T. S. Purewal, *Ostwald Ripening and the Stability of Emulsion Systems: An Explanation for the Effect of an Added Third Component.* Journal of Colloid and Interface Science

1981. **80**(2): p. 4.

18. Zambaux, M.F., et al., *Influence of experimental parameters on the characteristics of poly(lactic acid) nanoparticles prepared by a double emulsion method.* Journal of Controlled Release, 1998. **50**(1-3): p. 31-40.
19. Jarrod A. Hanson1, C.B.C., Sara M. Graves, Zhibo Li, Thomas G. Mason, Timothy J. Deming, *Nanoscale double emulsions stabilized by single-component block copolypeptides.* Nature, 2008. **455**: p. 5.
20. Seifriz, W., *Studies In Emulsions 1-2.* J. Phys. Chem., 1925. **29**: p. 14.
21. Ficheux, M.-F., et al., *Some Stability Criteria for Double Emulsions.* Langmuir, 1998. **14**: p. 5.
22. Matsumoto, S., Y. Kita, and D. Yonezawa, *An attempt at preparing water-in-oil-in-water multiple-phase emulsions.* Journal of Colloid and Interface Science, 1976. **57**(2): p. 353-361.
23. Anton, N., J.-P. Benoit, and P. Saulnier, *Design and production of nanoparticles formulated from nano-emulsion templates—A review.* Journal of Controlled Release, 2008. **128**: p. 15.
24. Anton, N. and T.F. Vandamme, *The universality of low-energy nano-emulsification.* International Journal of Pharmaceutics, 2009. **377**: p. 6.
25. Shay, R., *Flavor Manufacturing*, in *Source Book of Flavors* G. Reineccius, Editor. 1994, Springer-Science+Business Media. p. 68.
26. Jafari, S.M., Y. He, and B. Bhandari, *Nano-Emulsion Production by Sonication and Microfluidization—A Comparison.* International Journal of Food Properties, 2006. **9**: p. 11.
27. Maa, Y.-F. and C.C. Hsu, *Performance of Sonication and Microfluidization for Liquid–Liquid Emulsificatio.* Pharmaceutical Development and Technology, 1999. **4**: p. 8.
28. Vandamme, T.F. and N. Anton, *Low-energy nanoemulsification to design veterinary controlled drug delivery devices.* International Journal of Nanomedicine, 2010. **5**: p. 7.
29. Miller, C.A., *Spontaneous Emulsification Produced by Diffusion - A Review.* Colloids and Surfaces,, 1988. **29**: p. 14.
30. Kilin, V.N., et al., *Counterion-enhanced cyanine dye loading into lipid nano-droplets for single-particle tracking in zebrafish.* Biomaterials, 2014. **35**(18): p. 4950-4957.

4.2 Production of contrast agent-loaded nanolipogels by spontaneous emulsification

ABSTRACT

Nanogels have attracted substantial interest in different fields thanks to their controllable and three-dimensional physical structure, good mechanical properties and biocompatibility. Many technologies have been proposed for their preparation and design, however they result in broad size distributions and a poor control on their size. Thus the preparation of nanogels with monodispersed sizes by simple emulsification is a real challenge still in abeyance to date. In this study we propose an original low energy emulsification approach for the production of nanogels whose final size can be easily controlled in the range 30 to 400 nm. The procedure consists in the preparation of an oil-in-water nano-emulsion by spontaneous emulsification in which a bi-functional acrylate monomer was used as an additive. The nanodroplets size was found to depend on the additive and surfactant to oil weight ratios. Then the nano-emulsions were polymerized by UV light to achieve the production of lipophilic nanogels. Nanogels loaded with iron-oxide and gold nanoparticles were also produced as a kind of contrast agent nanovectors whose structure was confirmed by TEM.

4.2.1 Introduction

Nanogels can be defined as a three-dimensional crosslinked polymeric network nano object swollen by a fluid. They have receive considerable attraction in many aspects due to their potential applications such as sensing,[1] diagnostics,[2, 3] bioengineering[4] and drug delivery.[5] Unlike usual polymer nanoparticles, which exhibit a densely packed structure, nanogels can trap small molecules inside a nanocompartment within the polymer network. It allows a versatile control release of small molecules by the change of nano-dimension in response to different triggers. Nanogels have been synthesized by various strategies, which were mainly classified into two categories. First of them, polymeric networks were formed by covalently bound polymer chains. In this case, nanogels are obtained by gelation of nano- or micro-emulsion,[6] cross-linking of block copolymer micelle[7] and nano template method.[8] Different chemistries have been developed to offer optimal properties of nanogels such as crosslinking on disulfide groups, similarly to those existing in in biological environment.[9] On the other hands, polymeric network can be also

generated by non-covalent interactions between polymer chains, such as i hydrophobic interactions, hydrogen bonding, van der Waals interactions and so forth. However, physiochemical properties of this latter family of gels appears difficult to control.

Generally, the commonly used method to synthesize nanogels faces some challenges, like the encapsulation of lipophilic molecules. Indeed, most of the methods reported in literature for the fabrication of hydrogels and nano-hydrogels concern water-soluble polymers.[10, 11] Regarding the synthesis and formulation of nanogels able to encapsulate lipophilic or hydrophobic molecules, only few solutions were reported, such as the crosslinking of micelles,[12] or the chemical modification of polymers including grafting of lipophilic chains.[9]

In this paper, we propose a new methodology to synthetize lipophilic nanogels based on nano-emulsions, through the crosslinking of lipophilic polymers pre-solubilized in the oil core of droplets. The nano-emulsions were i) formulated with a mixture of a difunctional monomer and medium chain triglycerides, ii) obtained by a low-energy nano-emulsification method (spontaneous emulsification) and finally ii) photopolymerized. As a result of the spontaneous emulsification, nano-emulsions and then nanogels were obtained with a controllable size and homogeneous size distribution. Such nanogels have potential to encapsulate hydrophobic cargos for drug delivery.

4.2.2 Experimental section

4.2.2.1 Materials

A mixture of medium chain triglycerides (Labrafac® WL 1349, Gattefossé S.A., Saint-Priest, France), tri(propylene glycol) diacrylate (TPGDA, supplied by Aldrich) and a photoinitiator 1-hydroxycyclohexyl phenyl ketone (HCPK, 99% purity, supplied by Aldrich) was used in the preparation of nano-emulsions. Note that TPGDA also acts as a crosslinker due to its two double bonds. The water phase comprised distilled water and a nonionic hydrophilic surfactant (Kolliphor ELP®, BASF, Ludwigshafen, Germany), which is a polyethoxylated-35 castor oil with a Hydrophilic-Lipophilic Balance (HLB) of 12~14 and playing a crucial role in the spontaneous emulsification. Iron oxide nanoparticles were obtained according to the thermal decomposition method reported elsewhere [13].

4.2.2.2 Preparation of nanogels

Figure 5 **Schematic drawings of the low-energy nano-emulsification device (a) and continuous-flow UV polymerization setup (b).** depicts the schematic drawing of the low-energy nano-emulsification device use to generate the nano-emulsions and also shows the continuous-flow UV polymerization setup to produce the nanogels. The mixture of Labrafac® and TPGDA was used as the oily phase for the emulsification process; the two components are extremely miscible, which has orientated our choice. Low-energy nano-emulsification methods have been described through several methods like spontaneous emulsification or phase inversion temperature method which was recently shown to be based on similar mechanisms.[14] In general, the formulation of oil-in-water emulsions is performed by mixing one aqueous phase (that can be pure water) with the oily phase containing a high-HLB non-ionic surfactant (fully miscible in certain conditions of temperatures). When these phases are mixed, the water-miscible surfactants diffuse into the water phase, fast enough that turbulence thereby generated along with spinodal-like decomposition cause oil droplets to form [15]. Spontaneous emulsification takes benefit of the intrinsic physicochemical properties of the surfactants, co-surfactants and excipients in the formulation, to create the dispersion of the oily phase at the nanometric scale, in the continuous phase (aqueous solution).

The idea here was to take advantage of the spontaneous emulsification to serve the fabrication of nano-emulsions, using the mixture of Labrafac® and TPGDA, assuming that all the nanodroplets generated have the similar composition of both compounds. Spontaneous emulsification was performed by beforehand mixing the mixture of Labrafac® and TPGDA with the high-HLB nonionic surfactant Kolliphor ELP® at 75ºC. Then, when the mixture was homogeneous, the aqueous phase was rapidly poured in the oily one. This system was finally homogenized by vortexing (Figure 5a) at low RPM resulting in the formation of a nano-emulsion. Therefore, the impact of the different formulation parameters on the dispersion properties (size, size distribution, polydispersity index (PDI)) were studied. These formulation parameters were defined as *(i)* the weight ratio of Labrafac® and TPGDA in oil phase, *(ii)* the weight ratio between high-HLB surfactant and oil phase: SOR = $100 \times w_{surfactant} /(w_{surfactant} + w_{oil})$, where w indicates the weight of the different compounds, and *(iii)* the weight ratio between {surfactant + oil} and aqueous phase: SOWR = $100 \times w_{surfactant} + w_{oil} / (w_{surfactant} + w_{oil} + w_{water})$. In the current study, we mainly investigated the influence of the two former parameters, ratio of Labrafac / TPGDA and SOR, whereas SOWR was kept constant at 40% throughout this study (since its influence is negligible, only impacting on the droplet concentration). The freshly prepared nano-

emulsions were polymerized by UV irradiation in a tube-in-tube device shown in Figure 5b. The above nano-emulsions were charged in a 5 mL plastic syringe (HSW, Norm-Ject, France). Then the syringe was placed in the holder of a syringe pump (PHD 2000, Harvard Apparatus) aiming at delivering the nano-emulsion through a 22 cm long (Polytetrafluoroethene) PTFE tubing (1.68 mm ID x 3.2 mm OD) at a constant flowrate of 0.025 mL/min. The PTFE tubing was inserted inside a 4 cm ID stainless steel tube equipped at both ends with a T-junction (Swagelok) in which were set the two light guides of an UV source (Lightningcure LC8, Hamamatsu) operating at λ = 365 nm; a wavelength corresponding to the maximum of absorbance of the photo-initiator added into the nano-emulsion monomer phase. Given the size of the PTFE tubing and the flow rate, the residence time of the nano-emulsion under the UV irradiation was about 20 min. At the end of the PTFE tubing, the polymerized nano-emulsion, *i.e.* the colloidal suspension nanogel particles, was collected in a vial.

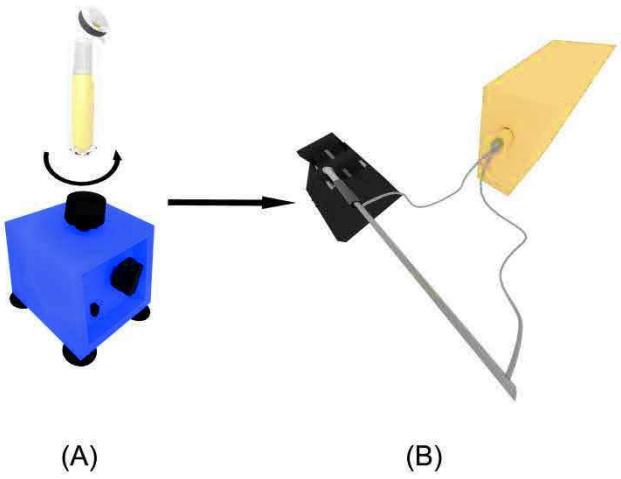

Figure 5 Schematic drawings of the low-energy nano-emulsification device (a) and continuous-flow UV polymerization setup (b).

4.2.2.3 Preparation of encapsulated iron oxide nanogels

Iron oxide nanoparticles in dichloromethane (DMC supplied by Aldrich) were first added into pure Labrafac® at a weight content of 16 wt.%. Then the solution was heated at 75ºC to evaporate DMC. Afterwards TPGDA was added to the suspension of iron oxide nanoparticles in Labrafac® at a weight content of 50 wt.%. The resulting mixture was finally used as the Labrafac® / TPGDA oil phase in the aforementioned procedure for the production of unloaded nanogels in which SOR was fixed at 40 %.

4.2.2.4 Dynamic light scattering

The size and size distribution of the nanogels were assessed by dynamic light scattering (DLS) using a Malvern Nano ZS instrument (Malvern, Orsay, France). The helium-neon laser (4 mW) was operated at 633 nm, the scatter angle was fixed at 173° and the sample temperature was maintained at 25°C. The polydispersity index of the particle size distribution (PDI) is a measure of the broadness of the size distribution and it is commonly admitted that PDI values below 0.2 corresponds to monomodal distributions. Measurements of nanosuspensions size were performed in triplicates by pouring 0.02 mL of the nanosuspension into 1 mL of Ultrapure water.

4.2.2.5 Transmission electron Microscope

Iron oxide nanoparticles nanogels were characterized by transmission electron microscopy. A drop of susp nanosuspension was placed on a carbon grid (carbon type-A, 300 mesh, copper, Ted Pella Inc. Redding, PA) and dried at 40ºC. Observations were carried out using a Philips Morgagni 268D electron microscope.

4.2.3 Results and discussion

4.2.3.1 Nanogels size

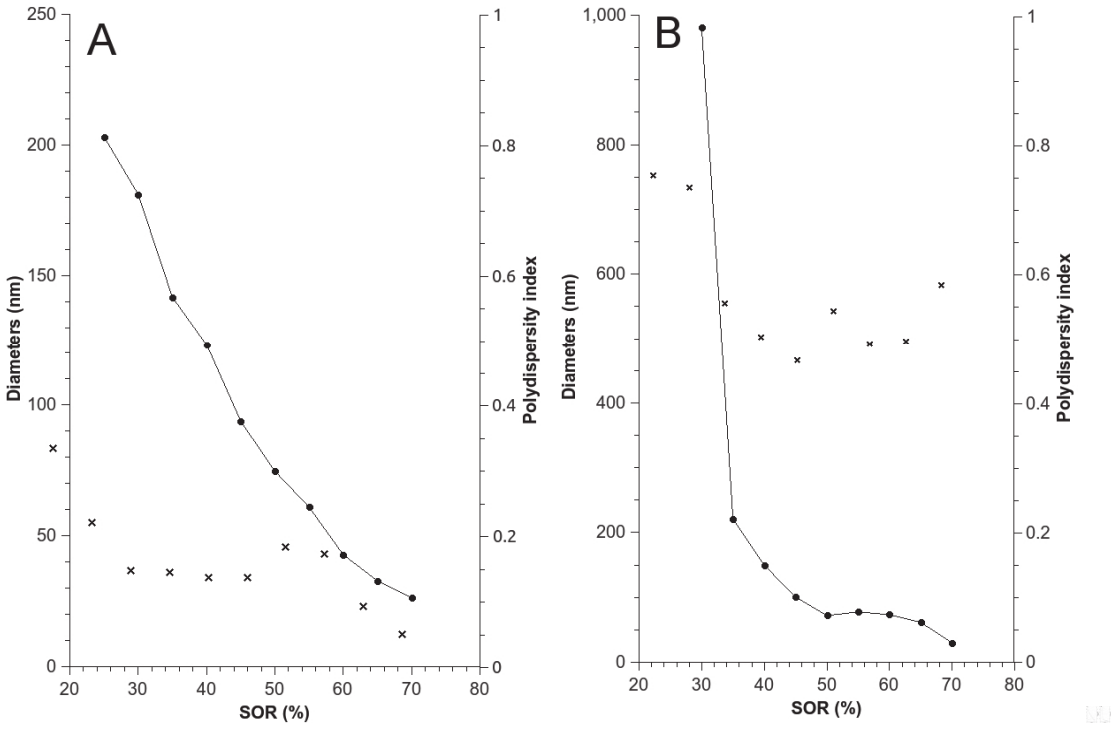

Figure 6. (A) Nano-emulsions formulated with pure Labrafac®, (B) Nanogel formulated with pure TPGDA. Hydrodynamic diameter (filled circles) and PDI (cross) are plotted against the surfactant oil weight ratio.

First, the effect of SOR on the hydrodynamic nanogels diameter and PDI was studied, and the results are presented in Figure 6 f for pure Labrafac® and pure TPGDA. It appears that the spontaneous emulsification allows the production of oil nanodroplets using indifferently Labrafac® or TPGDA; however PDI value for the former are significantly lower. Figure 6 shows that the droplet size follows a sharp decrease along with the SOR. Nano-emulsions size synthesized with Labrafac® can be tuned from 203.1 to 26.36 nm, which correspondent the PDI from 0.335 to 0.051. The results stem from the principle of spontaneous emulsification, in which nano-droplets are generated by turbulent displacement. During the procedure, turbulent displacement can be controlled with a fast diffusion of nonionic surfactant Kolliphor ELP® from organic phase into aqueous phase. Based on this principle, the higher the weight content of Kolliphor ELP® (i.e. SOR), the stronger is the turbulence displacement and the smaller is the nano-emulsions size. Higher size PDI emphasized the significant difference in affinity of the Kolliphor ELP® for the oil phase. It was worth noticing that one can deduct from the PDI values shown in Figure 6 that the best affinities of the nonionic surfactant are for the medium chain triglycerides.

Similar experiments were then implemented using the mixture of Labrafac® and TGPDA. Results are reported in Figure 6, and show a global trend similar to that of the one reported in Figure 6, i.e. a sharp decrease of the nano-emulsions size with SOR.

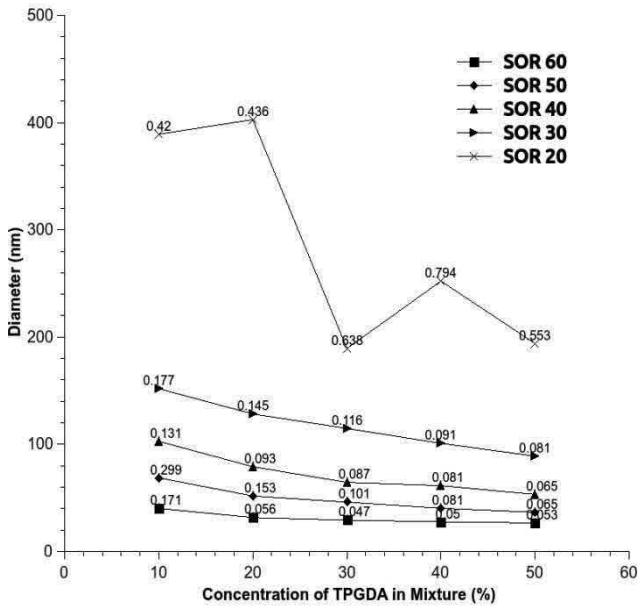

Figure 7. Nanogels formulated with the mixture of TPGDA and Labrafac®. Hydrodynamic diameter and PDI are plotted against the TPGDA weight content.

Interestingly, the mixture of TPGDA and Labrafac® allowed the production of the smallest nano-emulsions sizes and PDIs. At a SOR of 30%, the nano-emulsions size decreases from 151.9 nm (PDI=0.177) down to 89.01 (PDI=0.081) for 10 to 50 wt.%

TPGDA in oil, respectively. In contrast and for the same SOR, the size of nanogels formulated with pure Labrafac® reached 181 nm (PDI=0.221) and 43 nm for a SOR of 60%. Whereas nano-emulsion size prepared at 50 wt.% TPGDA in oil phase reached 53 nm for a SOR of 40%. These results emphasized that the mixture of TPGDA and Labrafac® found a synergetic effect, able to decrease the nano-emulsion droplet sizes even smaller than the ones obtained with the individual pure compounds. These results may open doors to new alternative formulations to get homogenous nano-emulsions at lower SOR.

4.2.3.2 Versatility of nanogels

As previously mentioned and due to their intrinsic structure, nanogels formulated with the mixture of TPGDA and Labrafac® have potential to be applied in pharmaceutics field. Indeed, one can imagine a structure such as the one illustrated in Figure 8. The nanogels consist in a crosslinked network of Poly(TPGDA) chains swollen by Labrafac®; thus forming a bi-continuous structures able to entrap and encapsulate efficiently lipophilic active ingredients or contrast agent for cargo delivery of biomedical imaging.

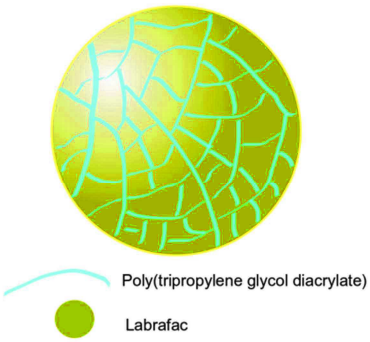

Figure 8. Schematic illustration of nanogels synthesized with a mixture of TPGDA and Labrafac® by spontaneous emulsification

As a proof of concept, nanogels have been designed to encapsulate iron oxide or gold nanoparticles which were mixed with the mixture of Labrafac® and TPGDA as oil phase. The nano-emulsions were formulated at a SOR of 40 % and a 50 wt.% of TPGDA in oil phase, following the procedure described in Figure 5. As a result, nanogels encapsulating either iron oxide or gold nanoparticles appeared quite close in size, *ca.* 65.99 nm (PDI=0.151) and 78.91 nm (PDI=0.116), respectively. These DLS results were confirmed by TEM pictures (Figure 9) presenting sizes around 50 nm for

both systems. While iron oxide NPs are shown in rather spherical shape that reflects the location of the nanogel droplet, the gold nanoparticles, more contrasted, appear more randomly agglomerated. On can think that iron oxide nanoparticles or gold nanoparticles have been successfully encapsulated in the nanogels although not directly observed.

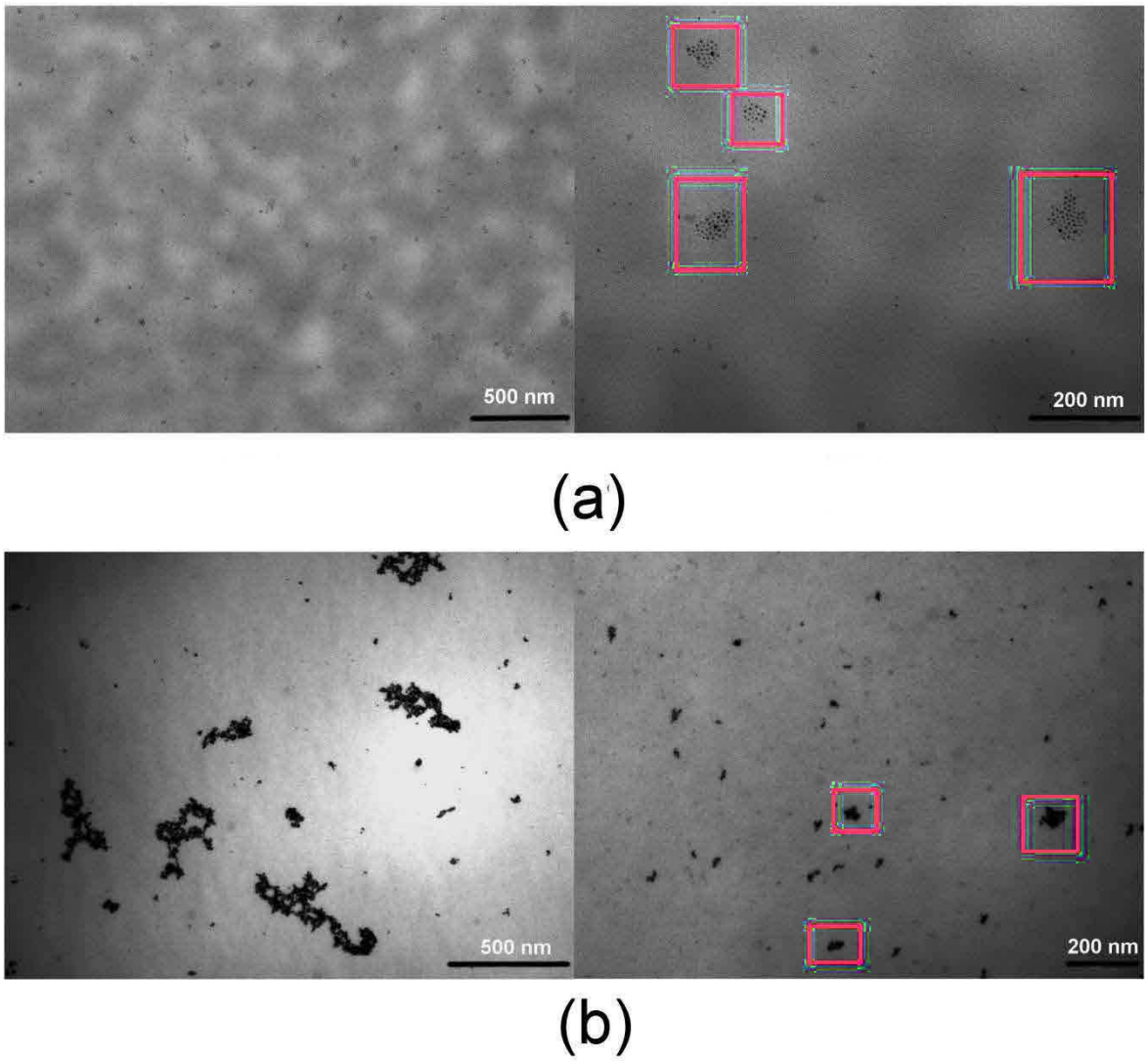

Figure 9. TEM micrographs of encapsulated iron oxide (a) and gold (b) nanoparticles nanogels

4.2.4 Summary

A new and facile route to the synthesis of lipophilic nanogels filled with one type of oil (Labrafac®) is presented. The approach follows a two-step procedure. First, a TPGDA / Labrafac® oil-in-water nano-emulsion was produced by spontaneous emulsification using a high-HLB nonionic hydrophilic surfactant. Then the

difunctional TPGDA monomer was photopolymerized to give rise to a colloidal suspension of nanogels. Results showed that this method can be used to produce monodisperse nanogels at low surfactant to oil ratios (SOR), with a size easily tunable from *ca.* 400 nm down to *ca.* 30 nm according to the formulation parameters (i.e. TPGDA / Labrafac® weight ratio and SOR). As a proof of concept, contrast agents (iron oxide or gold NPs) were encapsulated in such nanogels. Their effective encapsulation in nanogels of 65 nm in size (measured by DLS) was confirmed by TEM analyses which in addition have exhibited the same size range (around 50-60 nm diameter for both systems). The main advantage of such route is the high loading capacity of nano-emulsions but with a reinforced structure that could prevent the potential leak of active principles or contrast agents during applications.

4.2.5 References

1. Peng, H.S., et al., *A nanogel for ratiometric fluorescent sensing of intracellular pH values.* Angewandte Chemie - International Edition, 2010. **49**(25): p. 4246-4249.
2. Oishi, M., S. Sumitani, and Y. Nagasaki, *On-off regulation of 19F magnetic resonance signals based on pH-sensitive PEGylated nanogels for potential tumor-specific smart 19F MRI probes.* Bioconjugate Chemistry, 2007. **18**(5): p. 1379-1382.
3. Hasegawa, U., et al., *Nanogel-quantum dot hybrid nanoparticles for live cell imaging.* Biochemical and Biophysical Research Communications, 2005. **331**(4): p. 917-921.
4. Hayashi, C., et al., *Osteoblastic bone formation is induced by using nanogel-crosslinking hydrogel as novel scaffold for bone growth factor.* Journal of Cellular Physiology, 2009. **220**(1): p. 1-7.
5. Qiao, Z.Y., et al., *Multi-responsive nanogels containing motifs of ortho ester, oligo(ethylene glycol) and disulfide linkage as carriers of hydrophobic anti-cancer drugs.* Journal of Controlled Release, 2011. **152**(1): p. 57-66.
6. McAllister, K., et al., *Polymeric nanogels produced via inverse microemulsion polymerization as potential gene and antisense delivery agents.* Journal of the American Chemical Society, 2002. **124**(51): p. 15198-15207.
7. Chacko, R.T., et al., *Polymer nanogels: A versatile nanoscopic drug delivery platform.* Advanced Drug Delivery Reviews, 2012. **64**(9): p. 836-851.
8. Sasaki, Y. and K. Akiyoshi, *Nanogel engineering for new nanobiomaterials: From chaperoning engineering to biomedical applications.* Chemical Record, 2010. **10**(6): p. 366-376.
9. Ryu, J.H., et al., *Surface-functionalizable polymer nanogels with facile hydrophobic guest encapsulation capabilities.* Journal of the American Chemical Society, 2010. **132**(24): p. 8246-8247.
10. Ryu, J.-H., et al., *Self-Cross-Linked Polymer Nanogels: A Versatile Nanoscopic Drug Delivery Platform Supporting Info.* Journal of the American Chemical Society, 2010. **3**(c): p. 2-10.
11. Torchilin, V.P., *Recent advances with liposomes as pharmaceutical carriers.* Nature reviews. Drug discovery, 2005. **4**(2): p. 145-160.
12. O'Reilly, R.K., C.J. Hawker, and K.L. Wooley, *Cross-linked block copolymer micelles: functional nanostructures of great potential and versatility.* Chemical Society reviews, 2006. **35**(11): p. 1068-1083.

13. Sun, S., et al., *Monodisperse MFe_2O_4 (M) Fe, Co, Mn) Nanoparticles.* J. AM. Chem. Soc., 2004. **126**: p. 6.
14. Vandamme, T.F. and N. Anton, *Low-energy nanoemulsification to design veterinary controlled drug delivery devices.* International Journal of Nanomedicine, 2010. **5**: p. 7.
15. Miller, C.A., *Spontaneous Emulsification Produced by Diffusion - A Review.* Colloids and Surfaces,, 1988. **29**: p. 14.

CHAPTER 5
CONCLUSION AND PERSPECTIVES

5.1 Context and objectives

Nanocarriers including polymeric nanoparticles, liposomes, polymerosomes, (double) emulsions, or nanogels have attracted a substantial attention in pharmaceutics due to their high potential to serve as efficient drug delivery or contrast agent vehicles. However, the methods conventionally used to produce such vehicles suffer from several drawbacks that impede their further development. To the foremost, the large size distribution of these objects which reduce their properties (e.g. reproducibility in delivering a given amount of drug over a specified timeframe). Also, most of them are produced from an initial step that consists in the emulsification of a liquid in another immiscible liquid. Conventional apparatus used to achieve this emulsification are quite energy consuming (e.g. high pressure homogenizer), not really suitable for continuous flow production (e.g. sonificator) and poorly suitable to achieve the production of size-controlled double nanoemulsions. Therefore there is a need for low energy methods that can produce such nanocarriers while achieving a good control on their size and *in fine* of their reproducible properties.

In this context, this work aimed at combining advanced technologies for mixing and emulsification to produce nanocarriers with controlled features, which include size, size distribution, drug loading and delivery rate or morphology like double nanodroplets.

5.2 Results

During this Ph.D. work, three different methods, namely micromixer-assisted nanoprecipitation, microfluidic-assisted elongational-flow nanoemulsification and spontaneous emulsification, were successfully applied to produce a large variety of nanocarriers whose cargos were either a model drug or a contrast agent.

First method allowed the production of monodisperse Ketoprofen-loaded PMMA NPs whose size can be easily tuned from 200 nm down to 110 nm upon an increase in the flow rate of the non-solvent (water) which promotes the precipitation of the polymer

solution (admixed with drug). Once produced, the nanocarriers were dried by means of a commercial spray drying apparatus. NPs size was found to be moderately affected by the drying process while the sustain drug release profile was significantly altered by the size of the NPs (increasing for smaller NPs) and by the spray-drying step (lower by 10 to 15% depending in NPs size). However it was proved that drug-loaded NPs can be simply produced, dried, stored and re-dispersed while still exhibiting a pretty decent release rate (above 40% over 6 hours).

This method was also used to produce 200 nm PMMA nanoparticles loaded with superparamagnetic iron oxide nanoparticles (SPIONs) at a weight content of up to 60 wt.%.

Second method was used to double the mass fraction of SPIONs-loaded PMMA NPs in final colloidal suspension and to get more spherical nanoparticles of lower size (100 nm).

Third method was developed to produce double nanoemulsions ($w_1/O/W_2$) whose inner nanodroplets were loaded with a florescent probe (5(6)-carboxyfluorescein). This method involves two steps: i) the preparation, by means of a commercial emulsification device (microfluidizer), of the primary w1/O emulsion whose aqueous phase (w_1) was composed of a PBS buffer solution admixed with the contrast agent and a thickener (Maltodextrin) while oil phase (O) contained a parenteral-grade oil (Labrafac) and a nonionic low-HBL surfactant (PGPR); ii) the spontaneous emulsification of the primary oil phase by addition of a nonionic emulsifier (Cremophor) followed by a large amount of PBS buffer solution (W_2). Primary emulsion size (range 50 - 200 nm) was found to be moderately affected by the weight amount of thicker (increasing with Maltodextrin weight amount) but largely affected by the weight amount of surfactant in oil phase (decreasing with an increase in PGPR weight amount). If like for the primary emulsion, the Maltodextrin weight content has a moderate effect on the double nanodroplets size, the Cremophor to primary emulsion weight contents ratio (SOR) is the primary parameter which control the final size of the double nanoemulsion. An increase in SOR from 20 to 40% induces a sharp decrease in double nanocarriers size from 160 down to 80 nm. When the aqueous

phase of primary emulsion (w1) contained a polymerizable formulation (acrylamide monomer, crosslinker and photoinitiator), this two-step method allowed the production of poly(acrylamide) nanohydrogels surrounded by an oil shell (Labrafac). These double nanohydrogels were found to significantly increase the florescent probe encapsulation efficiency (EE(f)) up to 50% compared to the low EE(f) of 2 to 12% obtained without monomer.

The spontaneous emulsification was also used to produce nanolipogels when the previous w_1/O emulsion was replaced by a lipophilic mixture composed of a difunctional acrylate monomer (tripropyleneglycol diacrylate, TPGDA), a photoinitiator and Labrafac. Upon addition of Cremophor and PBS buffer solution, nanodroplets of the lipophilic mixture were obtained and then polymerized by UV irradiation to form nanolipogels, whose matrix was composed of crosslinked poly(TPGDA) swollen by Labrafac oil, in suspension into an aqueous phase. It was found that nanolipogels size depends on SOR parameter and TPGDA weigh content in lipophilic mixture and can reach values as low as 57 nm. Finally these nanolipogels were successfully loaded with magnetic or gold nanoparticles to potentially serve as contrast agent nanocarriers.

5.3 Perspectives

If this work allowed developing new methods for producing morphologically-complex nanocarriers, there are still many unknowns which impede their further optimization:

- How the size of polymeric nanoparticles obtained by the micromixer-assisted nanoprecipitation process is linked with the geometry of the micromixer? Or would the nature of the polymer affect this size? To answer these questions, one may consider combining experimental investigations, CFD simulations and thermodynamic considerations along with population balance equations.

- For the double nanohydrogels, on may wonder about the effect of the viscosity of the inner droplets on the drug encapsulation efficiency and spontaneous

emulsification? Or does a general rule exist, for the choice of the two surfactants and their respective concentration, that can predict an effective double emulsification? Answers would probably lie in a new campaign of experiments.

- For which reason the addition of TPGDA in the Labrafrac eases the spontaneous emulsification. Besides an experimental work, some physical-chemistry knowledge should be considered.

Another set of perspectives would concern:

- Whether it is possible to perform the production of a double nanoemulsion in continuous flow. This would imply to develop a specific process that would allow the formation of the primary emulsion continuously and to investigate under which operating conditions (e.g. residence time, mixing etc.) the spontaneous emulsification might be performed.

- Until now, only drugs or contrast agents were loaded in the nanocarriers that were developed. However it might be much interesting to encapsulate more than one cargo in the NPs. For instance two incompatible drugs for dual drug delivery, one in the shell and the other one in the core of the double nanoemulsions/nanohydrogels; or a drug and a contrast agent for delivery and diagnosis.

- Pushing even further the concept of multifunctional nanocarriers, the surface of the nanocarriers could be modified to bear some specific peptides which will confer to the NPs a recognition site for theranostic applications.

HBL: Hydrophilic-Lipophilic Balance
PMMA: poly(methyl methacrylate)
NPs: nanoparticles
PGPR: polyglycerol polyricinoleate
Labrafac: a mixture of capric and caprylic acid triglycerides as a model of parenteral-grade oil
PBS: phosphate buffer solution
CFD: computational fluid dynamics

5.4 Scientifique production

5.4.1 Articles

1. Shukai Ding, Nicolas Anton, Thierry F. Vandamme and Christophe A. Serra, Microfluidic nanoprecipitation systems for preparing pure drug or polymeric drug loaded nanoparticles: an overview, **Expert Opin. Drug Deliv., 13 (10) (2016) 1447-1460.**

2. Wei Yu, Christophe A. Serra, Ikram U. Khan, Shukai Ding, Rigoberto Ibarra Gomez, Michel Bouquey and René Muller, Development of an Elongational-Flow Microprocess for the Production of Size-Controlled Nanoemulsions: Batch Operation. **Macromol. React. Eng., accepted.**

3. Wei Yu, Christophe A. Serra , Ikram. U. Khan, Meriem Er-Rafik, Marc Schmutz, Isabelle Kraus, Shukai Ding, Lixiong Zhang, Michel Bouquey and René Muller. Development of an Elongational-Flow Microprocess for the Production of Size-Controlled Nanoemulsions: Application to the Preparation of Monodispersed Polymer Nanoparticles and Composite Polymeric Microparticles. **Macromol. React. Eng., accepted.**

4. Shukai Ding, Christophe A. Serra, Wei Yu, Nicolas Anton and Thierry F. Vandamme, Production of dry-state ketoprofen-encapsulated PMMA NPs by coupling micromixer-assisted nanoprecipitation and spray drying, **submitted to Int. J. Pharm.**

5. Shukai Ding, Mohamed F. Attia, Justine Wallyn, Christophe A. Serra, Nicolas Anton, Wei Yu and Thierry F. Vandamme, Microfluidic-assisted production of SPIONs-encapsulated PMMA nanoparticles, **in preparation**.

6. Shukai Ding, Nicolas Anton, Wei Yu, Salman Akram, Marc Schmutz, Halina Anton, Andrey Kymchenko, Thierry F. Vandamme and Christophe A. Serra, A new method for the formulation of double nano-emulsion, **submitted to Soft Matter**.

7. Shukai Ding, Nicolas Anton, Christophe A. Serra, Wei Yu and Thierry F. Vandamme, Production of contrast agent-loaded nanolipogels by spontaneous emulsification, **in preparation**.

8. Shukai Ding, Nicolas Anton, Christophe A. Serra, Wei Yu and Thierry F. Vandamme, Technologies of double emulsification for the preparation of Water-in-Barrier-in-Water systems: a review, **in preparation**.

5.4.2 Oral communication

1. Shukai Ding, Christophe A. Serra, Nicolas Anton and Thierry F. Vandamme, Coupling nanoprecipitation microfluidic techniques and spray drying for preparing high-quality dry-state drug-loaded monodisperse polymeric nanoparticles at high throughput, In Proc. of **9th World Drug Delivery Summit**, New Orleans (USA), 30 June – 2 July, 2016.

SHUKAI DING

Development of microfluidic and low-energy emulsification methods for the production of monodisperse morphologically-complex nanocarriers. Application to drug and contrast agent encapsulation

Résumé

L'objectif de ce travail fut de développer et d'appliquer des technologies avancées de mélange et d'émulsification pour la préparation de nanovecteurs de morphologies complexes potentiellement utilisables en tant que produits pharmaceutiques. Premièrement, un procédé de nanoprécipitation assisté par micromélangeur fut utilisé pour obtenir et contrôler la taille de nanoparticules de PMMA chargées en Kétoprofène (100-200 nm). Combiné avec un appareil de séchage par pulvérisation, des nanoparticules sèches purent être obtenues dont les propriétés physico-chimiques furent proches de celles des particules non séchées. Ce microprocédé de nanoprécipitation permit également d'encapsuler des nanoparticules d'oxyde de fer (6 nm) dans des nanoparticules de PMMA de 200 nm avec une fraction massique de 60%. Pour augmenter la fraction solide de ces nanosuspensions et obtenir des particules sphériques de tailles plus petites (100 nm), une méthode de nanoémulsification basée sur un fort écoulement élongationnel fut employée. Deuxièmement, des émulsions et nanohydrogels doubles encapsulant un médicament hydrophile modèle dans leur cœur aqueux furent obtenus par couplage d'un microfluidiseur commercial pour l'obtention de l'émulsion primaire et d'une méthode d'émulsification basse énergie (émulsification spontanée) pour la double émulsification. La taille des nanovecteurs doubles a pu être variée grâce au rapport massique surfactant/huile (SOR) dans la gamme 80-80 nm. La colocation de deux sondes fluorescentes, placées dans le cœur et dans l'écorce, a pu être confirmée par microscopie confocale en fluorescence. La méthode d'émulsification spontanée fut également employée pour produire des nanolipogels (60 nm) chargées ou non de nanoparticules d'oxyde de fer et d'or (6 nm).

Mots-clés : microfluidique, émulsification spontanée, nanoprécipitation, nanoémulsification, nanoparticules polymères, nanoémulsions doubles, nanogels, délivrance de principe actifs, agent de contraste.

Abstract

The aim of this work was to develop and apply advanced technologies in mixing and emulsification for the preparation of morphologically-complex nanocarriers for potential uses in pharmaceutics. Firstly, a micromixer-assisted nanoprecipitation process was used to get and to easily tune the size of Ketoprofen-loaded PMMA nanoparticles (100-200 nm). Combined with a commercial spray dryer, dry-state drug-loaded polymeric nanoparticles (NPs), which main physicochemical properties were close to those of non spray-dried NPs, were successfully produced. This nanoprecipitation microprocess also allowed encapsulating 6 nm iron oxide NPs into 200 nm PMMA nanoparticles with a weight ratio of 60%. To increase the solid content of the above nanosuspension and get spherical polymeric NPs of smaller sizes (100 nm), an elongational-flow nanoemulsification method was used. Secondly, double nanoemulsions/nanohydrogels encapsulating a hydrophilic model drug in the aqueous core droplets/hydrogel were obtained by the combination of a commercial microfluidizer for the primary emulsion and a low energy emulsification method (spontaneous emulsification) for the double emulsification. The size of the double nanocarriers was varied by means of the surfactant to oil ratio (SOR) in the range 80 to 180 nm. Colocation of two fluorescent probes located in the core and in the shell was confirmed by fluorescence confocal microscopy. The spontaneous emulsification method was also employed to produce nanolipogels whose size could be tuned down to 60 nm. These nanolipogels were also loaded with iron oxide nanoparticles (6 nm) or gold nanoparticles (6 nm).

Keywords: microfluidics, spontaneous emulsification, nanoprecipitation, nanoemulsification, polymeric nanoparticles, nano double emulsions, nanogels, drug delivery, contrast agent.